

# Surface Scaling Mechanism and Prediction for Concrete

by

Youngjae Kang

A dissertation submitted in partial fulfillment  
of the requirements for the degree of  
Doctor of Philosophy  
(Civil Engineering)  
in The University of Michigan  
2010

## Doctoral Committee:

Professor Will Hansen, Chair  
Professor Jwo Pan  
Associate Professor Claus Borgnakke  
Associate Professor Vineet R. Kamat

# Table of Contents

<b>List of Figures</b>	<b>v</b>
<b>List of Tables</b>	<b>x</b>
<b>ABSTRACT</b>	<b>xi</b>
<b>CHAPTER 1</b>	
<b>INTRODUCTION</b>	<b>1</b>
<b>CHAPTER 2</b>	
<b>LITERATURE REVIEW</b>	<b>3</b>
2.1 INTRODUCTION	3
2.2 SALT SCALING	5
2.3 BASIC CHARACTERISTICS OF CONCRETE	7
2.3.1 Hardened Portland Cement (HPC)	7
2.3.2 Bleeding and segregation	9
2.4 WATER	10
2.5 ICE	11
2.6 FLOW IN CONCRETE	13
2.6.1 Moisture uptakes mechanism	13
2.6.2 Diffusivity	16
2.6.3 Permeability of cement paste	17
2.7 THE AIR VOID SYSTEM	18
2.7.1 Spacing factor for durable concrete	18
2.7.2 Influence of air entrainment on durability of concrete	20
2.8 BASIC THEOMODYNAMICS	21
2.8.1 Transport	23
2.9 MICRO-ICE-LENS	25
2.9.1 Micro-Ice-Lens theory	25
2.9.2 Micro-Ice-Lens pumping between water and salt solution	26
2.9.3 Pressures in pore water	27
2.10 THERMAL EXPANSION MISMATCH MECHANISM (BI-MATERIAL MECHANISM) [30]	29
2.11 COMPOSITE MATERIAL LAYER	33
2.12 THE MICROSTRUCTURE OF THE CONCRETE SURFACE	35
2.12.1 The weak surface layer	36
2.12.2 Interfacial transition zone (ITZ)	36
2.13 CHEMICAL PARAMETERS	38
2.13.1 The composition of Portland cement and Ground-Granulated Blast Furnace Slag	39
2.13.2 Carbonation	39
2.14 HYPOTHESIS REGARDING THE MECHANISM OF SURFACE SCALING	41
2.14.1 Moisture uptake	41
2.14.2 Microscopic pores	41

2.14.3 Macroscopic pores	42
2.14.4 Bulk system	42
2.15 THE VARIABLE AFFECTING SURFACE SCALING	42
2.15.1 Air Content	43
2.15.2 Water-binder ratio (w/b)	44
2.15.3 Supplementary Cementing Materials (SCM)	44
2.15.4 Aggregate	45
2.15.5 Curing Duration	46
<b>CHAPTER 3</b>	
<b>MATERIALS MATRIX AND EXPERIMENTAL METODS</b>	<b>47</b>
3.1 INTRODUCTION	47
3.2 EXPERIMENTAL REGIME	48
3.2.1 Materials	48
3.2.2 Material Matrix	48
3.3 TESTING METHODS	51
3.3.1 RILEM CIF/CDF Test	51
3.3.2 Test Specimens	51
3.3.3 Test Procedure	53
3.3.4 Measurements	55
3.3.5 Air void analysis	57
3.3.6 Low Temperature Dilatation (LTD)Test	59
<b>CHAPTER 4</b>	
<b>PRELIMINARY LABORATORY STUDIES WITH FIELD SPECIMENS</b>	<b>61</b>
4.1 INTRODUCTION	61
4.2 AIR VOID SYSTEMS OF FIELD SPECIMENS	61
4.2.1 Air Contents and Spacing Factors of field specimens	61
4.2.2 Air voids distribution.	63
4.2.3 Air voids infilling	65
4.3 RILEM CIF AND CDF TEST	72
4.3.1 Pre-saturation stage	73
4.3.2 Freezing-Thawing cycles	74
4.3.3 Internal damage VS surface scaling	78
4.3.4 Similarity in scaling mechanism between F-T testing in water and 3% sodium chloride solution	81
4.4 SUMMARY OF FINDINGS	84
<b>CHAPTER 5</b>	
<b>MECHANISMS OF SURFACE SCALING</b>	<b>86</b>
5.1 INTRODUCTION	86
5.2 EXISTING MECHANISMS	87
5.2.1 Hydraulic pressure	87
5.3 CRYOGENIC SUCTION PUMP MECHANISM	88
5.3.1 Background	88
5.3.2 Local Frost Actions	91
5.4 EXPERIMENTAL STUDIES	93
5.4.1 Low Temperature Dilatometer Test	93
5.4.2 Specimen Preparation and Pre-saturation	94

5.4.3 Results and discussion	96
5.5 QUALITATIVE SEQUENTIAL SURFACE SCALING MODEL	100
5.5.1 When there is no outer liquid reservoir on surface	100
5.5.2 When there is a water reservoir on the surface	103
5.5.3 When there is a de-icing salt solution reservoir on the surface	104
5.6 Conclusions	107
<b>CHAPTER 6</b>	
<b>FLOW AND EXPANSION BY CRYOGENIC PUMP EFFECT</b>	<b>109</b>
6.1 INTRODUCTION	109
6.2 PORE PRESSURE DIFFERENCES AND DIFFUSION IN CONCRETE	110
6.3 LOW TEMPERATURE DILATATION TESTS	114
6.4 THE RELATIONSHIP BETWEEN CRYOGENIC PUMP AND SURFACE SCALING	122
6.5 MICROSCOPIC OBSERVATION ON THE SURFACE AFTER LTD TEST	123
6.5.1 Cryogenic pump expansion < 100 micro strain	123
6.5.2 Cryogenic pump expansion > 100 micro strain	125
6.6 SUMMARY OF FINDINGS	126
<b>CHAPTER 7</b>	
<b>METHODOLOGY FOR IMPROVING SURFACE SCALING RESISTANCE OF CONCRETE</b>	<b>128</b>
7.1 INTRODUCTION	128
7.2 FROST ACTIONS OF WET CONCRETE PASTE DURING FREEZE-THAW CYCLE	129
7.3 IMPROVED PASTE QUALITY BY SUPPLEMENTARY CEMENTING MATERIAL (GGBFS)	131
7.3.1 Absorptivity of concrete containing GGBFS	132
7.3.2 Comparison of form surface scaling resistance between ordinary Portland cement concrete and concrete containing GGBFS	133
7.3.3 Comparison of cut surface scaling resistance between ordinary Portland cement concrete and concrete containing GGBFS	135
7.4 EFFECTS OF AIR VOID DISTRIBUTION AND INTERFACIAL TRANSIT ZONE (ITZ) ON SURFACE SCALING RESISTANCE	138
7.4.1 Test specimens	138
7.4.2 Critical spacing factor and flow distance	144
7.4.3 Expelling air by cryogenic pump	145
7.4.4 Air voids clustering and ITZ	149
7.5 TEST RESULTS WITH LABORATORY CONCRETE SPECIMENS	178
7.5.1 LTD test	178
7.5.2 Microscopic examination into damage of LTD specimens of OPC concrete	179
7.5.3 Microscopic examination into damage of LTD specimens of HPC concrete	181
7.5.4 Surface scaling test	186
7.6 SUMMARY OF FINDINGS	187
<b>CHAPTER 8</b>	
<b>MAJOR FINDINGS AND RECOMMENDATIONS FOR FUTURE WORK</b>	<b>191</b>
8.1 Major Findings	192
8.2 RECOMMENDATIONS FOR FUTURE RESEARCH	194
<b>References</b>	<b>197</b>



## List of Figures

FIGURE 1- 1 A) EXAMPLE OF SALT-SCALING DAMAGE, B) EXAMPLE OF FREEZE-THAW DAMAGE	2
FIGURE 2- 1 A) THE CONCRETE SURFACE AFTER 24 FREEZE/THAW CYCLES IN 3% NACL SOLUTION B) THE CONCRETE SURFACE AFTER 24 FREEZE/THAW CYCLES IN WATER	6
FIGURE 2- 2 DIFFERENT MOISTURE RANGES IN REGARD TO THE BASIC WATER ABSORPTION MECHANISM[12]	13
FIGURE 2- 3 A CAPILLARY ABSORPTION TEST OF A THIN SLAB. THE STEEP LINE CORRESPONDS TO MOISTURE RANGES 1 AND 2. THE BREAKING POINT CORRESPONDS TO CAPILLARY SATURATION IN FIGURE 2.2. THE SLOW ABSORPTION AFTER THE BREAKING-POINT CORRESPONDS TO MOISTURE RANGE 3. [12]	15
FIGURE 2- 4 SCHEMATIC OF CONSTRICTIVITY, CONNECTIVITY AND TORTUOSITY OF A PORE NETWORK [40]	17
FIGURE 2- 5 ILLUSTRATION OF PARAMETERS USED IN EQUATION 2.21	19
FIGURE 2- 6 SET-UP IN WET FROST EXPOSURE [25]	24
FIGURE 2- 7 VOLUME FRACTION OF ICE IN SOLUTIONS OF NACL AT THE INDICATED CONCENTRATIONS VERSUS TEMPERATURE	31
FIGURE 2- 8 CALCULATED STRESSES AND VOLUME FRACTION OF ICE IN SOLUTION CONTAINING 0.01% NACL, WHERE THE VOLUME FRACTION OF ICE IS NEAR 1	32
FIGURE 2- 9 CALCULATED STRESSES AND VOLUME FRACTION OF ICE IN SOLUTION CONTAINING 3% NACL	33
FIGURE 2- 10 EXAMPLE OF DILATOMETRIC TESTS	34
FIGURE 2- 11 THE CONCRETE SURFACE AFTER 5CDF CYCLES IN 3% NACL SOLUTION	38
FIGURE 2- 12 IMPACT OF THE CARBONATION ON THE VOLUME [28]	40
FIGURE 3- 1 SAWING OF TEST SPECIMENS AND PTFE PLATE	52
FIGURE 3- 2 F-T MACHINE TEMPERATURE CYCLE	53
FIGURE 3- 3 TEMPERATURE CONTROLLED CHEST & TEST CONTAINER	54
FIGURE 3- 4 CONCRETE POLISHER	58
FIGURE 3- 5 A) SAMPLE SURFACE AFTER POLISHING, AND B) IS SAME SURFACE AFTER TREATMENT	59
FIGURE 3- 6 DILATOMETER FOR LTD TEST	60
FIGURE 4- 1 AIR CONTENT FOR EACH CLASS (ENTRAINED AIR).	63
FIGURE 4- 2 CHORD LENGTH FREQUENCY FOR EACH CLASS (ENTRAINED AIR).	64
FIGURE 4- 3 AIR CONTENT FOR EACH CLASS (ENTRAPPED AIR)	64
FIGURE 4- 4 CHORD LENGTH FREQUENCY FOR EACH CLASS (ENTRAPPED AIR)	65
FIGURE 4- 5 AIR VOIDS SYSTEM OF NON DURABLE CONCRETE, SPECIMEN #3.	66

FIGURE 4- 6 AIR VOIDS SYSTEM OF ORDINARY CONCRETE, SPECIMEN #4.	67
FIGURE 4- 7 AIR VOIDS SYSTEM OF DURABLE CONCRETE, SPECIMEN #11.	68
FIGURE 4- 8 SOLUBILITY OF SODIUM SULFATE IN WATER. COOLING THE LIQUID FROM 30 °C TO 10 °C WITHOUT CRYSTALLIZATION CREATES SUPER SATURATION.	69
FIGURE 4- 9 AIR VOIDS INFILLINGS OF SPECIMEN #1	70
FIGURE 4- 10 AIR VOIDS INFILLINGS OF SPECIMEN #3	71
FIGURE 4- 11 SKETCH OF A PRISMATIC F-T SPECIMEN OBTAINED FROM A CORE	73
FIGURE 4- 12 MOISTURE UPTAKES IN WATER DURING PRE-SATURATION STAGE	74
FIGURE 4- 13 MOISTURE UPTAKES IN 3% NACL DURING PRE-SATURATION STAGE	74
FIGURE 4- 14 THE EVALUATION OF INTERNAL DAMAGES IN WATER	75
FIGURE 4- 15 THE EVALUATION OF INTERNAL DAMAGES IN 3% NACL SOLUTION	75
FIGURE 4- 16 THE EVALUATION OF SURFACE SCALING IN WATER	76
FIGURE 4- 17 THE EVALUATION OF SURFACE SCALING IN 3%NACL SOLUTION	76
FIGURE 4- 18 THE MOISTURE UPTAKES IN WATER	77
FIGURE 4- 19 THE MOISTURE UPTAKES IN 3% NACL SOLUTION	77
FIGURE 4- 20 INTERNAL DAMAGE VERSUS MASS LOSS RATE	78
FIGURE 4- 21 SCALING SENSITIVITY TO REMAINING ENTRAINED AIR (%)	79
FIGURE 4- 22 SCALING SENSITIVITY TO SPACING FACTOR (MM)	80
FIGURE 4- 23 INTERNAL DAMAGE VERSUS ENTRAINED AIR CONTENT	80
FIGURE 4- 24 INTERNAL DAMAGE VERSUS SPACING FACTOR (MM)	81
FIGURE 4- 25 SURFACE SCALING OF SPECIMEN #1 IN CIF AND CDF TEST	82
FIGURE 4- 26 SURFACE SCALING OF SPECIMEN #6 IN CIF AND CDF TEST	82
FIGURE 4- 27 SURFACE SCALING OF SPECIMEN #10 IN CIF AND CDF TEST	83
FIGURE 4- 28 SURFACE SCALING OF SPECIMEN #11 IN CIF AND CDF TEST	83
FIGURE 5- 1 PRESSURE DIFFERENCE AND LIQUID AND VAPOR FLOW TOWARD AN ICE CRYSTAL	91
FIGURE 5- 2 (A) SURFACE VOIDS (B) BULK VOIDS	92
FIGURE 5- 3 (A) FROST ACTION IN COARSE PORES OR VOIDS UNDERNEATH THE SURFACE, (B) FROST ACTION FAR BELOW THE SURFACE	92
FIGURE 5- 4 TEMPERATURE PROFILE FOR LTD TEST	94
FIGURE 5- 5(A) LTD TEST PRISM WITHOUT SURFACE LIQUID RESERVOIR, (B) WITH SURFACE LIQUID RESERVOIR	95
FIGURE 5- 6 PRE-SATURATION	95
FIGURE 5- 7 COMPLETE SPECIMEN	95
FIGURE 5- 8 MOISTURE UPTAKES DURING PRE-SATURATION	96
FIGURE 5- 9 LTD TEST RESUTLS FOR FIELD SEPCIMEN #6 WITH SURFACE LIQUID (DE-MINERALIZED WATER)	96
FIGURE 5- 10 LTD TEST RESUTLS FOR FIELD SEPCIMEN #6 WITH SURFACE LIQUID (3% NACL SOLUTION)	97
FIGURE 5- 11 DILATATION VS TEMPERATURE DURING FREEZING THAWING (#6)	98
FIGURE 5- 12 DILATATION VS TIME DURING FREEZING THAWING CYCLE (#6)	99
FIGURE 5- 13 LTD TEST RESUTLS FOR FIELD SEPCIMEN #6 WITHOUT SURFACE LIQUID (3% NACL SOLUTION)	100

FIGURE 5- 14 DILATATION CURVES WITHOUT SURFACE LIQUID	101
FIGURE 5- 15 STEP 1 AND PORE LIQUID FREEZING	102
FIGURE 5- 16 STEP 2 AND STEP 3	102
FIGURE 5- 17 STEP 4 AND STEP 5	103
FIGURE 5- 18 CAPILLARY SUCTION AND CRYOGENIC PUMP EFFECT	104
FIGURE 5- 19 DILATATION CURVES WITH SURFACE LIQUID (3% NaCl SOLUTION)	105
FIGURE 5- 20 STEP 1 AND PORE LIQUID FREEZING	105
FIGURE 5- 21 STEP 2 AND STEP 3	106
FIGURE 5- 22 STEP 4	106
FIGURE 5- 23 STEP 5 WHEN PORE ICE CRYSTALS START MELTING AND STEP 5 WHEN SURFACE ICE STARTS MELTING	107
FIGURE 6- 1 VAPOUR FLOW FROM SATURATED HARDENED CONCRETE PASTE TOWARDS VOID [41]	110
FIGURE 6- 2 DIFFUSION INTO AN AIR VOID WITH A SHELL OF CEMENT PASTE [43]	111
FIGURE 6- 3 TRANSPORT RATE INTO AN AIR VOID (AVERAGE RADIUS) BY CRYOGENIC PUMP VS. SPACING FACTOR	112
FIGURE 6- 4 TRANSPORT RATE INTO AN AIR VOID BY CRYOGENIC PUMP VS. AVERAGE VOID RADIUS	112
FIGURE 6- 5 PRESSURE DIFFERENCES OF FIELD SPECIMENS BY CRYOGENIC PUMP VS. SPACING FACTOR	113
FIGURE 6- 6 PRESSURE DIFFERENCES OF FIELD SPECIMENS BY CRYOGENIC PUMP VS. AVERAGE VOID RADIUS	114
FIGURE 6- 7 DILATATION OF NON-DURABLE CONCRETE (#1) DURING A FREEZE-THAW CYCLE	115
FIGURE 6- 8 DILATATION OF NON-DURABLE CONCRETE (#2) DURING A FREEZE-THAW CYCLE	115
FIGURE 6- 9 DILATATION OF MODERATE CONCRETE (#6) DURING A FREEZE-THAW CYCLE	116
FIGURE 6- 10 DILATATION OF DURABLE CONCRETE (#10) DURING A FREEZE-THAW CYCLE	116
FIGURE 6- 11 EXPANSION DUE TO CRYOGENIC PUMP EFFECT	117
FIGURE 6- 12 THE RELATIONSHIP BETWEEN MASS LOSS RATE AND MAX CRYOGENIC EXPANSION	118
FIGURE 6- 13 DILATATION OF NON-DURABLE CONCRETE (#1) WITH ONLY WATER ON SURFACE DURING A FREEZE-THAW CYCLE	119
FIGURE 6- 14 DILATATION OF NON-DURABLE CONCRETE (#2) WITH ONLY WATER ON SURFACE DURING A FREEZE-THAW CYCLE	119
FIGURE 6- 15 DILATATION OF MODERATE CONCRETE (#6) WITH ONLY WATER ON SURFACE DURING A FREEZE-THAW CYCLE	120
FIGURE 6- 16 EXPANSION DUE TO CRYOGENIC PUMP EFFECT WITH ONLY WATER ON SURFACE	120
FIGURE 6- 17 THE RELATIONSHIP BETWEEN MASS LOSS RATE AND MAX CRYOGENIC EXPANSION	121

FIGURE 6- 18 MASS LOSS RATE VS CRYOGENIC PUMP EXPANSION	122
FIGURE 6- 19 A) LATERAL SURFACE OF #10 LTD PRISM BEFORE FREEZE THAW CYCLES B) SAME LOCATION AFTER 3 FREEZE THAW CYCLES	124
FIGURE 6- 20 A) LATER SURFACE OF #6 LTD PRISM BEFORE FREEZE THAW CYCLES B) SAME LOCATION AFTER 3 FREEZE THAW CYCLES	124
FIGURE 6- 21 A) TOP SURFACE OF SPECIMEN #2 AFTER 3 FREEZE THAW CYCLES OF LTD TEST B) LATERAL SURFACE OF SAME SPECIMEN	125
FIGURE 6- 22 A) TOP SURFACE OF SPECIMEN #1 AFTER 3 FREEZE THAW CYCLES OF LTD TEST B) LATERAL SURFACE OF SAME SPECIMEN	126
FIGURE 7- 1 SCHEMATIC EXPLANATION OF ICE SHRINKAGE IN A VOID	129
FIGURE 7- 2 SCHEMATIC EXPLANATION OF FLOW TOWARD A VOID	130
FIGURE 7- 3 ABSORPTIVITY TEST RESULTS WITH VARIOUS CONTENTS OF GGBFS	133
FIGURE 7- 4 SURFACE SCALING OF OPC AND 50S	134
FIGURE 7- 5 CUT SURFACE SCALING OF OPC AND 50S	135
FIGURE 7- 6 DISTRIBUTION OF CHORD LENGTH FREQUENCY (<0.5MM)	140
FIGURE 7- 7 DISTRIBUTION OF CHORD LENGTH FREQUENCY (>0.5MM)	140
FIGURE 7- 8 CHORD LENGTH FREQUENCY OF OPC 1 AND HPC 2	142
FIGURE 7- 9 CHORD LENGTH FREQUENCY OF OPC 2 AND HPC 3	142
FIGURE 7- 10 CHORD LENGTH FREQUENCY OF NON AEA AND OPC	143
FIGURE 7- 11 CHORD LENGTH FREQUENCY OF NON AEA AND HPC	143
FIGURE 7- 12 AT A GIVEN, CRITICAL WATER CONTENT IN A UNIT CELL, THE ACTUAL FLOW DISTANCE EQUALS THE CRITICAL VALUE [12]	144
FIGURE 7- 13 SCHEMATIC EXPLANATION OF EXPELLING AIR BURBLES IN SALT SOLUTION DURING FREEZING	145
FIGURE 7- 14 MICROSCOPIC PHOTO OF THE ICE LAYER ON CONCRETE SURFACE AT -20C (3%NACL SOLUTION, 2F-T CYCLES)	146
FIGURE 7- 15 SCHEMATIC EXPLANATION WHEN SURFACE LIQUID IS WATER	147
FIGURE 7- 16 MICROSCOPIC PHOTO OF THE ICE LAYER ON CONCRETE SURFACE AT -20C (WATER, 2F-T CYCLES)	148
FIGURE 7- 17 SCHEMATIC IMPRESSION OF THE INTERFACIAL TRANSITION ZONE [48]	150
FIGURE 7- 18 POLISHED SURFACE OF OPC-I SPECIMEN	151
FIGURE 7- 19 SPOT A AND B OF OPC-I SPECIMEN IN FIGURE 7.18	152
FIGURE 7- 20 POLISHED SURFACE OF OPC-II SPECIMEN	153
FIGURE 7- 21 SPOT A AND B OF OPC-II SPECIMEN IN FIGURE 7.20	153
FIGURE 7- 22 INTERFACE BETWEEN AGGREGATES AND PASTE (OPC-I)	154
FIGURE 7- 23 INTERFACE BETWEEN AGGREGATES AND PASTE (OPC-II)	155
FIGURE 7- 24 POLISHED SURFACE OF HPC-II SPECIMEN	156
FIGURE 7- 25 SPOT A AND B OF HPC-II SPECIMEN IN FIGURE 7.24	156
FIGURE 7- 26 INTERFACE BETWEEN AGGREGATES AND PASTE (HPC-II)	157
FIGURE 7- 27 INTERFACE BETWEEN AGGREGATES AND PASTE (HPC-III)	158
FIGURE 7- 28 ITZ AND AIR VOIDS IN THE ZONE (OPC-I)	159
FIGURE 7- 29 AIR VOIDS IN ITZ OF OPC-I	161
FIGURE 7- 30 AIR VOIDS IN ITZ OF OPC-II	162

FIGURE 7- 31 AIR VOIDS IN BULK PASTE OF OPC-I	163
FIGURE 7- 32 AIR VOIDS IN BULK PASTE OF OPC-II	164
FIGURE 7- 33 ANOTHER EXAMINATION OF AIR VOIDS IN BULK PASTE OF OPC-II	165
FIGURE 7- 34 INTERFACE OF HPC-II	166
FIGURE 7- 35 AIR VOIDS IN INTERFACE OF HPC-II	167
FIGURE 7- 36 AIR VOIDS IN INTERFACE OF HPC-III	168
FIGURE 7- 37 AIR VOIDS IN BULK PASTE OF HPC-III	169
FIGURE 7- 38 ANOTHER AIR VOIDS IN BULK PASTE OF HPC-III	170
FIGURE 7- 39 AIR VOIDS IN BULK PASTE OF HPC-III	171
FIGURE 7- 40 SCHEMATIC EXPLANATION OF EXPANSION IN ITZ DURING F-T CYCLES	173
FIGURE 7- 41 ITZ STRAIN (ITZ WIDTH =30MICRON, AGGREGATE CONTENT = 70% AND AVERAGE DIAMETER OF COARSE AGGREGATES = 25MM) FOR LTD TEST PRISM (LENGTH=90MM)	174
FIGURE 7- 42 DILATATION OF OPC-2 DURING A F-T CYCLE	175
FIGURE 7- 43 OPC-II SPECIMEN AFTER 4 F-T CYCLES IN 3% NAACL SOLUTION	176
FIGURE 7- 44 OPC-II (AFTER 4 F-T CYCLES IN 3% NAACL SOLUTION)	177
FIGURE 7- 45 OPC-II (AFTER 10 F-T CYCLES IN 3% NAACL SOLUTION)	177
FIGURE 7- 46 EXPANSION OF OPC CONCRETE SPECIMENS DUE TO CRYOGENIC PUMP EFFECT ( $\Delta\varepsilon$ )	178
FIGURE 7- 47 EXPANSION OF HPC CONCRETE SPECIMENS DUE TO CRYOGENIC PUMP EFFECT ( $\Delta\varepsilon$ )	179
FIGURE 7- 48 THE LOCATIONS OF SURFACES OF LTD PRISM	179
FIGURE 7- 49 THE TEST SURFACE OF OPC I LTD PRISM AFTER 5 FREEZE-THAW CYCLES	180
FIGURE 7- 50 SPOT A AND B OF OPC-I LTD PRISM IN FIGURE 7.49	180
FIGURE 7- 51 THE LATERAL SURFACE OF OPC I LTD PRISM AFTER 5 FREEZE-THAW CYCLES	180
FIGURE 7- 52 SPOT A AND B OF OPC-I LTD PRISM IN FIGURE 7.51	181
FIGURE 7- 53 THE TEST SURFACE OF HPC-II LTD PRISM AFTER 5 F-T CYCLES	181
FIGURE 7- 54 SPOT A AND B OF HPC-II LTD PRISM IN FIGURE 7.53	182
FIGURE 7- 55 THE TEST SURFACE OF HPC-II LTD PRISM AFTER 10 F-T CYCLES	182
FIGURE 7- 56 SPOT A AND B OF HPC-II LTD PRISM IN FIGURE 7.55	183
FIGURE 7- 57 THE LATERAL SURFACE OF HPC-II LTD PRISM AFTER 5 F-T CYCLES	183
FIGURE 7- 58 SPOT A AND B OF HPC-II LTD PRISM IN FIGURE 7.57	184
FIGURE 7- 59 THE LATERAL SURFACE OF HPC-II LTD PRISM AFTER 10 F-T CYCLES	184
FIGURE 7- 60 SPOT A AND B OF HPC-II LTD PRISM IN FIGURE 7.59	185
FIGURE 7- 61 AFTER 130 F-T CYCLES IN 3%NAACL SOLUTION (CONCRETE CONTAINING GGBFS (LEFT) AND ORDINARY PORTLAND CEMENT CONCRETE (RIGHT))	186
FIGURE 7- 62 THE EVALUATION OF SURFACE SCALING OF LABORATORY SPECIMENS	187

## List of Tables

TABLE 2- 1 A) CLASSIFICATION OF PORES [8]	9
TABLE 2- 2 MATERIAL DATA FOR CONCRETE SHOWING RELATION BETWEEN RELATIVE HUMIDITY, $\phi$ , MOISTURE CONTENT, W, AND KIRCHHOFF POTENTIAL, $\psi$ [13]	16
TABLE 3- 1 FROST DAMAGE RATES OF FIELD SPECIMENS	49
TABLE 3- 2 CHEMICAL COMPOSITIONS OF MATERIALS	50
TABLE 3- 3 MATRIX FOR TEST SPECIMENS	51
TABLE 4- 1 AIR VOIDS PROPERTIES OF FIELD SPECIMENS	62
TABLE 4- 2 TOTAL AIR CONTENT AND IN-FILLING AIR CONTENT BY 3000 POINTS COUNT	72
TABLE 7- 1 SCALED SURFACE BY F-T ATTACK	136
TABLE 7- 2 SCALED CUT SURFACES OF OPC AND 50S SPECIMENS BY F-T ATTACK	137
TABLE 7- 3 MATRIX FOR TEST SPECIMENS	139
TABLE 7- 4 AIR VOIDS PARAMETERS OF TEST SPECIMENS	139

## ABSTRACT

Severe deterioration of concrete joints has developed at a rapid rate for several Michigan highway projects. This deterioration was found to be linked to deicer salt applications during the winter season. Surface scaling was found to be associated with frost deterioration of the portland cement mortar from exposure to a salt solution on the surface during a freeze-thaw cycle. Inadequate entrained air content in the portland cement paste was found to be the major factor.

A variety of mechanisms and associated models have been proposed in the literature. So far no clear consensus has been developed due to the lack of detailed measurements based mainly on macroscopic observations. From the experiments in this study the major findings are:

The driving force responsible for developing surface scaling can be explained by means of an exiting theory known as the Cryogenic Suction Pump. This mechanism is thermodynamic-based. As ice starts forming inside a large pore, capillary transport will form within triple-phases zone. If the surface liquid is unfrozen, then a cryogenic pump stays active within a surface region. Surface liquid consisting of salt-water is an example, because salt-water does not freeze instantly as opposed to pure water. This is because the solutes lowers the freezing point while removal of water increases the solute concentration in the remaining solution, so an initial 3% salt solution stays unfrozen above the eutectic point ( $-21.2^{\circ}\text{C}$ ).

Surface scaling can develop as a result of excessive internal pore pressure from either critically saturated pores within the paste without air-entrainment as pressure relief, or when surface liquid is present, then the cryogenic pump exacerbates the problem as this creates an additional source for ice formation.

This study is the first to identify a link between surface scaling from exposure to pure water and salt-water (i.e. 3 % sodium chloride concentration) on the surface. For pure water the cryogenic suction pump is limited to capillary pore-suction since external liquid is not available for ice-crystal growth.

Another first, this study found a connection between surface scaling and the Interfacial Transit Zone (ITZ) localized zone around the aggregate, which is a higher porosity zone. In this case the cryogenic pump initiates in the ITZ region. Scaling is localized and propagates with depth and width. This type of scaling is more severe than regular surface scaling, which is spread out over more surface area, but less deep. Substantial improvement in resistance to surface scaling resistance was achieved by eliminating the weak-ITZ by means of pozzolanic reactions between the Portland cement paste and ground granulated blast-furnace slag (GGBFS). The pozzolanic reactions further reduced capillary sorptivity (i.e. rate of capillary suction versus square-root time) as seen from water sorption results. A decrease in capillary sorptivity reduces the rate of transport by the cryogenic suction pump during freezing.

Entrained air was found to be the major factor in mitigating the cryogenic suction pump. The cryogenic suction pump starts as soon as freezing develops inside the larger pores. This was concluded from results using a unique experimental procedure called low temperature dilation. Initial freezing in these pores is due to pure water from the



fully saturated capillary pores. Ice crystal growth inside the surface pores due to the cryogenic pump is reduced with increasing entrained air content as air decreases pore-filling and creates capillary discontinuity, which inhibits suction.

However, increased entrained air alone cannot stop the cryogenic suction pump as long as surface liquid is available during freezing (i.e. temperatures down to  $-20^{\circ}\text{C}$ ). Freezing exposure to pure surface water is much less severe as liquid transport is only possible within the pore system. Increasing entrained air content in a fully saturated pore-system can prevent internal frost damage, but cannot prevent salt-scaling surface damage.

Paste sorptivity was found to be a measure of the liquid transport property as affected by entrained air content, and pozzolanic reactions. Once the expansion was initiated, a gradient of expansion was related with a cryogenic pump flow rate which was controlled by paste sorptivity. The cryogenic suction pump accelerates critical saturation levels in the paste.

# CHAPTER 1

## INTRODUCTION

Concrete is the most common material for construction material because it is inexpensive material and has many structural benefits. On the other hand, concrete is difficult to repair and remove and causes large amounts of construction waste at the end of the service life. Thus, people expect that concrete structure and pavement will remain in good shape for at least a couple of decades. However, the service life of concrete structure can be shortened by durability problem without structural failure. In cold regions especially, concrete experiences deterioration caused by freezing and thawing. Deicing salts exacerbate this problem. Two types of deterioration are observed. One is surface scaling (Figure 1.1) which is critical only in the presence of deicing salt. The other is internal damage (Figure 1.2). Frost deterioration might shorten the service life of concrete structure, especially slab or pavement. It has been believed that the internal damage might be caused by ice expansion when the critical degree of saturation is reached. Thus, no Portland cement concrete could be placed in below freezing weather without thermal protection such as entrained air. In contrast, the mechanisms causing surface scaling have been unknown. Besides, it is not clear to which factors salt scaling resistance of concrete is more sensitive.

Therefore, the purpose of this study is to contribute to the knowledge of those

mechanisms and to suggest optimal concrete mix design for deicing salt scaling resistance. More specifically, several questions related to salt scaling including internal frost attack need to be answered. First, what causes the occurrence of salt scaling of concrete and which factors contribute most to salt scaling? Also, how do present protection methods improve salt scaling resistance? This study will also examine what is an optimal concrete mix design and construct procedure? And finally, what criteria are available for avoiding salt scaling? Addressing these questions will be the major objective of this study.



**Figure 1- 1 a) Example of salt-scaling damage, b) Example of freeze-thaw damage**

# CHAPTER 2

## LITERATURE REVIEW

### 2.1 INTRODUCTION

Porous materials such as concrete experience frost deterioration, internal damage and surface scaling under cyclic freeze/thaw conditions. The deterioration is more severe in the presence of a de-icing salt solution than water. Damage might occur when saturation reaches a critical degree before freezing. Saturation might not be reached at a critical degree by osmotic pressure or it might take too long to happen in the field. To explain this contradiction, the micro-ice-lens model is suggested by Max J. Setzer. [1]

Since the radius of the porosity in concrete is very small, condensed matter in pores can coexist stably as liquid, solid and vapor much below a bulk freezing point (up to  $-20^{\circ}\text{C}$ ). This triple-phase condition in the pores can generate negative pressure with decreasing temperature. The pressure difference might cause microstructure shrinkage or damage. As temperature increases, the pressure difference decreases. However, the liquid is entrapped in the micro-ice-lenses. This submicroscopic pump leads to an artificial saturation with repeated freeze/thaw cycles. This micro-ice-lens model might explain part of the surface scaling mechanism as well as internal damage even though there is no agreement regarding the surface scaling mechanism yet.

Microstructure of the surface cannot be considered to be the same as bulk concrete. M. Pigeon, C. Talbot, J. Marchand and H. Hornain observed an extremely porous layer at the surface [2]. This porous layer at the surface (Weak Zone) might weaken the scaling resistance during the early cycles. This fact is also supported by my own test results in this study. The depth and porosity of the weak zone may be related to the amount of the supplementary cementing materials (SCM) such as GGBFS or fly ash as well as water-binder ratio (w/b).

When a concrete surface is exposed to de-icing salt solution, the microstructure of the surface might be changed by a chemical reaction such as carbonation. The chemical reaction leads to changes in the pore size distribution. The change of the pore size distribution can effect the saturation as well as the salt scaling resistance. Even if it is not clear yet whether the deterioration by the chemical reaction is very serious and whether it occurs under real conditions, alterations of the microstructure and pore solution through carbonation must be considered in order to more precisely understand surface scaling. In [3], the test result shows that the interfacial transition zone (ITZ), which foamed between the aggregate and the cement paste by the chemical reaction, may cause the deterioration of the frost durability as well as the surface scaling.

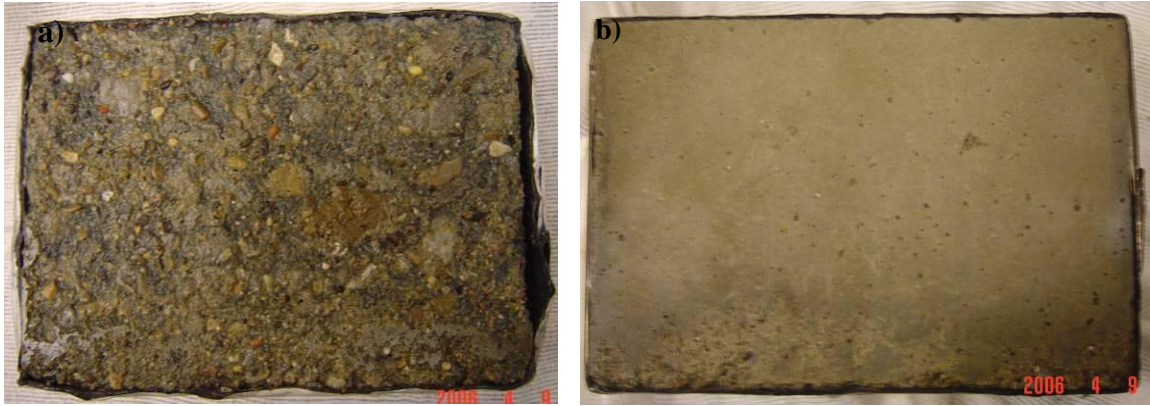
There is no exact agreement of the mechanism of the surface scaling while ice crystal expansion in the pores might be the major reason of the internal damage. The mechanism of the salt scaling could be multiple phenomena. Even though the reasons are not yet clear, several variables, which affect salt scaling, have been determined by many researchers [3,4,5,6]. These variables are air content, water-binder ratio (w/b), the amount of cement replacement by supplementary cementing material (SCM) such as GGBFS or

fly ash, aggregate and curing duration.

By observing the change of the scaling amount by such variables, we can more precisely approach the mechanism of the salt scaling.

## **2.2 SALT SCALING**

When it snows in severe climate regions, de-icing salts are commonly spread on roads and sidewalks for removing ice or preventing snow from freezing. Thus, the roads experience cyclic freeze/thaw in the presence of a salt solution. It has been well documented that the combination of de-icing salts and frost causes serious degradation of concrete structures. The degradation mainly affects the surfaces of a structure and tends to be more severe when the concentration of de-icer in the solution is rather moderate, i.e. around 3%. Concrete particles are taken off by the salt-frost attack. This degradation is often referred to as salt scaling. The result is severe. If a concrete structure has the poor resistance of salt scaling and if the surface of concrete is exposed to salt solution in a cyclic freeze/thaw climate environment the entire concrete cover would be removed in just a few cycles. In addition, the depth of scaling can be a few centimeters. These observations were supported by this researcher's test results. See Figure 2-1.



**Figure 2- 1 a) The concrete surface after 24 freeze/thaw cycles in 3% NaCl solution  
b) The concrete surface after 24 freeze/thaw cycles in water**

As shown in Figure 2.1, it is obvious that the salt scaling takes place only in the presence of salt solution. When the de-icer frost attack has destroyed the entire concrete cover, the adhesion of the reinforcement to the concrete is reduced, resulting in serious loss of structural strength. In this severe case, the salt scaling may shorten the service life of the structure.

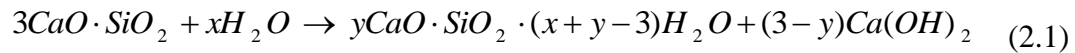
Unfortunately, the exact mechanism of the salt scaling is not clear at this time. Thus, we cannot avoid the degradation perfectly until the true mechanism is revealed. Therefore, tests with variables which can affect the scaling resistance and possible mechanism suggested by many researchers appears to be the best way to approach and pinpoint the contribution of mechanisms or to develop a better model for salt scaling.

Before examining the variables which can affect scaling resistance, it is necessary to review the basic characteristics of Portland cement paste and thermodynamics.

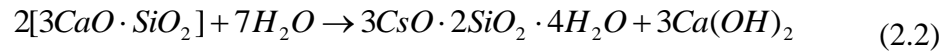
## 2.3 BASIC CHARACTERISTICS OF CONCRETE

### 2.3.1 Hardened Portland Cement (HPC)

Hardened Portland Cement is a porous material and consists of a crystalline calcium silicate hydrate ( $3CaO \cdot 2SiO_2 \cdot 4H_2O$ ) and crystalline  $Ca(OH)_2$ . Tricalcium silicate and dicalcium silicate together make up 75-80% of Portland cement. In the presence of a limited amount of water, the reaction of  $C_3S$  with water is represented as follows:



or typically



This calcium silicate hydrate is denoted C-S-H gel or cement gel. The dimension of its particles is less than  $1\mu m$ .

When mixing concrete, hydration, which is the reaction of cement and water, begins immediately and continues in the presence of water. During hydration, water is chemically bound to cement. For ordinary Portland cements, the degree of hydration,  $\alpha$ , can be calculated by equation (2.3)

$$\alpha = \frac{W_n}{0.25C} \quad (2.3)$$

Where,

$W_n$  = weight of chemically bound water

$C$  = weight of cement

The amount of chemically bound water for OPC at complete hydration is approximately 0.25g.



The porosity of the HPC is related with the degree of hydration and water-cement ratio. Powers and Brywnyard [7] suggested the equations of the porosity of the hardened cement paste as follows:

$$P_{paste} = \frac{w/c - 0.19\alpha}{0.32 + w/c} \quad (2.4)$$

Where,

$P_{paste}$  = total porosity

$\alpha$  = degree of hydration

w/c = water cement ratio

0.32 = specific volume of Portland cement [l/kg]

The gel porosity is due to the porosity of the cement gel and its typical width ranges up to 30nm. The capillary porosities are larger than gel pores and are not filled with reaction products. The part of the total paste porosity due to the porosity of the gel is called gel porosity and is calculated:

$$P_{gel} = \frac{0.20\alpha}{0.32 + w/c} \quad (2.5)$$

As a result, the capillary porosity can be as follows:

$$P_{capillary} = P_{paste} - P_{gel} = \frac{w/c - 0.39\alpha}{0.32 + w/c} \quad (2.6)$$

The pore system is rather heterogeneous where transport phenomena take place. The physical and chemical behavior in this system is not only subjected to macroscopic bulk phenomena but also to submicroscopic surface physics and chemistry. To separate the different effects M.J.Setzer distinguished between gel pores, capillaries and coarse pores [8]. See Table 2.1. In gel pores surface physics are at least not negligible or even

dominant. In capillaries water behaves mostly macroscopically. However, due to interfaces capillary suction takes place.

### 2.3.2 Bleeding and segregation

In a freshly placed concrete which is still plastic, settlement of solids is followed by the formation of a layer of water on the surface. This is known as bleeding. In lean mixes, localized channels develop and the seepage of water transports some particles to the surface. Bleeding may thus give rise to laitance, a layer of weak, nondurable material containing diluted cement paste and fines from the aggregate.

**Table 2- 1 Classification of pores [8]**

Name	$R_H$	Characteristics	Type of pore water
Coarse		Empty	
Macro Capillaries	< 1mm	Suction : Instantly	Macroscopic Bulk water
Meso Capillaries	< 30 $\mu$ m	Suction : minutes to week	
Micro Capillaries	< 1 $\mu$ m	Suction : no macroscopic equilibrium	
Meso gel pores	< 30nm	Transition from bulk to surface physics	Prestructured condensate
Micro gel pores	< 1nm	Surface Physics	Structured surface water

During the handling of a concrete mixture, there may be some separation of coarse aggregates from concrete mass. This is known as segregation. Segregation may lead to flaws in the final product and honeycombing may occur in some instances. Segregation may result during handling, placing, vibrating, or finishing operations. The primary cause of segregation is the differences in the size of the particles and specific gravity of the mix. The tendency to segregate increases with slump, reduction in cement content, or increase in the maximum size and amount of aggregate.

## 2.4 WATER

For better understating of water flow during freeze/thaw action, the properties of water such as density, heat capacity and surface energy need to be observed. The density of water varies with temperature. The density can be calculated as follows [9]:

$$\rho = -3479.56 + 46.301T - 0.1591T^2 + 1.8171 \cdot 10^{-4}T^3 \quad (2.7)$$

Where,

$\rho$ = the density of water ( $kg/m^3$ )

T= temperature (K)

Thus, the molar volume is:

$$V_{m,l} = -3.4228 \cdot 10^{-12}T^3 + 2.9896 \cdot 10^{-9}T^2 - 8.6806 \cdot 10^{-7}T + 1.0182 \cdot 10^{-4} \quad (2.8)$$

The density of water contained in the pores of hardened Portland cement paste is higher than that of bulk water even though the exact difference is not known. The density of the deicing agent solution may depend on its concentration. In case of NaCl solution, the density at 20°C can be expressed as the following [10]:

$$\rho(c) = 7.2416c + 997.98 \quad (2.9)$$

in which  $c$  is the concentration of NaCl in % by weight of the solution. This relation is valid up to 26%.

The surface tension of water or deicing agent solution is related with the characteristic of pore water. The surface tension of a surface liquid water-vapor varies with temperature and content of solutes in the liquid. The surface tension is described as a function of the concentration of NaCl by:

$$\sigma_{l-v}(c)_{293k} = \frac{72.72 + 0.325c}{1000} \quad (2.10)$$

in which  $\sigma(c)$  is given in  $J/m^2$  and the concentration of NaCl ( $c$ ) is given in % by weight of the solution [10]. In the interval  $265 < T < 298K$ , the temperature dependence of the surface tension of a surface liquid water-vapor is as follows [10]:

$$\sigma_{l-v}(T) = -0.1484 \cdot 10^{-3}T + 0.11623 \quad (2.11)$$

## 2.5 ICE

There are two types of nucleation. Ice nucleation may be homogeneous if nucleation takes place in the liquid so that the ice crystal is entirely surrounded by the liquid and an ice-liquid interface is created. The other case is that the ice nucleation may be heterogeneous if it nucleates and grows on a foreign surface. The solid-liquid interface of homogeneous nucleation causes a rise in the free energy of the system which must be overcome by the loss of free energy due to the phase transition itself in order for nucleation to occur. Thus, a nucleus smaller than a certain size at a certain temperature is

thermodynamically unstable and immediately melts. The critical radius of a spherical ice nucleus as a function of temperature can be expressed as the following:

$$r_s = \frac{2\sigma_{s-l}V_{m,s}}{0.0997T^2 - 76.4532T + 13444.483} \quad (2.12)$$

Where,

$T$  = temperature [K]

$V_{m,s}$  = molar volume of ice,  $m^3/mol$

$\sigma_{l-s}$  = free energy of the interface liquid-solid,  $J/m^2$

It is well known that the density of ice is lower than that of water. In fact, the density of ice at 0°C is  $916.4 \text{ kg}/m^3$  [11]. As the density of water at the same temperature is  $999.8395 \text{ kg}/m^3$ , the phase transition brings about an expansion of 9.1%. This is the most apparent reason of frost damage. The density of ice as a function of temperature may be estimated from the following equation:

$$\rho(T) = \frac{\rho(273.15)}{(1 + \alpha(T - 273.15))^3} \quad (2.13)$$

Where,

$\rho(T)$  = density at temperature  $T$

$\rho(273.15)$  = density at  $T=273.15\text{K}$ , 1 atm ( $916.4 \text{ kg}/m^3$ )

$\alpha$  = coefficient of linear expansion

The surface energy of ice at different temperatures may be estimated from:

$$\sigma_{l-s} = \frac{33 + 0.2\theta}{1000} \quad (2.14)$$

or

$$\sigma_{l-s} = \frac{0.2T - 21.63}{1000} \quad (2.15)$$

An alternative equation by studying spontaneous freezing of small water droplets has been expressed by Hesstvedt as follows:

$$\sigma_{l-s} = 0.0305 \cdot \{1 - 0.0093(T_0 - T)\} \quad (2.16)$$

## 2.6 FLOW IN CONCRETE

### 2.6.1 Moisture uptakes mechanism

The moisture uptake is not only an important variable of frost damage but also it is complicated to calculate the amounts. G. Fagerlund[12] suggested three ranges of the moisture levels depending on the major mechanism for water absorption.

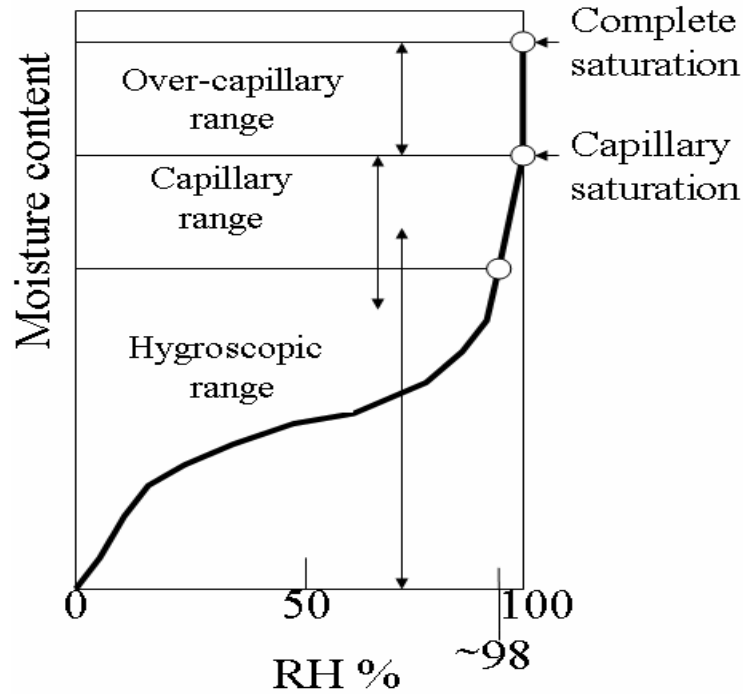


Figure 2- 2 Different moisture ranges in regard to the basic water absorption mechanism[12]

The “hygroscopic range” is determined by water absorption by capillary condensation of water vapor and capillary suction. Moisture transport in the hygroscopic range when there is no temperature gradient can be calculated by [12]:

$$q = -\delta_c (dc / dx) \quad (2.17)$$

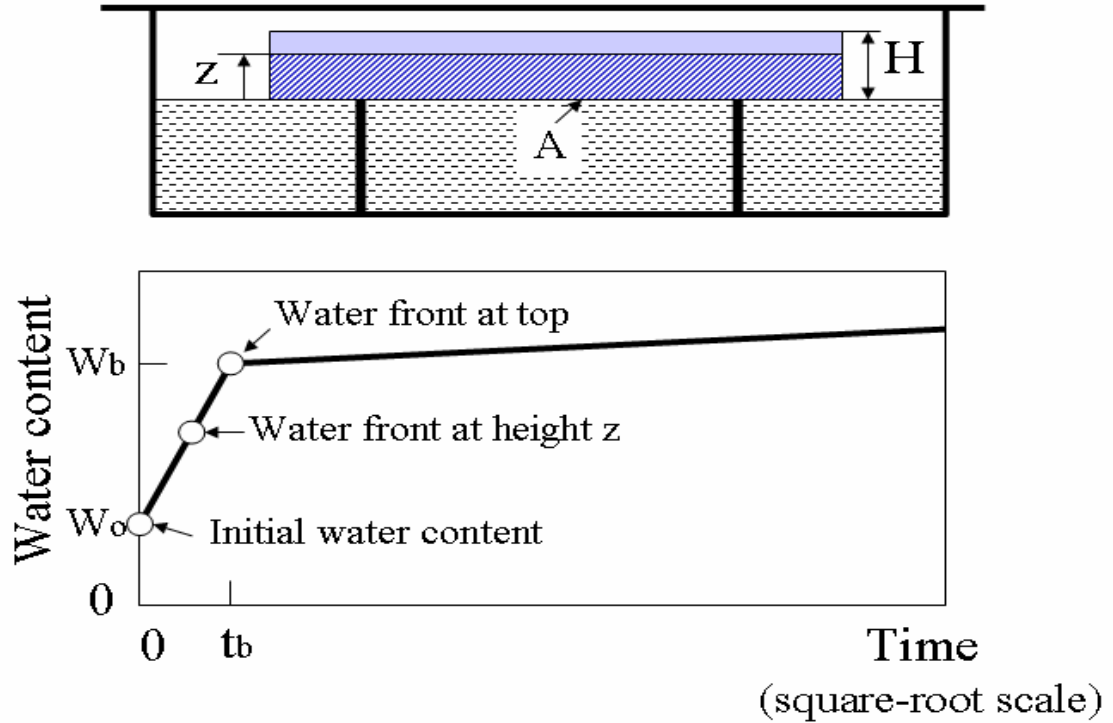
Where,

$q$  = the water flux [ $kg/(m^2 \cdot s)$ ]

$\delta_c$  = the transport coefficient [ $m^2 / s$ ]

$dc / dx$  = the vapor concentration [ $kg/m^3 \cdot m$ ]

Within the capillary range, water is absorbed by capillary suction from a free water surface. When pores are still unfilled and the water front has not reached the top surface, water content increases rapidly. Once the water front gets through the top surface, the absorption rate is very low and depends on a mechanism other than capillary forces. When no more water can be absorbed by capillary suction, the concrete has reached capillary saturation. (Figure 2.3)



**Figure 2- 3 A capillary absorption test of a thin slab. The steep line corresponds to moisture ranges 1 and 2. The breaking point corresponds to capillary saturation in Figure 2.2. The slow absorption after the breaking-point corresponds to moisture range 3. [12]**

The gradient of water transport in the capillary range is expressed in terms of water content,  $w[kg/m^3]$ . Then, the water transport equation becomes:

$$q = -\delta_w(dw/dx) \quad (2.18)$$

Transport data for concrete in the capillary range have been determined as follows:



**Table 2- 2 Material data for concrete showing relation between relative humidity,  $\varphi$ , moisture content,  $w$ , and Kirchhoff potential,  $\psi$  [13].**

$\varphi$ (%)	$w$ ( $kg/m^3$ )	$\psi$ ( $kg/ms$ )
0	0	0
50	42	$3 \cdot 10^{-10}$
60	54	$6 \cdot 10^{-10}$
70	68	$10 \cdot 10^{-10}$
80	84	$16 \cdot 10^{-10}$
90	110	$30 \cdot 10^{-10}$
93	120	$38 \cdot 10^{-10}$
95	130	$57 \cdot 10^{-10}$

### 2.6.2 Diffusivity

Diffusivity is one of the important factors in terms of liquid flow in porous materials such as concrete. The effective diffusion coefficient describes diffusion through the pore space of porous media. The effective diffusion coefficient for transport through the pores,  $D_e$ , is estimated [39] as follows:

$$D_e = \frac{D \varepsilon_t \delta}{\tau} \quad (2.19)$$

Where,

$D$  = diffusion coefficient in gas or liquid filling the pores ( $m^2 s^{-1}$ )

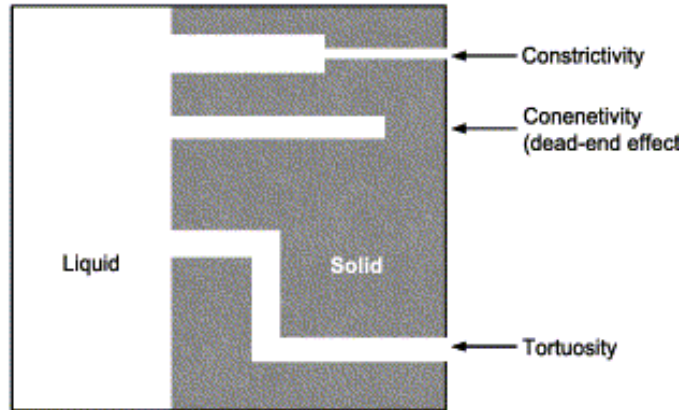
$\varepsilon_t$  = porosity available for transport (dimensionless)

$\delta$  = constrictivity (dimensionless)

$\tau$  = tortuosity (dimensionless)

The diffusion channels in concrete paste are tortuous and constricted or disconnected.

The characteristics of channels are explained in Figure 2. 4.



**Figure 2- 4 Schematic of constrictivity, connectivity and tortuosity of a pore network [40]**

### 2.6.3 Permeability of cement paste

The rate of movement of water through concrete under a pressure gradient, termed permeability has an important bearing upon the durability of concrete. The measure of the rate of fluid flow is sometimes regarded as a direct measure of durability.

Nyame and Illston [16] have used mercury intrusion data to define a parameter, termed the maximum continuous pore size ( $r_\alpha$ ), and related it to permeability. The relationship was found by linear regression to be

$$K = 1.684r_\alpha 3.284 * 10^{-22} \quad (2.20)$$

with a correlation coefficient of 0.9576 where K=permeability (m/s) and  $r_\alpha$ =maximum

continuous pore radius ( $\bar{A}$ ).

Permeability can be related to pore structure using the hydraulic radius theory, which relates flow rates to the viscous forces opposing flow. Permeability is related to hydraulic radius as follows:

$$\log K = 38.45 + 4.08 \log(\epsilon r_h^2) \quad (2.21)$$

Where,

$r_h$  = the hydraulic radius and  $\epsilon$  is the porosity.

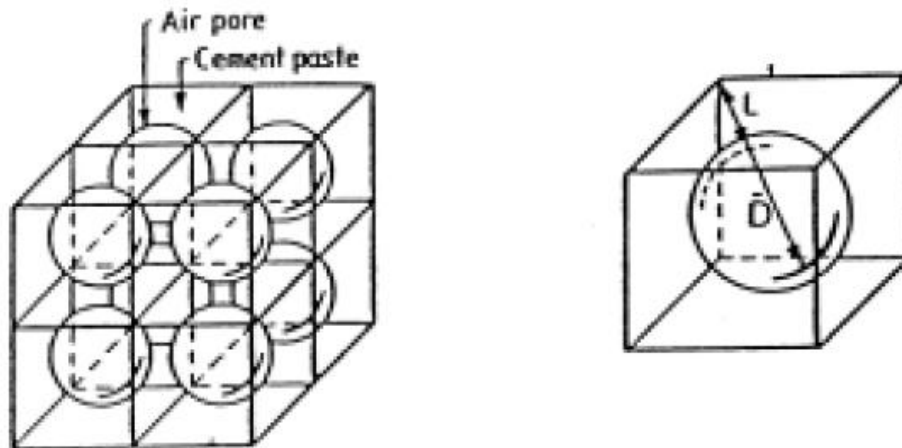
## **2.7 THE AIR VOID SYSTEM**

The effectiveness of air entrainment in providing frost resistance to concrete is well known to the industry. In order to make HCP frost resistant, an additive is used which, during the mixing of the concrete, forms foam. The bubbles thus formed are preserved in the hardened paste. Provided these cavities remain air-filled, they provide space for the volumetric expansion which occurs when pore water freezes. The extent to which such bubbles are able to protect the materials from frost deterioration is dependent on the total amount of air and on the distances across which water must be transported in order to relieve the pressure that rises occurring during ice formation.

### **2.7.1 Spacing factor for durable concrete**

The general consensus is that the Powers spacing factor must be less than 200 $\mu$ m if concrete is to be durable in freezing-and-thawing exposure. Assuming that the air bubbles are cubically arranged in the cement paste, Powers [17] defined a spacing factor which is

half the maximum distance between cubically arranged spheres with a diameter equal to the mean diameter of all the air bubbles in unit volume of the paste. See Figure 2.5



**Figure 2- 5 Illustration of parameters used in equation 2.21**

Powers derived the following relation between total air content, mean air bubble diameter and the spacing factor

$$a = \frac{D}{2} \left\{ 1.4 \left( \frac{V_p}{L} + 1 \right)^{1/3} - 1 \right\} \quad (\text{provided } V_p / L > 4.33) \quad (2.22)$$

Where,

$a$  = spacing factor [mm]

$D$  = mean diameter of the bubbles [mm]

$V_p$  = volume of paste [ $m^3 / m^3$ ]

$L$  = volume of air [ $m^3 / m^3$ ]

If the nature of the concrete or its exposure is not usual, the required spacing factor may be different. If the freezing rate is low, as is typical of mild exposure, larger spacing

factors have been shown to be adequate [18]. Critical spacing factors were found to be lower for protection during the salt-scaling test than for the standard freeze-thaw test [19].

### **2.7.2 Influence of air entrainment on durability of concrete**

Water experiences a volume increase when it freezes. This increase amounts to approximately nine percent. If the water in a critically saturated pore freezes and forces some unfrozen water out into and through the as yet unfrozen pore system of the cement paste, a hydraulic pressure would be generated. This pressure will be directly proportional to the flow rate and the flow path length, and inversely to the permeability of the medium being traversed. When the tensile stress generated by this pressure exceeds the strength of the material, it will fail. The role of air voids is to provide a lot of small, closely-spaced, empty escape places for the excess water when freezing occurs. If any flow path is not longer than the critical distance from a void, disruptive pressures cannot be generated.

Gel Water Diffusion generates another pressure on the pores. It was based on observations of expansion of cement pastes with time, as the temperature was held at some subfreezing level. Saturated, non-air-entrained pastes continued to expand, while air-entrained pastes not only did not expand but also even contracted. The freezing point of water in a pore is decreased below that of bulk water. Until temperature drops to a critical degree, i.e.  $-40^{\circ}\text{C}$  [20], all of the water does not freeze. Thus, ice particles are formed in larger pores while the water in small pores is not frozen at the higher temperature than the critical temperature. The free energy of the unfrozen water is higher than that of the ice. Thus, a potential exists to cause the water to migrate to the ice body

and generate pressure. In the case of salt solution, an osmotic component should be added. When salt solution freezes, the solid formed is pure ice, and the remaining unfrozen solution increases in concentration. Therefore an osmotic potential exists between the more concentrated solution in the partially frozen pore and the less concentrated solution in the unfrozen pores. This osmotic component is thought to be the main reason for the salt scaling of concrete. According to the gel-water-diffusion mechanism, entrained air bubbles protect against freezing distress by allowing an alternate path to the unfrozen water. Air voids are not fully saturated, so the unfrozen water can either travel to the ice-filled pore or to the ice in the air bubble. The first will increase the pressure, raising the free energy while the later will not.

## 2.8 BASIC THERMODYNAMICS

The chemical potential  $\mu$  of any phase (index k) can be given by:

$$\mu_k = \mu_k(T_0, p_0) - \int_{T_0}^T s_k dT + \int_{p_0}^p v_k dp \quad (2.23)$$

with: k=[L,S,V]

Where,

p is pressure, v the molar volume, s the molar entropy and T the temperature. The phases are liquid (L), solid ice (S), and vapor (V).

At the triple phases point (273.16K), ice and water are in equilibrium, i.e. their chemical potentials are equal. For infinitesimal changes in pressure and temperature, the change in chemical potential of each is:

$$d\mu = \mu - \mu_0 = -SdT + VdP \quad (2.24)$$

If the equilibrium is maintained by the changes in temperature and pressure, then:

$$d\mu_l = d\mu_s \quad (2.25)$$

and thus:

$$-S_l dT + V_l dP_l = -S_s dT + V_s dP_s \quad (2.26)$$

If temperature and pressure are both equal in both phases, this leads to:

$$(S_l - S_s) dT = V_l dP_l - V_s dP_s \quad (2.27)$$

For a reversible change, the entropy change of the system is equal to its change of molar enthalpy divided by the temperature, at which it occurs, so that:

$$S_l - S_s = \frac{\Delta H_f}{T} \quad (2.28)$$

Where,

$\Delta H_f$  = enthalpy on freezing (J)

T=freezing temperature of water (K).

$$\Delta H_f = \Delta h_f \cdot w_{f,T} \cdot m_{spec} \quad (2.29)$$

Where,

$w_{f,T}$  = freezable water content (kg/kg dry material) of the porous material at temperature T(°C)

$\Delta h_f$  = heat of fusion of freezable water (J/kg) assumed constant

$m_{spec}$  = mass of specimen (kg).

This results in Clapeyrons equation in the form:

$$V_l dP_l - V_s dP_s = \frac{\Delta H_f}{T} dT \quad (2.30)$$

Three possible ways of transferring additional absolute pressure ( $\Delta P$ ) in a highly saturated and freezing pore system can be deduced from equation. (2.30) [25].

At first, if the pressures of ice and unfrozen liquid are equal,

$$dP = \frac{\Delta H_f dT}{(V_l - V_s)T} \Rightarrow \Delta P = \frac{\Delta H_f}{(V_l - V_s)} \ln\left(\frac{T}{273.16}\right) \quad (2.31)$$

Secondly, if the pressure of the unfrozen liquid is unchanged while the pressure of the ice changes, then  $dP_w = 0$ .

$$dP_s = -\frac{\Delta H_f}{V_s T} dT \Rightarrow \Delta P = \frac{\Delta H_f}{V_s} \ln\left(\frac{T}{273.16}\right) \quad (2.32)$$

Finally, if the pressure of ice is unchanged while the pressure of the unfrozen water changes, then  $dP_s = 0$ .

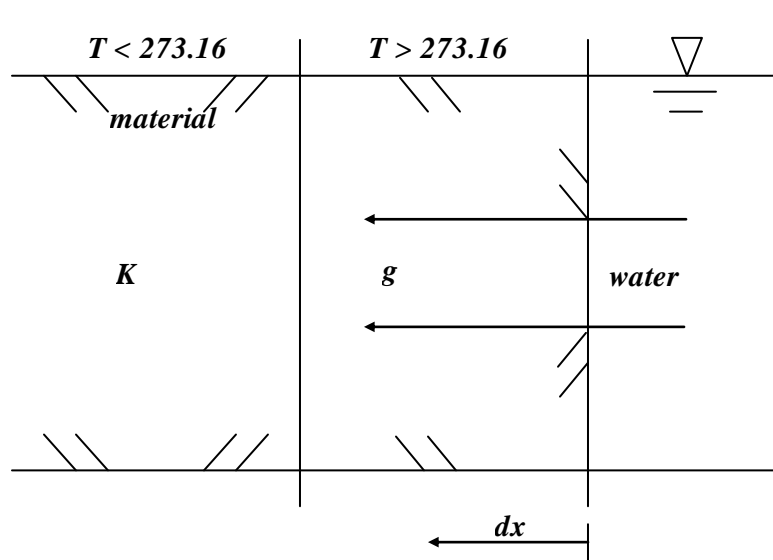
$$dP_l = \frac{\Delta H_f}{V_l T} dT \Rightarrow \Delta P = \frac{\Delta H_f}{V_w} \ln\left(\frac{T}{273.16}\right) \quad (2.33)$$

In the case of a highly saturated porous material, equation (2.31) appears most realistic.

### 2.8.1 Transport

If a gradient of temperature,  $dT/dx$  (K/m), is negative from a wet surface, a flow may take place inwards. Figure 2.6 illustrates this case.





**Figure 2- 6 Set-up in wet frost exposure [25]**

Based on D'Arcy flow, the steady-state flow can be obtained. D'Arcy flow is as follows:

$$g = K \frac{dP}{dx} \quad (2.34)$$

Where,

$g$ = steady-state flow ( $kg/m^2 \cdot s$ )

$K$ = coefficient of permeability ( $kg/Pa'm's$ ) assumed constant with  $K=k/\eta$

where  $k$ =permeability ( $kg/m$ )

$\eta$ =viscosity ( $Pa's$ ).

Combining with equation(2.31) the steady-state flow illustrated in Figure 2.6 can be obtained.

$$g = \frac{K\Delta H_f}{(V_l - V_s)} \cdot \frac{1}{T} \cdot \frac{dT}{dx} \quad (2.35)$$

Where,

$g$  = steady-state flow through a section of temperature  $T$ .

The minimum radius where ice is forming at T is found by combining equation (2.31) with Kelvins law, which for cylindrical pore shape is [25]:

$$dP = -\frac{2\sigma}{r} \quad (2.36)$$

Where,

$\sigma$ =surface tension and  $r$ =pore radius (m).

## **2.9 MICRO-ICE-LENS**

### **2.9.1 Micro-Ice-Lens theory**

The freezing and melting point of liquid in concrete pores decreases with decreasing pore radius. Since concrete matrix has very small pores, condensed matter in pores can coexist stably as liquid, solid and vapor over a wide temperature range (up to  $-20^{\circ}\text{C}$ ). This is because the surface tension at internal surfaces of the matrix increases when ice is formed. Besides, the surface tension of the salt solution is higher than water, and the maximum surface tension of salt solution is reached at around 3% concentration. Thus, the radius of the pores of the triple-phase condition might be higher in salt solution than in the water (Especially when the concentration of the solution is 3%).

Since the condition for the free mechanical potential is the free exchange of mass with the surrounding system the chemical potential is equal for all components in all phases. Thus, if they are stable in pores below bulk transition, high negative pressures are generated in the triple-phase region. This negative pressure increases with decreasing temperature. Therefore, pore water is squeezed out and freezing by the micro-ice crystals. In addition, pore microstructure might shrink or damage if the pressure difference is

higher than matrix tensile strength.

As temperature increases, a reversible phenomenon occurs. The pressure difference decreases and the ice front melts causing the pores to expand. However, the squeezed out water is entrapped at the micro-ice-lenses. Therefore, external water will be sucked into the pores if the external water is available. This process is called micro-ice-lens pumping. Thus, an artificial frost-saturation increases with every freeze-thaw cycle. However, the amount of sucking water by micro-ice-lens might be different between the water and salt solutions.

### 2.9.2 Micro-Ice-Lens pumping between water and salt solution

At first, the radius of the pores, in which triple phases can coexist, might be larger in the salt solution than in the water due to its high surface tension. The surface tension might have a maximum value when its concentration is around 3%. As the maximum radius of the pore increases, the amount of the microscopic transport may increase. The mean flow velocity  $\bar{v}_l$  of the pressure gradient through a pore system with constant cross section is:

$$\bar{v}_l(r) = \frac{\partial \mu_l}{\partial t} = \int_{r_{\min}}^{r_{\max}} T(r) \frac{r^2}{8\eta} \frac{\partial p}{\partial l} V_p(r) dr \quad (2.37)$$

when  $\eta$  is the viscosity of pore water. The functions represent the differential pore size distribution  $V_p$  and a characteristic tortuosity  $T$ .  $r_{\max}$  is the largest pore radius filled with unfrozen water. Since the function is decreasing very fast  $r_{\min}$  can be set to zero. If we assume pore size distribution and tortuosity as constant.  $T \approx 1$  and  $V_p = V_{total} / r_{g,\max}$  with the total porosity, then equation (2.37) can be integrated to:

$$\bar{v}_l(r) = \frac{T \cdot V_{total} r_{max}^3}{24 r_{g,max} \eta} \frac{\partial p}{\partial t} \quad (2.38)$$

As shown in equation (2.37) and (2.38), the flow velocity will rapidly increase with increasing  $r_{max}$ . In addition, an external water source may be available for longer time since pure water in bulk system does not melt until the temperature reaches 0°C while this occurs at much below 0°C in the salt solution even though its phase is liquid or gel type.

As a result, in the salt solution, more porous system act as the pipes of the micro-ice-lens pump and pumping duration is longer than water. Thus, the porous material might reach the critical degree of the saturation quickly in the salt solution.

### 2.9.3 Pressures in pore water

As mentioned above, the triple phase condition in pores generates negative pressure in the pore matrix. The pressures in pore water before and after freezing have been presented [21]. If the liquid is water and no ice is presented in the pore system, water pressure in a porous material is governed by Kelvin's equation

$$p - p_0 = \frac{RT}{v_w} \ln \left( \frac{p_v}{p_{v0}} \right) \quad (2.39)$$

in which T is ambient temperature presented in Kelvins,  $p$  is the pressure of water,  $p_0$  denotes the reference pressure, which has been chosen as the atmospheric pressure 0.1 Mpa.  $p_v$  is the vapor pressure in the pore system and  $p_{v0} = p_{v0}(T, p_0)$  is the saturated vapor pressure of the liquid in the pressure  $p_0$  is the saturated vapor pressure of the

liquid in the pressure  $P_0$  at the ambient temperature.  $R$  is the gas constant 8.314 J/mol/K and  $v_w$  is the specific volume of the liquid. The relative humidity of the pore system  $\phi$  equals  $P_v / P_{v0}$ .

When ice forms in the pore system of a porous material freezing-induced pressures are generated. Penttala [23,24] has derived a theory by which the liquid pressure can be calculated in a freezing porous material.

$$\begin{aligned}
 p - p_0 &= \frac{RT}{v_i} \ln \left( \frac{P_v}{\gamma_w x_{unf} P_{v0}} \right) + \frac{\Delta h_{wi}^\circ}{v_i T_0} (T_0 - T) \\
 &+ \frac{1}{v_i} \int_{T_0}^T \int_{T_0}^T \frac{c_{pi}^\circ - c_{pw}^\circ}{T} dT dT \quad (2.40)
 \end{aligned}$$

$$\begin{aligned}
 p - p_0 &= \frac{\Delta h_{wi}^\circ}{(v_i - v_w) T_0} (T_0 - T) \\
 &+ \frac{1}{(v_i - v_w)} \int_{T_0}^T \int_{T_0}^T \frac{c_{pi}^\circ - c_{pw}^\circ}{T} dT dT \quad (2.41)
 \end{aligned}$$

Equation (2.40) represents the situation when ice is forming in a pore partially filled with gas and pore liquid while Equation (2.41) gives pore pressures when the freezing pore is totally free of gas bubbles and all pores are filled with liquid.  $\Delta h_{wi}^\circ$  is the freezing heat of the liquid at the reference temperature  $T_0$  and  $v_i$  is the specific volume of the solid phase of the liquid. The specific heat capacities of ice and water,  $c_{pi}^\circ$  and  $c_{pw}^\circ$ , cannot be considered constant in the rather large temperature range in question and therefore the following equations will be used [22].

$$c_{pi}^\circ(T) = 38.052[1 + 373.7 \times 10^{-5}(T - T_0)] \quad (2.42)$$

$$c_{pw}^\circ(T) = 75.996[1 - 54.0 \times 10^{-5}(T - T_0)] \quad (2.43)$$

The term  $x_{unf}$  denotes the mole fraction of pore water before freezing, and if no additional salt has been dissolved into the pore water  $x_{unf} = 1$ . The activity coefficient  $\gamma_w$  has the value of 1 in the case of ideal solution in which both solvent and solute obey Raoult's law.

## 2.10 THERMAL EXPANSION MISMATCH MECHANISM (BI-MATERIAL MECHANISM) [30]

In addition to the hydraulic pressure, the potential between water and ice and the osmotic potential between the more concentrated solution and the less concentrated solution, another cause generating tensile stress on the concrete surface has been suggested by John J. Valenza II and George W. Scherer [30].

The stress is related to the physical properties of ice: since ice has a much higher thermal expansion coefficient than concrete. In fact, the thermal expansion coefficient of ice,  $\alpha_i$ , is about  $50 \text{ ppm}/^\circ \text{C}$  while that of concrete,  $\alpha_c$ , is about  $10 \text{ ppm}/^\circ \text{C}$ .

When a saturated surface layer is frozen, the thermal strain of the surface is equal to that of the bulk concrete system since the ice layer cannot force the concrete to deform. Thus, the stress in the frozen layer can be calculated as follows:

$$\sigma_x = \frac{E_i (\alpha_i - \alpha_c) (T_m - T)}{1 - \nu_i} \quad (2.44)$$

Where,

$E_i$  = Young's modulus of ice

$\nu_i$  = Poisson's ratio of ice

$T_m$  = the melting temperature.

When outer liquid is pure water, this equation is easy to apply. In case of salt solution, however, pure water ice begins to form and the concentration of remaining solution increases when a solution starts freezing.

At the end of the first temperature step below the melting point, a certain volume fraction of ice has formed and is stress free. In each subsequent temperature decrement, new stress-free ice is formed, while the stress increases in all of the previously existing ice. The total stress in the ice network at any given temperature is

$$\sigma_x(T) = \int_T^{T_L} B(T)(a_i - a_c)dT \quad (2.45)$$

where,

B= the volume-averaged biaxial modulus

However, this elastic solution provides a serious overestimate of the stress, because ice exhibits rapid creep. When creep occurs, the thermal mismatch strain,  $\varepsilon_T$ , has to be corrected by subtracting the creep:

$$d\varepsilon_T = (\alpha_i - \alpha_c)dT + d\varepsilon_s \quad (2.46)$$

Thus, stress development in solid ice is as follows:

$$\sigma_x(T) = \int_T^{T_L} B(T)(\alpha_i - \alpha_c + A\sigma_x^n \exp(-Q/T)/q)dT \quad (2.47)$$

Where,

$$q = dT / dt$$

$$\frac{d\varepsilon_s}{dt} = A\sigma_x^n \exp(-Q/T) \quad (2.48)$$

If  $dT < 0$ , the positive creep strain will offset negative thermal strain.

The average tensile strength reported for ice/brine composites by Weeks,  $\sigma_T$ , is given approximately by

$$\sigma_T (Mpa) \approx 2.47 - 5.15\sqrt{1 - v_i} \quad (2.49)$$

Where,

$v_i$  = Volume fraction of ice in the composite

The tensile strength is the function of the volume fraction of ice in the composite. As shown in Figure 2.6, the volume fraction of pure water ice rises to near 1 just below melting point. Thus, the strength of pure ice ( $\sigma_T$ ) is about 2.5Mpa and the calculated stresses remain below the strength of pure ice for the rates used in a typical scaling test. This indicates that no cracks should occur in pure ice. See Figure 2.7.

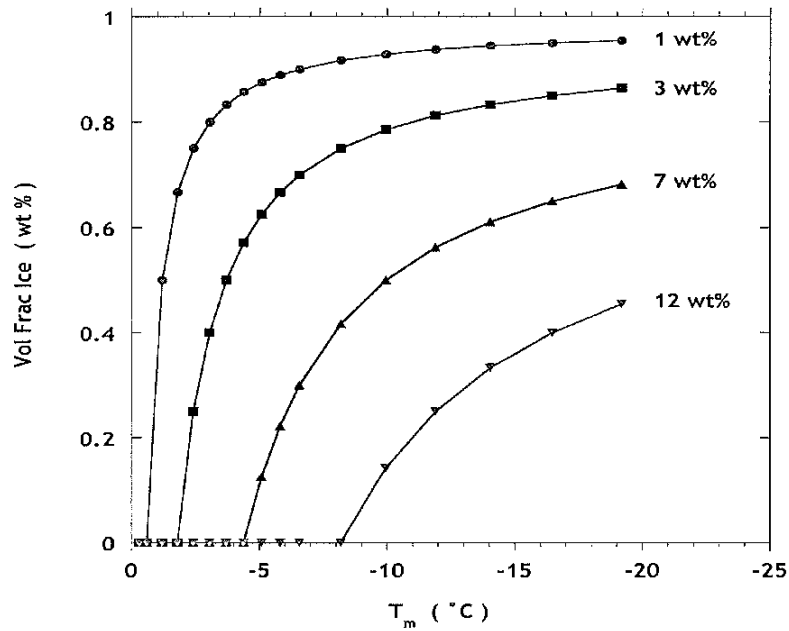
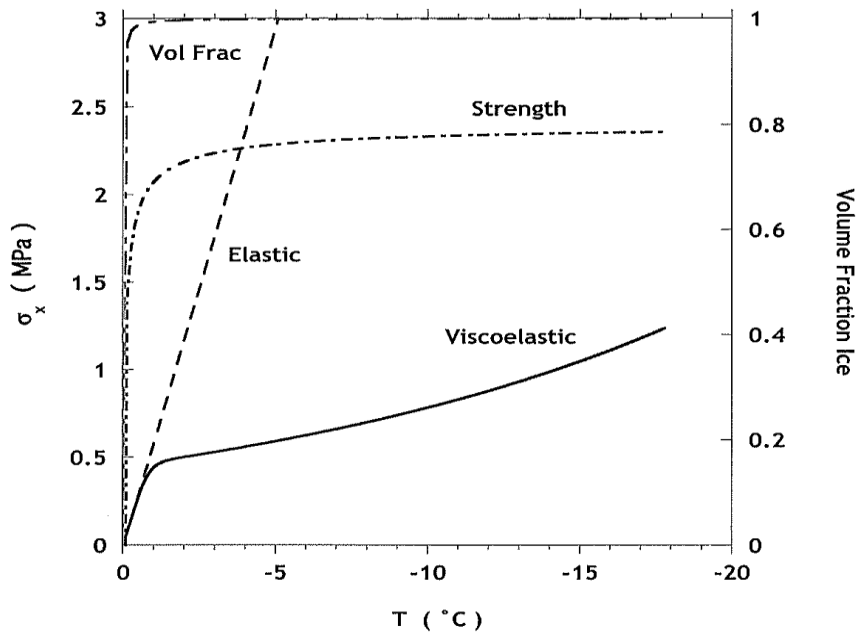


Figure 2- 7 Volume fraction of ice in solutions of NaCl at the indicated



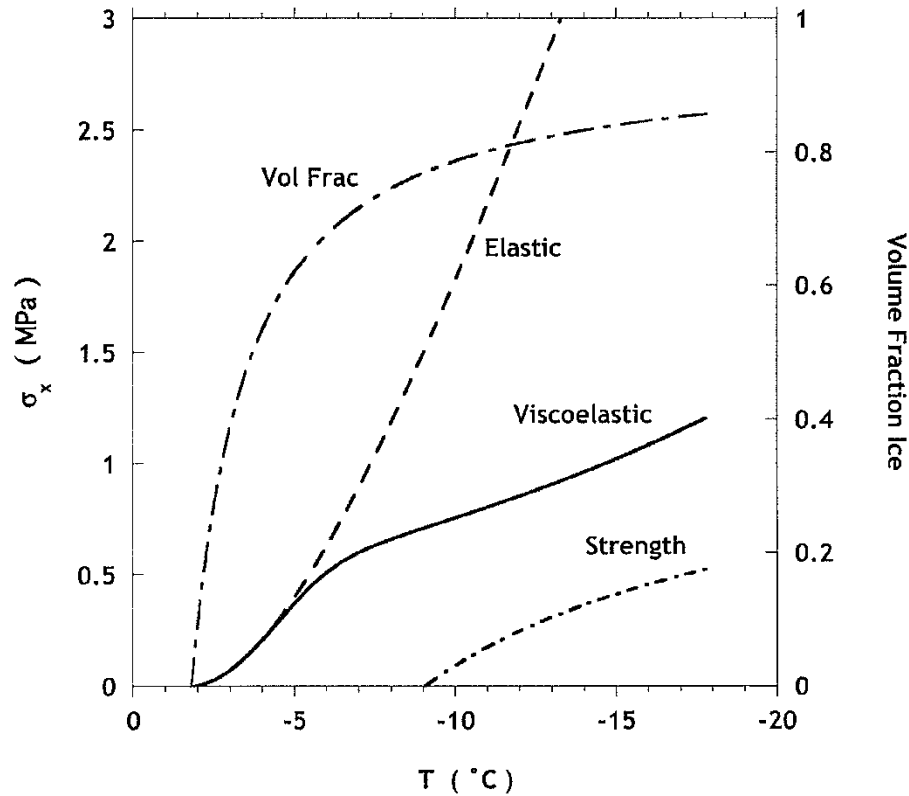
## concentrations versus temperature



**Figure 2- 8 Calculated stresses and volume fraction of ice in solution containing 0.01% NaCl, where the volume fraction of ice is near 1**

When the calculation is repeated for a solution containing 1% NaCl, the stresses are predicted to be about equal to the strength of the layer, and when the salt content rises to 3%, as shown in Figure 2.8, the stress exceeds the strength. A brine containing 7% NaCl only contains  $v_i \approx 0.7$  at  $-20^\circ\text{C}$ , so it would have no tensile strength, according to equation (2.36). Thus, a layer of pure water ice on the surface of concrete is predicted to remain uncracked, whereas any brine containing  $> 1\%$  NaCl should crack upon freezing. Ice containing 3% NaCl only acquires strength when the temperature drops below  $-10^\circ\text{C}$ , which accounts for the observation that scaling damage does not occur if the minimum temperature of the cycle is higher than  $-10^\circ\text{C}$ . At salt contents exceeding 5%, the frozen layer is expected to have negligible strength, so it cannot exert significant stress on the concrete. The pessimum occurs because pure water ice does not crack, whereas ice with  $>$

1% solute does. The cracking causes damage to the underlying substrate; however, when the salt content is high, the ice layer is too soft to exert enough stress to harm the substrate.

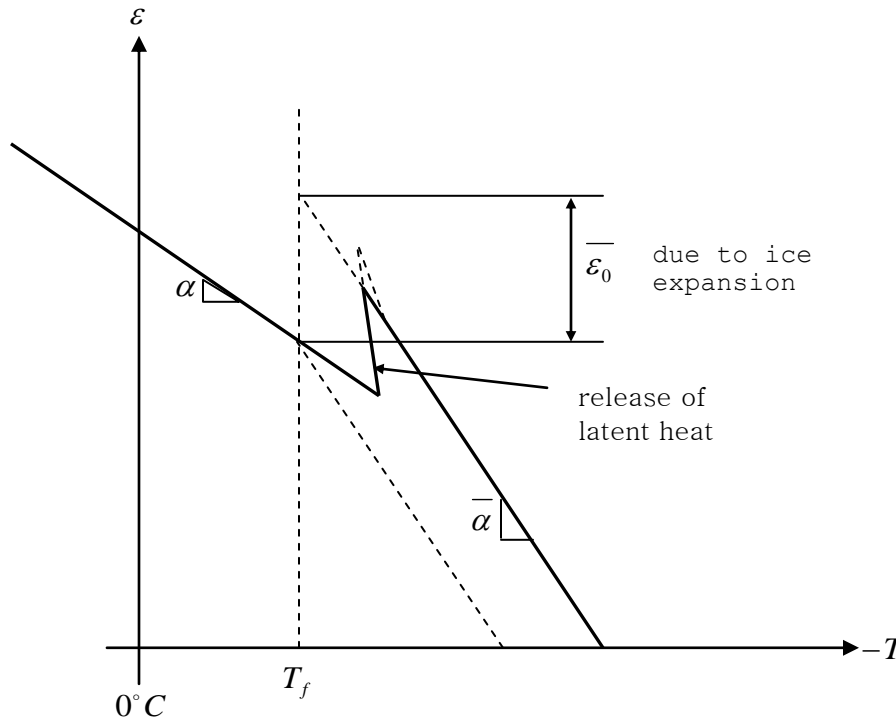


**Figure 2- 9 Calculated stresses and volume fraction of ice in solution containing 3% NaCl**

## 2.11 COMPOSITE MATERIAL LAYER

When the concrete surface is exposed to an outer solution and experiences freeze/thaw cycles, the part of freezable pores are filled with solution. If the temperature drops below the freezing point, ice expansion will occur in the concrete and the slope of dilatation

curve is changed after freezing. The condensed layer should be considered as composite material. To analyze this, a simple composite model was suggested by Zdenek P. Bazant *et al* [31]. See Figure 2.10.



**Figure 2- 10 Example of dilatometric tests**

The equilibrium of longitudinal normal stresses in the specimen requires:

$$\sigma = (1 - n)\sigma_c + n\sigma_i \quad (2.50)$$

Where,

$n$  = the volume fraction of freezable pores in concrete

$\sigma$  = the total stress

$\sigma_c$  = the normal stress in the solid structure of concrete

$\sigma_i$  = the normal stress in ice

A reduced strain is

$$\varepsilon_0' = q\varepsilon_0 \quad (2.51)$$

Where  $\varepsilon_0$  is the volume expansion of water of water on freezing and  $q$  indicates a reduction in volume decrease due to the fact that pore volume  $n$  may be filled by liquid water only partially or that part of the water may be expelled from these pores before it freezes. The strain of the composite layer after freezing can be calculated as follows:

$$\varepsilon = \bar{\alpha}T + \bar{\varepsilon}_0 + \sigma / \bar{E} \quad (2.52)$$

The elastic modulus of the composite layer,  $\bar{E}$ , can be calculated by equation (2.53)

$$\bar{E} = (1-n)E_c + nE_i \quad (2.53)$$

in which  $E_c$  and  $E_i$  are elastic moduli of concrete and of ice. Finally, one can obtain the thermal coefficient of the composite layer after freezing,  $\bar{\alpha}$ , and the strain of the composite layer due to ice expansion,  $\bar{\varepsilon}_0$ , as the following:

$$\begin{aligned} \bar{\alpha} &= \frac{(1-n)E_c\alpha_c + nE_i\alpha_i}{\bar{E}} \\ \bar{\varepsilon}_0 &= \frac{E_i}{E}qn\varepsilon_0' \end{aligned} \quad (2.54)$$

in which  $\alpha_c$  and  $\alpha_i$  are linear coefficients of thermal expansion of concrete and ice. If the freezing temperature,  $T_f$ , is known, the values of  $n$  and  $q$  can be calculated and consequent stress due to the ice expansion and the change of slope after freezing.

## 2.12 THE MICROSTRUCTURE OF THE CONCRETE SURFACE

The microstructure of the concrete surface is strongly related with its durability since the permeability of the surface is determined by its microstructure. There is an extremely

porous layer at the surface and an interfacial transition zone (ITZ) between cement paste and coarse aggregate.

The microstructure of the concrete surface cannot be considered the same as the bulk of the material. In [2], an extremely porous layer was observed at the surface. The existence of this porous layer might increase permeability decreasing the salt scaling resistance. Even though it may not be able to explain precisely the reasons, the properties can be affected by w/b ratio and SCM.

An interfacial transition zone exists around the coarse aggregate. In this zone, the porosity is much higher than that of bulk paste [3,4] and the ITZ has a significant effect on the permeability and durability of concrete.

#### **2.12.1 The weak surface layer**

As the porosity of the concrete increases, the permeability increases causing the reduction of the surface scaling resistance. The porosity is extremely high at surface layers with a high water/binder ratio. The porosity decreases with depth from surface. The use of SCM increases the thickness and the porosity of the surface layer.

#### **2.12.2 Interfacial transition zone (ITZ)**

There is an interfacial transition zone around coarse aggregate. This transition zone exists as a thin shell between aggregate particles and hydrated cement paste. Since the porosity of the ITZ is higher than that of the bulk paste, the ITZ has a significant effect on the permeability and durability of concrete.

The properties of ITZ might be related with w/b ratio and the use of SCM. However, it

has been determined that the size of the coarse aggregate has a significant effect on the properties of the zone. Two possible reasons are suggested in [4]. When the size of the coarse aggregate increases, there is a reduction in the tortuosity of the flow path, which tends to increase the permeability. The second reason is that when larger size coarse aggregates are used, the possibility of the bleed water getting collected below the coarse aggregate increases, which leads to an increase in local water-cement ratio and hence the porosity.

In fact, cement paste covering aggregates at the surface and around the aggregates were flaked off during the first few freeze/thaw cycles. This region might be ITZ. Thus, the salt scaling may begin from ITZ so that the aggregate underneath the cement paste was revealed after a few freeze/thaw cycles. Figure 2.11 shows the concrete surface which has experienced 5 freeze/thaw cycles in 3% NaCl solution.



**Figure 2- 11 The concrete surface after 5CDF cycles in 3% NaCl solution**

### **2.13 CHEMICAL PARAMETERS**

The question has been raised as to whether chemical reaction has a direct effect on salt scaling mechanisms since a true mechanism of salt scaling is not clear yet. Some researchers insist that significant stress is generated by the crystallization of salt in pores [26, 27]. However, the crystallization may occur under relatively low humidity circumstances which affect solubility and the pores as the outer surface are probably always saturated. Thus, the stress by crystallization might not be a big concern. Instead, alterations of the microstructure and pore solution through carbonation must be considered since the microstructure of concrete plays a significance role in salt scaling. The effect of carbonation is probably due mainly to its effect on the permeability of the

surface zone. In fact, carbonation causes a denser pore structure for ordinary Portland cement-based materials while cements rich in ground granulated blast furnace slag (GGBFS) become coarser [28].

### **2.13.1 The composition of Portland cement and Ground-Granulated Blast Furnace Slag**

Portland cement consists of the Portland cement clinker mixed with a few percent of gypsum ( $CaSO_4 \cdot 2H_2O$ ) or anhydrate ( $CaSO_4$ ). Portland cement clinker contains four major phases: tricalcium silicate ( $C_3S$ ),  $\beta$ -dicalcium silicate ( $\beta-C_2S$ ), tricalcium aluminate ( $C_3A$ ), and ferrite solid solution ( $C_2(A,F)$ ) (in the cement nomenclature,

$C = CaO$ ,  $S = SiO_2$ ,  $A = Al_2O_3$ ,  $H = H_2O$ ,  $F = Fe_2O_3$ ,  $M = MgO$  and  $\hat{S} = SO_4$ ).

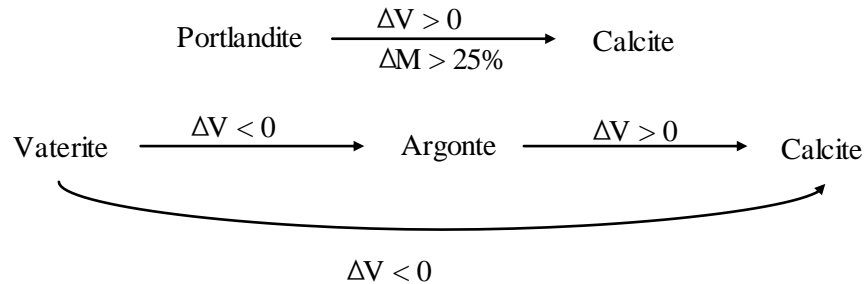
The main reaction product of Portland cement is a very poor crystalline calcium silicate hydrate,  $C-S-H$ . This is produced by the hydration of  $C_3S$  and  $\beta-C_2S$ .  $C-S-H$  is often designated as a gel when there are other phases admixed on a sub-micrometer scale. It is generally accepted that the  $Ca/Si$  molar ratio of  $C-S-H$  gel is in the range of 1.5-2, and in most cases around 1.7.  $C-S-H$  gel represents the primary binding phase in Portland cement and controls the strength development of the paste.

### **2.13.2 Carbonation**

Temperature change could have a strong impact on the stability of certain cement stone phases, which would induce salvation and crystallization processes in the matrix. This



reaction causes secondary ettringite formation in cold climate of calcium aluminate monosulphate and the formation of the metastable calcium carbonate phases vaterite and aragonite in the concrete with high GGBFS content. The volume changes due to re-crystallization are shown in figure 2.12.



**Figure 2- 12 Impact of the carbonation on the volume [28]**

Vaterite and aragonite are mainly discovered in GGBFS concretes with slag content over 65%. A re-crystallization from vaterite to calcite leads to a volume reduction while a re-crystallization from aragonite to calcite leads to an enlargement and probably to a crystallization pressure in the matrix. It can be generally observed that portlandite transfers to calcite in an ordinary Portland cement-based material when it is carbonated. This kind of carbonation leads to a volume enlargement and to a shift of the pore size distribution to lower values. Thus, the carbonation of OPC can make the surface denser, resulting less permeability. On the other hand, the transformation from vaterite to aragonite and calcite, which can be generally observed for high slagged blast-furnace concrete, leads to a volume reduction and to a shift of the pore size distribution to larger pores. This kind of carbonation causes a coarser surface and consequent high

permeability. J. Stark [29] showed that the reason for the heavy scaling of concretes made with blast furnace cement is the carbonation of a thin surface layer as well as the formation of the metastable  $CaCO_3$  modifications vaterite and aragonite.

## **2.14 HYPOTHESIS REGARDING THE MECHANISM OF SURFACE SCALING**

### **2.14.1 Moisture uptake**

When concrete is exposed to a reservoir of liquid, capillary suction occurs above the freezing point. When an ice lens forms in the pore system of hardened cement paste, micro-ice-lens pumping might accelerate moisture uptake with cyclic freezing/thawing. The saturation starts from the surface of the concrete. In addition, the surface layer may be easily saturated due to its high permeability while permeability decreases along the depth from surface. Therefore, the surface layer might be locally saturated up to the critical degree before the bulk system reaches the critical degree of the saturation.

### **2.14.2 Microscopic pores**

At the triple point of water, ice and water are in equilibrium. As temperature drops below the freezing point, the free energy of the water increases more than that of the ice because the entropy of liquid water is higher than that of ice. Consequently, a transition of molecules from the liquid to the ice will reduce the free energy of the system. However, if they are stable in pores below the bulk freezing point, high negative pressures are generated in the triple phase region. If the negative pressure were too high, it would cause

damage. In the case of salt solution, an osmotic potential exists between the more concentrated solution in the partially frozen pores and the less concentrated solution in the unfrozen pores, causing more pressure.

### **2.14.3 Macroscopic pores**

When the surface layer is saturated locally, the ice expansion leads to additional hydraulic pressure directed toward the surface layer rather than the entire system since the surface layer is weaker than the bulk system. If there were not enough space to release the pressure, it would cause surface heaving and salt scaling.

### **2.14.4 Bulk system**

The critically saturated surface layer may expand when the ices in the pores of the surface layer freeze and expand. However, the bulk concrete system, which is not saturated yet, shrinks as the temperature decreases. This dilatation difference between the bulk system and the surface layer might generate stress at the boundary.

## **2.15 THE VARIABLE AFFECTING SURFACE SCALING**

Surface scaling can be affected by outer environmental conditions such as temperature cooling rate, available duration for the outer water reservoir, as well as the concentration of the de-icing salt solution.

If the cooling rate is too low, the effect of the micro ice-lens pumping would decrease. In this study, a constant cooling rate of 10K/h is taken as RILEM recommended. The

cooling rate of 10K/h may be severe since a cooling rate is rarely reached at 10K/h in situ.

During the freeze/thaw test, the specimens were always stored in 10mm de-icing salt solution even though this appears not to happen in the field. Salt scaling might be proceeded only in the presence of the de-icing salt solution. Besides, the degree of the scaling may be various with the concentration of the solution. There is the apparent existence of a "pessimum" de-ice concentration. This is around 3%. Thus, the 3% NaCl solution is used in this study.

Since the outer condition is set up as severe, the variables affecting the properties of concrete, chemical reactions such as carbonation as well as specimen preparation procedure such as curing are focused on in the study.

### **2.15.1 Air Content**

Entrained air voids have an important role to prevent internal damage and surface scaling. Air voids perform as extra space in which the ice crystal grows releasing the pressure due to the ice expansion and osmotic pressure due to potential between ice and pore water and between more and less concentrated solution. During the melting phase, the compressed air by the ice expansion expands and pushes the water, which was sucked in during the cooling phase, out.

However, after all voids are filled with the solution resulting entrained air out, air voids may not prevent further frost damage. An air content of 6% or above is believed to be a reasonable value. Too much air content might cause enfeeblement of concrete strength. It is still not clear whether air voids are well distributed through the whole system, for instance, between the surface and inner part.

In addition, it is already known from numerous investigations that the frost-deicing salt resistance of blast furnace cement concrete rich in granulated slag cannot satisfactorily be improved by adding air-entraining agents. The addition of air-entraining agents to super-sulphated cement concrete will even lead to a further increase in the amount of scaling. [29]

### **2.15.2 Water-binder ratio (w/b)**

In general, lower water-binder ratios produce more durable concrete. Many studies have shown that the lower the water/binder ratio, the lower the diffusion coefficient. Thus, a low water/binder ratio raises not only strength but also the durability of concrete. In addition, low water/binder ratio might improve the density of the concrete surface causing the reduction of its permeability and the amount of the freezable water in pores. In fact, many test results show that the concrete with low w/b ratio such as around 0.3 has satisfactory scaling resistance irrespective of other variables.

### **2.15.3 Supplementary Cementing Materials (SCM)**

The use of Supplementary Cementing Materials such as Fly Ash (FA) or Ground Granulated Blast-Furnace Slag (GGBFS) can result in numerous potential benefits. In fact, they reduce long-term chloride penetrability, mitigation of alkali-silica reaction, and temperature in mass and hot weather concreting. However, the SCM used in concrete was found to increase the bleeding of concrete. Thus, the addition of SCM was found to increase the thickness and the porosity of the surface layer [2].

In contrast to this, J. Stark insists that the degree of hydration and, consequently, the

pore size distribution of the concrete do not have a significant effect on salt scaling and that the frost-deicing salt resistance of concretes made with cement rich in GGBFS might be dependent on the state of the carbonated surface layer [29].

Although there is not an agreement of the effect of the SCM on salt scaling, salt scaling and microstructure of the surface layer might be affected by use of SCM..

#### **2.15.4 Aggregate**

The interfacial transition zone (ITZ), which has much higher porosity and permeability than the bulk material, exists around coarse aggregate. Due to its high porosity, the transition zone is considered to influence the transport processes in the concrete. In addition, the diffusion coefficient of chloride ions can be 6-12 times greater in the transition zone compared to the bulk paste [3,4].

When the size of coarse aggregate and the proportion of larger size coarse aggregate increases in a mix, there is an associated increase in interfacial transition zone porosity volume and permeability.

Several investigators used the pre-soaked lightweight aggregate (LWA) as internal water reservoirs, to ensure the correct content of water needed for the hydration process. The surface layers of concrete with lightweight aggregate should be denser than traditional concrete, and therefore more resistant to scaling. However, in one observation [5], replacement of LWA was shown to be effective only for low water/binder ratio concretes.

### **2.15.5 Curing Duration**

It has been known that reducing the moist curing period results in the concrete microstructure remaining more porous since for cement to properly hydrate sufficient curing conditions are required to prevent moisture loss. This condition is more sensitive for SCM concrete since the SCM concrete has longer hydration duration than OPC. In fact, there exists a linear relationship between the degree of hydration and the frost resistance of GGBFS concrete. This relates to the amount of capillary pores that decrease with an increasing degree of hydration. As a result the amount of freezable water in the concrete is reduced [29].

In addition, the amount of scaling observed in concrete containing supplementary cementitious materials is greatly increased with increased drying time. The drying front penetrates deeper into the concrete the longer the specimen dries and the increase in permeability depends on the w/c ratio, degree of hydration, and extent of drying. Also, the microstructure of the surface becomes coarse during drying.

# **CHAPTER 3**

## **MATERIALS MATRIX AND EXPERIMENTAL METHODS**

### **3.1 INTRODUCTION**

A detailed experimental program was developed to evaluate the mechanisms associated with frost damage and to understand the relationships between these mechanisms and the mechanical properties of concrete. This research focuses on pavement concrete and building materials with typical strength development. Thus, laboratory concrete specimens were designed with typical strength development in mind.

As discussed in previous chapters, the emphasis of this study is the frost protection properties of air voids. Thus, field specimens with various levels of frost damage have been chosen to evaluate the effects of air voids system on frost durability from 11 different field locations.

The beneficial effect of supplementary cementitious materials (SCMs) on frost durability has been argued. As a result, Ground Granulated Blast Furnace Slag (GGBFS) has been used as a SCM in this study. The lab specimens have been prepared with varying GGBFS portions and air contents.

This chapter describes the materials, the lab and field concrete specimens, and the



experimental methods that were used to evaluate their frost resistance properties.

## **3.2 EXPERIMENTAL REGIME**

### **3.2.1 Materials**

For this thesis, field pavement concretes from 11 different locations were used to incorporate the effect of air voids systems with actual frost damage rates. The damage rates of the field concretes are shown in Table 3.1.

In addition to field samples of concrete, concrete specimens produced in the laboratory were prepared for study. The laboratory mixes contained Ordinary Portland Cement (OPC) from two sources (I and II) and GGBFS. The chemical compositions are listed in Table 3.2.

### **3.2.2 Material Matrix**

To be able to find out significant conclusion about the mechanisms of frost damages and the roles of variables, it is important to narrow down the variables for one series of specimens. The water-to-cement ratio and curing time are not varied because this study is targeted at normal strength and hydrated concrete.

The OPC mix was used to evaluate frost durability and surface scaling mechanisms of ordinary Portland cement concrete, and also served as a reference mix for the blended cement concrete. Four binary mixtures containing GGBFS were prepared at a water-to-binder ration (w/b) of 0.45. The cement replacement levels by GGBFS were 25%, 35%, 50% and 65% by weight, respectively. The target air contents of these mixes was 0% (no

entrained entrainment), 4% (moderate air entrainment), and 7% (high air entrainment). The specimens were de-molded after 24 hours and were moisture cured for 28 days. See Table 3.3.

**Table 3- 1 Frost damage rates of field specimens**

Frost damage rate in field	Location I.D. number
Severely damaged	#1, #2 and #3
Moderately damaged	#4, #5, #6, #7, #8 and #9
Barely damaged	#10 and #11

**Table 3- 2 Chemical compositions of materials**

% By weight	Cement I (type I)	GGBFS I	Cement II (type I)	$C_3S$
$SiO_2$	20.4	37.49	20.6	25
$Al_2O_3$	5.04	7.77	4.7	1
$Fe_2O_3$	2.51	0.43	2.6	<0.02(trace)
$CaO$	62.39	37.99	65.1	73
$MgO$	3.43	10.69	2.7	0.5
$Na_2O$	0.25	0.28		<0.01(trace)
$K_2O$	0.67	0.46		
$Cl$	0.03			
$SO_3$	2.75	3.21	2.5	
$C_3S$	53.66	-	66.4	
$C_2S$	18.01	-	9.24	
$C_3A$	9.11	-	8.06	
$C_4AF$	7.64	-	7.91	
$(Na_2O)_{eq}^*$	0.69	0.58	0.52	
Loss on Ignition			1.45	
Insoluble residue			0.4	
Free Lime			1.31	
Blaine $(cm^2 / g)$	4290	6020	3650	

$$^*(Na_2O)_{eq} = Na_2O + 0.658K_2O$$

$$C_3S = 4.071 \times CaO - 7.6 \times SiO_2 - 6.718 \times Al_2O_3 - 1.43 \times Fe_2O_3 - 2.852 \times SO_3$$

$$C_2S = 2.867 \times SiO_2 - 0.7544 \times C_3S$$

$$C_3A = 2.65 \times Al_2O_3 - 1.692 \times Fe_2O_3$$

$$C_4AF = 3.043 \times Fe_2O_3$$

### 3.3 TESTING METHODS

#### 3.3.1 RILEM CIF/CDF Test

Adequate resistance of concrete to freeze-thaw attack should be verified by laboratory tests such as the CIF (Capillary suction, Internal damage and Freeze-thaw) test. The CIF test is based upon the RILEM recommendation of the CDF-test (Capillary Suction, De-icing agent and Freeze-thaw Test), where precision data for scaling has been determined, and complements this test.

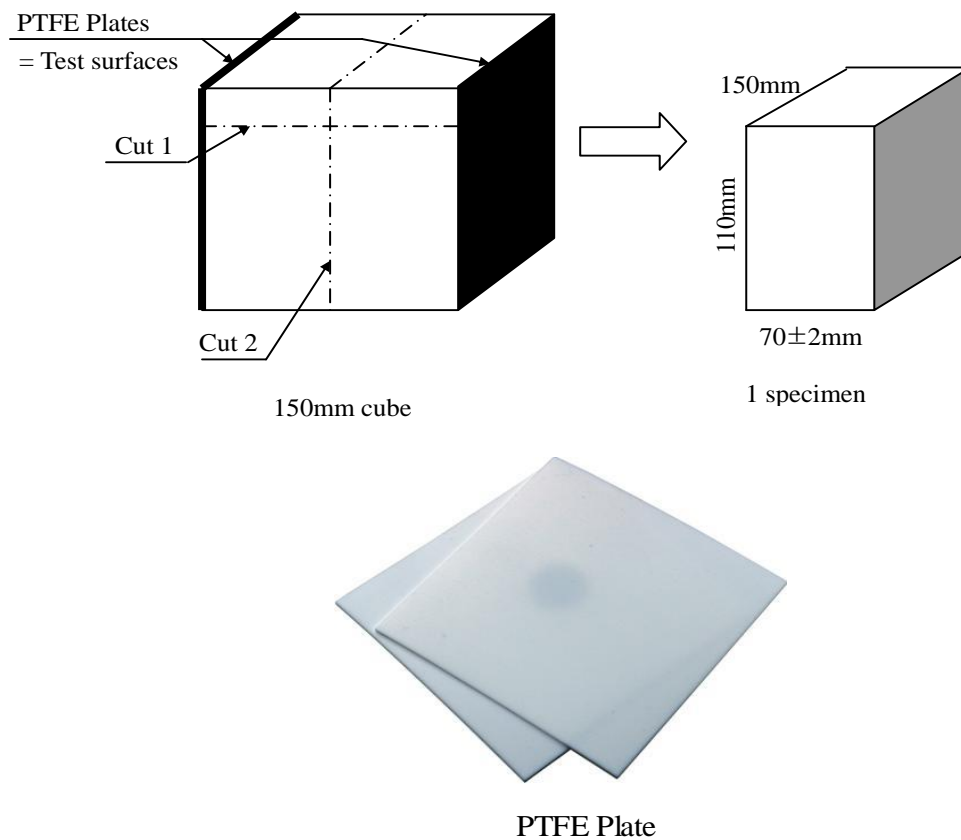
**Table 3- 3 Matrix for test specimens**

Sample ID	Cement I (Type I&II)	GGBFS	w/b	Target Air(%)	Curing duration
OPC	100		0.45	7	28days
25S	75	25	0.45	7	28days
50S	50	50	0.45	7	28days
65S	35	65	0.45	7	28days
OPC I	100		0.45	4	28days
OPC II	100		0.45	8	28days
HPC I	65	35	0.45	0	28days
HPC II	65	35	0.45	3	28days
HPC III	65	35	0.45	6	28days

#### 3.3.2 Test Specimens

The dimensions of the standard test specimen is 150mm wide by 110mm long by 70mm thick (5.9\*4.33\*2.76in). For testing concrete mixes or concrete constituents in a

mix, the test specimens are cast and compacted on a vibrating table in a 150mm (5.90 in.) cube moulds according to prEN-ISO 2736/2. The concrete surface at the poly-tetra-fluoro-ethylene (PTFE) plate (Figure 3.1) is the test surface. The PTFE plate which is non-sticky material can be easily detached from test surface without de-molding oil so that the test surface is not only not damaged by de-molding but also not contaminated by de-molding oil. After  $24 \pm 2$  hours of curing the specimens are removed from the mould and submersed in tap water at 20 °C. After storage under water, the specimens are cut into rectangular prisms measuring 150mm by 110mm by  $70 \pm 2$ mm. The first cut is made along the top (rough) upper side at 110mm. See Figure 3.1.

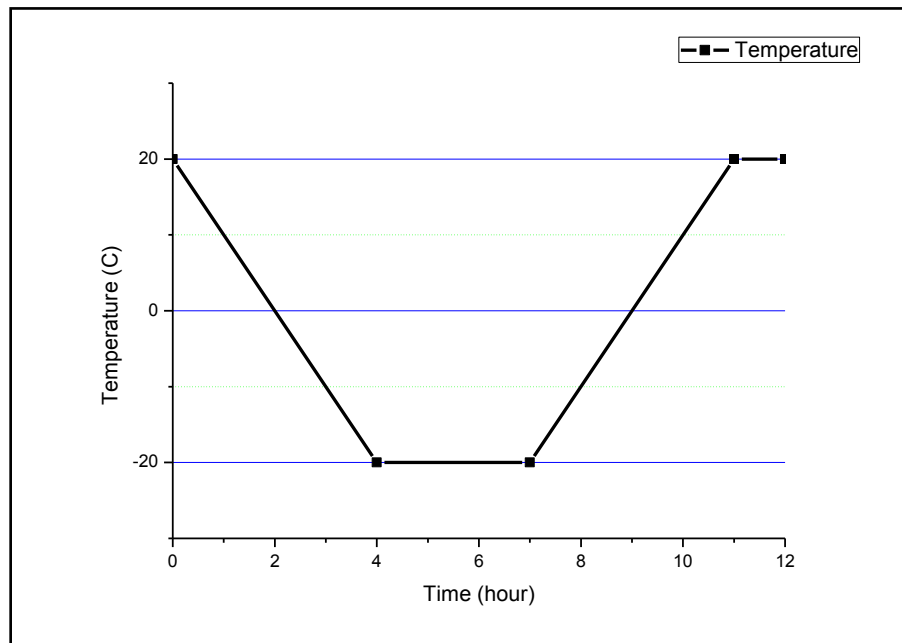


**Figure 3- 1 Sawing of test specimens and PTFE Plate**

After cutting, the specimens must be sealed on their lateral surface. For this study, aluminum foil with butyl rubber is used for lateral sealing.

### 3.3.3 Test Procedure

The test specimens are stored on test liquid (de-mineralized water for CIF and 3% NaCl solution for CDF test) for 7 days so that a degree of saturation reaches to similar condition with field. Then, freeze-thaw cycles start. Apply a 12 hours freeze-thaw cycles to the prepared specimens.. Starting at 20°C(+68 °F) the temperature is lowered in 4 hours with a constant cooling rate of 10°C (18 °F/hr). It is kept constant for 3 hours at – 20 °C (– 68°F) and increased in 4 hours with a constant heating rate of 10 °C (18°F/hr). Then, it is kept constant for 1 hour at 20°C (+68°F). The temperature profile is shown in Figure 3.2.



**Figure 3- 2 F-T machine température cycle**

The specimens are exposed to a freeze-thaw cycle in a temperature controlled chest.

Figure 3.3 shows the temperature controlled chest and the test container.



**Figure 3- 3 Temperature controlled chest & Test container**

### 3.3.4 Measurements

#### 3.3.4.1 Sequence of Measurement with Respect to Scaling, Moisture Uptake and Internal Damage

Measurements are taken at the start of the freeze-thaw test (0 freeze-thaw cycles) and after every 4<sup>th</sup>-6<sup>th</sup> freeze-thaw cycle. The following sequence of the measurement is imperative: Surface scaling, Moisture uptake, and Internal damage (ultrasonic transit time as reference method).

#### 3.3.4.2 Determination of Surface Scaling

Once freezing-thawing cycles start, the test surface is damaged by frost action. The damaged concrete flakes fall down on the bottom of container (figure 3.3). The scaled materials are collected in a filter paper. The total amount of scaled material,  $m_n$ , related to the test surface after the nth cycle is to be calculated for each measuring interval and each specimen:

$$m_n = \frac{\sum \mu_s}{A} \quad (3.1)$$

Where,

$m_n$  = the total mass of scaled material related to the test surface after each measuring interval, in  $g/m^2$

$\mu_s$  = the mass of scaled material at each measuring interval, in grams  $\pm 0.01g$ .

$A$  = the area of the test surface, in  $m^2$ .



### 3.3.4.3 Measurement of Moisture Uptake

The relative increase in mass of each specimen,  $\Delta w_n$ , after nth cycle is calculated by:

$$\Delta w_n = \frac{w_n - w_1 + \sum \mu_s}{w_0} * 100 \quad (3.2)$$

Where,

$\Delta w_n$  = the moisture uptake in mass of each specimen after the nth cycle, in M-%

$\mu_s$  = the mass of total scaled material at each measuring interval, in grams with an accuracy of 0.01g. The sum is taken over all measurements of the mass of the scaled material until the nth cycle.

$w_0$  = the reference mass of the each specimen without mass of aluminum foil with butyl rubber for lateral sealing after 7days pre-storage on test liquid, in grams.

$w_1$  = the mass of each specimen including sealing mass before re-saturation starts, in grams.

$w_n$  = the mass of each specimen at each measuring interval, in grams.

### 3.3.4.4 Evaluation of the Internal Damage

The transit time in the coupling medium,  $t_c$ , is calculated using the following relation:

$$t_c = \frac{l_c}{v_c} \quad (3.3)$$

Where,

$t_c$  = the transit time in the coupling medium, in ms

$l_c$  = the transit length  $l_{c1} + l_{c2}$  in the coupling medium, in mm

$v_c$  = the velocity of the ultrasonic signal in the coupling medium, which can be assumed to 1490 m/s for water between  $20C \pm 5C$ .

The change of relative transit time  $\tau_n$  after n freeze-thaw cycles is calculated separately for each specimen and transit axis by:

$$\tau_n = \frac{t_{cs} - t_c}{t_n - t_c} \quad (3.4)$$

Where,

$\tau_n$  = the relative transit time

$t_{cs}$  = the total transit time in ms before the first freeze thaw cycle

$t_n$  = the total transit time after n freeze-thaw cycles (ftc), in ms

Instead of expressing internal damage as the change of relative transit time it is convenient to use the dynamic modulus of elasticity of ultrasonic transit time,  $R_{u,n}$ . In this test procedure the relative change in dynamic modulus of elasticity after n freeze-thaw cycles is calculated by the relation:

$$R_{u,n} = \tau_n^2 \quad (3.5)$$

### 3.3.5 Air void analysis

As mentioned before, one of the most important parameters that affects the durability of concrete is the amount of entrained air voids. RapidAir 457 is an automated image analysis system that performs the analysis of the air void distribution within hardened concrete according to the ASTM C 457 : “Standard Method for Microscopical Determination of Parameters of the Air-Void System in Hardened Concrete” method A and B, and EN 480-11: “Admixtures for concrete, mortar and grout – test methods – Part

11: Determination of air void characteristics in hardened concrete”.

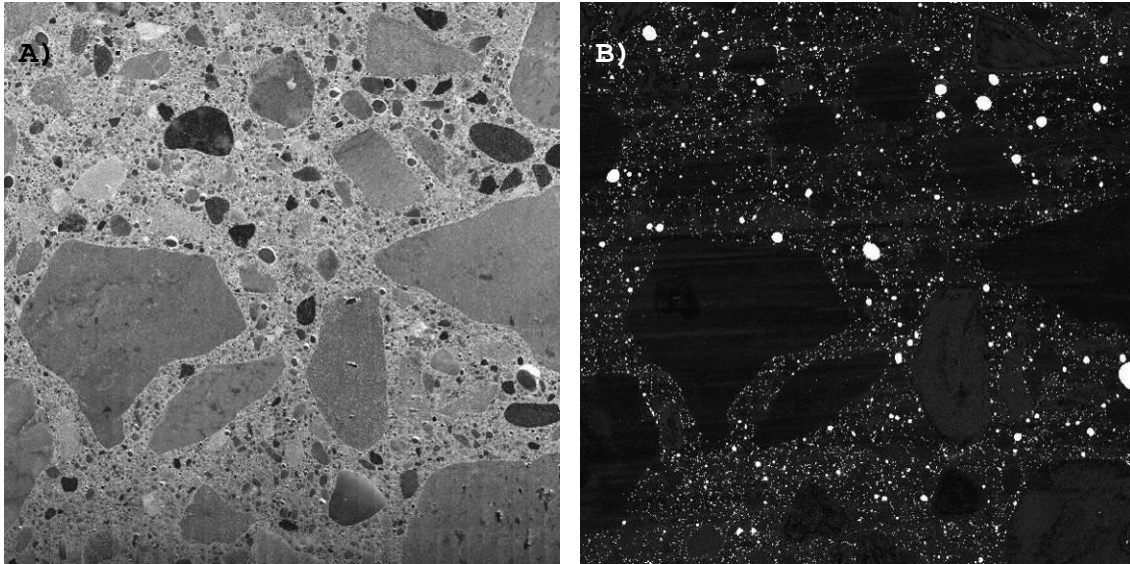
### 3.3.5.1 Test sample

The dimensions of the test samples are 100mm by 100mm (4 in. by 4 in). The samples are polished using the concrete polisher (Figure 3.4), a lapping device, which is constructed to lap concrete plane sections.



**Figure 3- 4 Concrete Polisher**

The concrete samples to be analyzed using automatic analysis performed by RapidAir 457 are prepared using a surface contrast enhancement technique that results in a black surface with white air voids. After polishing the specimens, the sample surface is colored by black ink and air voids are filled with a white fine-grained powder ( $\text{BaSO}_4$ ) so that the best contrast enhancement is given. Fig. 3.5 shows a polished sampled surface and a final sample surface.



**Figure 3- 5 A) Sample surface after polishing, and B) is same surface after treatment**

RapidAir 457 determines the volume of air (percent volume), specific surface, the spacing factor, the void frequency, and the average chord length. Results are provided in three categories: chord sizes less than 0.5mm in. (0.02in.), less than 1.0mm (0.04in.) and all chord sizes. RapidAir 457 also calculates the modal chord length and the zero-order standard deviation of a lognormal representation of the normalized chord length frequency versus the chord length.

### **3.3.6 Low Temperature Dilatation (LTD) Test**

The LTD test is a precision measurement of the continuous length change versus surface temperature during a F-T cycle. The freezing temperature of the pore-liquid and specimen expansion during freezing as well as permanent length change due to internal damage is obtained from this test. The concrete dilatometer is shown in Figure 3.6. A typical prismatic specimen has dimension of length 90mm (3.55in.) and cross section dimensions of 10mm by 10mm (0.4in. by 0.4in.).



**Figure 3- 6 Dilatometer for LTD test**

# **CHAPTER 4**

## **PRELIMINARY LABORATORY STUDIES WITH FIELD SPECIMENS**

### **4.1 INTRODUCTION**

Michigan has a very severe wet-freeze climate with many freeze-thaw (F-T) cycles per year. To assure a concrete pavement sustains its inherent long term durability requires several factors be performed properly during design and construction. Some of concrete pavements exposed to the severe climate have experienced severe frost damages while some pavements do not seem to have any problem with the weather conditions. To understand what factors cause the differences, macro and microscopic tests and observations were carried out.

### **4.2 AIR VOID SYSTEMS OF FIELD SPECIMENS**

#### **4.2.1 Air Contents and Spacing Factors of field specimens**

Entrained air is the most general frost protection method. The air voids system of concrete is very important as it influences the properties of the material such as frost durability. Therefore, most concrete pavements were designed to be constructed with

sufficient entrained air. It is, however, still obscure how much air contents are sufficient and what parameters of air voids affect the durability. In order to evaluate these relationships, air voids systems of field specimens have been analyzed. See Table 4.1.

In terms of entrained air contents, Specimens #1 to #3 which have poor frost scaling resistance are under 3% while specimens # 4 to #9 with ordinary resistance have 3% to 5% air contents of entrained air. The specimens #10 and #11 which were seldom damaged by frost action in the field have over 6% entrained air contents. The spacing factors of nondurable concrete specimens are over 200  $\mu\text{m}$  while that of durable concrete is less 100  $\mu\text{m}$ . In the range of this study, entrained air content and spacing factor are the variables independently affecting concrete scaling resistance.

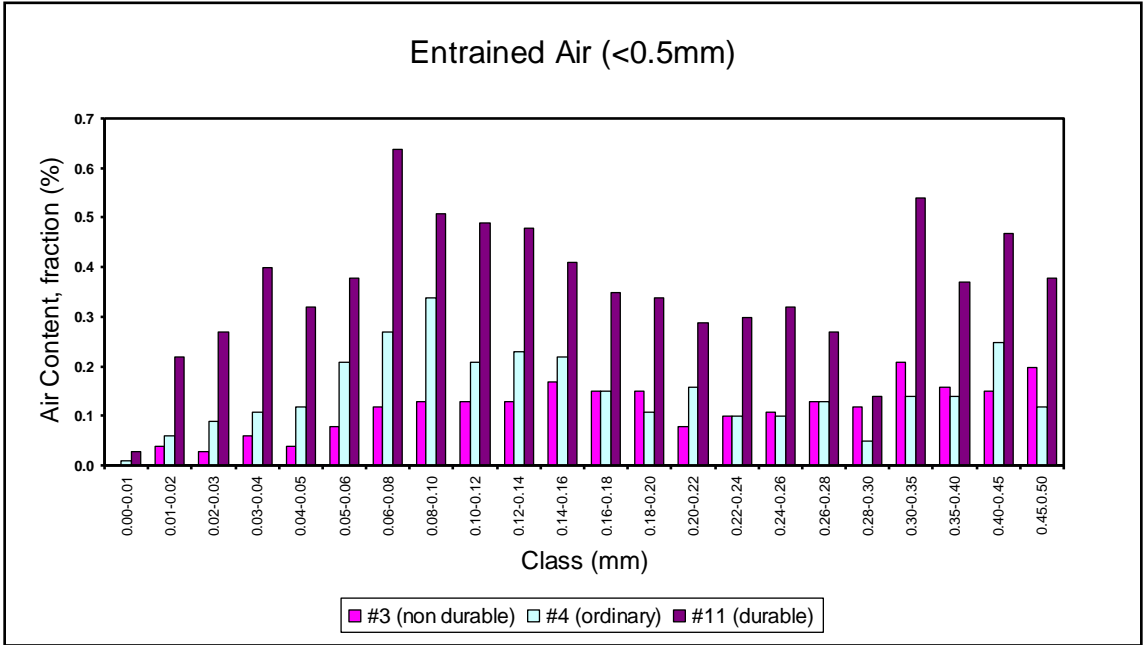
**Table 4- 1 Air voids properties of field specimens**

No.	Total Air (%)	Entrained Air (%) (<0.5mm)	Spacing Factor $\bar{L}$ ( $10^{-3}$ m)	Average radius of air voids, $\bar{r}$ ( $10^{-3}$ m)	Frost damage in field
1	3.8	1.47	0.29	0.24	Severely damaged
2	4.3	2.42	0.22	0.16	Severely damaged
3	3.8	2.49	0.22	0.173	Severely damaged
4	4.24	2.67	0.20	0.143	Moderately damaged
5	5.9	3.01	0.13	0.153	Moderately damaged
6	5.7	3.19	0.18	0.17	Moderately damaged
7	6.3	3.58	0.15	0.18	Moderately damaged
8	5.8	3.87	0.10	0.124	Moderately damaged
9	6.93	4.29	0.12	0.127	Moderately damaged
10	8.14	6.5	0.07	0.1	Little damaged
11	9.57	7.71	0.08	0.1	Little damaged

**4.2.2 Air voids distribution.**

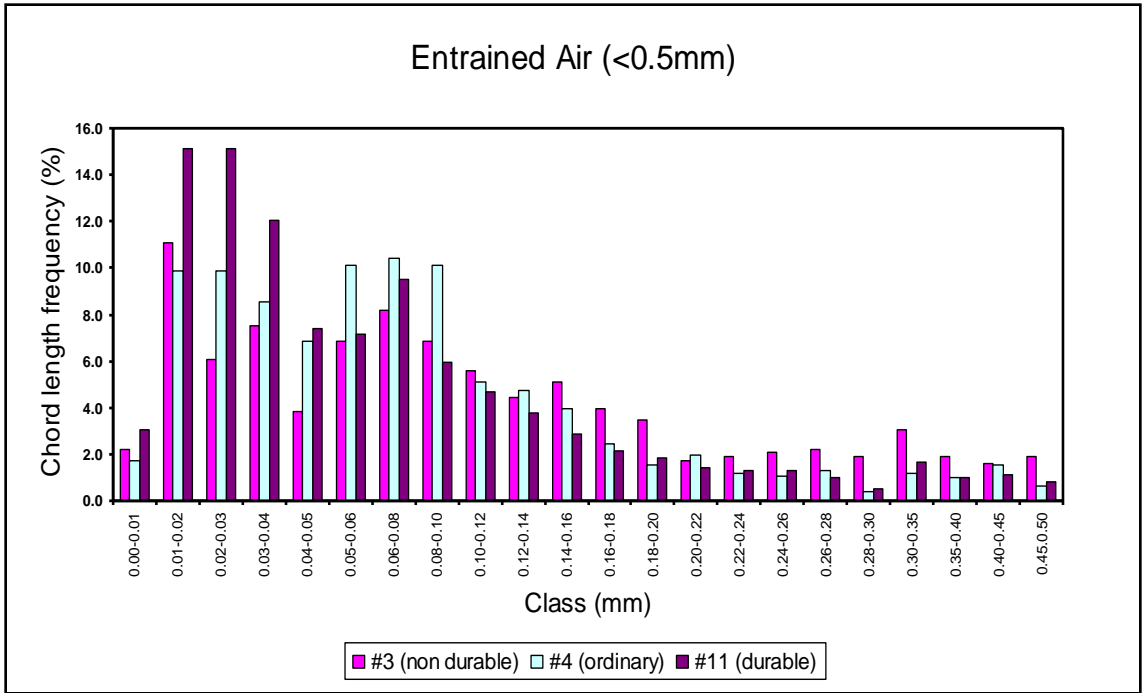
In addition to quantitative properties of air voids, one important qualitative property of air voids is distribution. Air content and chord length frequency for each class are shown in Figure 4.1 to 4.4. Appendix A contains are the air voids distributions of all specimens.

Figure 4.1 shows air content for each class up to 500  $\mu m$  and Figure 4.3 over 500  $\mu m$ . The durable concrete has higher air contents of all classes up to 1mm. On the other hand, specimen #11, durable concrete, has higher frequencies of small void classes. In fact, the sum of frequencies up to 50  $\mu m$  voids of specimen #11 is 53% while that of specimen #3 and 4 are 31% and 37%, respectively.

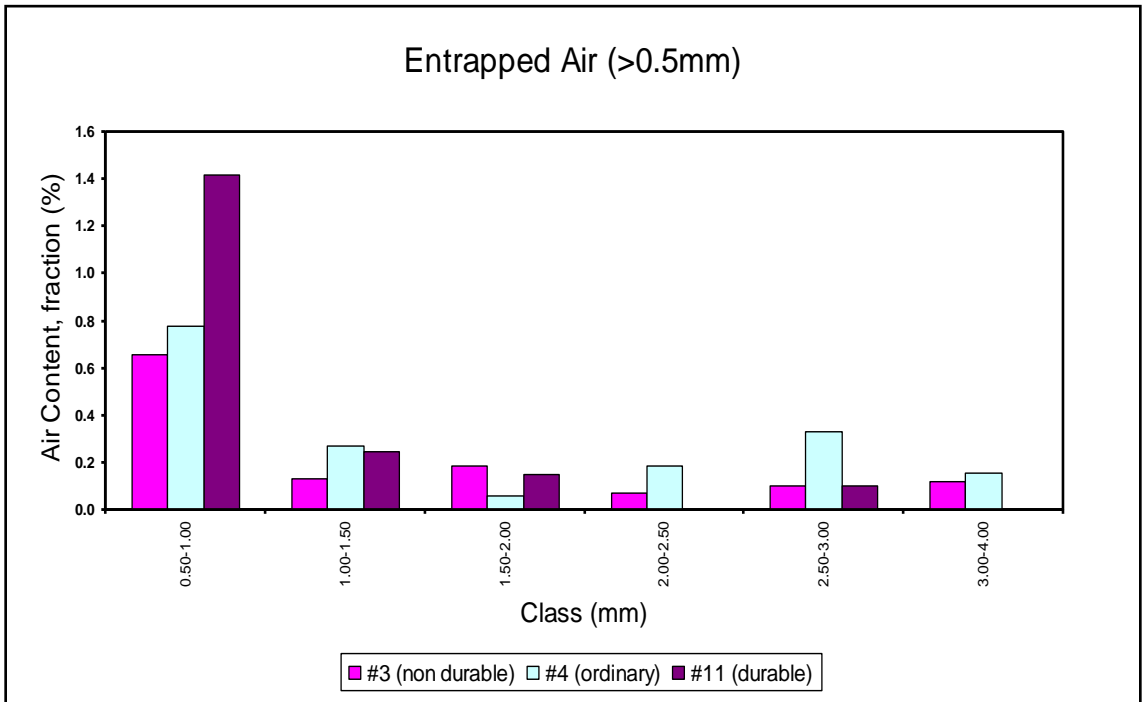


**Figure 4- 1 Air content for each class (Entrained air)**

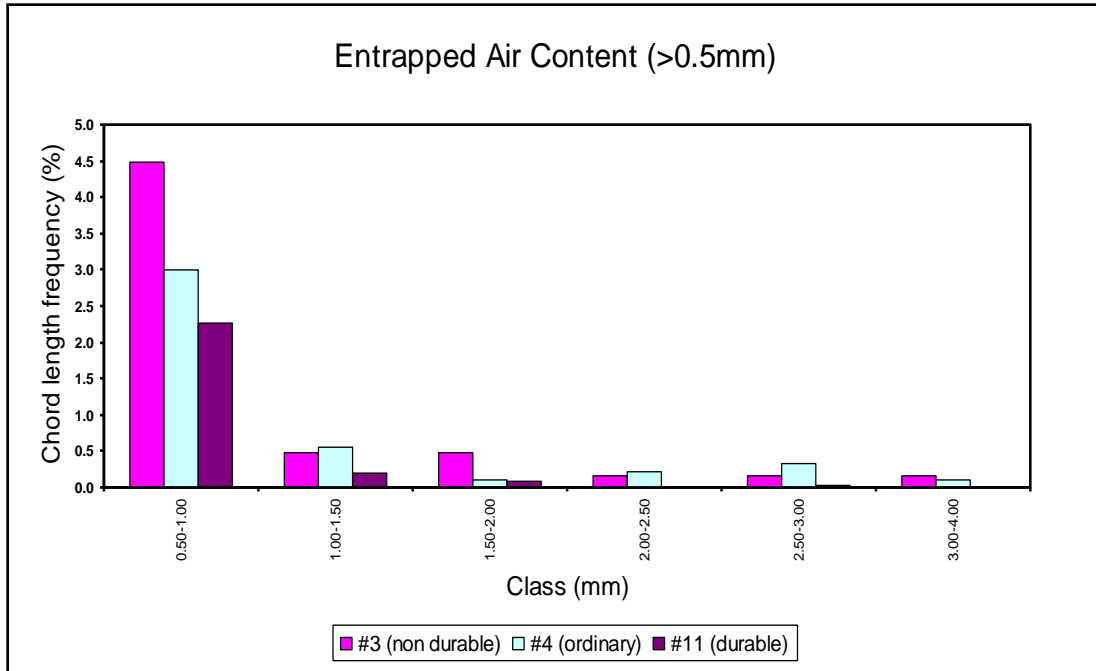




**Figure 4- 2 Chord length frequency for each class (Entrained air)**



**Figure 4- 3 Air content for each class (Entrapped air)**

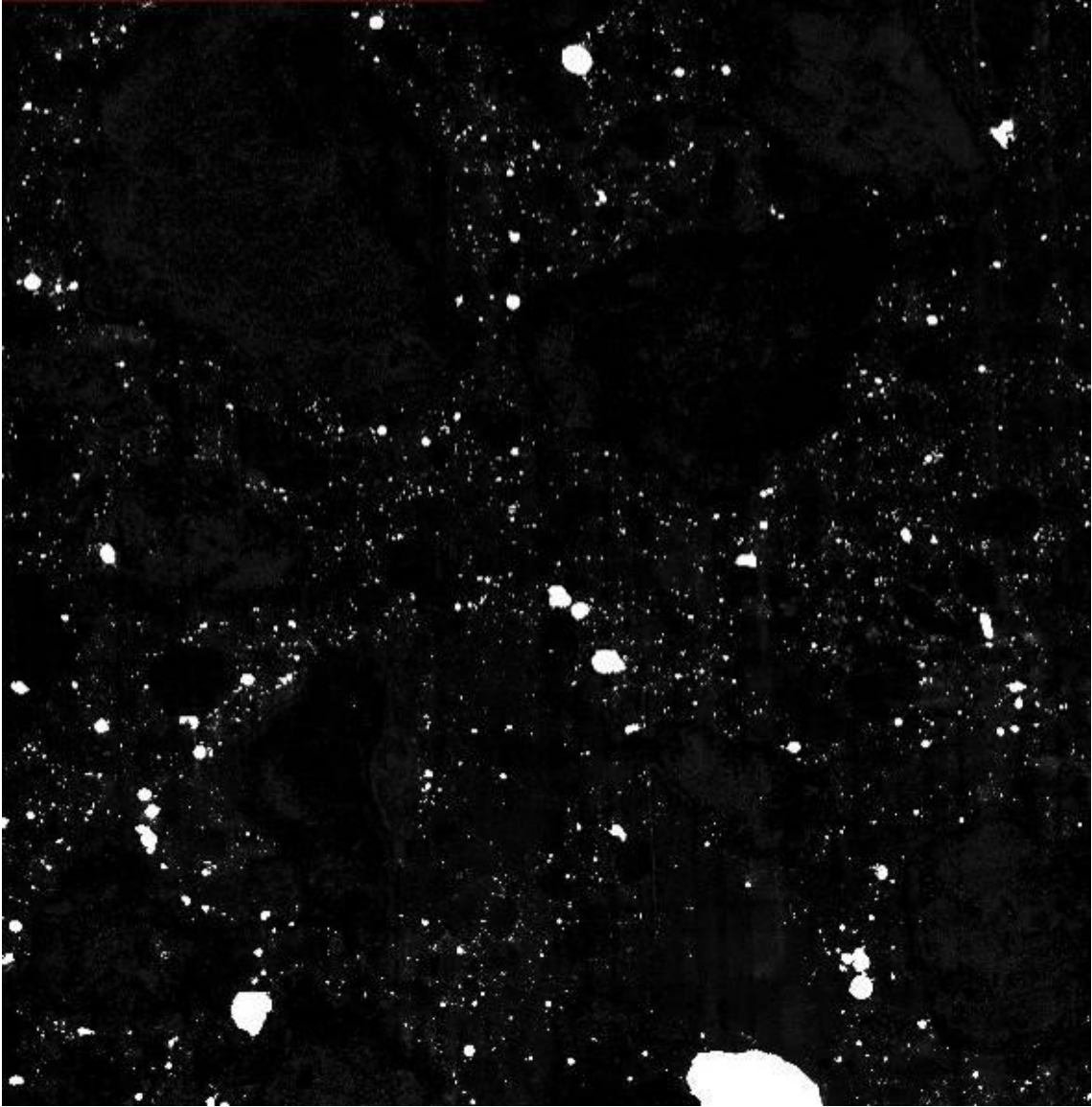


**Figure 4- 4 Chord length frequency for each class (Entrapped air)**

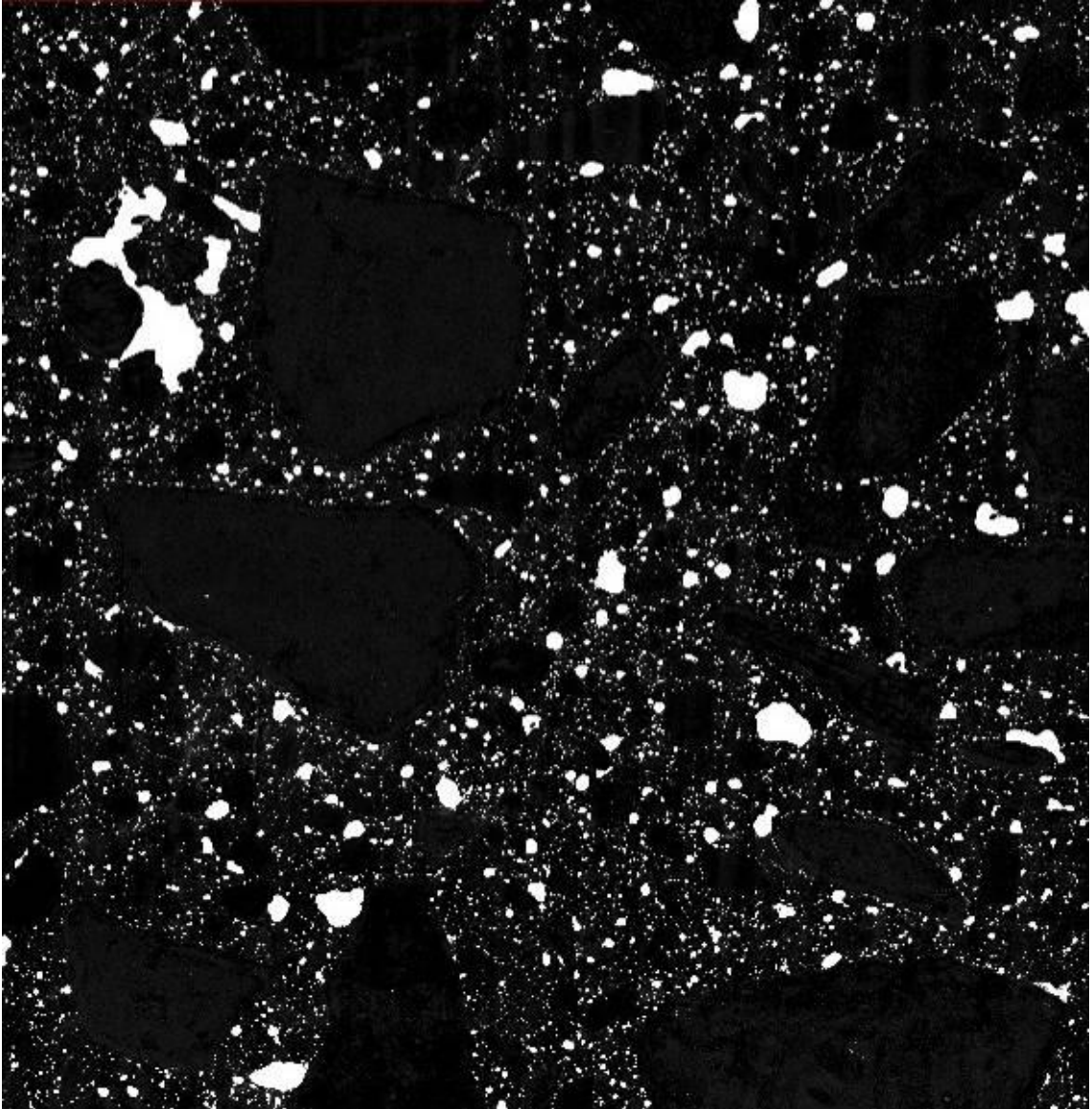
Figure 4.5 to 4.7 show the test surface of air voids blocks of specimens #3, #4 and #11. In the figures, white represents air voids. Paste and aggregates are colored by black ink. It can be clearly seen that the durable concrete, #11, has many small air voids and the air voids system is well distributed throughout the entire surface.

#### **4.2.3 Air voids infilling**

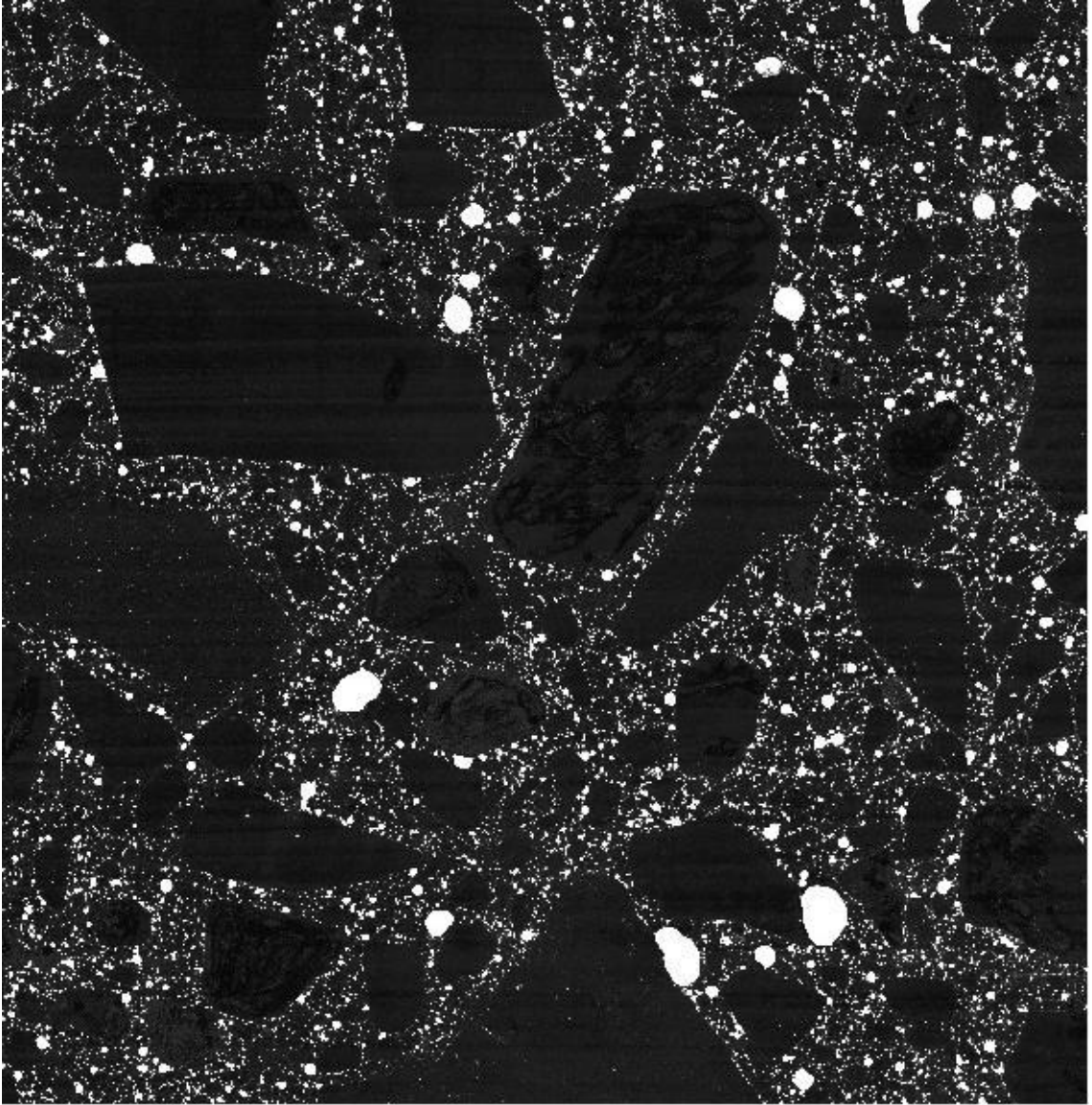
If liquid in capillary and voids contains salt, crystallization can occur. According to [33, 34], super-saturation of salts can result from capillary rise and evaporation, or from cycles of wetting and drying and solubility of sodium sulfate in water decreases dramatically when the temperature drops below 32 °C (Figure 4.8). Besides, as ice begins to freeze out of the salt water, the fraction of water in the solution becomes even lower, and the concentration of remaining solution increases. At some point the solution will become saturated



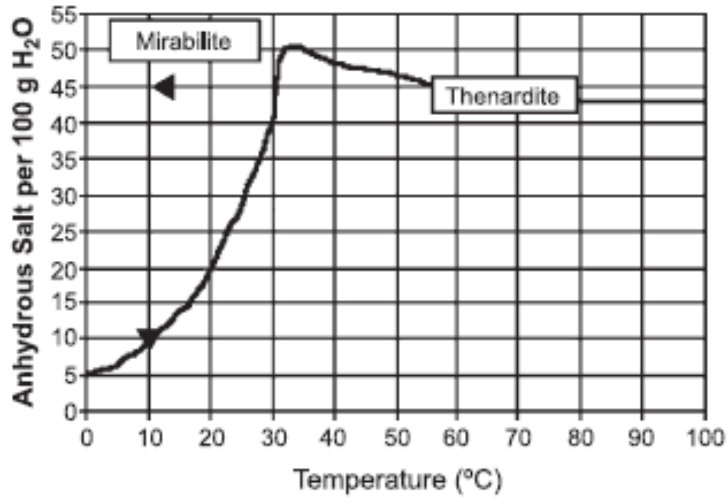
**Figure 4- 5 air voids system of non durable concrete, specimen #3.**



**Figure 4- 6 air voids system of ordinary concrete, specimen #4.**



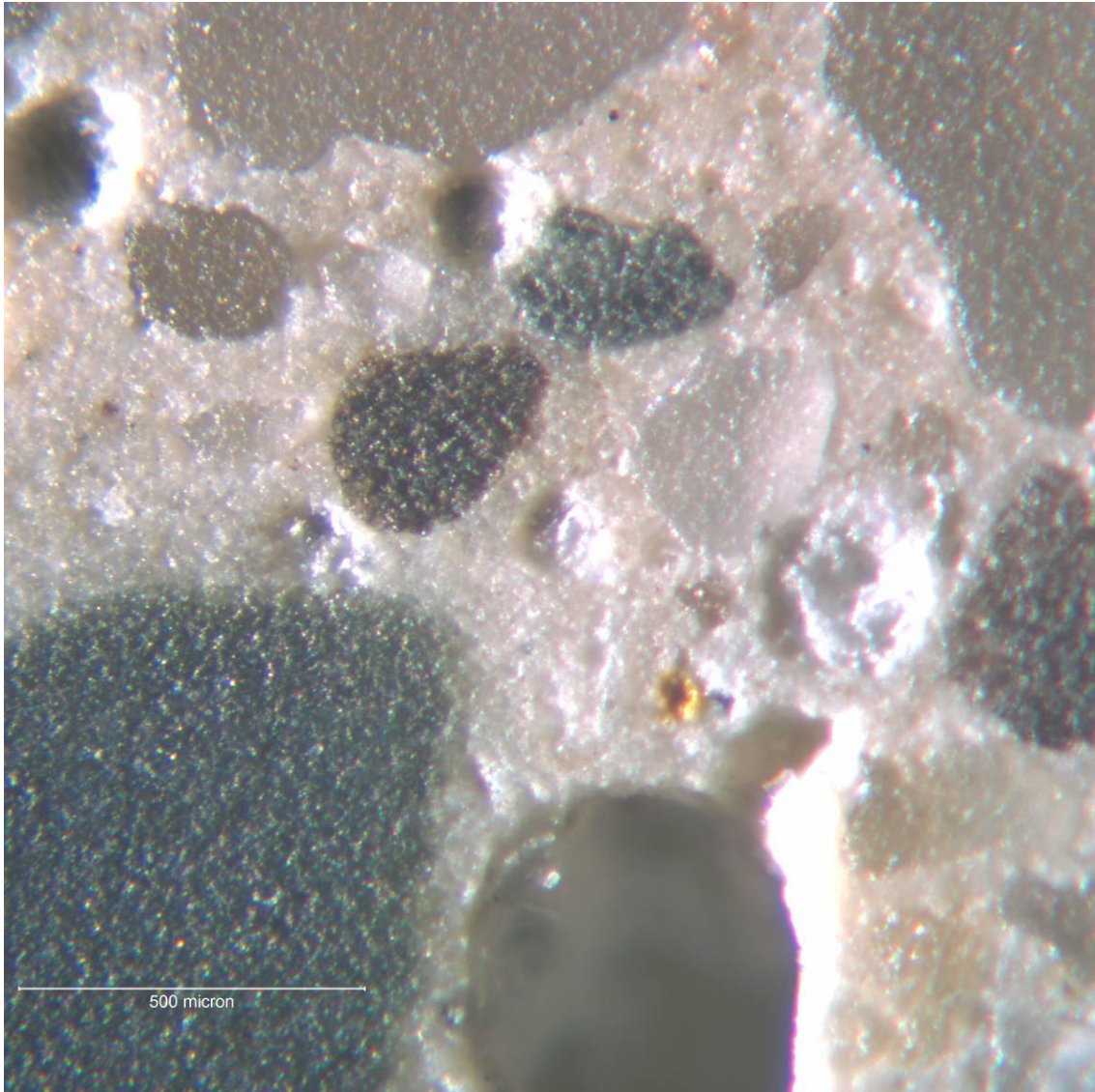
**Figure 4- 7 air voids system of durable concrete, specimen #11.**



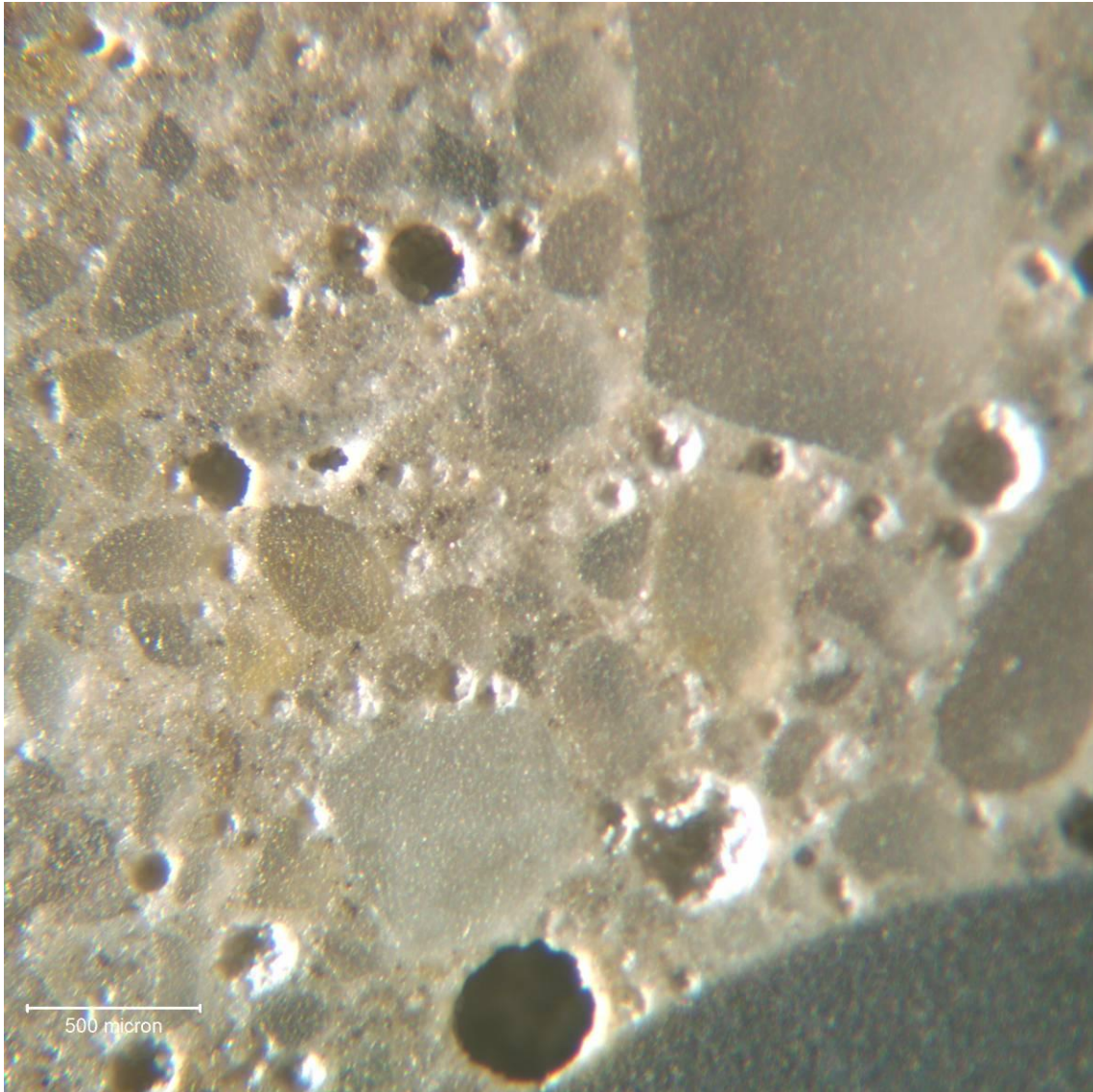
**Figure 4- 8 Solubility of sodium sulfate in water. Cooling the liquid from 30 °C to 10 °C without crystallization creates super saturation.**

with salt. This happens for salt in bulk water at -21.1 °C , which therefore is the coldest a saturated solution of salt and water can get. At that temperature, the salt begins to crystallize out of solution, along with the ice, until the solution completely freezes. Thus, the amount of salt crystals in voids grows with repeated drying and wetting cycles as well as freezing and thawing cycles. It may cause air voids infilling and consequently worsen air voids properties. Figure 4.9 and 4.10 show some voids with infillings.





**Figure 4- 9 Air voids infillings of specimen #1**



**Figure 4- 10 Air voids infillings of specimen #3**

Due to severe weather condition in Michigan,  $6.5\% \pm 1.5\%$  of air for pavement concrete is recommended. However, non durable concretes have less than 4% of total air and 2.5% of entrained air. To evaluate how much air content has been lost by infilling, the ASTM C 457 point count method has been performed. The number of points is 3000. See Table 4.2.



**Table 4- 2 Total air content and In-filling air content by 3000 points count**

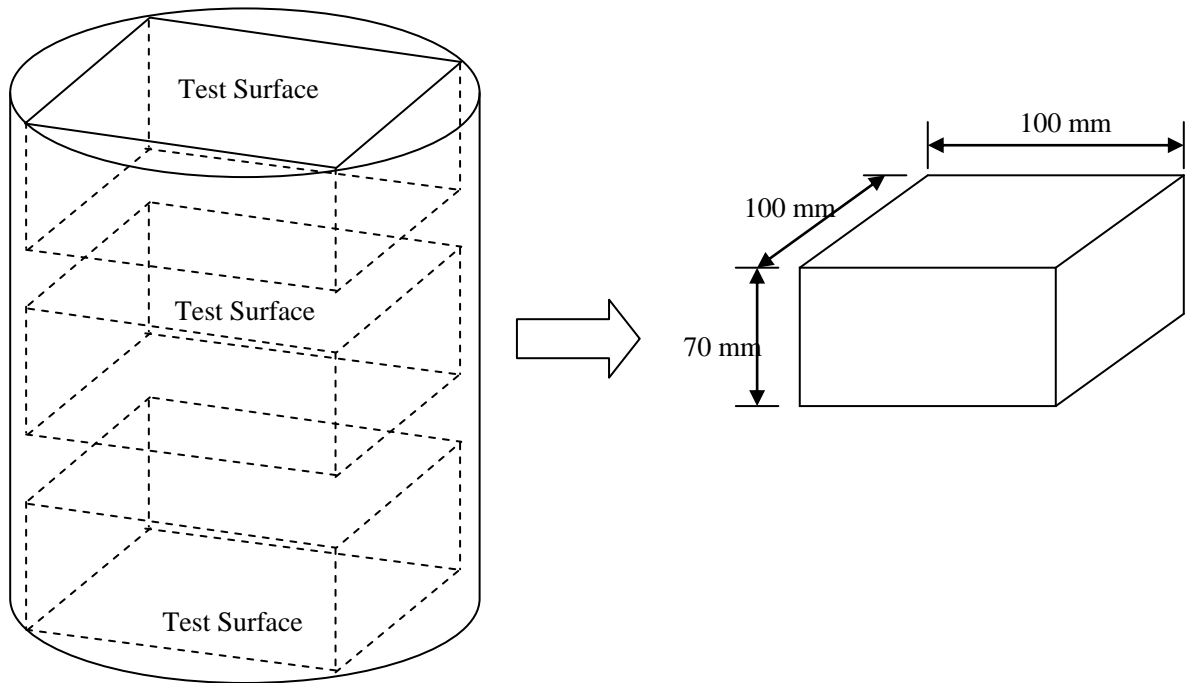
Specimen I.D.	Total air content (%) By Point Count	In-filling (% of total) By Point Count
1	5.8	34
2	5.8	26
3	4.8	21
4	6.3	19
5	7.5	21
6	6.7	15
7	7.2	13
8	6.8	15
9	7.7	18

Based on the point count results (Table 4.2), most field concretes had approximately 6% air at the beginning of service. After many repeated freezing and thawing cycles, parts of the air voids lost their frost protection properties. Nondurable concrete specimens had relatively low air contents (4.8% and 5.8%) at the beginning compared to other specimens. Furthermore, they have lost more air voids by infilling.

### **4.3 RILEM CIF AND CDF TEST**

The RILEM CIF and CDF tests have been conducted with the field specimens obtained from field cores. Dimensions of specimens are 100mm by 100mm in width and 70mm in height as shown in Fig. 4.11. Once cut from cores, the specimens have been dried in an

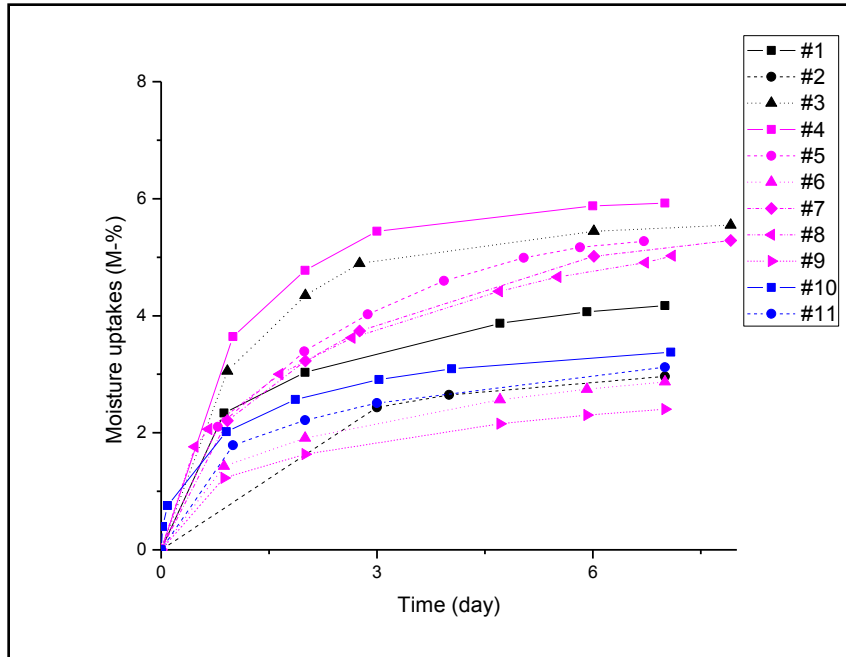
oven of  $45^{\circ}\text{C} \pm 5^{\circ}\text{C}$  until the weights of the specimens were not changed. Therefore, it can be sure that there is no evaporable liquid in the field specimens.



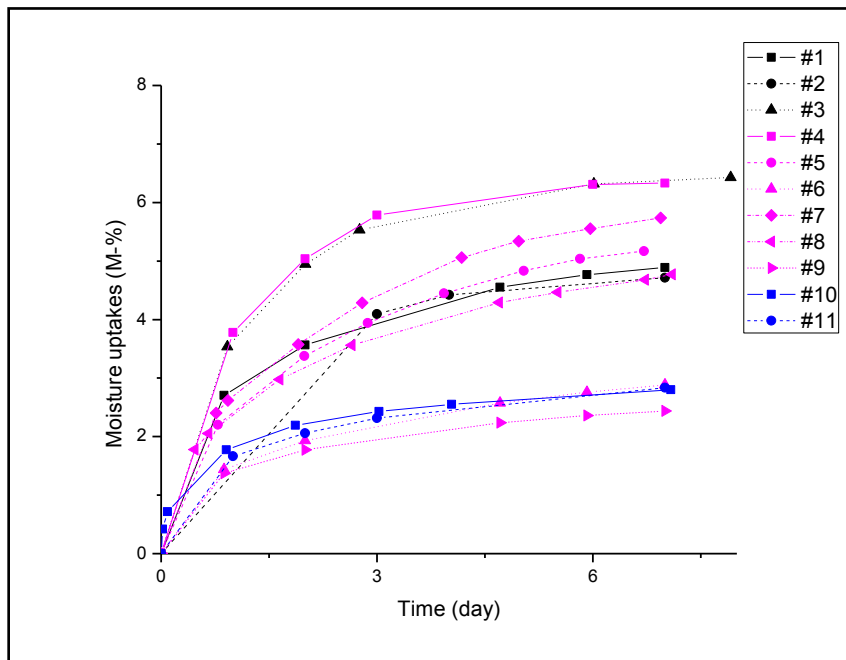
**Figure 4- 11 Sketch of a prismatic F-T specimen obtained from a core**

#### **4.3.1 Pre-saturation stage**

Prior to freezing-thawing cycles, the specimens have been stored in test liquids (water for CIF test and 3% NaCl solution for CDF test) for 7days. The weight gains have been monitored. See Figure 4.12 and 4.13.



**Figure 4- 12 Moisture uptakes in water during pre-saturation stage**

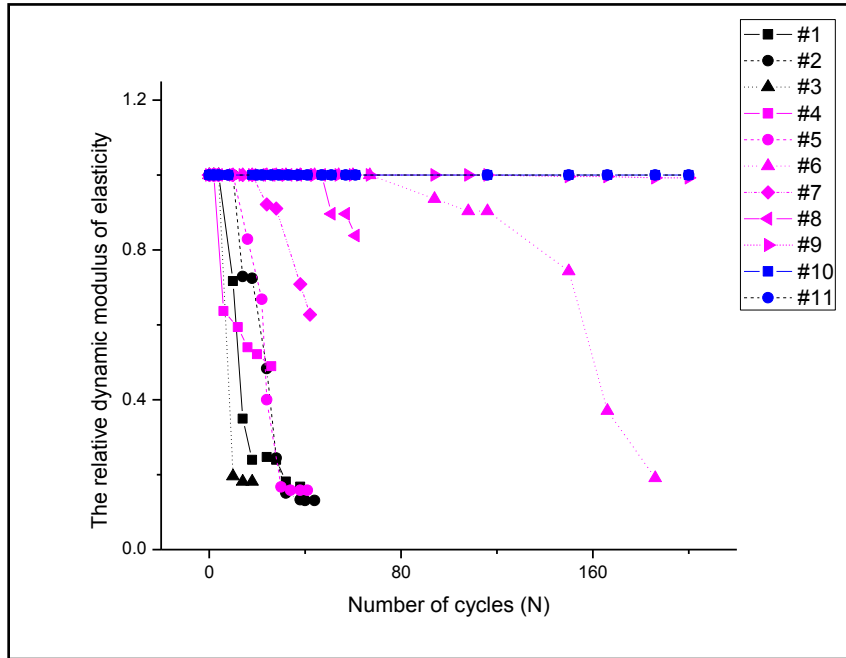


**Figure 4- 13 Moisture uptakes in 3% NaCl during pre-saturation stage**

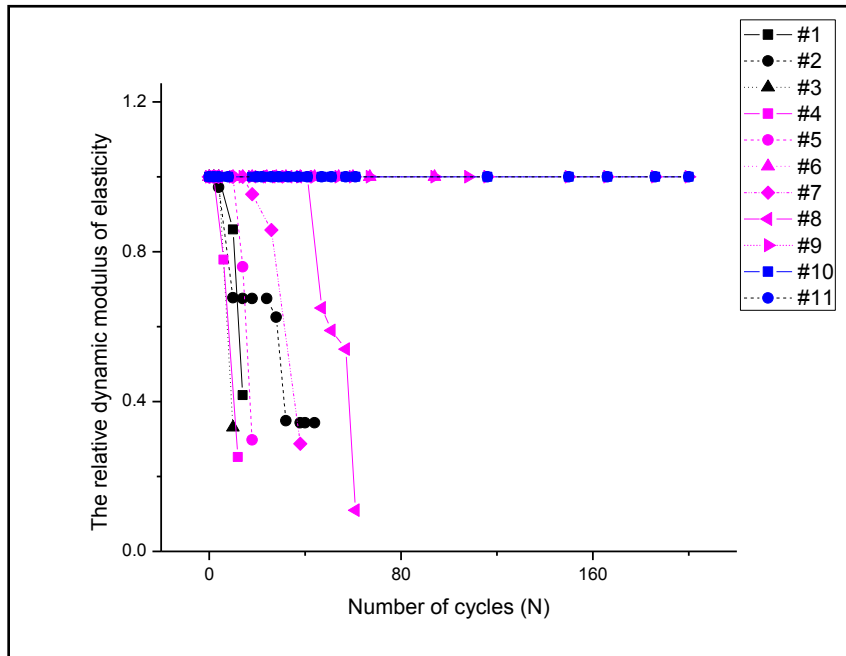
### 4.3.2 Freezing-Thawing cycles

After the pre-saturation stage, Freezing-Thawing cycles were started. To evaluate the

frost durability of the specimens, the relative dynamic modulus of elasticity, the mass loss and the moisture uptakes have been observed up to 200 freezing-thawing cycles. See figure 4.14 to 4.19.



**Figure 4- 14 The evaluation of internal damages in water**



**Figure 4- 15 The evaluation of internal damages in 3% NaCl solution**

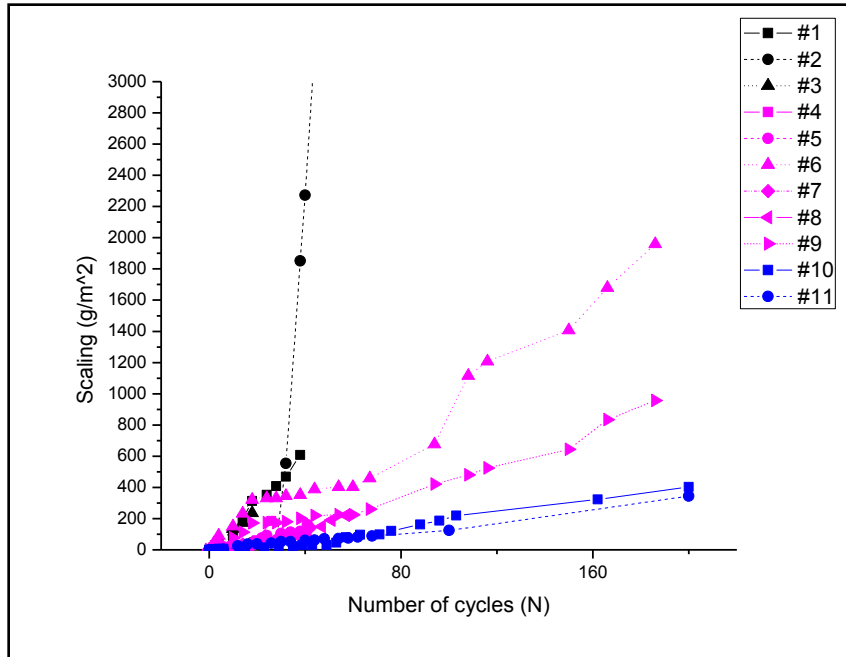


Figure 4- 16 The evaluation of surface scaling in water

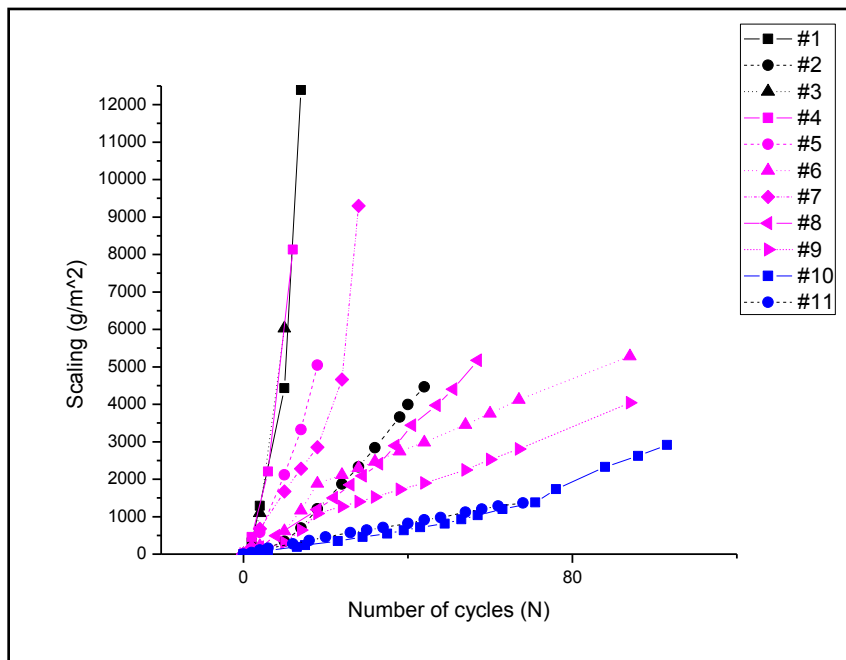
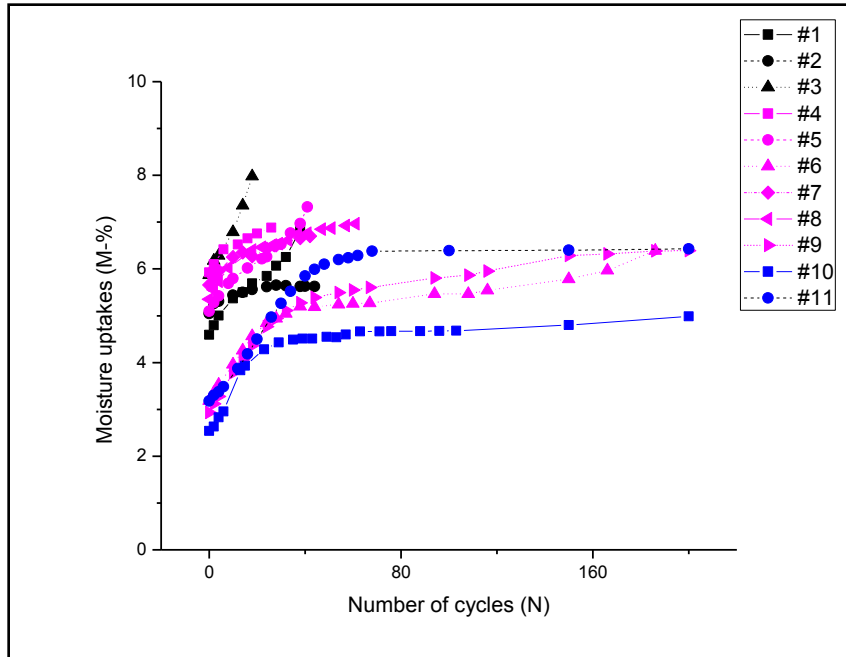
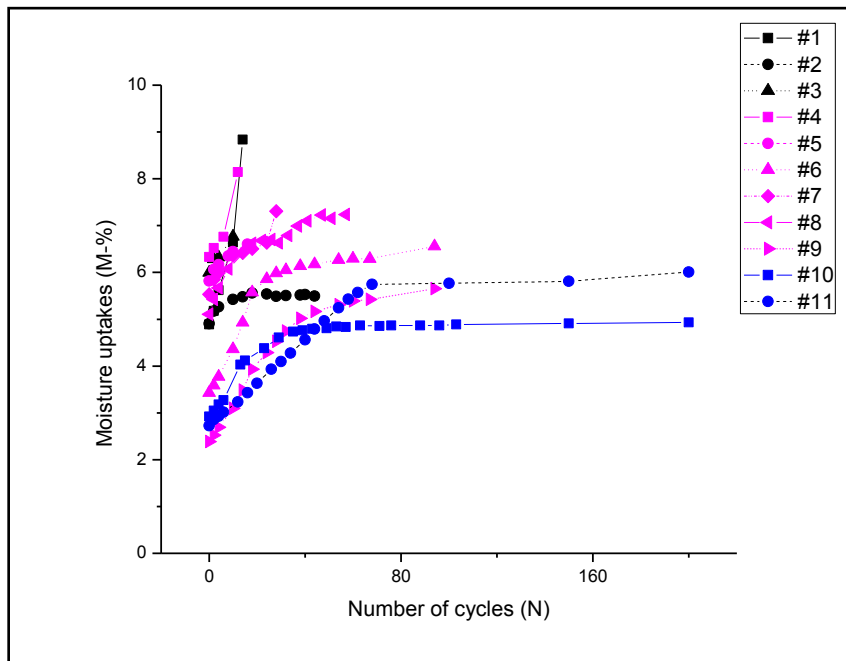


Figure 4- 17 The evaluation of surface scaling in 3%NaCl solution



**Figure 4- 18 The moisture uptakes in water**



**Figure 4- 19 The moisture uptakes in 3% NaCl solution**

**4.3.3 Internal damage VS surface scaling**

As shown in Figure 4.16 and 4.17, the mass loss due to surface scaling tends to increase linearly. Thus, the gradients of the mass loss plotting can be considered as mass loss rate. The mass loss rate can be calculated by equation 4.1.

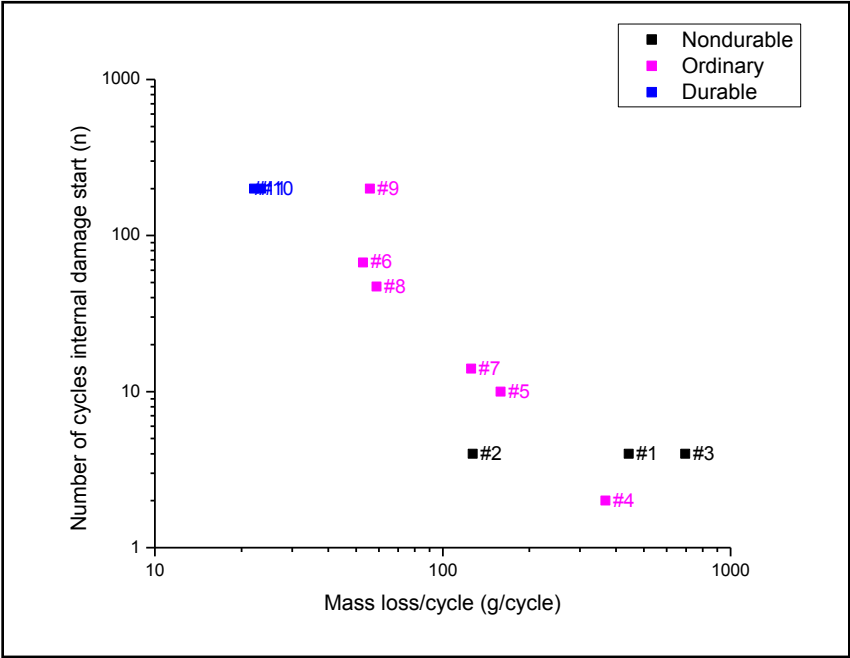
$$M a s s L o s s R a t e \Delta_T / N_T \tag{4.1}$$

Where,

$\Delta_T =$  Total mass loss ( g / m<sup>2</sup> )

$N_T =$  Total number of freezing thawing cycles

The mass loss rates have been compared with the number of freezing thawing cycles when internal damages start. See Figure 4.20.

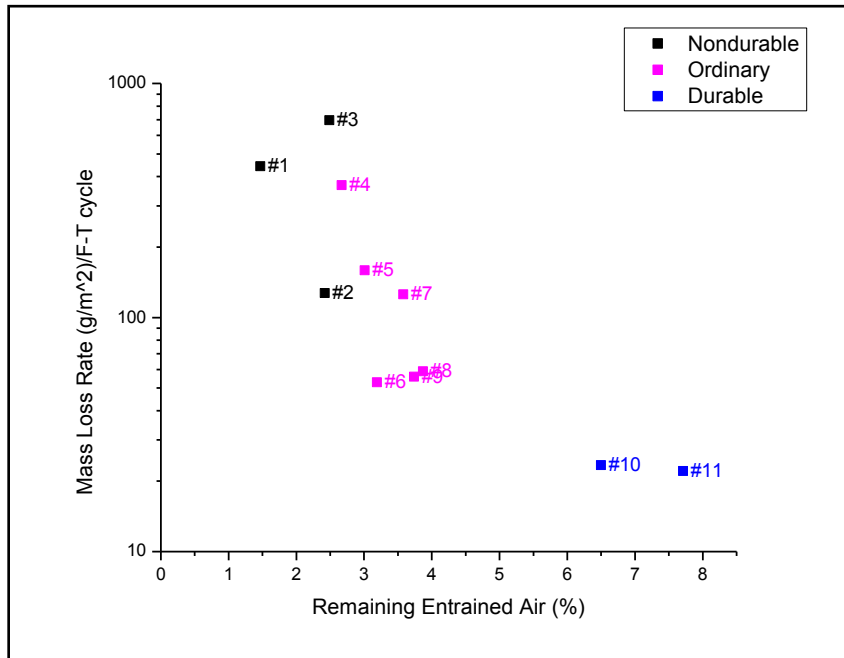


**Figure 4- 20 Internal damage versus mass loss rate**

A good correlation was found between the two F-T test methods. This was concluded from results in Fig. 4.20. The concrete samples which did not have any reduction in

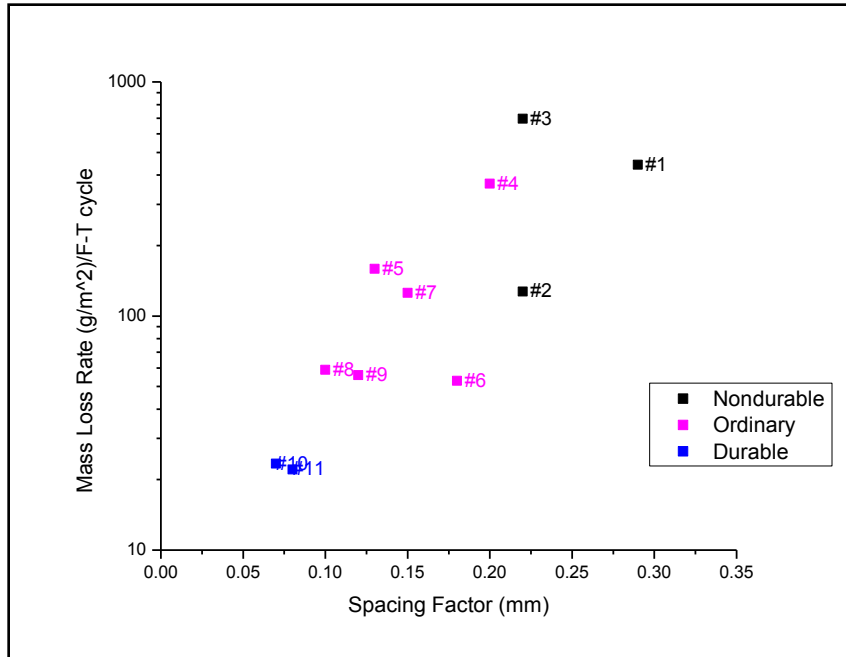
dynamic elastic modulus within the more than 100 F-T cycles of exposure to water (upper left corner) also had the lowest mass-loss rate from the deicer scaling test. The concretes in the lower right-hand corner failed within 10 F-T cycles in water and also exhibited highest mass-loss rates from the deicer scaling test. These findings span a range of nearly 50 between the lows and the highs for each exposure condition.

Both test methods correlate well with entrained air content and spacing factor as seen from Figure 4.21 to 4.24. Therefore, entrained air content is the single-most important factor in avoiding surface scaling. However, good resistance to deicer surface scaling requires more air than for good resistance to F-T exposure in water. This is consistent with recommendations by the NRMCA CIP2-Scaling Concrete Surfaces[33], which recommends 6%-7% air content in fresh concrete for severe exposure conditions.

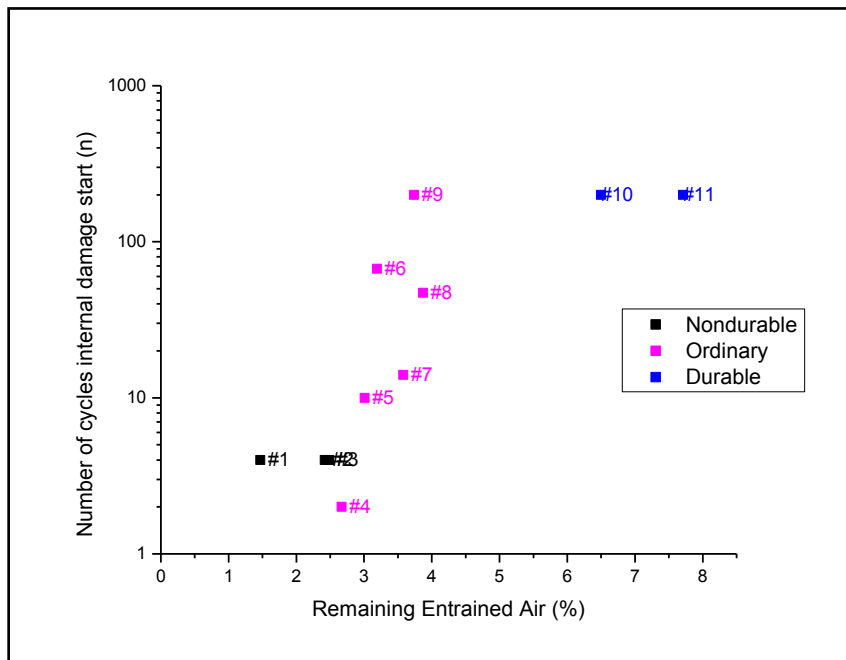


**Figure 4- 21 Scaling sensitivity to remaining entrained air (%)**

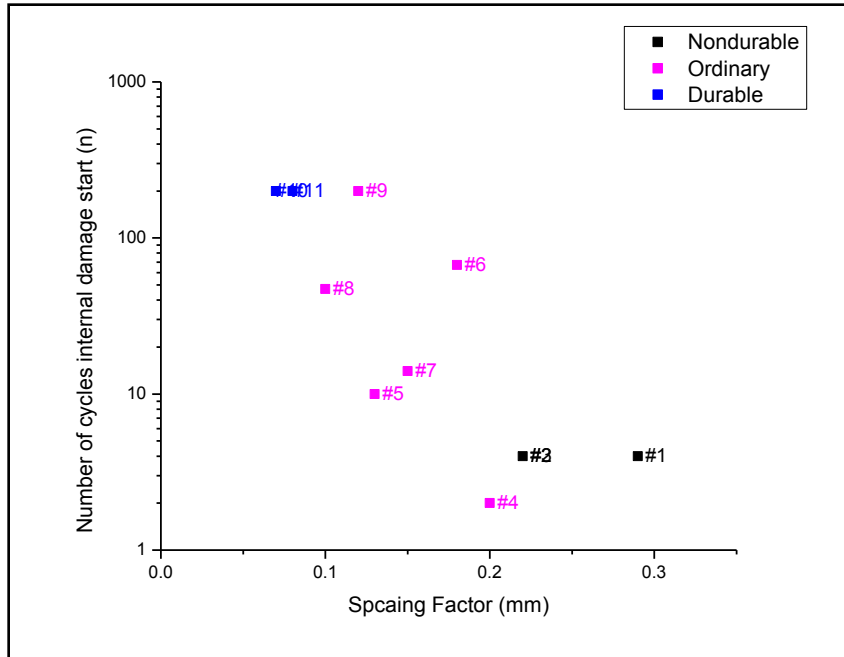




**Figure 4- 22 Scaling sensitivity to spacing factor (mm)**



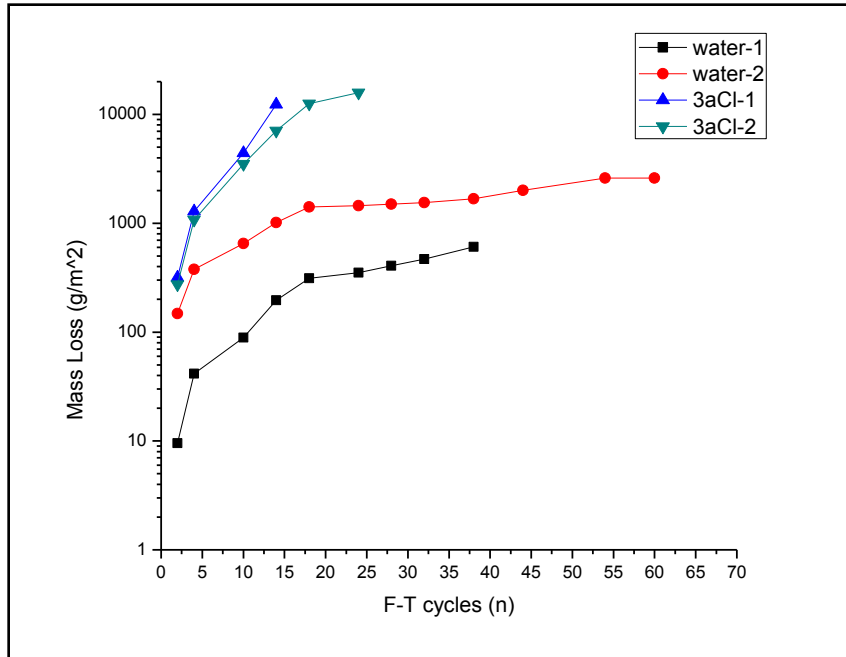
**Figure 4- 23 Internal damage versus entrained air content**



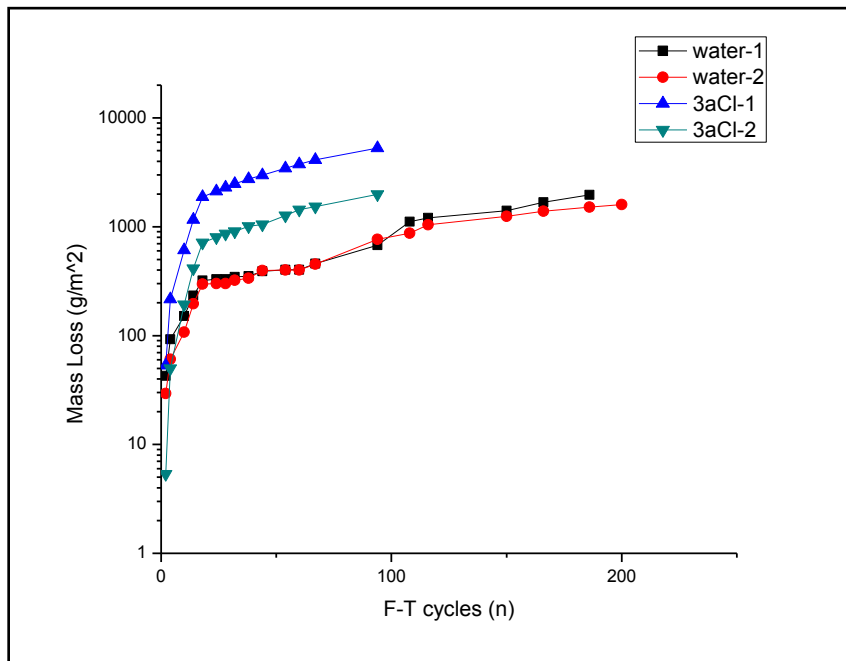
**Figure 4- 24 Internal damage versus spacing factor (mm)**

#### **4.3.4 Similarity in scaling mechanism between F-T testing in water and 3% sodium chloride solution**

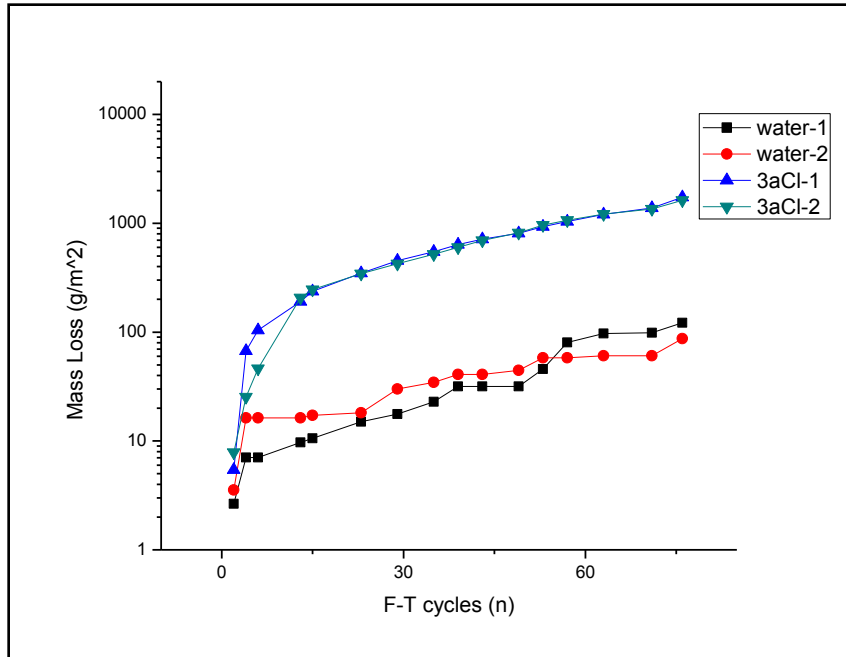
Figure 4.25 through 4.28 show that surface scaling occurs for both exposure conditions and that deicer scaling mass-loss is about 10 times as much as freezing in water. This suggests that the mechanism of surface deterioration is the same in 3% sodium chloride solution and in water. For these concretes the mass-loss is nearly linearly proportional to F-T cycle, except initially. Mass-loss data for duplicate specimens for the laboratory concrete specimens were found to have excellent reproducibility.



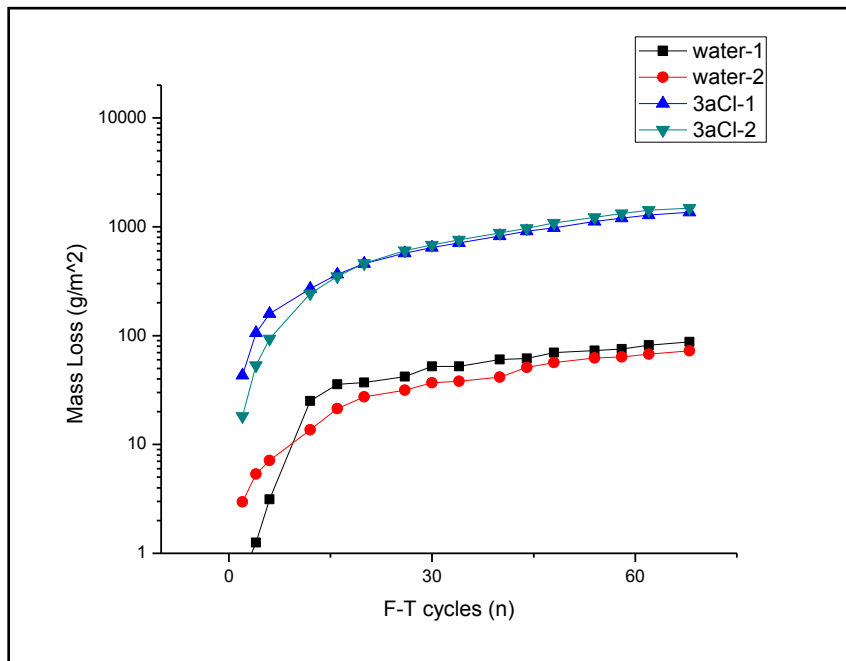
**Figure 4- 25 Surface scaling of specimen #1 in CIF and CDF test**



**Figure 4- 26 Surface scaling of specimen #6 in CIF and CDF test**



**Figure 4- 27 Surface scaling of specimen #10 in CIF and CDF test**



**Figure 4- 28 Surface scaling of specimen #11 in CIF and CDF test**

#### 4.4 SUMMARY OF FINDINGS

The objective of this chapter is to determine what characteristics of concrete contributed to frost durability in the field. In order to connect information on laboratory performance to field performance, 11 specimens cored from 11 different fields were categorized into three groups as 'Nondurable' (Severely damaged), 'Moderate' (Moderately damaged) and 'Durable' (Barely damaged). Then, the laboratory tests, air voids system analysis according to ASTM C 457, RILEM CIF-CDF and microscopic observations were carried out with the field specimens. The following findings and indications have been made:

##### Air voids system analysis

- Field performance seems to be closely correlated with air voids contents and properties. In the range of this study, nondurable concrete had less than 2.5% of entrained air content and over 200 micro meters of spacing factor while durable concrete had more than 6% of entrained air content and less than 100 micro meters of spacing factor.
- Durable concrete seems to have more entrained air frequency. The tendency is more significant in the classes of less than 50 micro meters chord lengths.
- Parts of air voids have been filled with white crystals. The amounts of infillings are in the range between 13% and 34% of total air contents. More air voids seem to have been filled in nondurable concrete. The hypothesis of infillings has been suggested.

### RILEM CIF-CDF Test

- Nondurable concrete specimens failed both in water and 3% sodium chloride solution within 20 freeze-thaw cycles in terms of internal damage while durable concrete successfully remained without any internal damage throughout 200 freeze-thaw cycles.
- Mass losses of nondurable concrete specimens exposed to 3% sodium chloride solution were extremely high during freezing-thawing cycles. Surface scaling rates per freeze-thaw cycle are proportionally related with air contents and spacing factors in this study.
- Surface scaling of specimens exposed to water had similar tendencies with that of specimens exposed to 3% sodium chloride although the scaling was much less severe.
- The number of F-T cycles of internal damage and the surface scaling rate seems to be proportionately correlated not only to the air voids system but also to each other.

# **CHAPTER 5**

## **MECHANISMS OF SURFACE SCALING**

### **5.1 INTRODUCTION**

In wet-freeze regions such as in the mid-west states like Michigan, Illinois, Wisconsin, Minnesota etc, concrete frost resistance in the presence of deicer salts is of major concern. Many researchers have suggested that pore pressure build-up due to freezing expansion of saturated pores in concrete can cause internal cracking within the porous paste. Sufficient amounts of entrained air with a spacing factor less than 200 micro meters can release the pore pressure successfully. As a result, excessive internal stress build-up in air-entrained concrete can be avoided through air-entrainment.

Deicer scaling is a surface scaling phenomenon associated with frost damage of a concrete surface layer in the case where the surface is exposed to a salt solution. Therefore, salt or surface scaling is another type of frost damage, which can be mitigated through air-entrainment. Typically, surface scaling in laboratory tests starts after only a few freeze-thaw cycles and progresses at an almost linear rate with F-T cycles. The detailed physical process that causes this phenomenon is still debated. In this Chapter, differences of freezing and thawing actions between bulk concrete and the surface concrete containing a liquid reservoir are suggested. In addition, an improved mechanism

and a qualitative surface scaling model are suggested.

## **5.2 EXISTING MECHANISMS**

Although the surface scaling is very significant in presence of deicing salt under freezing temperature, there is not a consensus of the actual mechanism. There are several existing mechanisms, the bi-material mechanism due to a coupling between the surface and the interior [30, 34], a salt crystallization induced pressure buildup [27] and hydraulic pressure in pores due to freezing expansion [25, 35].

### **5.2.1 Hydraulic pressure**

The 9% increase in volume as water transforms to ice can cause a hydraulic pressure. It is widely believed that frost damage is caused by this pressure. In fact, G. Fagerlund suggested the critical degree of saturation at which the destructive pressure can be created [12]. It is clear in this mechanism how the air voids help to protect the concrete matrix from hydraulic pressure and how the pressure can cause internal damages. However, it may take a long time to reach the critical degree of saturation by capillary suction. Max J. Setzer explains how cyclic freezing thawing accelerates the degree of saturation by the micro ice lens model [1]. This model still needs improvements because the surface scaling occurs within a couple of freeze-thaw cycles even when the degree of saturation stays under the critical saturation state at the end of the cycle.



## 5.3 CRYOGENIC SUCTION PUMP MECHANISM

### 5.3.1 Background

The freezing point of pore liquid varies with pore sizes. As the radius of liquid channel decreases, the freezing point is depressed. The relationship between liquid channel radius and the freezing point depression is shown in [23, 52].

$$r = \frac{2\gamma_{CL}}{\sum_m (T_m - T)} \quad (5.1)$$

Where,

$r$  = the radius of the pore where the current solid-liquid interface

$\gamma_{CL}$  = the crystal-liquid interface energy

$\sum_m$  = the melting entropy

$T_m$  = the melting point

$T$  = the temperature

In the equation 5.1,  $r$  is the radius of the smallest channels where the ice crystals can be formed at the temperature,  $T$ . Therefore, liquid in the pores and capillaries having smaller radius than  $r$  remains as liquid while the pores having a greater radius than  $r$  freezes.

Microstructures of porous materials such as concrete are comprised of gel-pores, capillaries and voids (entrained/entrapped air) of various sizes [1]. As a result, a triple phase zone consisting of ice, liquid, and vapor, coexist. Due to coexistence of different phases, a pressure difference is created at an interface between ice and liquid. An equation for these pressure differences was derived by Setzer as shown in the following

[1]:

The chemical potential  $\mu$  of any phase (index k) can be given by:

$$\mu_k = \mu_k(T_0, p_0) - \int_{T_0}^T s_k dT + \int_{p_0}^p v_k dp \quad (5.2)$$

with : k=[L,S,V]

Where,

P= pressure

v= the molar volume

S= the molar entropy

T= temperature.

The phases are liquid (L), solid ice (S), and vapor (V). The chemical potentials must be equal in all phases. The chemical potential can be separated by a temperature term

( $\int_{T_0}^T s_k dT$ ) and a pressure term ( $\int_{p_0}^p v_k dp$ ). The pressure term between ice and liquid is

given by:

$$\Delta\mu_{p,SL} = \mu_{p,S} - \mu_{p,L} = -v_L \Delta p_{LS} + (v_s - v_L)(p_s - p_0) \quad (5.3)$$

With  $\Delta p_{LS} = p_L - p_S$

The temperature term can given by:

$$\Delta\mu_{T,SL} = \mu_{T,S} - \mu_{T,L} = \int \Delta s_{SL} dT \quad (5.4)$$

With  $\Delta s_{SL} = s_S - s_L = \Delta s_{SLO} + \int_{T_0}^T \left( \frac{c_S - c_L}{T} \right) dT - (v_S \alpha_S - v_L \alpha_L)(p_S - p_0) + v_L \alpha_L \Delta p_{LS}$

Where,

$c$  = the specific molar heat capacity

$\alpha$  = the coefficient of thermal expansion

Temperature term (equation 5.4) should be balanced by the pressure term (equation 5.5) because the chemical potential must be equal in all phases. Therefore, pressure differences are created as the temperature drops below the bulk freezing point. The pressure difference can be given as follows [8]:

$$\begin{aligned}\Delta p_{LS} &= p_S - p_L \\ &= -\frac{1}{v_L} \int_{T_0}^T \Delta s_{SL} dT + \left( \frac{v_S}{v_L} - 1 \right) (p_S - p_0)\end{aligned}\quad (5.5)$$

Where,

Index S= Solid

Index L= Liquid

$v$  = the molar volume

T= Temperature

Index 0= the bulk values at triple point where the chemical potentials of all three-bulk-phases are equal.

The equation can be expressed approximately:

$$\Delta p_{LS} = \frac{\Delta s_{SLO}}{v_L} \left( (T - T_0) + \left[ \frac{c_S - c_L}{T_0 \Delta s_{SLO}} - \alpha \right] \frac{(T - T_0)^2}{2} \right) \quad (5.6)$$

The pressure difference can cause artificial suction as driving forces. Assuming a linear pressure gradient and saturated flow, Ficks' first law applies [25]:

$$\frac{dp}{dx} = \frac{g}{\delta_p} \quad (5.7)$$

Where,

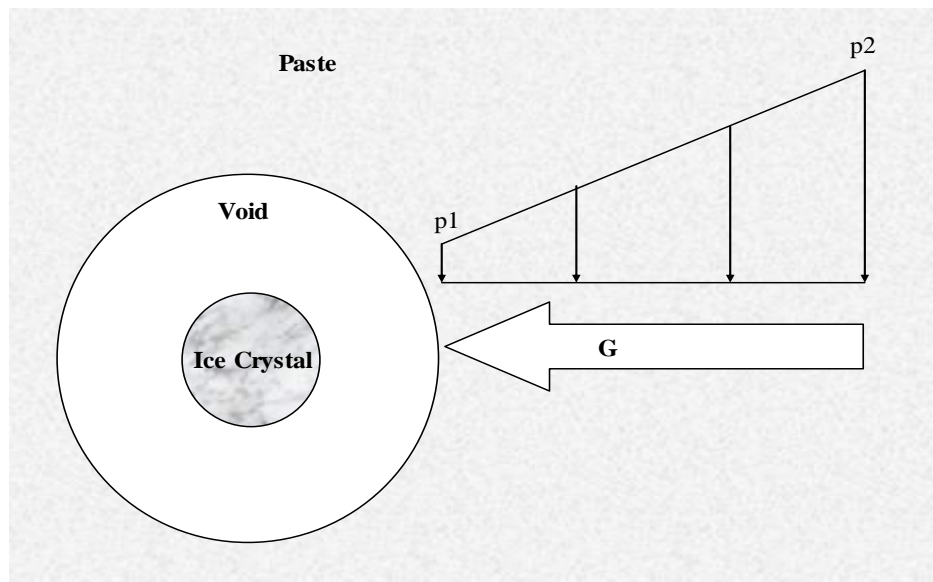
$dp$  = pressure difference in Pa

$dx$  = flow travel length to void where the pressure is released

$g$  = transport rate in  $(kg/(m^2s))$

$\delta_p$  = vapor diffusivity of permeability in  $(kg/(mPas))$

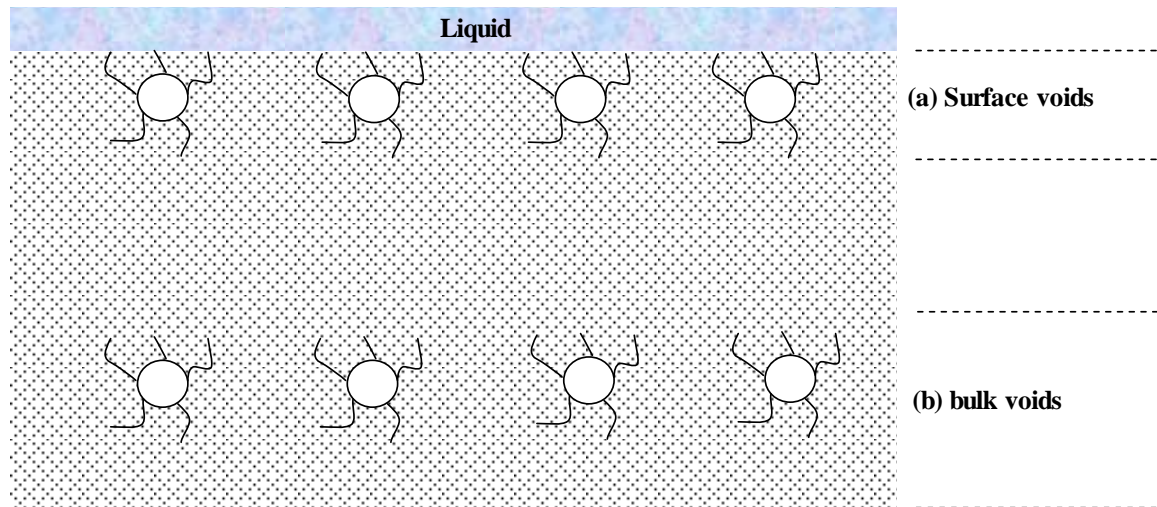
Figure 5.1 illustrates this case.



**Figure 5- 1 Pressure difference and liquid and vapor flow toward an ice crystal**

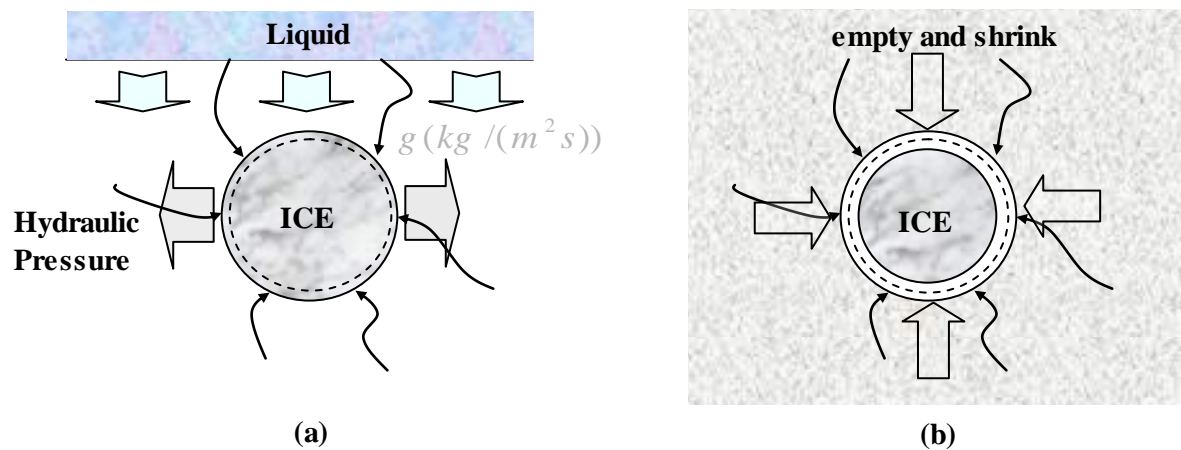
### **5.3.2 Local Frost Actions**

As shown above, when saturated concrete undergoes freezing, pressure differences and liquid transport toward ice crystals in air-voids are generated. Consequently, the degree of saturation can approach a critical value for a given paste system, which causes destructive hydraulic pressure [38]. However, capillary pores and voids just below the surface should be considered separately from voids and pores further below the surface as surface pores and voids are directly connected to the surface liquid through channels. See Figure 5.2



**Figure 5- 2(a) Surface voids (b) bulk voids**

Thus, liquid flow develops between the surface liquid and surrounding near-surface capillaries towards ice crystals while ice crystals further below the surface can empty and shrink. See Figure 5.3.



**Figure 5- 3 a) Frost Action in coarse pores or voids underneath the surface, (b) Frost Action far below the surface**

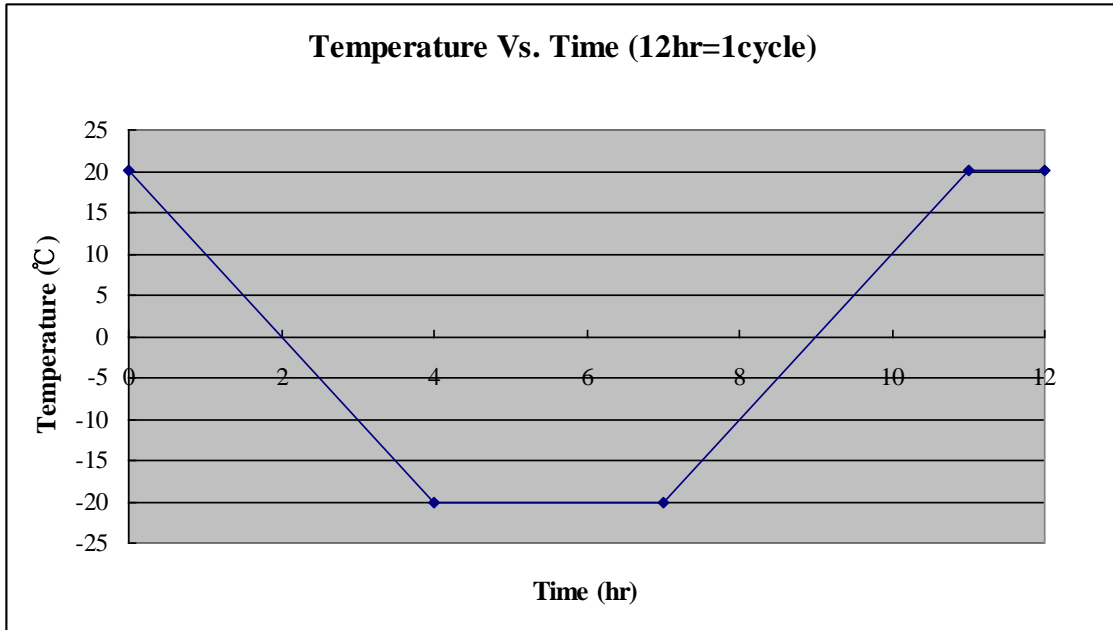
The small pores and capillaries at the surface are refilled with outer liquid if unfrozen liquid is available on the surface (Figure 5. 3 (a)). The ice crystals keep growing while the temperature stays under the freezing point. The voids far below the surface are not

connected with surface liquid directly so the small pores and capillary around ice crystals are dried and contracted (Figure 5. 3 (b)). As the coefficient of thermal expansion (CTE) of ice is much larger than concrete's CTE, the hydraulic pressure is modified by the shrinking of the ice volume so as the temperature drops it tends to lessen the effect of the ice-pressure buildup. The hydraulic pressures in the surface pores are then a balance of the two effects and it can be reduced by proper air-entrainment content to act as a buffer, consequently improving the surface scaling resistance. The amount of air-entrainment needed depends on the concrete surface density and number of liquid channels. Also the microstructure of concrete is not homogeneous. Surface scaling initiates in the largest pores, either ITZ pores or air-voids. [2,3,4]

## **5.4 EXPERIMENTAL STUDIES**

### **5.4.1 Low Temperature Dilatometer Test**

This freeze-thaw test method is a cyclic process subjecting the sample to repeated freeze-thaw periods. A 12h freeze-thaw cycle is applied. Starting at +20°C the temperature is lowered in 4h with a constant cooling rate of 10K/h. It is kept constant for 3h at -20°C and increased in 4h with a constant heating rate of 10K/h and finally kept constant for 1h at +20°C [1]. The temperature profile is shown in Figure 5.4.



**Figure 5- 4 Temperature Profile for LTD test**

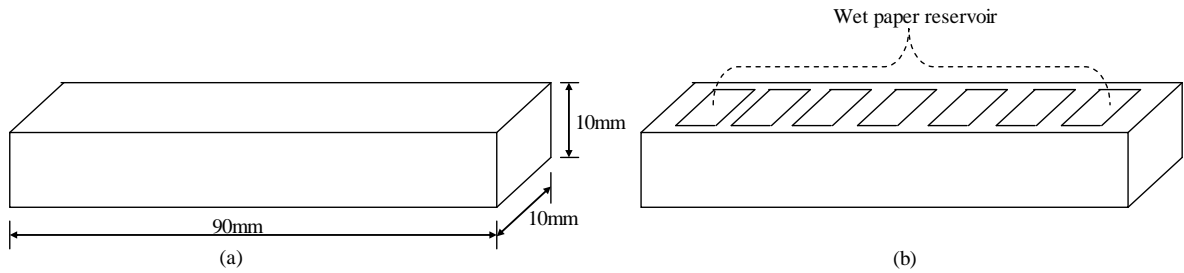
To measure the length change during freeze-thaw cycles, a Low Temperature Dilatation (LTD) apparatus was used. These measurements are performed to glean additional information from the overall process.

#### **5.4.2 Specimen Preparation and Pre-saturation**

A typical specimen is made as a prism with dimension of 90mm\*10mm\*10mm by sawing and stored in an oven at  $50 \pm 5C^{\circ}$  until the evaporable water in the specimen is dried up so that the mass is not changed. Then the specimen is placed in contact with a test liquid for pre-saturation (Figure 5. 6) . The weight gain by moisture uptake is monitored and plotted versus square root time as shown in Figure 5. 8. The temperature profile for 1 F-T cycle is same as the CIF-CDF test profile shown in Figure 5. 4. Two different test liquids (de-mineralized water and 3% NaCl Solution) are used and the LTD tests have been carried out with and without surface liquid (Figure 5. 5). The LTD test

without surface liquid represents the frost action of bulk concrete far below the surface and those with liquid represent a deicer surface scaling exposure test.

Soaked paper towels are placed on the top surface in order to provide a surface liquid reservoir. Then, the LTD prism is wrapped with plastic foil in order to avoid drying during the test (Figure 5. 7)



**Figure 5- 5(a) LTD test prism without surface liquid reservoir, (b) with surface liquid reservoir**



**Figure 5- 6 Pre-Saturation**



**Figure 5- 7 Complete specimen**



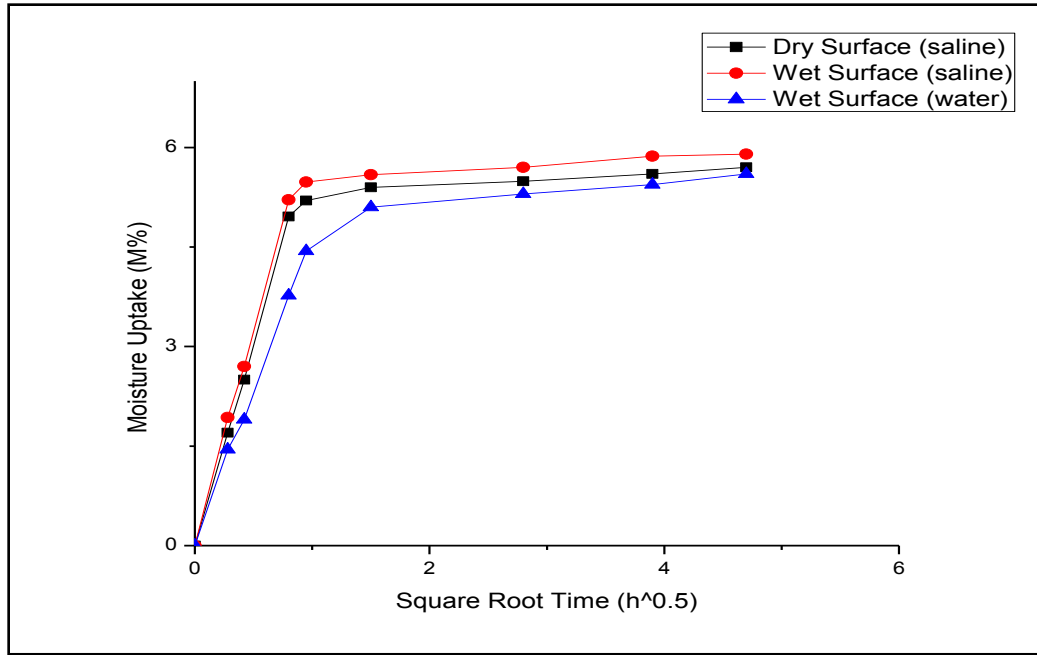


Figure 5- 8 Moisture uptakes during pre-saturation

### 5.4.3 Results and discussion

#### 5.4.3.1 Specimen conditioning prior to F-T exposure.

Case 1: Pre-conditioning in water and surface liquid (Water) during F-T testing.

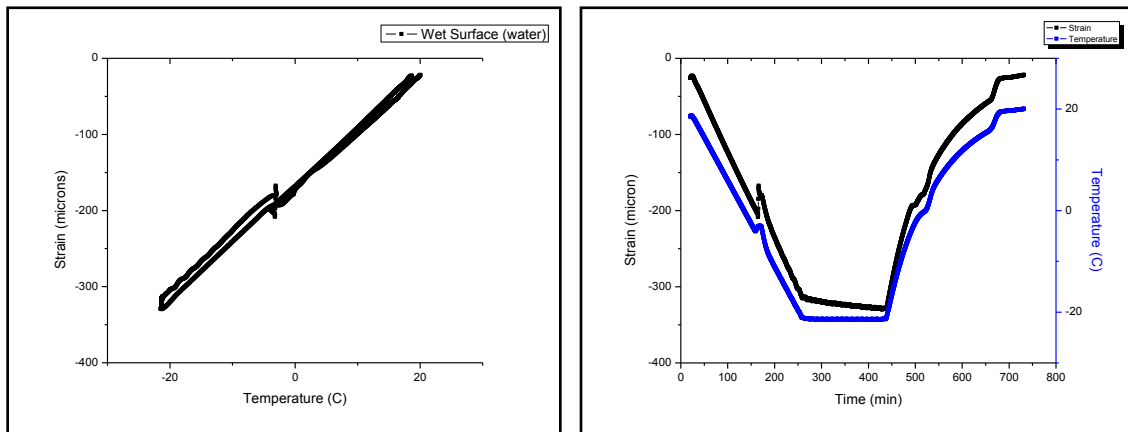
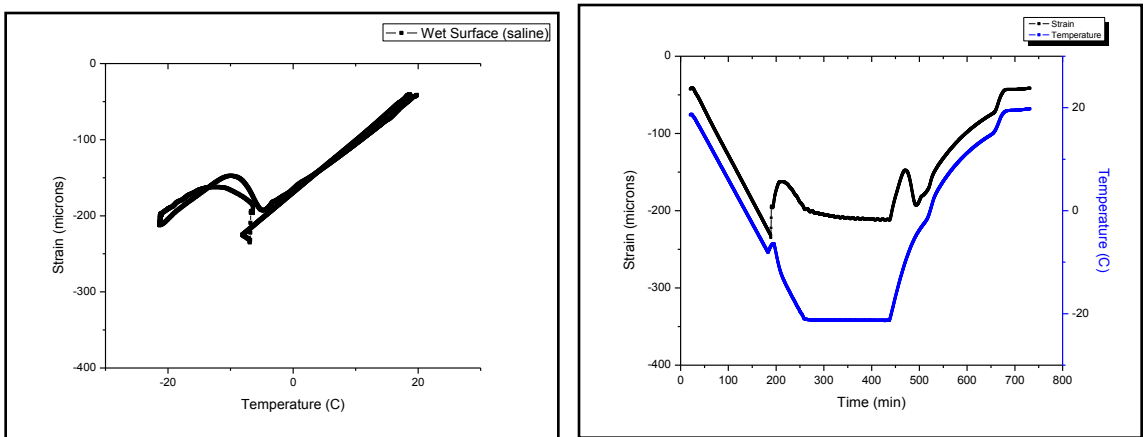


Figure 5- 9 LTD test results for field specimen #6 with surface liquid (de-mineralized water)

When the pore liquid freezes the expansion occurs, but after further freezing the specimen contracted at the rate of the concrete matrix. In this case since the liquid on the surface also freezes no liquid is able to add to the internal ice formation. Since no additional ice was formed inside the pores and voids there is no significant influence from the melting process except to see that the expansion of the ice-matrix combination is higher than the expansion of the liquid-matrix combination per degree of temperature rise.

**Case 2: Pre-conditioning in 3% NaCl solution and surface liquid (3% NaCl solution ) during F-T testing.**



**Figure 5- 10 LTD test results for field specimen #6 with surface liquid (3% NaCl solution)**

As shown in Figure 5.10 a much larger and broader expansion develops during first freezing. As opposed to case 1 (Figure 5.9) the expansion increases after freezing starts. The rate of strain reduction does relax towards the matrix reduction but tapers off to a constant level as the lower temperature limit (-20C) is reached. This indicates that ice continues to form in the pores. However, this process is counter-balanced by the shrinking of the ice volume as the temperature drops. During the constant temperature

period only small strain changes take place. During the heating period the ice expands more than the concrete matrix putting a stress on it, this expansion slowly disappears as the ice melts causing a contraction and after the melting process is complete it reverts to the thermal expansion of the combined system.

### Case 3 Dry Surface Versus Wet Surface (water or 3% NaCl).

The test results from the three different cases are compared in Figure 5. 11 and 5. 12. The three cases are nearly identical during the part of the process where water is in the liquid phase that is before it freezes during the cool down and after it melted in the heat-up period.

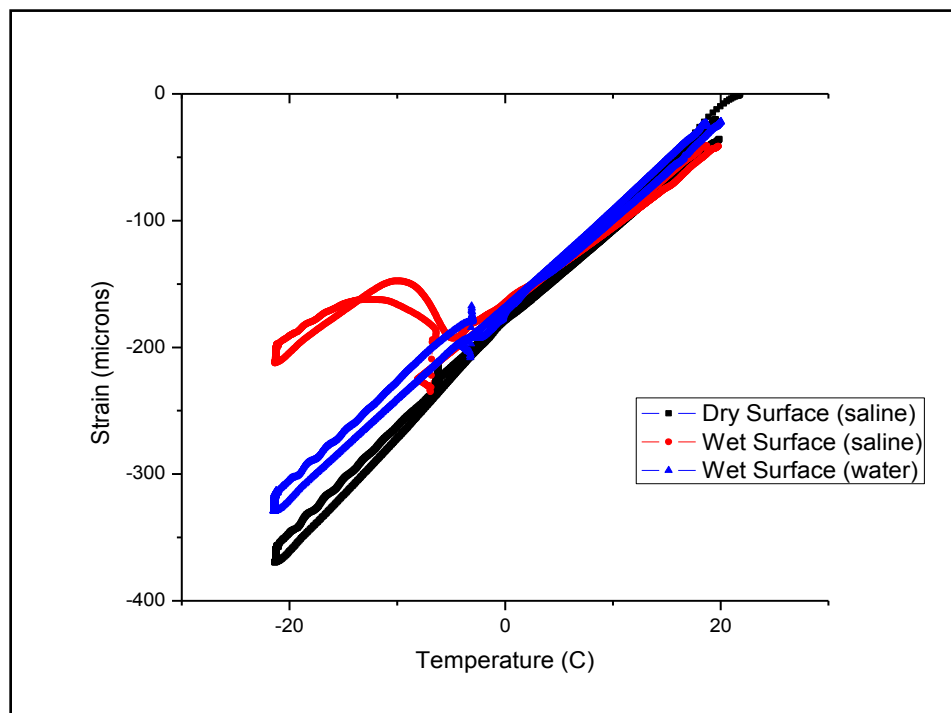
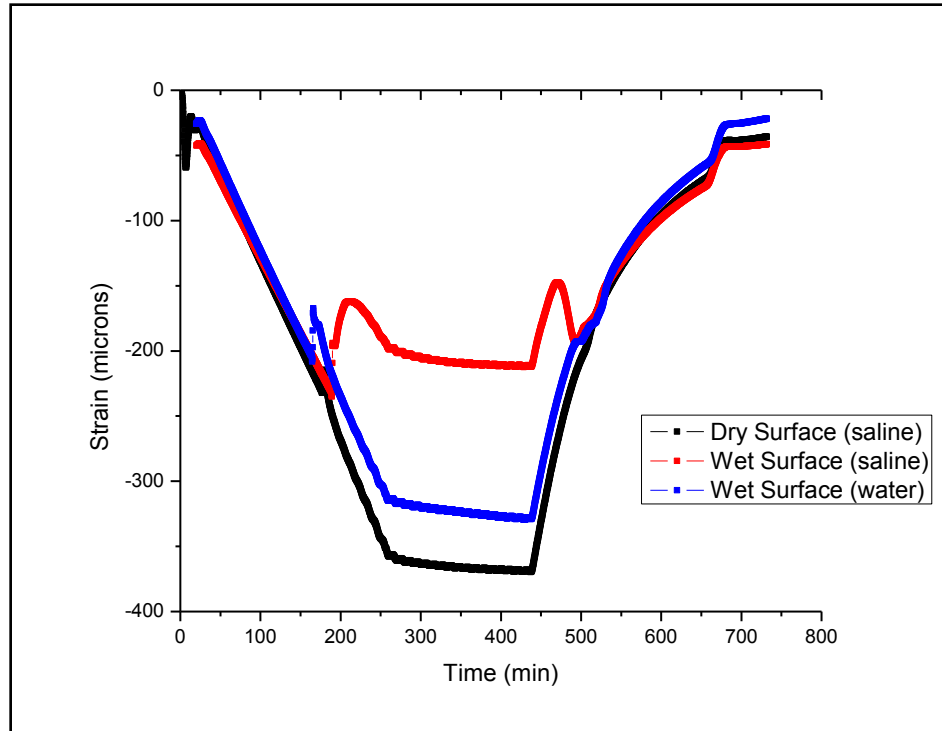


Figure 5- 11 Dilatation VS Temperature during Freezing Thawing (#6)



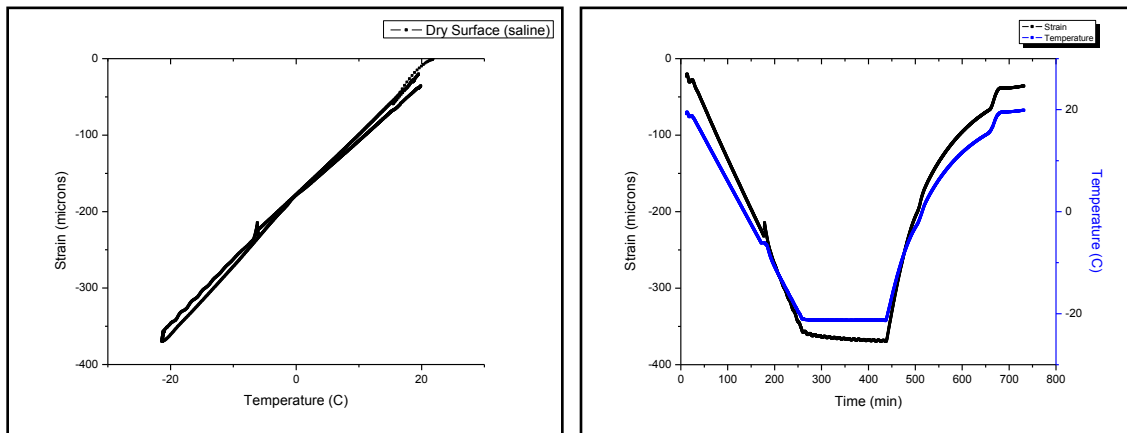
**Figure 5- 12 Dilatation VS time during Freezing Thawing cycle (#6)**

However there are relatively large differences among three test conditions during the freezing temperature range. When the test liquid is a 3% NaCl solution and surface liquid is available the difference of the combined expansion is about 200 microns compared to the case of no surface liquid and 170 microns when the test liquid is water. It is noticed that in the case of pure water the ice formation does reduce the total shrinkage of the specimen by about 50 microns compared to the dry surface and salt solution in the pores. Since the salt solution stays as a liquid longer it is squeezed out of the smaller pores into larger pores and voids. As some of the water forms ice the remaining solution becomes stronger in salt concentration with a further reduction in its freezing temperature.

**Case 4: Capillary pore-saturation with 3% NaCl solution Pore liquid without surface liquid**

Field Specimen #6 has average frost durability. First, the specimen was stored in 3%

NaCl solution for a day. The moisture uptake (M%) was 5.7% and the LTD test was carried out without surface liquid.



**Figure 5- 13 LTD test results for field specimen #6 without surface liquid (3% NaCl solution)**

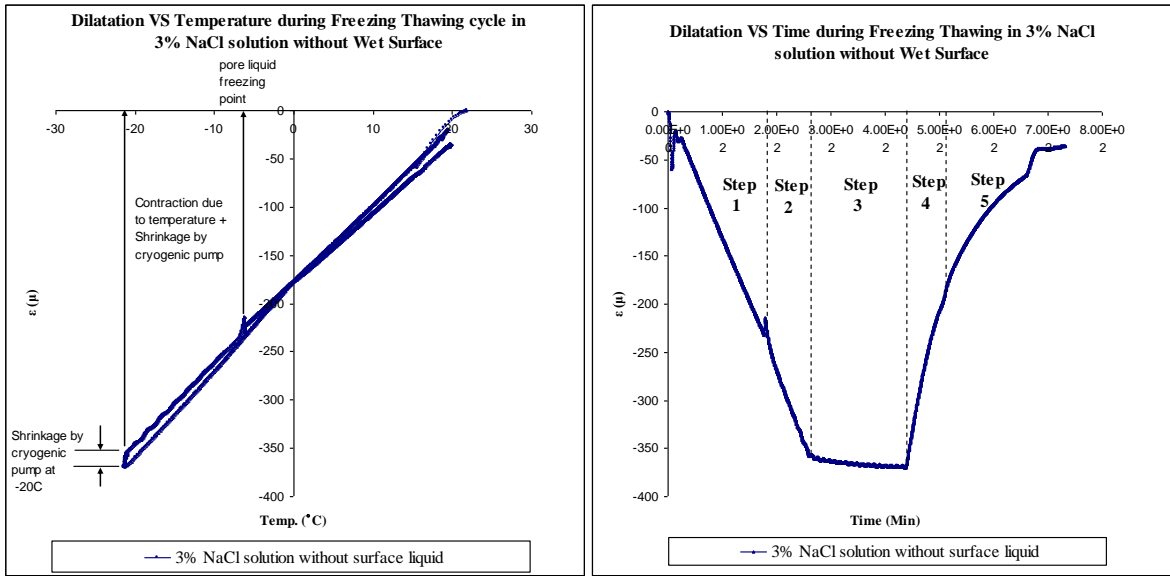
As shown in Figure 5.13, an expansion occurred when the pore liquid froze at about -6C. However, upon further cooling the ice formed in the pores contracts more than the matrix due to the higher CTE of ice. Thus, the pore-pressure is decreasing quickly upon further cooling, and the overall specimen contraction reduces to the one for the matrix. This indicates that the ice has enough available volume and the hydraulic pressure from the ice does not increase the volume. The second observation is that there is only a gradual effect of the melting process (volume reduction of the water) during the warm up period.

## 5.5 QUALITATIVE SEQUENTIAL SURFACE SCALING MODEL

### 5.5.1 When there is no outer liquid reservoir on surface

As the temperature decreases, the concrete contracts. If the concrete is saturated it

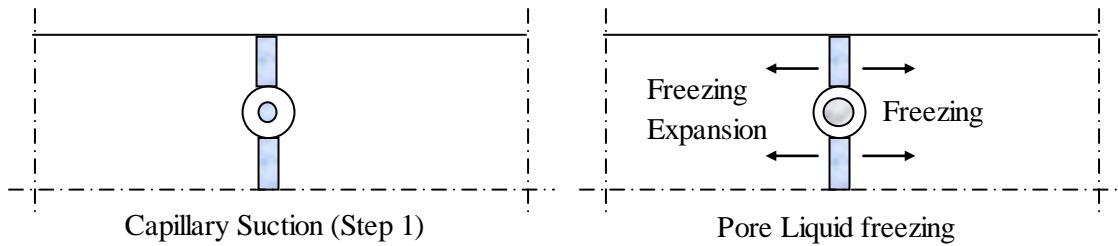
would expand when the pore liquid freezes. This expansion will be diminished because the ice contracts more than concrete as the temperature decreases. The pore liquid expansion will not cause a critical damage until the degree of saturation reach a critical point.



**Figure 5- 14 Dilatation curves without surface liquid**

**5.5.1.1 20°C to freezing point (Step 1) and Freezing point (Pore liquid freezing)**

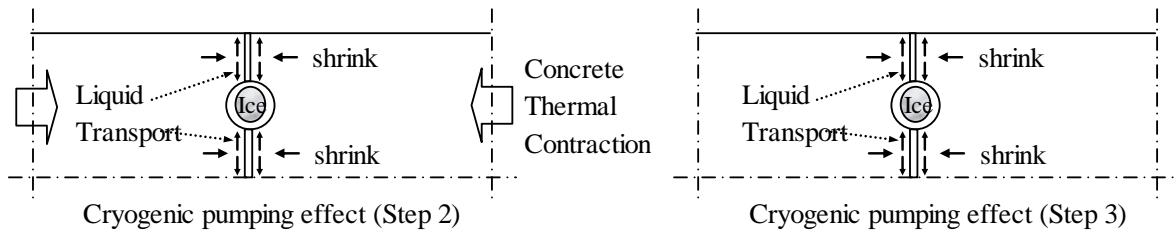
Step 1 shows the concrete specimen contracts as temperature decreases before the pore liquid freezes. When temperature drops under freezing point ice crystals are created and concrete specimen expands instantly.



**Figure 5- 15 Step 1 and Pore liquid freezing**

**5.5.1.2 Freezing point to  $-20^{\circ}\text{C}$  (Step 2) and Isothermal at  $-20^{\circ}\text{C}$  (Step 3)**

As temperature decreases As temperature decreases below the freezing point concrete specimen contracts and it shrinks as pore liquid transport toward ice crystal in the larger pores and air voids (Step 2). When temperature stays at  $-20$  thermal contraction stops but shrinkage by pore liquid transport is still working (Step 3) but it is a slow process leading to only minor shrinkage.

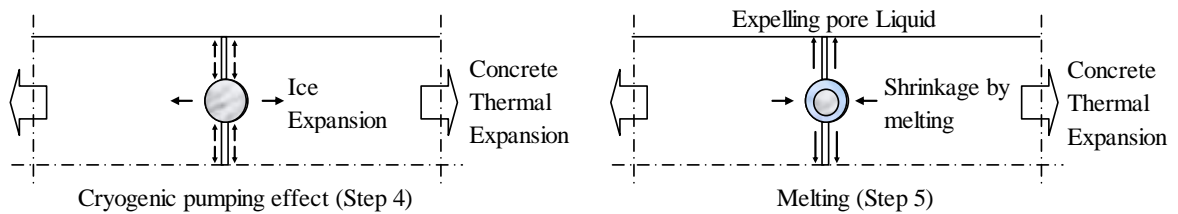


**Figure 5- 16 Step 2 and Step 3**

**5.5.1.3  $20^{\circ}\text{C}$  to melting point (Step 4) and melting point to  $20^{\circ}\text{C}$  (Step 5)**

The thermal coefficient of ice is larger than that of concrete, so the ice expands more than the concrete creating a higher pressure on the concrete wall until the temperature rises up to the melting point. Thus, the thermal expansion of concrete is affected by that of ice (Step 4). When the temperature reaches the melting point, the high pore pressure from the over expanded concrete is squeezing the melting liquid out (step 5) so the

thermal expansion is less than Step 4.

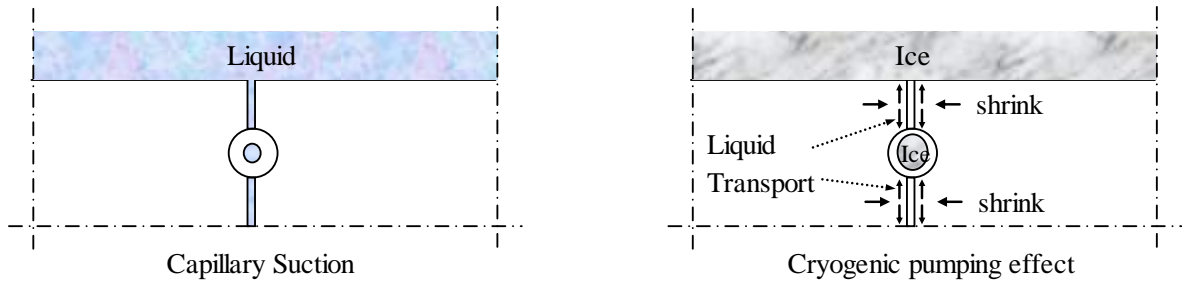


**Figure 5- 17 Step 4 and Step 5**

### 5.5.2 When there is a water reservoir on the surface

Surface pores connect to the outer liquid reservoir through channels depending on porosity and density. The source of liquid transport in bulk concrete is porous liquid in the vicinity of the larger pores. However, as liquid is transferred to the larger pores and voids the surface liquid is drawn into the porous structure keeping the transport process active. If surface liquid is not totally frozen after ice crystal is created in surface pores the liquid will transfer towards surface pores where the chemical potential is smaller. Then the degree of saturation of the surface pores will reach to a critical point locally depending on porosity and density. When pore ice crystal melts excess liquid will be pushed out because the high pore pressure and the surface concrete shrinks. In the most freeze thaw test methods the weight and the length changes are measured before freezing thawing cycle starts and after the cycle ends. With that data we cannot know what happens during the freezing and what differences accelerate the surface damages in presence of de-icing salt compared to pure water.



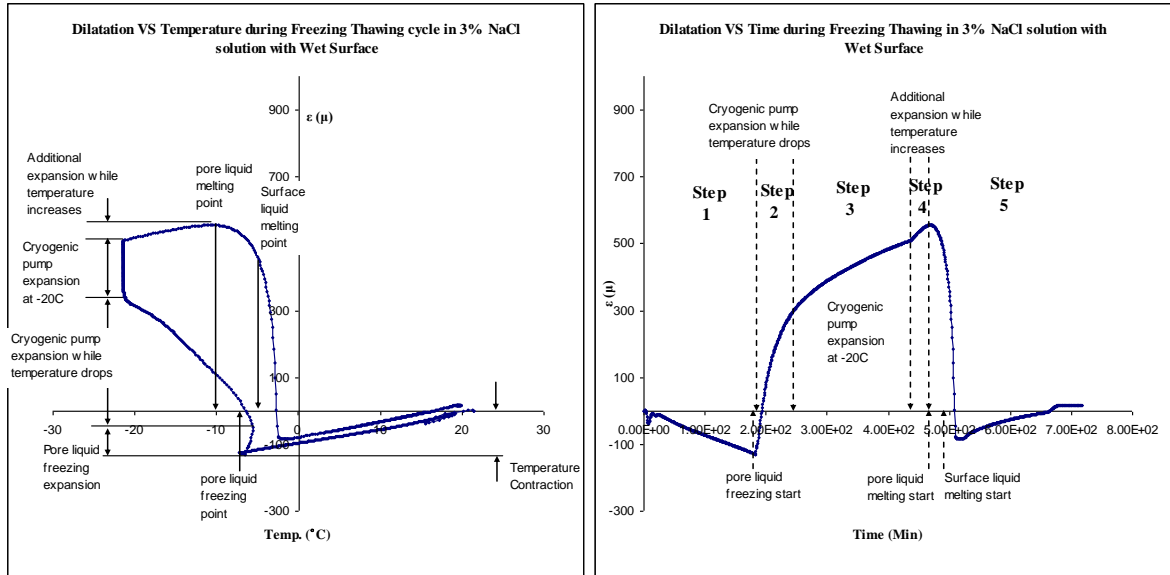


**Figure 5- 18 Capillary Suction and Cryogenic pump effect**

As shown in Figure 5. 18 capillaries and some of the voids and pores are filled with liquid within surface material. After temperature drops below the freezing point, surface liquid freezes instantly and micro ice crystals are created in the voids or the pores. After ice crystals form inside the structure, the ice crystal starts attracting available liquid. However, in case of pure water the outer liquid reservoir will be totally frozen before ice crystals forms inside.

### **5.5.3 When there is a de-icing salt solution reservoir on the surface**

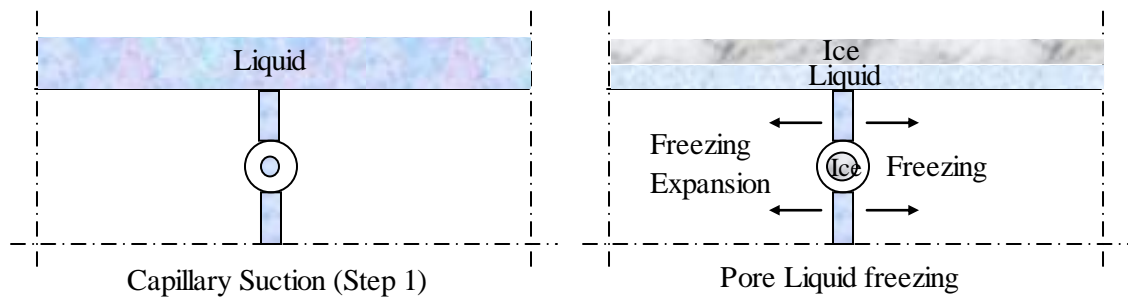
When the surface liquid is a salt solution or any other de-icing solution the liquid is not frozen instantly. Some part of it remains in the liquid phase below the first freezing point as water is removed the remaining solution becomes stronger lowering the freezing point.



**Figure 5- 19 Dilatation curves with surface liquid (3% NaCl solution)**

### 5.5.3.1 20 $^{\circ}\text{C}$ to freezing point (Step 1) and Freezing point (Pore liquid freezing)

Thermal expansion and pore liquid freezing expansion are very similar to the previous case up to the point where micro ice crystals are created in the pores.

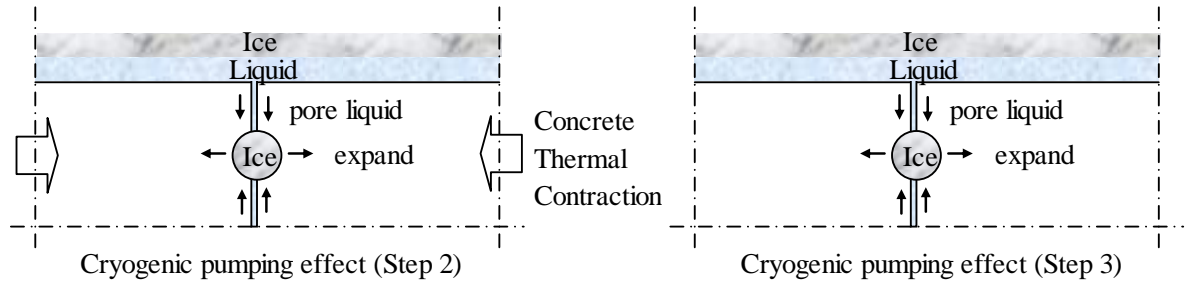


**Figure 5- 20 Step 1 and Pore liquid Freezing**

### 5.5.3.2 Freezing point to -20 $^{\circ}\text{C}$ (Step 2) and Isothermal at -20 $^{\circ}\text{C}$ (Step 3)

Once pore liquid is frozen the ice crystals start attracting unfrozen liquid from the surrounding structures. Surface pores are connected to surface liquid by capillary and

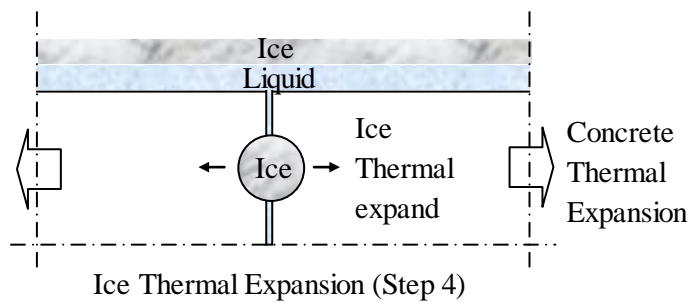
surface liquid is available down through Step 2 and Step 3. As temperature decreases cryogenic pumping effect increases (Step 2). Even when temperature stays at  $-20^{\circ}\text{C}$  the expansion keeps growing by cryogenic pump (Step 3).



**Figure 5- 21 Step 2 and Step 3**

#### 5.5.3.3 $-20^{\circ}\text{C}$ to melting point (Step 4)

Additional expansion occurs when the temperature increases up to the melting point because the thermal coefficient of ice is larger than that of concrete. Because degree of saturation already reached to very high point by cryogenic pump the additional expansion can be critical (Step 4).

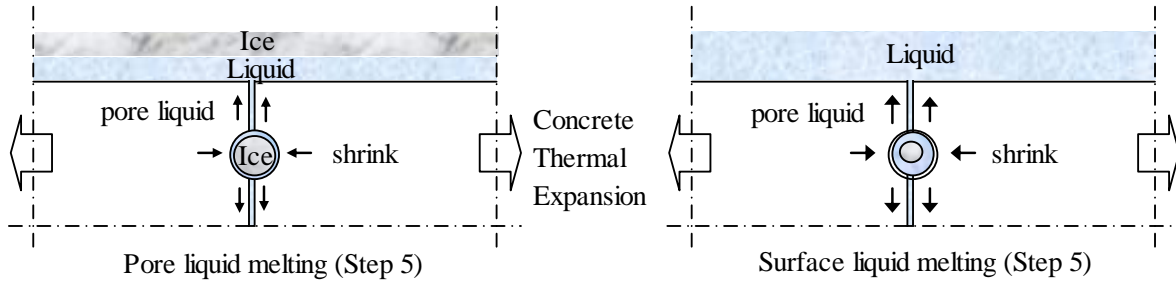


**Figure 5- 22 Step 4**

#### 5.5.3.4 Melting point to $20^{\circ}\text{C}$ (Step 5)

Ice crystals in pores starts melting before surface ice starts melting because pore ice crystals

are under extremely high pressure. When pore ice starts melting, the specimen shrinks slowly by expelling pore liquid even though the thermal expansion of concrete itself occurs. After temperature raises more so that surface ice melts, the rate the expelling pore liquid increases. Thus, the specimen shrinks so quickly (Step 5).



**Figure 5- 23 Step 5 when pore ice crystals start melting and Step 5 when surface ice starts melting**

## 5.6 Conclusions

There seems to be a limitation to improve surface scaling resistance because there is not a consensus regarding the mechanism involved. In fact, there are opposite opinions about the benefits of entrained air and GGBFS to surface scaling resistance.

The existing mechanisms were reviewed .. The salt crystallization mechanism seems to conflict with the fact that surface scaling is more severe with low-concentration salt solution. In addition, destructive hydraulic pressure is created after the degree of saturation reaches the critical point while surface scaling occurs during early freeze-thaw cycles.

Therefore, improved mechanisms of surface scaling were suggested based on the micro-ice-lens [1] and the flow by the hydraulic pump in wet concrete [2]. These mechanisms seem to fit well with frost actions during freeze-thaw cycles. The

mechanisms were supported by the LTD test results with various test conditions such as test liquid concentrations and the presence of surface liquid.

# **CHAPTER 6**

## **FLOW AND EXPANSION BY CRYOGENIC PUMP EFFECT**

### **6.1 INTRODUCTION**

The degree of saturation of surface concrete keeps increasing in pores or air voids by cryogenic pump effect as temperature drops down under freezing point. When the degree of saturation reaches to a certain point, destructive pressure would be created. The flow rate is related with the microstructure of concrete paste. In addition, if there are enough surfaces to store the inward flow, the expansion by cryogenic pump and consequently surface scaling can be reduced. In this chapter, relationships among flow rates, air voids, expansion during freezing and surface scaling have been studied so that more information for durable concrete can be provided. To identify surface scaling mechanism, dilatation test during freeze-thaw cycles were carried out with two different test liquids (de-mineralized water and 3% NaCl solution) and with and without surface liquid reservoir.

## 6.2 PORE PRESSURE DIFFERENCES AND DIFFUSION IN CONCRETE

Stefan Jacobsen has suggested in his research linear pressure gradient and saturated flow as following using Fick's first law [42].

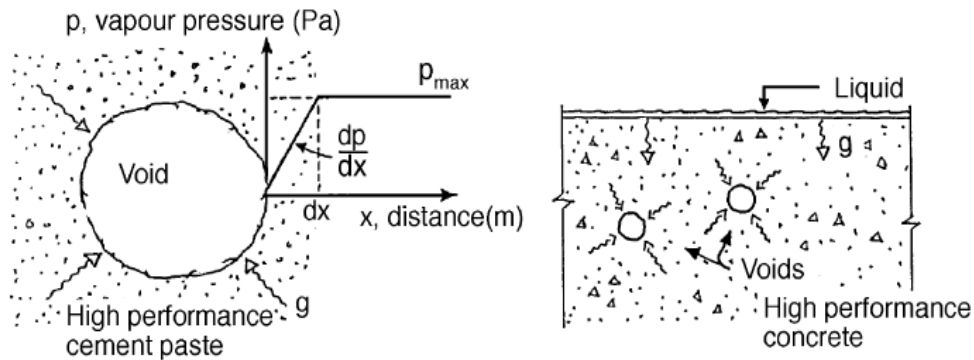
$$\frac{dp}{dx} = \frac{g}{\delta_p} \quad (6.1)$$

Where,  $dp$  (Pa) : Pore pressure difference

$dx$  (m) : length from saturated paste to void where pressure is released

$\delta_p$  (kg/(mPas)) : vapor diffusivity or permeability

$g$  (kg/(m<sup>2</sup>s)) : transport rate.



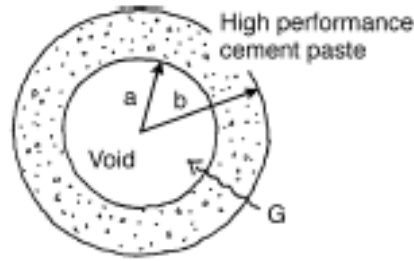
**Figure 6- 1 Vapour flow from saturated Hardened Concrete Paste towards void [41]**

Assuming  $g$  and  $\delta_p$  are constant,  $dp$  increases as  $dx$  increases. The transport into concrete during wet freeze-thaw exposure has been calculated by Crank [43].

$$G = 4\pi\delta_p \frac{ab}{b-a} \Delta p \quad (6.2)$$

Where,  $G$  (kg/s) : flow rate into the void

$\Delta p$  (Pa) : the vapor pressure difference over the shell (b-a)m (See Figure 6.2.)



**Figure 6- 2 Diffusion into an air void with a shell of cement paste [43]**

As shown in Figure 6.2, we can consider  $b-a$  as spacing factor ( $\bar{L}$ ) and  $a$  as the radius of void ( $\bar{r}$ ). The transport can be calculated as flow into a void of radius  $\bar{r}$ .

$$G = 4g\pi\bar{r}^2 \quad (6.3)$$

By Equation (6.2) + Equation (6.3)

$$g\bar{r}^2 = \delta_p \frac{ab}{b-a} \Delta p = \delta_p \frac{\bar{r} \cdot (\bar{r} + \bar{L})}{\bar{L}} \Delta p \quad (6.4)$$

Then, stationary transport into an air voids during Freezing Thawing cycles by cryogenic pump effect is

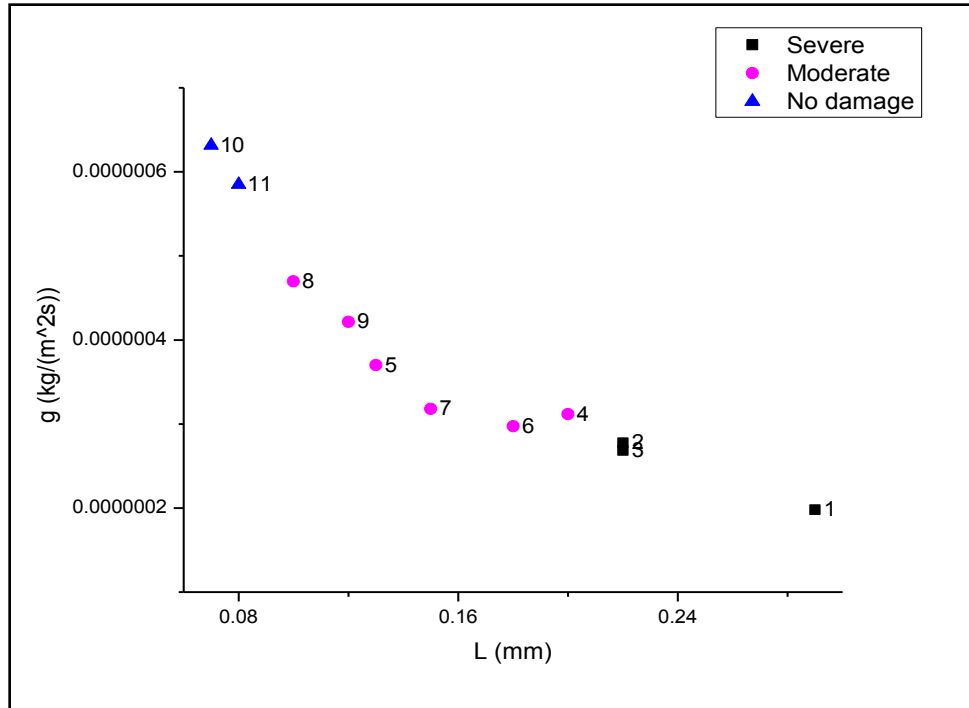
$$g = \delta_p \Delta p \frac{\bar{r} + \bar{L}}{\bar{r} \cdot \bar{L}} \quad (6.5)$$

The average radius of air voids and spacing factors of the field specimens are shown in Table 4.1. Assuming  $\delta_p$ , diffusivity, and  $\Delta p$ , pressure difference are constant,

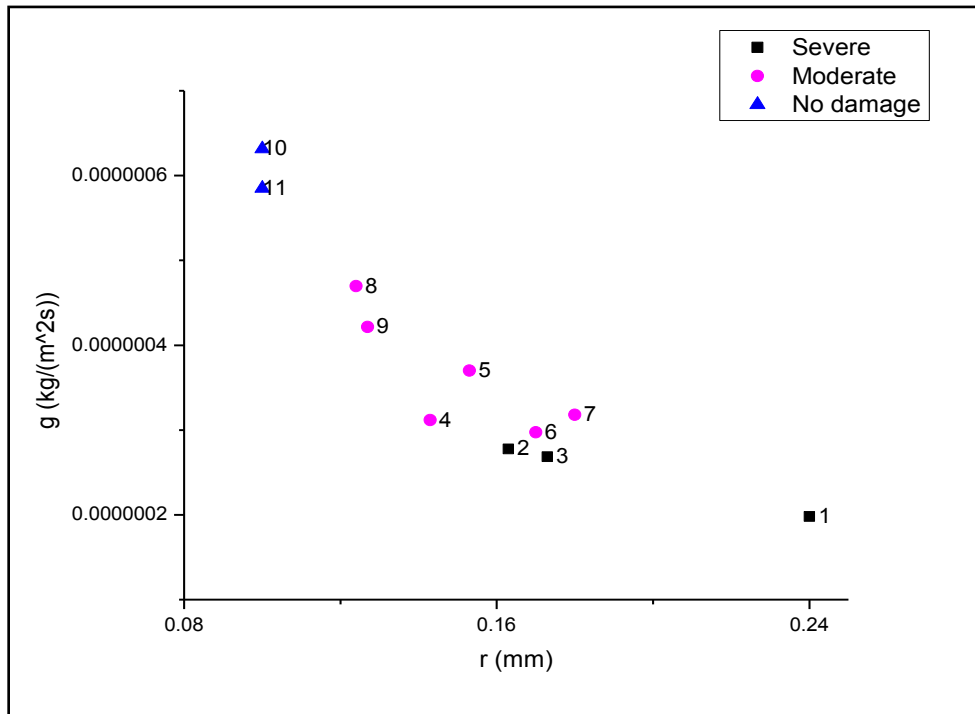
$g$  ( $kg/(m^2s)$ ) transport rate can be calculated using voids characteristics in Table 4.1.

Figure 6.3 and Figure 6.4 show the transport rate of field specimen.



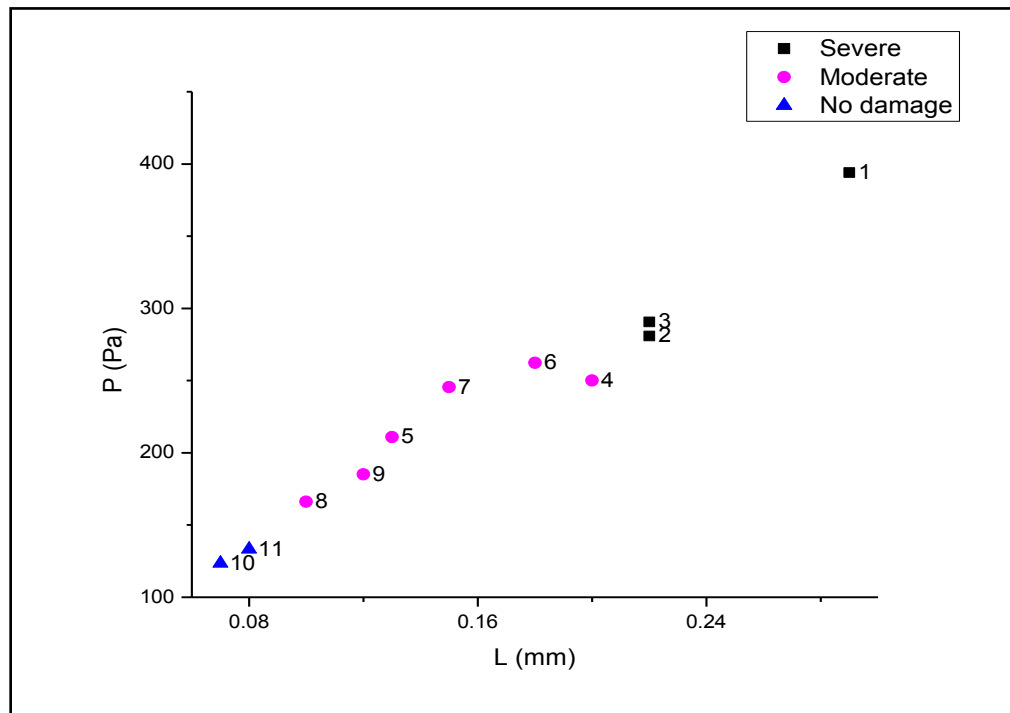


**Figure 6- 3 Transport rate into an air void (average radius) by cryogenic pump VS. Spacing Factor**

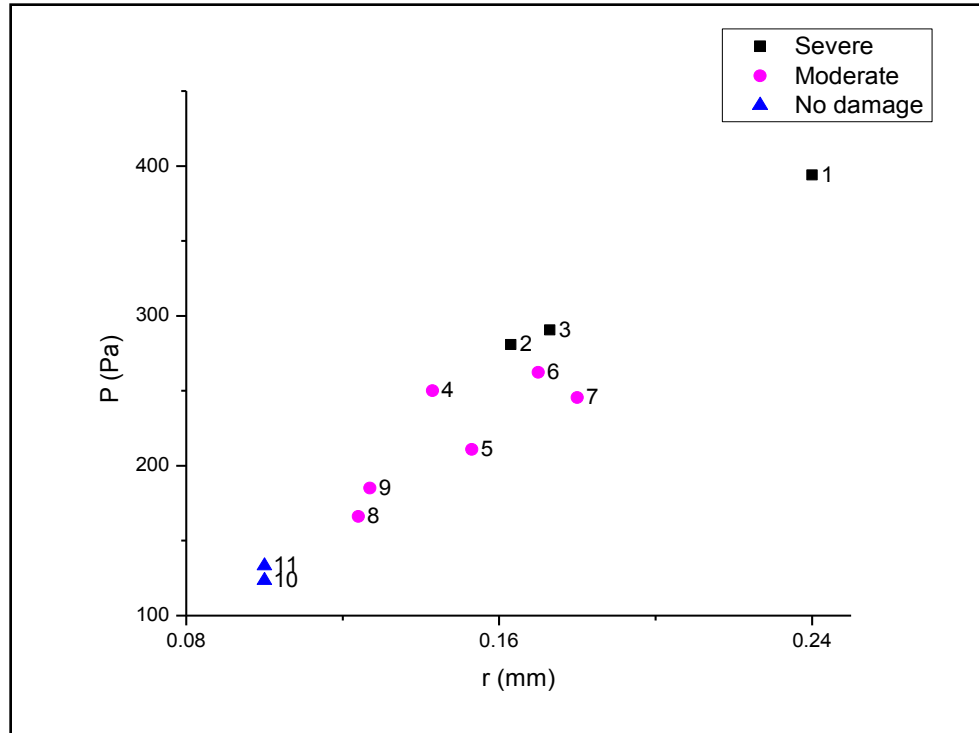


**Figure 6- 4 Transport rate into an air void by cryogenic pump VS. Average Void radius**

As shown in Figure 6.3 and Figure 6.4, Good scaling resistance concrete specimens (#10 and #11) need 3 times higher transport rate to create similar pressure difference compared with poor scaling resistance concrete specimens (#1, #2 and #3). If we can assume the transport rates are constant, the pressure differences can be calculated using the given information. Figure 6.5 and Figure 6.6 show the pressure differences of field specimens as function of void characteristics for  $g = 3.0 \times 10^{-7}$ .



**Figure 6- 5 Pressure differences of field specimens by cryogenic pump VS. Spacing Factor**

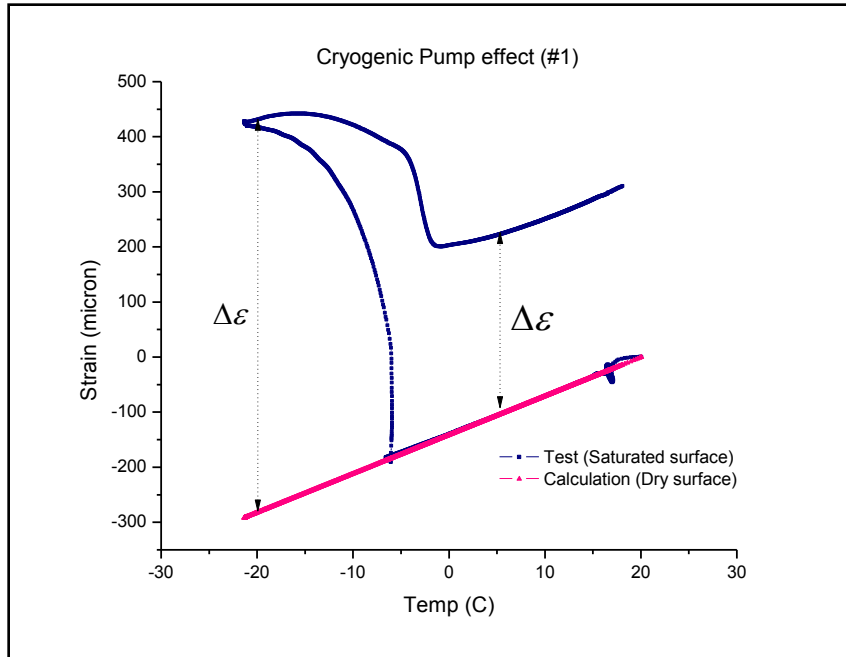


**Figure 6- 6 Pressure differences of field specimens by cryogenic pump VS. Average void radius**

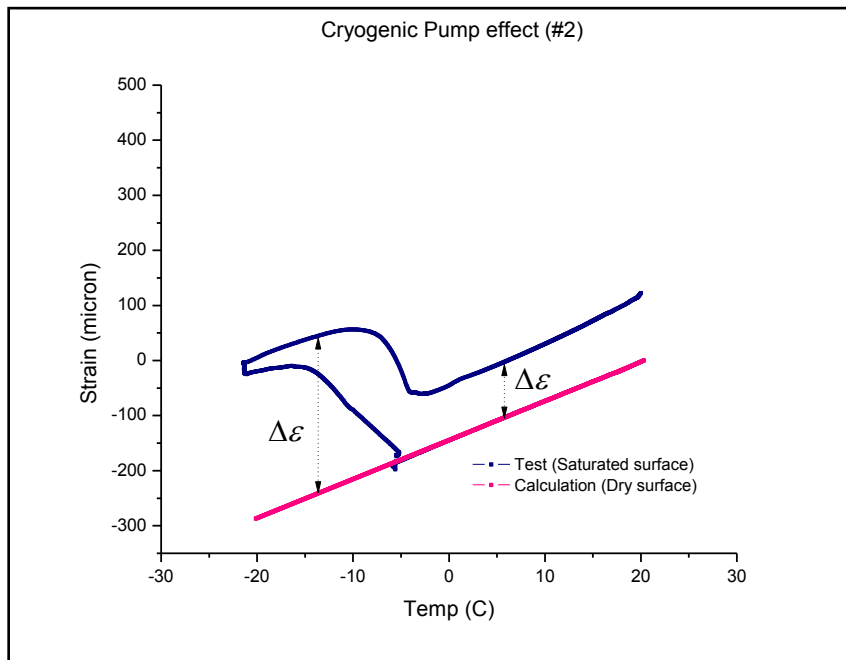
The pressure difference of specimen #1 is almost 3 times higher than that of specimen #10 and #11 which are durable concrete in field. Even though quality of concrete paste such as porosity, permeability and density are assumed as same, the flow rates and the pressure are very different due to air voids systems.

### 6.3 LOW TEMPERATURE DILATATION TESTS

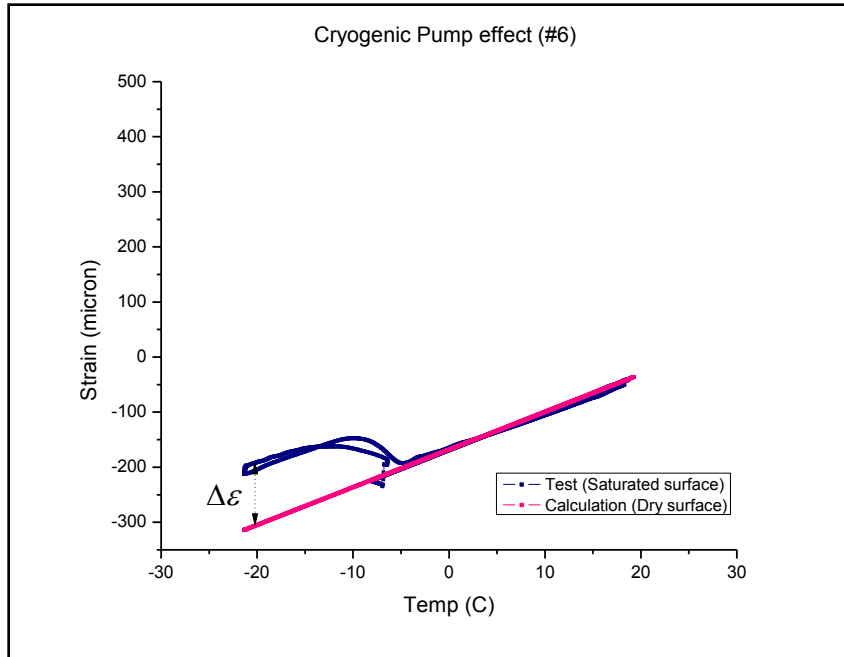
The flow rates of the field specimens during wet freezing have been studied. The higher flow rate can cause the bigger expansion by cryogenic pump mechanism. The Low Temperature Dilatation (LTD) tests have been performed with surface liquid. To find out cryogenic pump expansion, the test results have been compared with calculations based on dilatations before freezing.



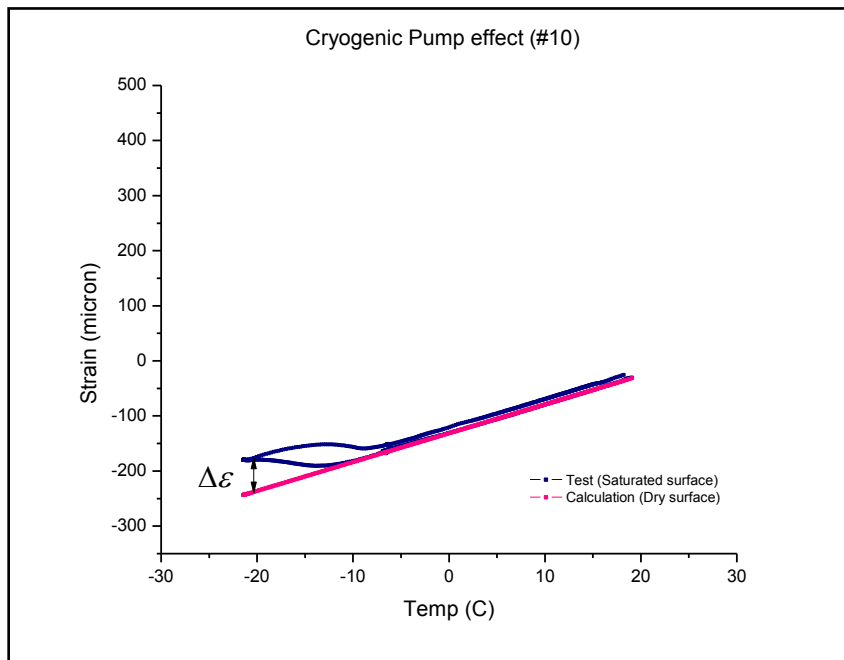
**Figure 6- 7 Dilatation of non-durable concrete (#1) during a freeze-thaw cycle**



**Figure 6- 8 Dilatation of non-durable concrete (#2) during a freeze-thaw cycle**



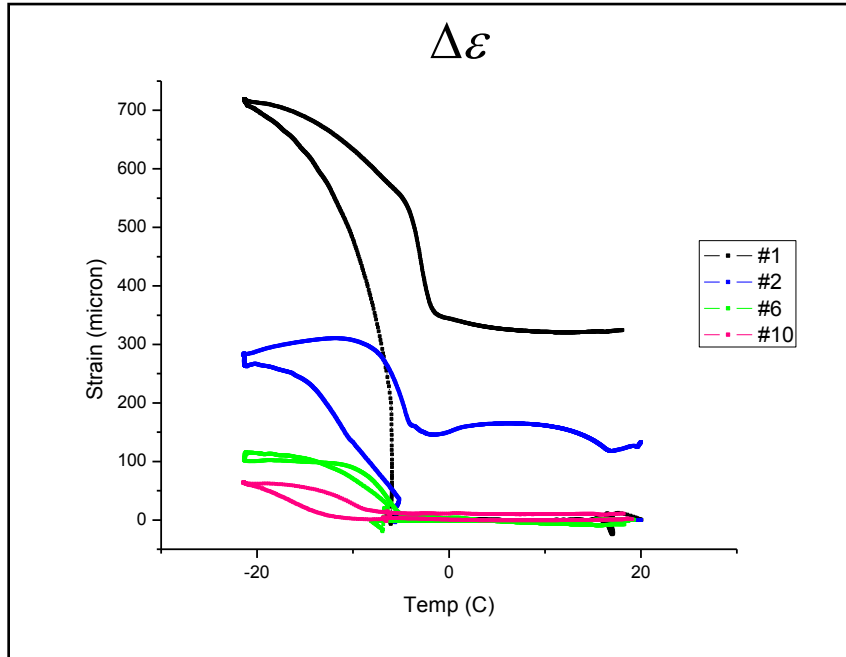
**Figure 6- 9 Dilatation of moderate concrete (#6) during a freeze-thaw cycle**



**Figure 6- 10 Dilatation of moderate concrete (#6) during a freeze-thaw cycle**

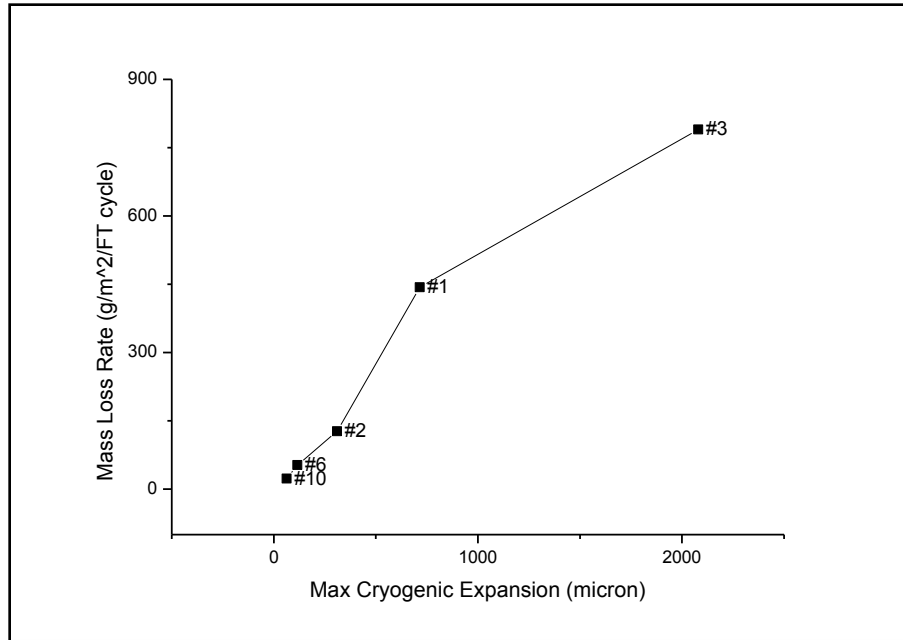
As shown in above, the surface concrete with surface liquid has experienced a huge expansion by cryogenic pump after pore liquid start freezing. The cryogenic expansion can be easily calculated by subtracting Calculation strain ( $\epsilon_C$ ) from test strain ( $\epsilon_T$ ).

$$\Delta\varepsilon = \varepsilon_T - \varepsilon_C \quad (6.6)$$



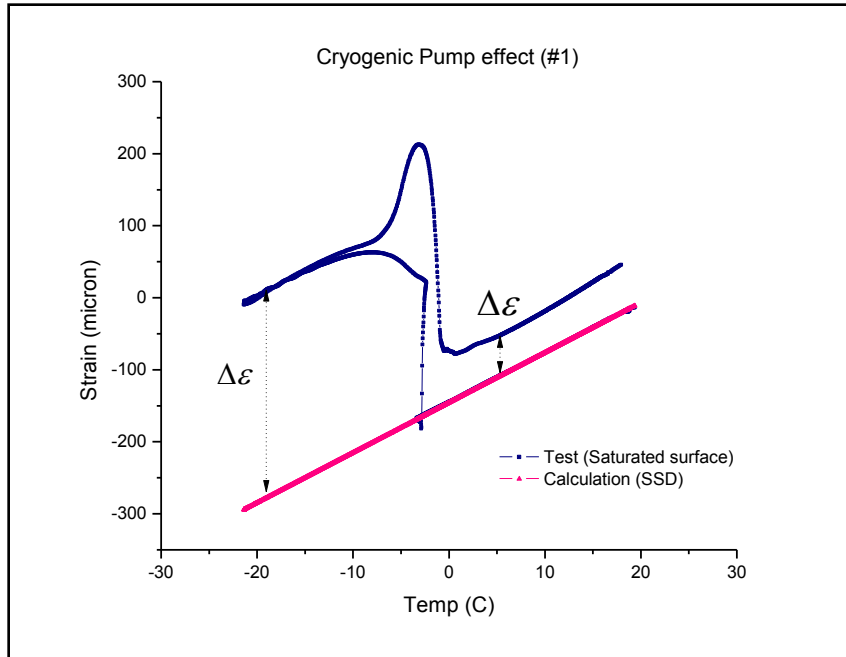
**Figure 6- 11 Expansion due to cryogenic pump effect**

Non-durable specimens (#1 and #2) have experienced huge expansions due to cryogenic pump. Besides, the amounts of the expansion are correlated with the flow rates. According to cryogenic pump surface scaling mechanism, surface scaling should be proportional to the expansions by cryogenic pump. The relationship between the cryogenic pump expansion and surface scaling is shown in Figure 6.12.

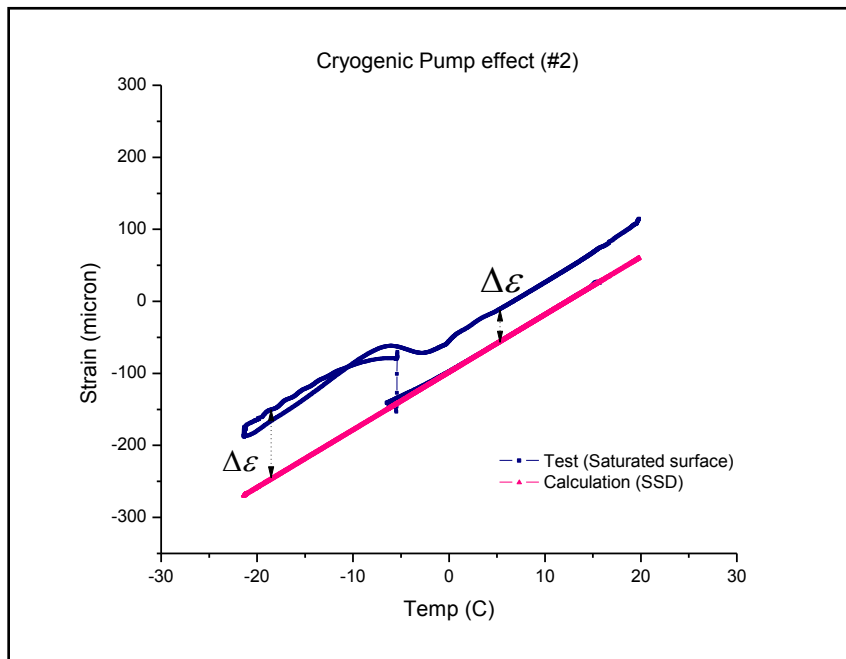


**Figure 6- 12 The relationship between mass loss rate and max cryogenic expansion**

No matter what liquid is inside pores, ice crystals in pores and voids draw liquid in capillary or small pores in the vicinity. The flows remain until the adjacent capillary or small pores are emptied. If air voids systems in concrete are not good enough and degree of saturation approaches to near a critical point, destructive pressure can be created even in case of water. Thus, Surface scaling happens not only in presence of salt solution but also water on surface under extreme conditions. Cryogenic expansion also happens even when there is water on surface even though the amounts are relatively small.

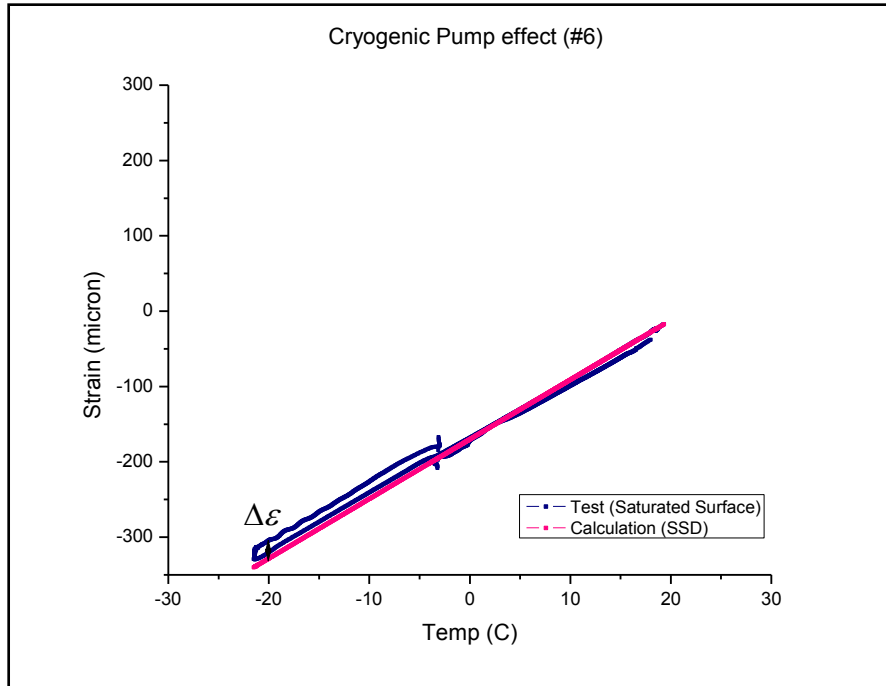


**Figure 6- 13 Dilatation of non-durable concrete (#1) with only water on surface during a freeze-thaw cycle**

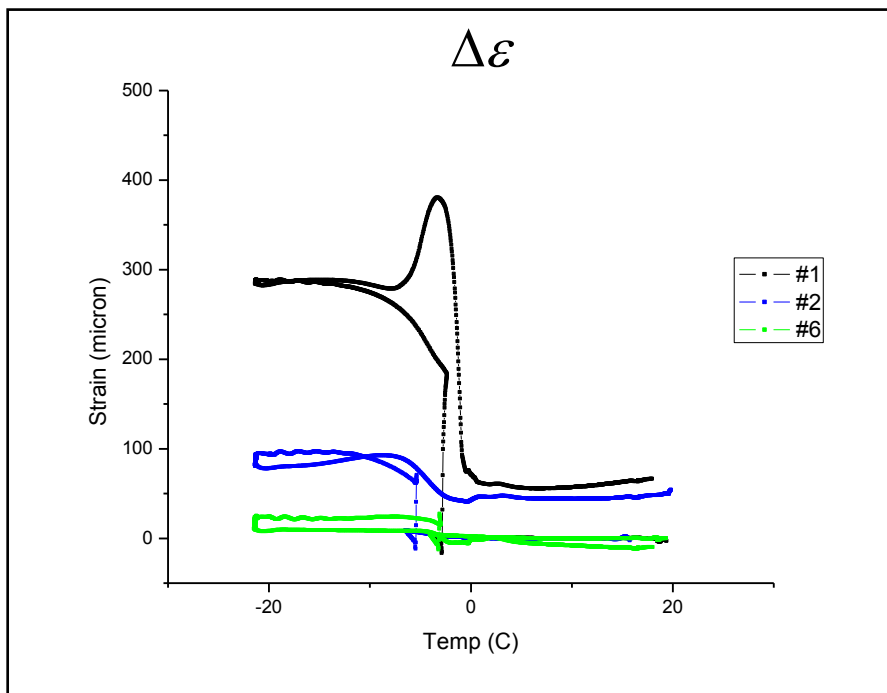


**Figure 6- 14 Dilatation of non-durable concrete (#2) with only water on surface during a freeze-thaw cycle**



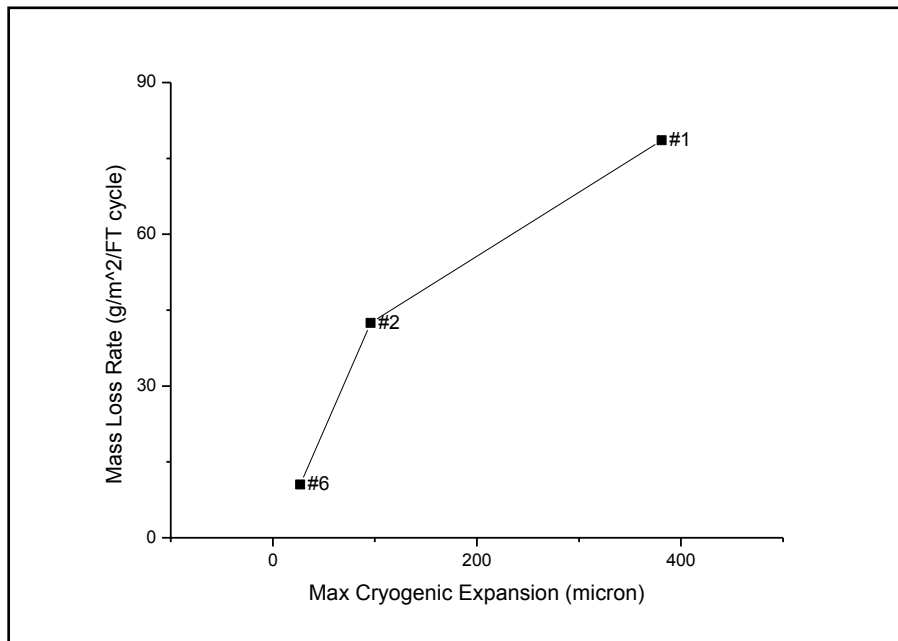


**Figure 6- 15 Dilatation of moderate concrete (#6) with only water on surface during a freeze-thaw cycle**



**Figure 6- 16 Expansion due to cryogenic pump effect with only water on surface**

Even though the test liquid was water, big expansions over 100 micro strains were generated in non-durable concretes (#1 and #2). In case of specimen #1, an extra expansion occurred as temperature went up to melting point. The ice crystals in pores grew as temperature went up but there were not enough spaces to store. Consequently, the extra expansion might be created. The amount of surface scaling should be proportional to the expansion due to cryogenic pump not only in presence of salt solution but also water.

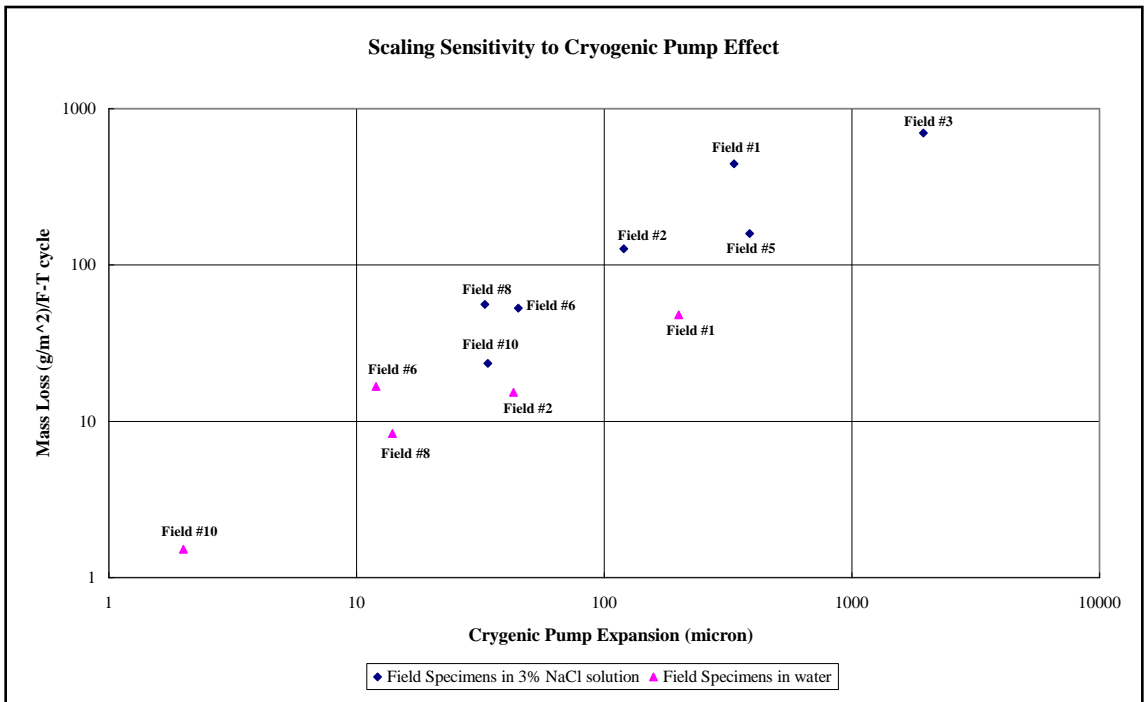


**Figure 6- 17 The relationship between mass loss rate and max cryogenic expansion**

As a result, a destructive expansion and consequent pressure can be generated both in salt solution and in water while salt can extremely magnify the expansion. Thus, de-icer may not be an essential factor causing surface damage during freeze-thaw cycles but an exacerbated factor and the surface damage is called as surface scaling instead of salt scaling in this study.

## 6.4 THE RELATIONSHIP BETWEEN CRYOGENIC PUMP AND SURFACE SCALING

Pore pressure is generated both in water and in salt solution even though the amount of pore pressure in salt solution is much higher than in water. Also the pore pressure in water is affected by cryogenic pump. Thus, mass loss rates should be related with the amounts of cryogenic pump expansion no matter what types of test liquid are used. The mass loss rates (Mass loss per cycle) from RILEM CIF-CDF test [3] are compared with the amounts of cryogenic pump expansion,



**Figure 6- 18 Mass loss rate VS Cryogenic pump expansion**

As shown in Figure 6. 18, mass loss rates of the field specimens are linearly related with cryogenic pump expansion both in de-mineralized water and in 3% sodium chloride solution. In other words, if the hydraulic pressure of the surface concrete causes the

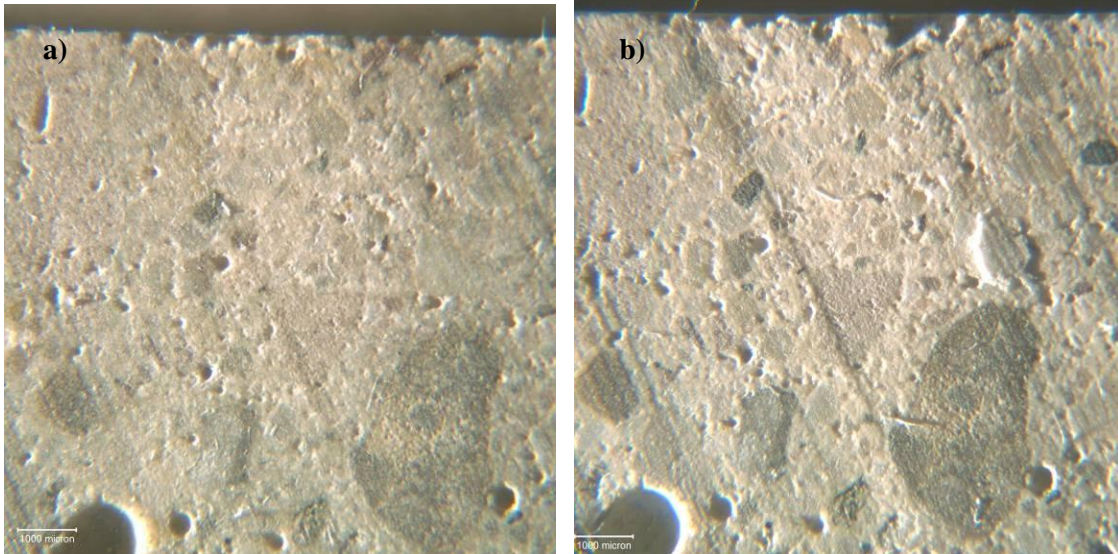
surface scaling, de-icing salt can accelerate the surface damage but it is not the essential variable.

## **6.5 MICROSCOPIC OBSERVATION ON THE SURFACE AFTER LTD TEST**

The LTD prisms have been observed under a microscope. Each prism has been exposed to 3 freeze-thaw cycles during the test. The prisms with dry surface and water wet surface have not been damaged at all after 3cycles test. The specimens with saline wet surface have been damaged by cryogenic expansion during the test.

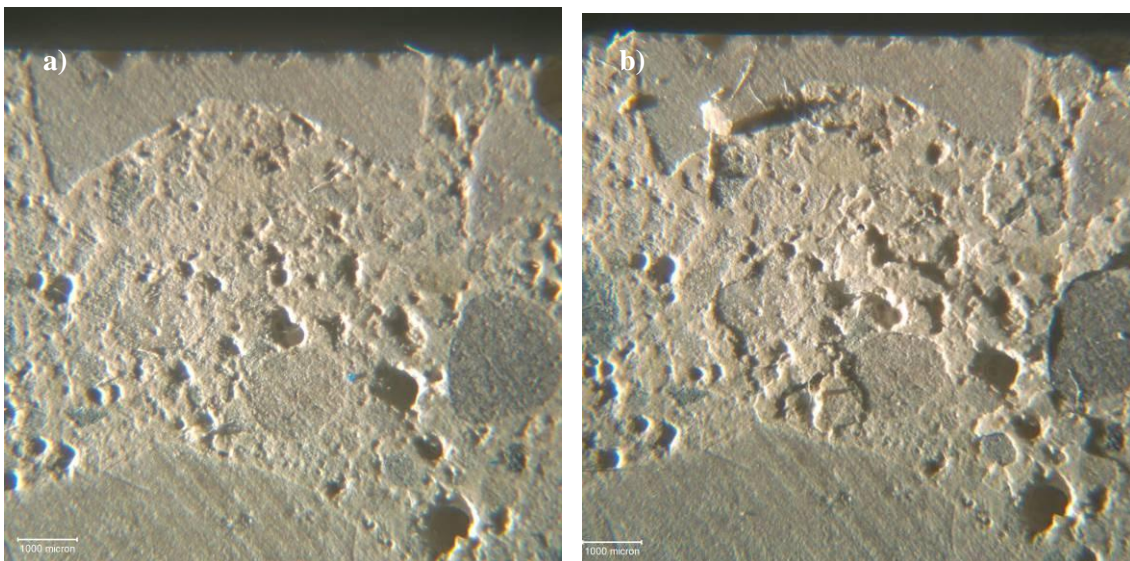
### **6.5.1 Cryogenic pump expansion < 100 micro strain**

The cryogenic expansion of the specimen #10 was less than 30 micron. The lateral surface which is not exposed directly to the surface liquid is compared between before and after test in Figure 6.19.



**Figure 6- 19 a) Lateral surface of #10 LTD prism before Freeze Thaw cycles b) Same location after 3 Freeze Thaw cycles**

The durable concrete, #10, had almost no damage except a few pieces pop out. Specimen #6 has a moderate resistance of surface scaling. Its cryogenic pump expansion was between 50 and 100 micro strain. See Figure 6.20.



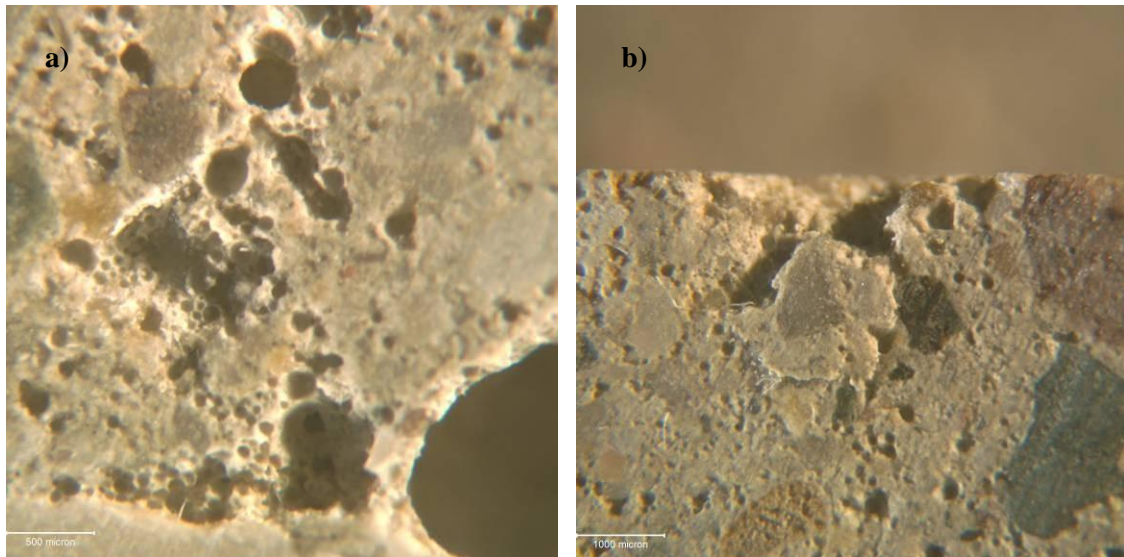
**Figure 6- 20 a) Lateral surface of #6 LTD prism before Freeze Thaw cycles b) Same location after 3 Freeze Thaw cycles**

The thin paste skin swelled up after 3 Freeze Thaw cycles even though the surface was

not directly exposed to surface liquid.

### 6.5.2 Cryogenic pump expansion > 100 micro strain

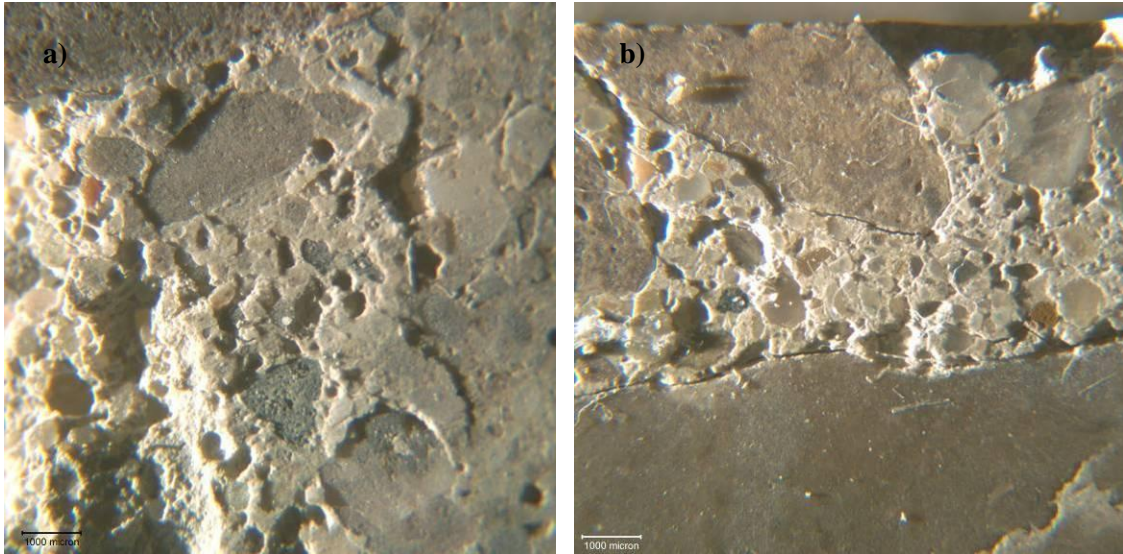
The cryogenic expansion of the specimen #2 was around 200 micro strains. The top surface which contact directly to surface liquid and the lateral surface after 3 freeze thaw cycles are shown in Figure 6.21.



**Figure 6- 21 a) Top surface of specimen #2 after 3 freeze thaw cycles of LTD test b) Lateral surface of same specimen**

After 3 freeze-thaw cycles, many spots of the test surface of specimen #2 popped out. The damages of lateral surface were progressed through the half of the depth (5mm). Specimen #1 is non durable concrete in the field. High expansion around 700 micro strains was created during the 3 freeze thaw cycles. The test surface and lateral surface after the LTD test are shown in Figure 6.22.





**Figure 6- 22 a) Top surface of specimen #1 after 3 freeze thaw cycles of LTD test b) Lateral surface of same specimen**

Most parts of the test surface were scaled off and the depths of scaling were deep. The cracks and swellings of lateral surface occurred through whole depth (10mm).

## **6.6 SUMMARY OF FINDINGS**

This study evaluates the frost actions of wet concrete. Flow rates into the voids of the field concrete specimens were calculated based on S. Jacobsen's work [25]. In order to support the cryogenic pump mechanism, the LTD tests were performed and the test results were compared with surface scaling rates and microscopic observations after the tests. The findings and indications are as follows.

### Flow from wet concrete toward voids

- It is almost impossible to quantify the flows from wet concrete paste toward voids at

this point due to a lack of information of micro-structure as well as its environmental of concrete paste. With reduced variables, the flows seem to be correlated well with flow path length and void radius. Nondurable concrete specimens tend to have high flow rates with a fixed pressure difference as well as high pressures with a fixed flow rate.

#### Expansion by cryogenic pump

- Nondurable concrete specimens experienced a very large expansion of over 300 microns during a freezing and thawing cycle while only small expansion less than 100 microns occurred in durable concrete specimens.
- The expansions due to cryogenic pump seem to be proportionally related with the scaling rates both in water and in 3% sodium chloride solution.

#### Microscopic observation after LTD test

- Not only were the surfaces exposed to surface liquid damaged but the lateral surfaces were also damaged. Most pastes of nondurable concrete were scaled off after 3 freeze-thaw cycles while aggregates seemed not to be damaged.
- The cracks and the scaling were expedited through the entire depth of the nondurable concrete specimen while cracks may not have been created along the depth of durable concrete. However, there was some damage on the surface exposed to the surface liquid.



# **CHAPTER 7**

## **METHODOLOGY FOR IMPROVING SURFACE SCALING RESISTANCE OF CONCRETE**

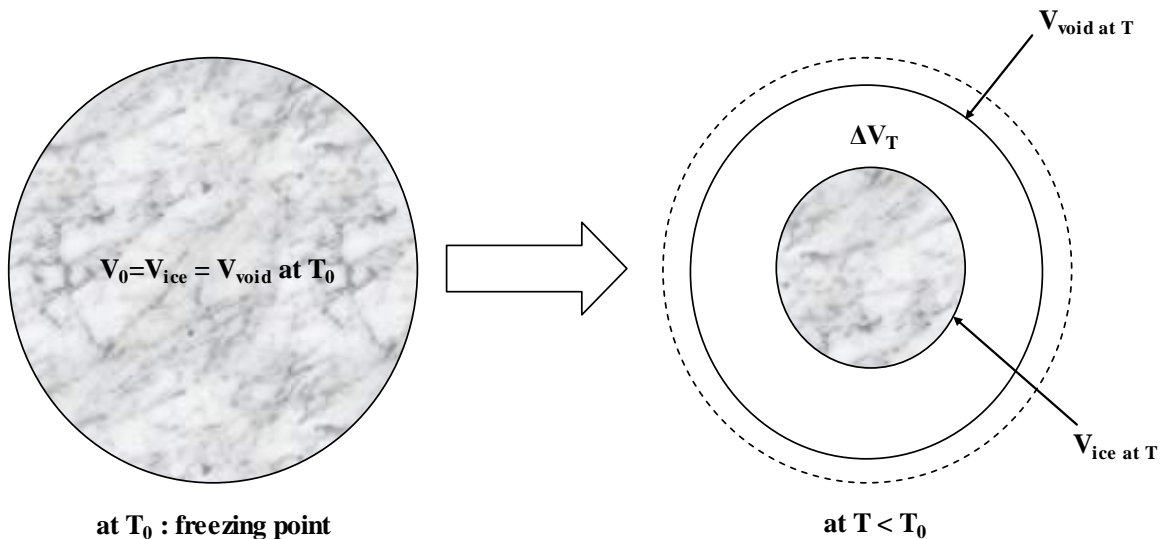
### **7.1 INTRODUCTION**

In the previous chapters, causes and mechanisms of frost damages have been studied. The objective of the study in this chapter is to optimize the concrete properties in terms of frost durability based on the finding in previous studies. Although it seems to be impossible to fully understand what happen in concrete during freezing and thawing, one major factor deteriorating the frost damage can be a flow toward pores and voids. In addition, entrained air as frost protection method seems to contribute not only to improving scaling resistance but also to reducing a flow rate. In order to improve one factor, another problem may arise. For instance, if water/cement ratio is reduced to improve density of paste, workability would be worsened. In fact, many researchers have suggested a lower water-cement ratio for scaling resistance. However, it is doubted if the water/cement ratio can be reduced and controlled in the field. Therefore, the water/cement ratio is fixed to 0.45 in this study. Also, it has been found out durability in previous chapters that the air content and properties seem to be proportionally related with frost. However, it has been reported that too much air content can reduce strength of

concrete. Thus, laboratory mix concrete specimens have been studied in this chapter to give more information on optimal concrete properties.

## 7.2 FROST ACTIONS OF WET CONCRETE PASTE DURING FREEZE-THAW CYCLE

For better understandings, cryogenic pump expansion process is simplified. For this explanation, assume that ice volume and void volume are same at a freezing point ( $T_0$ ). As a temperature drops down to subfreezing point,  $T$ , both the void and ice shrink. However, ice has a much higher thermal expansion coefficient than concrete so that a part of the void becomes empty as much as the difference of volumetric shrinkage between ice and air void. See Figure 7.1.



**Figure 7- 1 Schematic explanation of ice shrinkage in a void**

The difference between ice volume and void volume at temperature  $T$  can be calculated.

$$\Delta V_T = (\beta_{ice} - \beta_{concrete}) \cdot V_0 \cdot (T_0 - T) \quad (7.1)$$

Where,

$\Delta V_T$ : The empty volume of void at T(°C) in  $m^3$

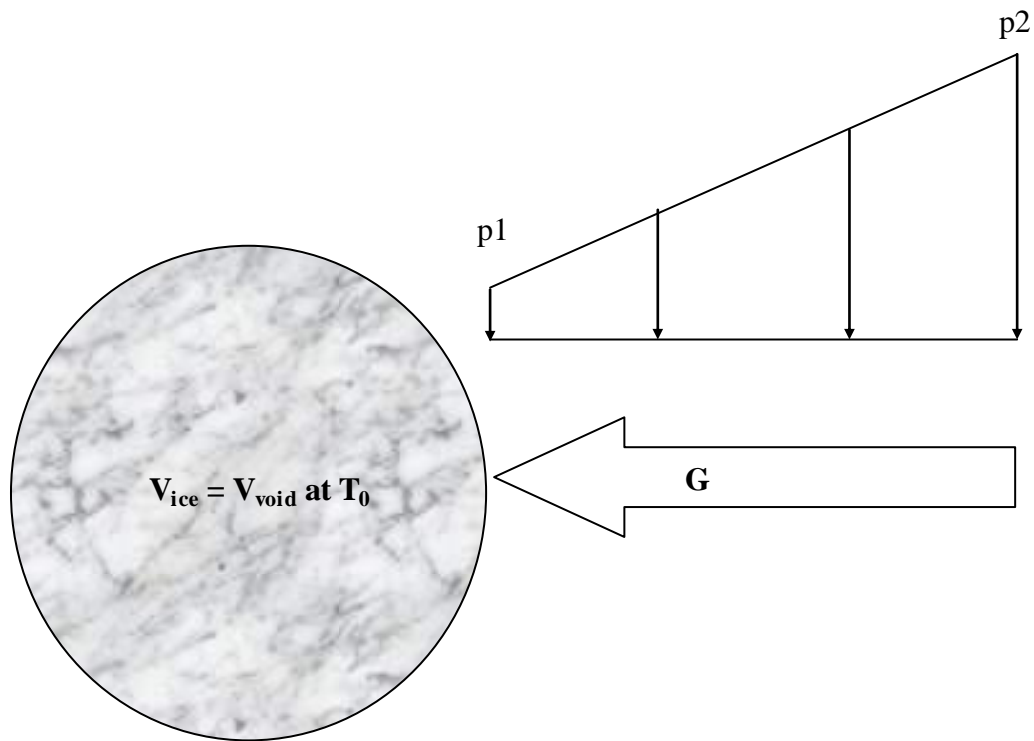
$V_0$ : The empty volume of void at freezing point,  $T_0$ (°C)

$\beta_{ice}$ : Volumetric thermal coefficient of ice = 153ppm

$\beta_{concrete}$ : Volumetric thermal coefficient of concrete = 36ppm

$T_0$ : Freezing point in °C

$T$ : Temperature in °C



**Figure 7- 2 Schematic explanation of flow toward a void**

After ice is created in a void, liquid may travel toward a void by pore pressure (Figure 7.2). If the liquid transport rate is less than the volume contracting rate;

$$G < \frac{\Delta V}{\Delta T} \quad (7.2)$$

Where,

$G$  : the liquid transport rate toward void in  $m^3 / ^\circ C$

$\frac{\Delta V}{\Delta T}$  :the volume contraction rate,  $(\beta_{ice} - \beta_{concrete}) \cdot V_0$ , in  $m^3 / ^\circ C$

the cryogenic pump expansion would not arise. In addition, the total volume of flow transport during freezing and thawing can be calculated as follows:

$$V_l = \int_{T_0}^T G \cdot dT \quad (7.3)$$

Where,

$V_l$  : The total volume of flow transport during a F-T cycle

If the total volume of flow transport is less than the total volume of air void, the expansion would occur. However, too much air content can cause to decrease concrete strength. The transport rate should be controlled. Unfortunately, it is almost impossible or too complicated to quantify the flow rate along temperature, time and so on. Instead, variables affecting the flow rate such as porosity, absorptivity and Interfacial Transition Zone (ITZ). In this study, Ground Granulated Blast-Furnace Slag (GGBFS) was used for improving quality of paste.

### **7.3 IMPROVED PASTE QUALITY BY SUPPLEMENTARY CEMENTING MATERIAL (GGBFS)**

The use of Supplementary Cementing Materials such as Fly Ash (FA) or Ground

Granulated Blast-Furnace Slag (GGBFS) can result in numerous potential benefits. In fact, it reduces long-term chloride penetrability, mitigation of alkali-silica reaction, and temperature in mass and hot weather concreting. Besides, using GGBFS can reduce the cost of construction materials, promote recycling and waste minimization and improve concrete durability [44]. However, SCM use was found to increase the bleeding of concrete. Thus, the addition of SCM was found to increase the thickness and the porosity of the surface layer [19].

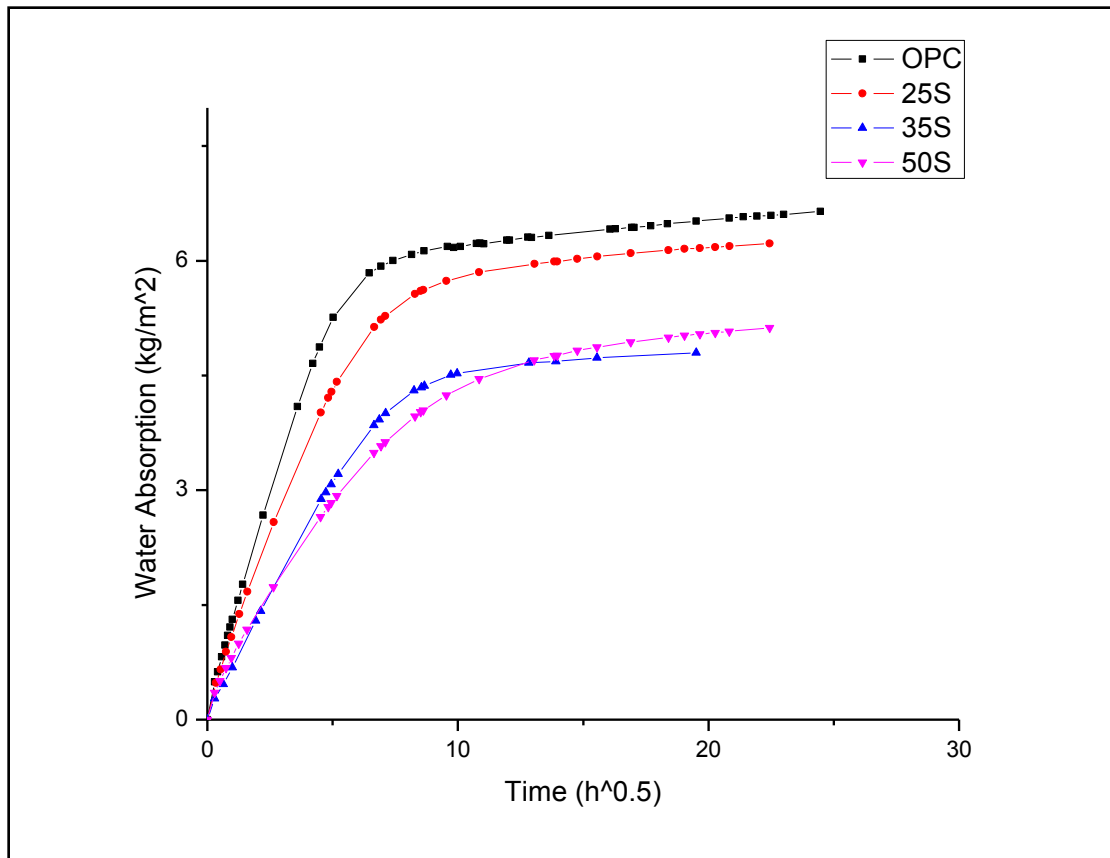
In contrast to this, J. Stark insists that the degree of hydration and, consequently, the pore size distribution of the concrete do not have a significant effect on salt scaling and that the frost-deicing salt resistance of concretes made with cement rich in GGBFS might be dependent on the state of the carbonated surface layer [29].

And also other researchers have found that GGBFS can improve the fluidity of fresh concrete, reduce its bleeding and delay the setting with replacing Portland cement by GGBFS[45, 46].

Although there is no agreement of the effect of the SCM on salt scaling, salt scaling and microstructure of the surface layer might be affected by use of SCM.

### **7.3.1 Absorptivity of concrete containing GGBFS**

In order to find out the effect of GGBFS on absorptivity, four disks of 50mm thickness were cut from each specimen, OPC, 25S, 35S and 50S and then the mean value of four results are shown in Figure 7.3.

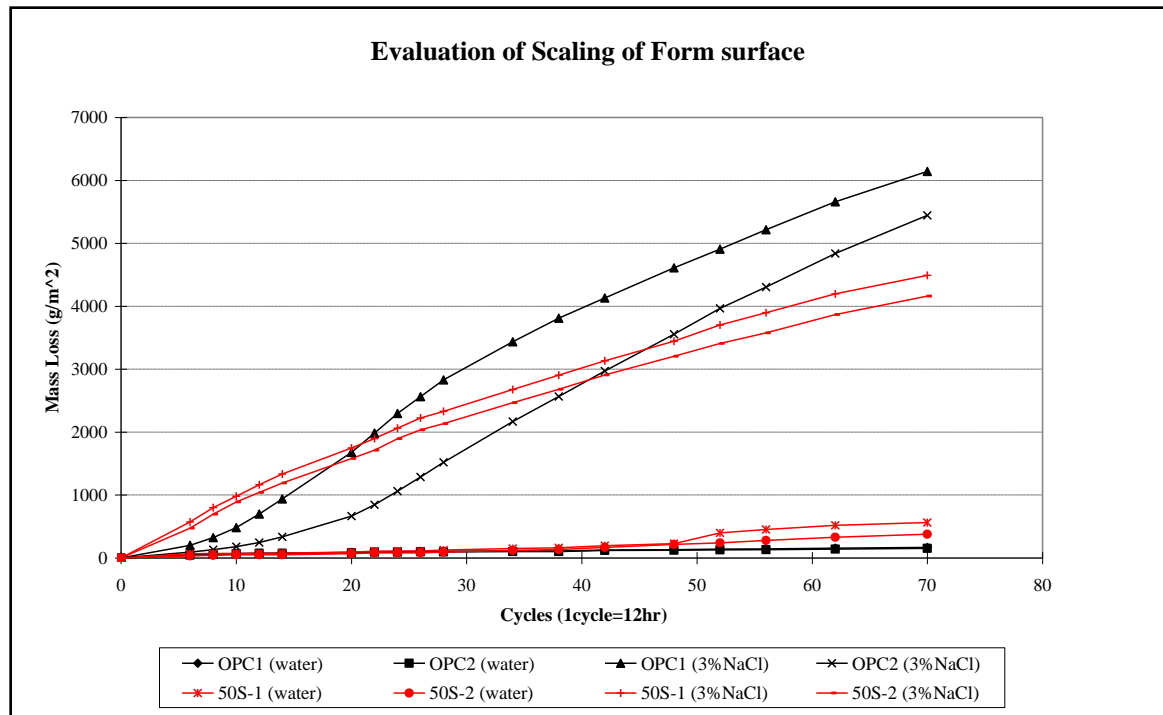


**Figure 7- 3 Absorptivity test results with various contents of GGBFS**

Absorptivity seems to be improved by increasing GGBFS content up to 35% while 50S specimens had similar absorptivity with 35S specimens. These results tell that GGBFS may contribute to denser paste as well as consequently lower absorptivity.

### **7.3.2 Comparison of form surface scaling resistance between ordinary Portland cement concrete and concrete containing GGBFS**

GGBFS has been limited to use because GGBFS has been believed to reduce frost durability. However, opposite results has been argued. Therefore, surface scaling tests were performed with OPC and 50S concrete specimens.



**Figure 7- 4 Surface Scaling of OPC and 50S**

GGBFS concrete may have a thicker weak surface than Type I concrete. Thus, 50%GGBFS specimens had more surface scaling during the early F-T cycles than Type I specimens. However, once the weak surface of 50% GGBFS specimens were removed the ratio of surface scaling decreased. In addition, the depth of damage by scaling of OPC concrete was deeper than 50s concrete while mass loss of 50S specimens were larger during early F-T cycles. Scaled surfaces have been observed in Table 7.1.

As shown in Table 7.1, concrete containing GGBFS were quickly scaled off in weak paste surface. However, the deterioration on GGBFS concrete was homogeneous while that on Type I was concentrated around aggregates in early F-T cycles. Besides, mass loss of 50% GGBFS concrete reduced after the weak surface was removed.

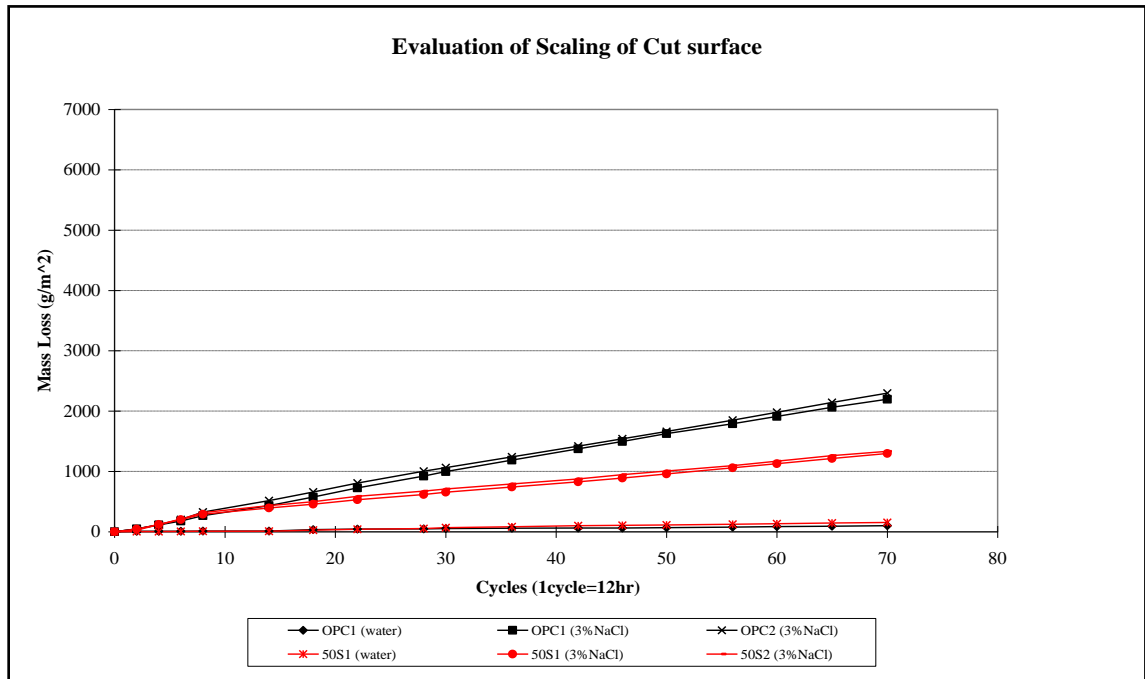
Surface scaling is evaluated by the amount of mass loss. Thus, concrete containing GGBFS reached to failure criteria ( $2000\text{g/m}^2$ ) in terms of mass loss. However, the depth

of scaling of OPC was deeper during early F-T cycles and long term scaling resistance of OPC concrete seems to be worse than concrete containing GGBFS.

Therefore, the quality of paste of concrete containing GGBFS seems to be homogeneous resulting uniform depth of scaling which can be optimal.

### 7.3.3 Comparison of cut surface scaling resistance between ordinary Portland cement concrete and concrete containing GGBFS

To avoid weak surface effect, a few millimeters of specimen's skin were removed before F-T test was started.

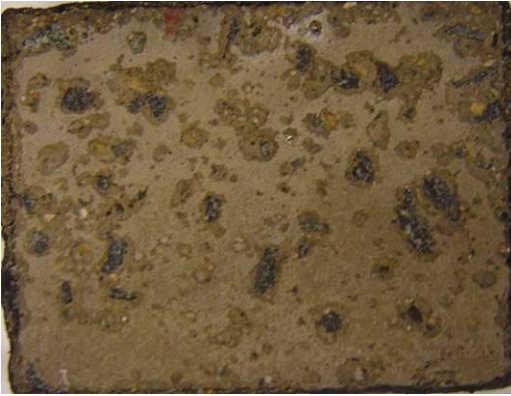

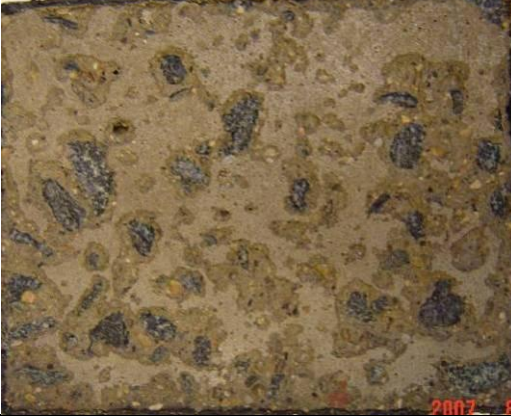
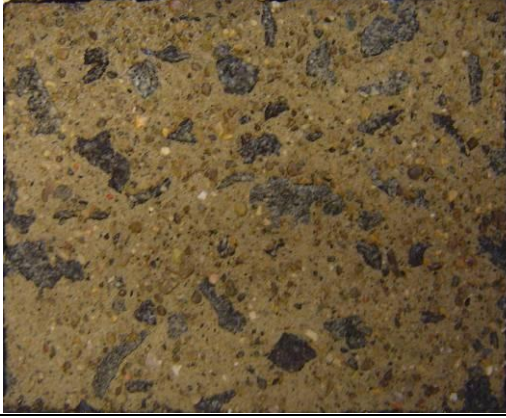




**Figure 7- 5 Cut Surface Scaling of OPC and 50S**

As shown in Figure 7.5, cut surfaces of 50% GGBFS specimens had about 40% less mass loss than that of Type I specimens. Surface deteriorations of cut surface specimens were monitored. See Table 7.2.









**Table 7- 1 Scaled surface by F-T attack**

F-T cycles	OPC in 3% NaCl solution	50S in 3% NaCl solution
20		
	Paste on and around aggregates was scaled off while other parts remained	Whole surface was evenly removed.
26		
	The scaling area was getting wider and deeper.	The depth of scaling was still homogenous.
70		
	A few mm of whole surface were removed	The depth of scaling was not deep as much as Type I specimens.



**Table 7- 2 Scaled cut surfaces of OPC and 50S specimens by F-T attack**

F-T cycles	Type I in 3% NaCl solution	50% GGBFS in 3% NaCl solution
12		
	<p>The deteriorations were getting deeper. Some of them became holes.</p>	<p>The depth of scaling became deeper a little.</p>
22		
	<p>The scaling area was getting wider and deeper.</p>	<p>The depth of scaling was still homogenous.</p>
42		
	<p>A few mm of whole surface were removed</p>	<p>The depth of scaling was not deep as much as Type I specimens.</p>

## **7.4 EFFECTS OF AIR VOID DISTRIBUTION AND INTERFACIAL TRANSITION ZONE (ITZ) ON SURFACE SCALING RESISTANCE**

Now it might be clear that air voids system is one of the most important factors of concrete surface scaling resistance. Not only the air contents improve the surface but the qualities of air voids such as spacing factors and distributions are strongly related. Besides, microstructures of paste which affect diffusivity, absorptivity and permeability have effects on durability of concrete, especially surface scaling resistance. The concrete paste has locally different properties of microstructure. There is very porous interface between paste and aggregates called Interfacial Transition Zone (ITZ) and air voids tend to be congregated around aggregates. These factors affect bond strength between paste and aggregates. Due to high porosity the ITZ has more moisture uptakes than bulk paste. As a result, the ITZ experiences higher stress and expansion during freezing thawing cycles. With these reasons the ITZ is weak point in terms of frost damages. The ITZ can be improved by replacement cement with GGBFS.

### **7.4.1 Test specimens**

The materials used and the mixture proportions for test series are summarized in Table 7.3.

The water-to-binder ratio of specimens is 0.45 respectively. The ordinary Portland cement (ASTM Type I) is used. Ground Granulated Blast Furnace Slag is used for supplementary cementitious materials (SCM). Parameters of air void system in hardened concrete have been determined. RapidAir C 457 has been used based on ASTM C 457

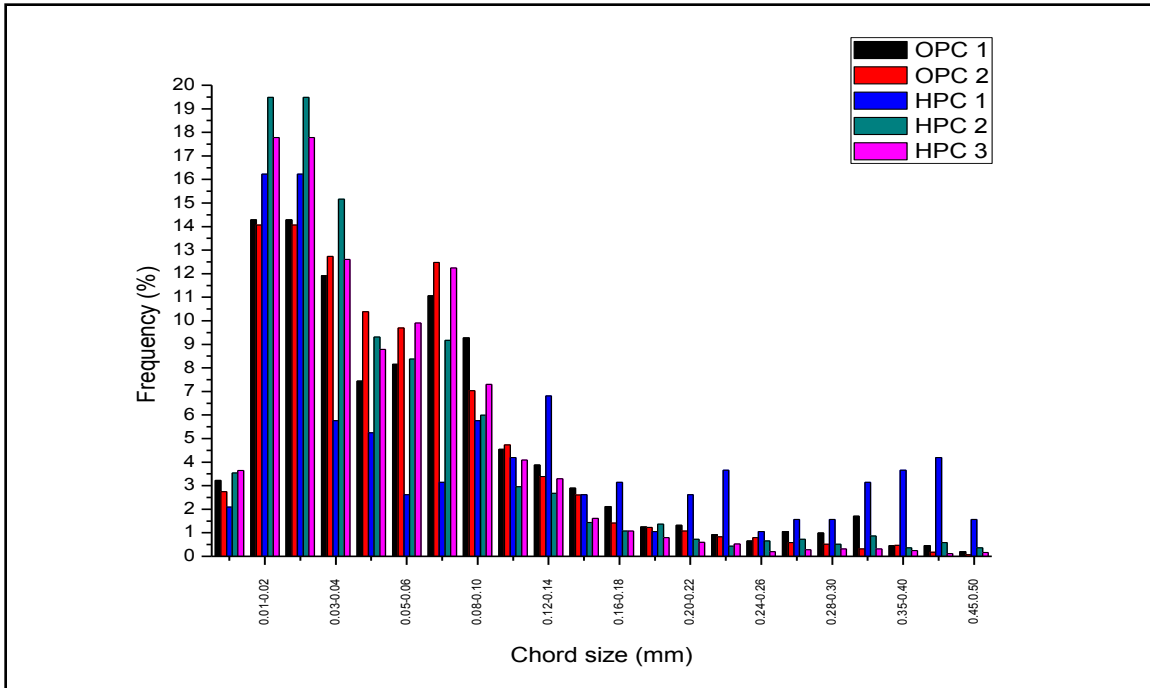
linear traverse method. The parameters and distributions are shown in Table 7.4 and Figure 7.6 and 7.7.

**Table 7- 3 Matrix for test specimens**

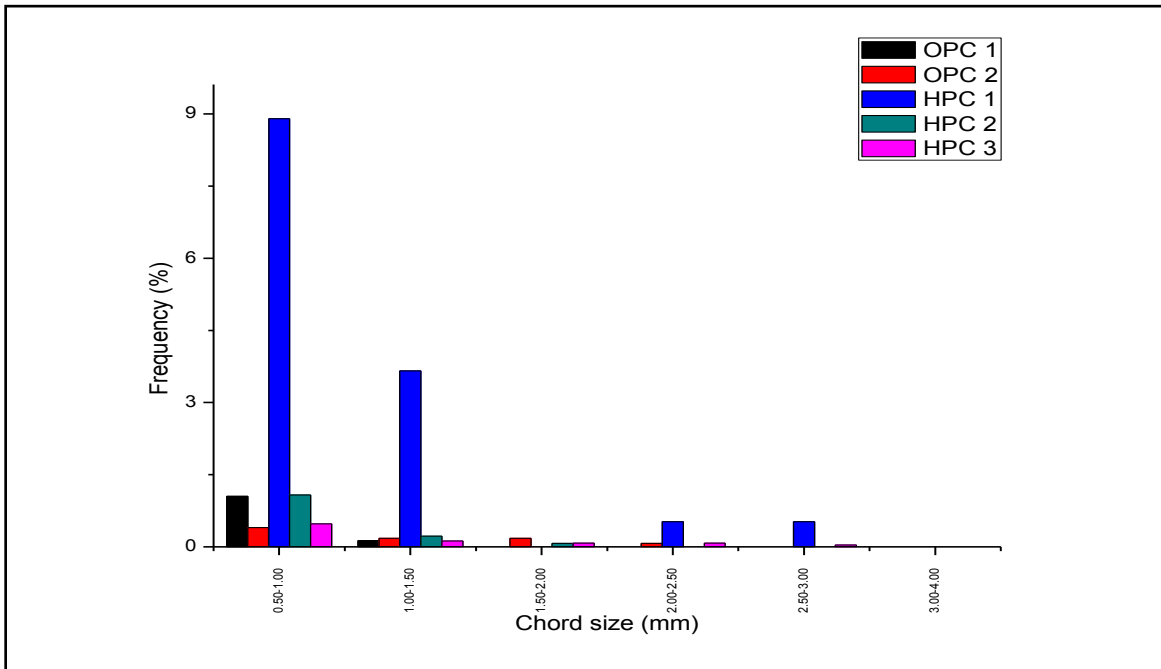
Specimen ID	w/b	OPC (% by wt.)	GGBFS (% by wt.)	Target air content
OPC-I	0.45	100	0	Medium (4%)
OPC-II	0.45	100	0	High (8%)
HPC-I	0.45	65	35	Low (0%)
HPC-II	0.45	65	35	Medium (3%)
HPC-III	0.45	65	35	High (6%)

**Table 7- 4 Air voids parameters of test specimens**

Specimen ID	Air Content (%)	Air Content (<0.5mm) (%)	Specific Surface (mm <sup>-1</sup> )	Spacing Factor (mm)	Average Chord Length (mm)
OPC-I	4.48	4.02	47.31	0.093	0.085
OPC-II	7.29	6.37	53.11	0.060	0.075
HPC-I	1.63	0.77	16.34	0.445	0.245
HPC-II	3.52	2.96	54.90	0.093	0.073
HPC-III	5.75	4.98	60.48	0.049	0.066



**Figure 7- 6 Distribution of chord length frequency (<0.5mm)**

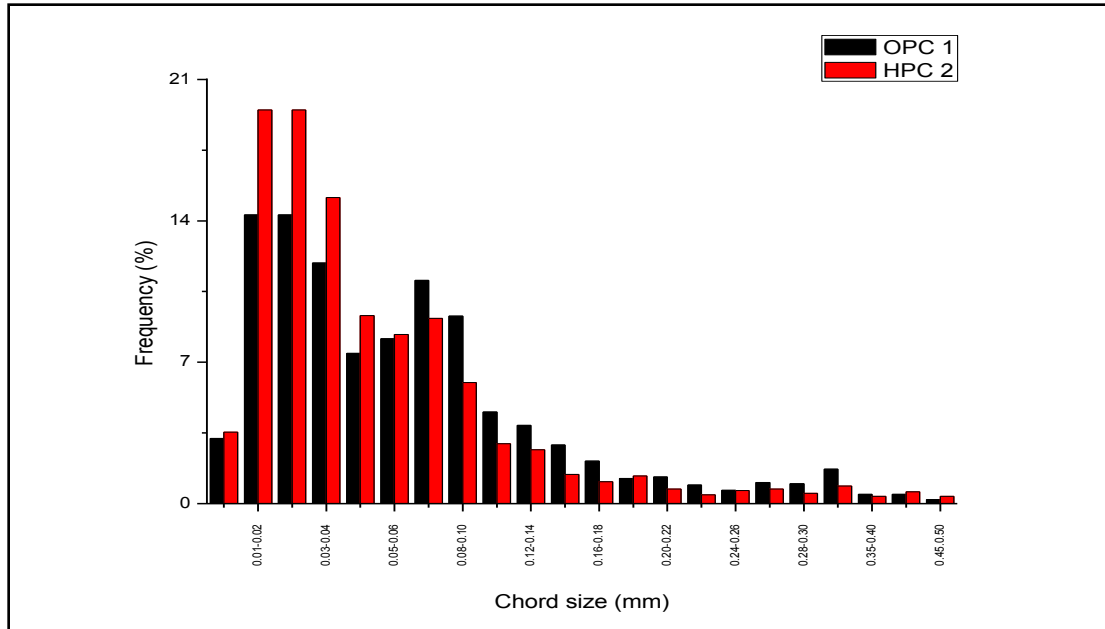


**Figure 7- 7 Distribution of chord length frequency (>0.5mm)**

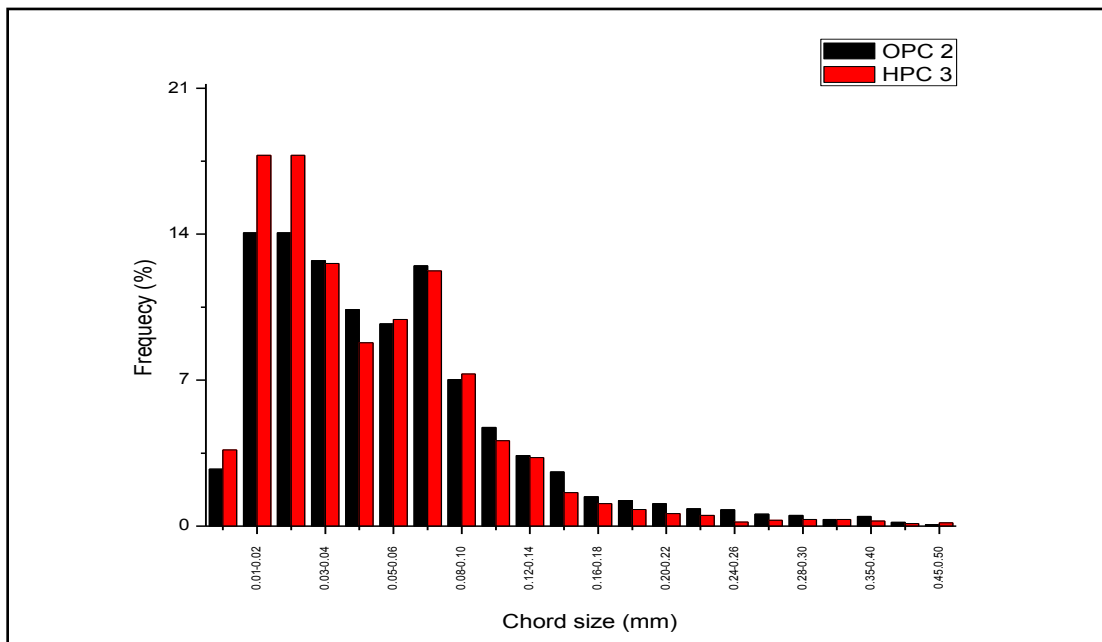
As shown in Figures, most entrained air voids are from 20 to 500 microns of diameters especially under 200 microns. The distributions of OPC 1 and HPC 2 which have medium air contents are compared in Figure 7.8.

HPC 2 has more fine voids from 10microns to 50microns while OPC 1 has many mid-size voids from 50microns to 200microns. Over 60% of HPC 2 air voids are in the ranges between 10 and 50microns. The distributions of OPC 2 and HPC 3 which have high air contents are compared in Figure 7.9.

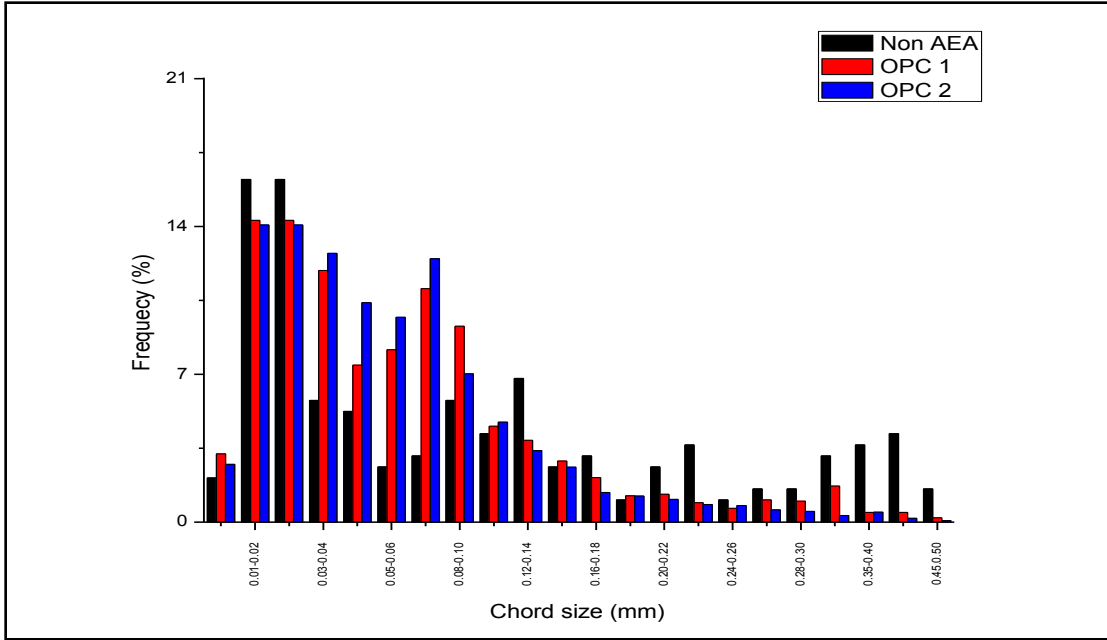
HPC 3 also has more fine air voids between 10 and 30 microns than OPC 2. The results may tell that concrete containing GGBFS creates finer air voids compared with OPC concrete independent of air contents. OPC 1 and 2 and HPC 2 and 3 are compared with HPC 1 which is non AEA concrete in Figure 7.10 and Figure 7.11.



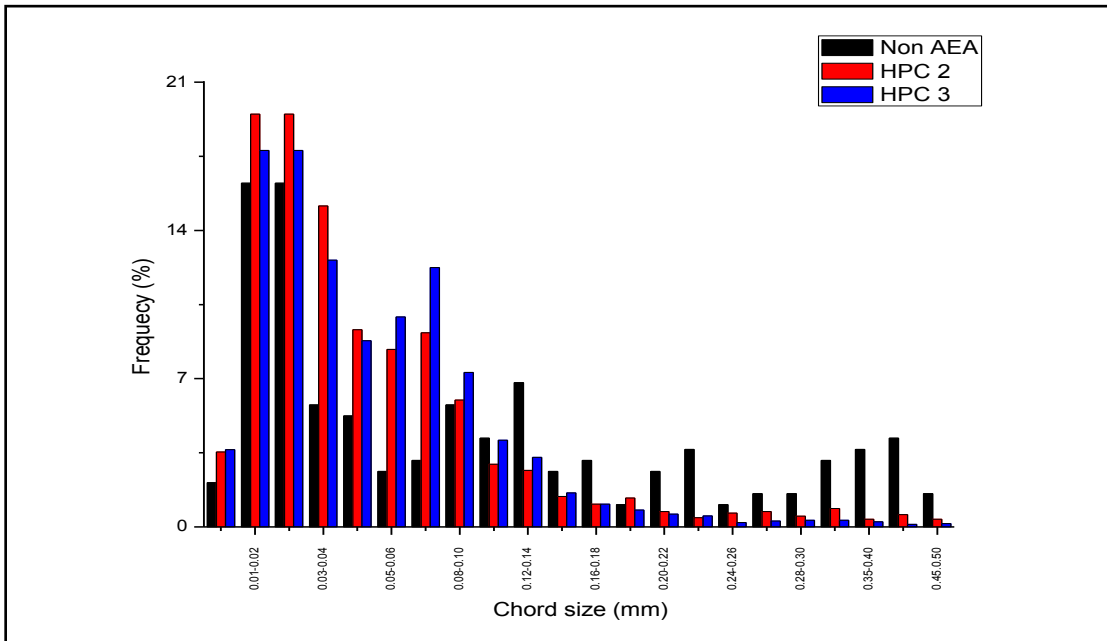
**Figure 7- 8 Chord length frequency of OPC 1 and HPC 2**



**Figure 7- 9 Chord length frequency of OPC 2 and HPC 3**



**Figure 7- 10 Chord length frequency of Non AEA and OPC**



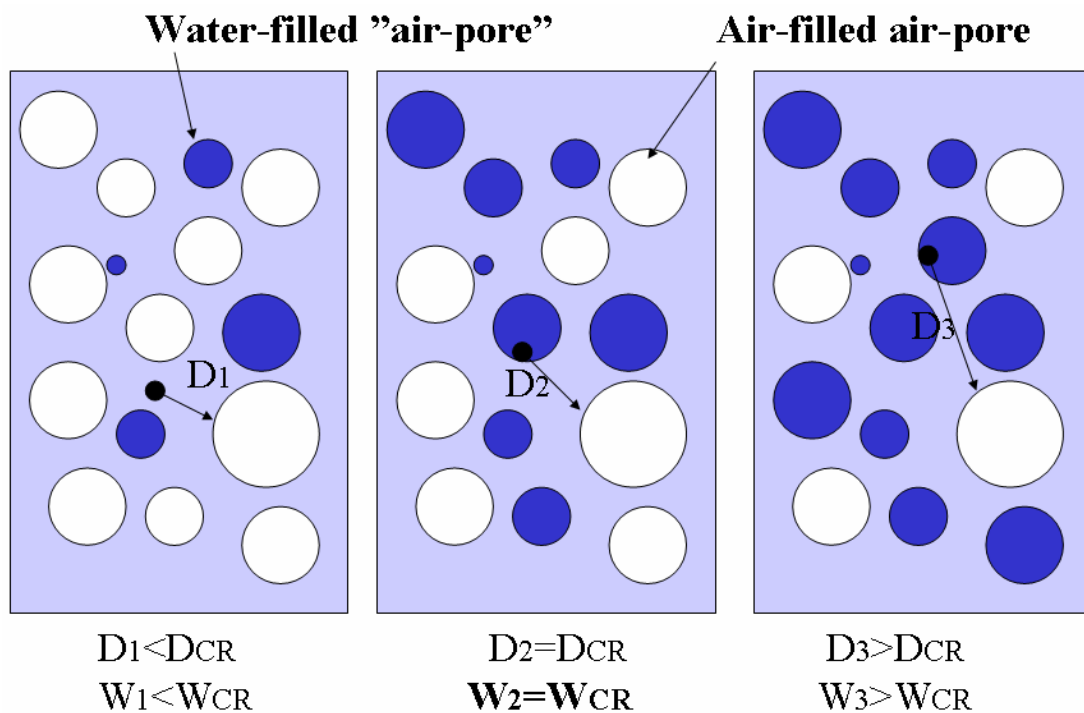
**Figure 7- 11 Chord length frequency of Non AEA and HPC**

Clearly, HPC specimens created sufficient small air voids which may reduce diffusivity and accordingly a pore pressure.



### 7.4.2 Critical spacing factor and flow distance

G. Fagerlund has suggested the critical degree of saturation theory. The relation between critical flow distance and critical water content is illustrated in Figure

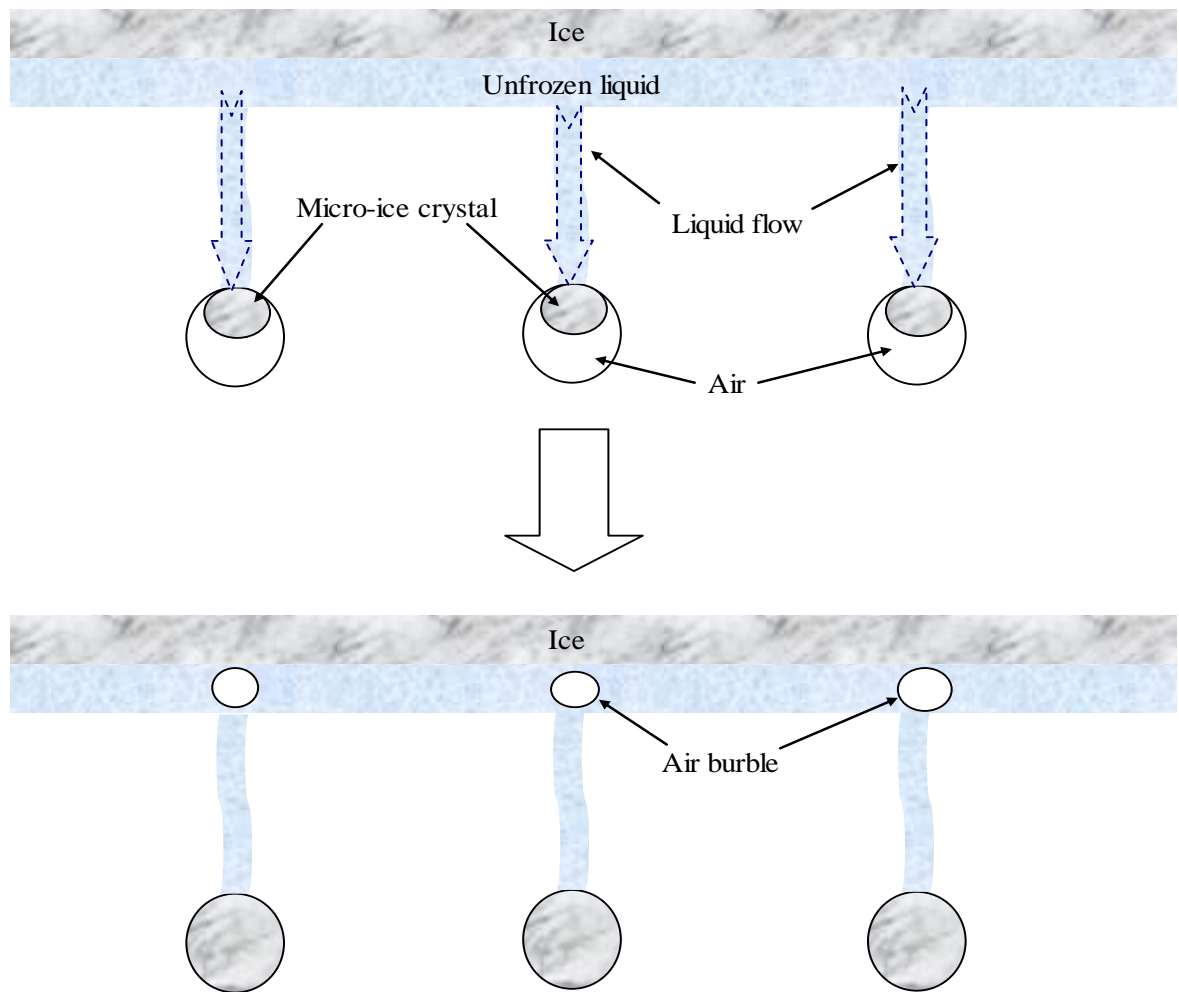


**Figure 7- 12 At a given, critical water content in a unit cell, the actual flow distance equals the critical value [12]**

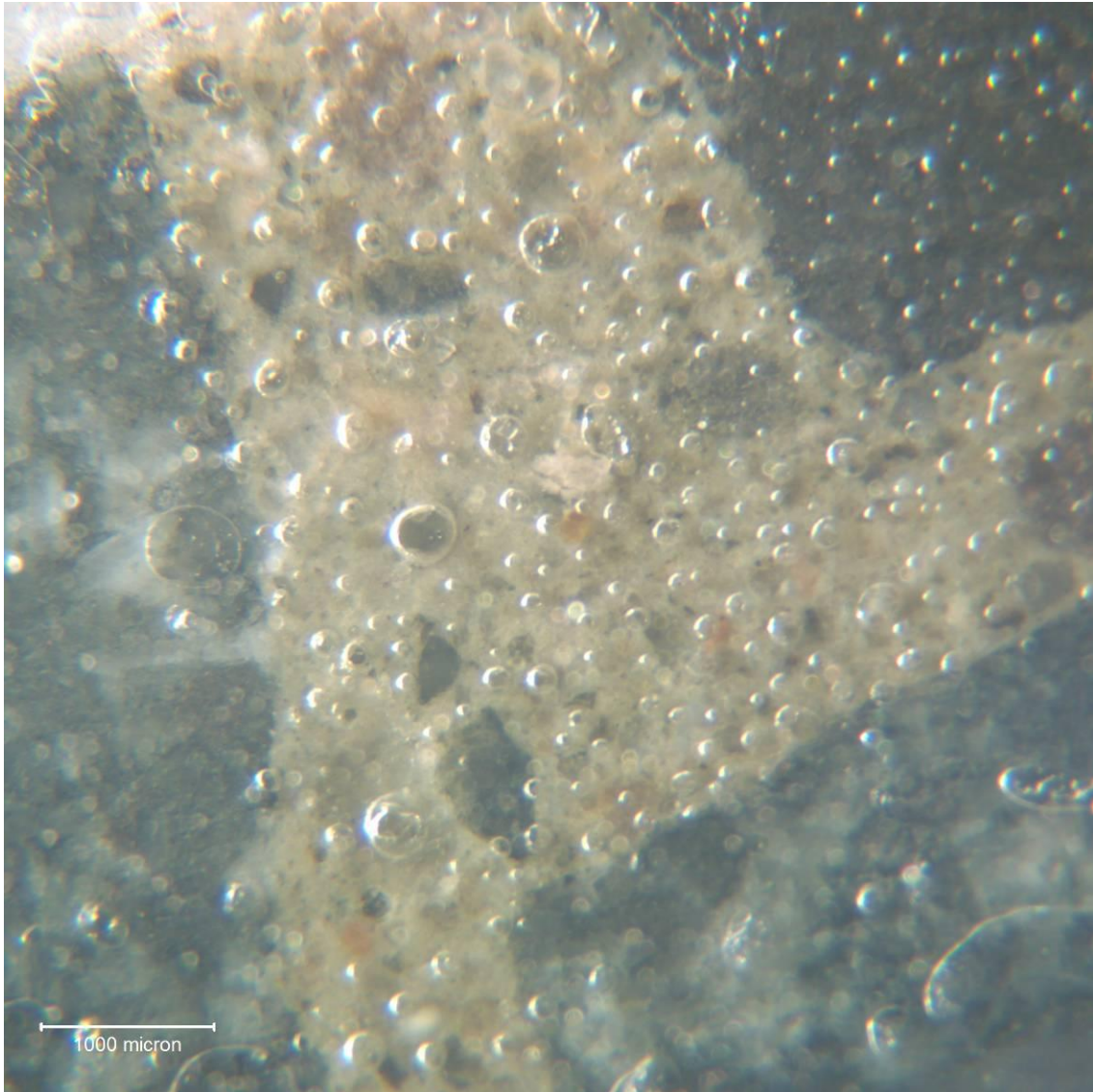
As explained before, the pore pressure increases as flow distance increases. According to the critical degree of saturation theory some air voids are filled with liquid as liquid content increases and it causes flow distance to be longer. Besides, the degree of saturation of surface paste of concrete becomes very high by cryogenic pump during freezing in presence of salt solution. Thus, destructive pore pressure can be generated in the area.

### 7.4.3 Expelling air by cryogenic pump

Once pore liquid freezes, micro ice crystals in large pores or voids suck the liquid from capillary and consequently outer liquid reservoir. The volume increase cause to expel excess liquid and air. The expelled air can be trapped in the surface ice because top surface of liquid is frozen before air come out. The phenomenon may occur when surface liquid is de-icing salt solution of low concentration. A schematic explanation is shown in Figure 7.13 and a microscopic photo of ice layer of 3% sodium chloride solution on concrete surface in Figure 7.14. Many air bubbles were entrapped in the ice layer.

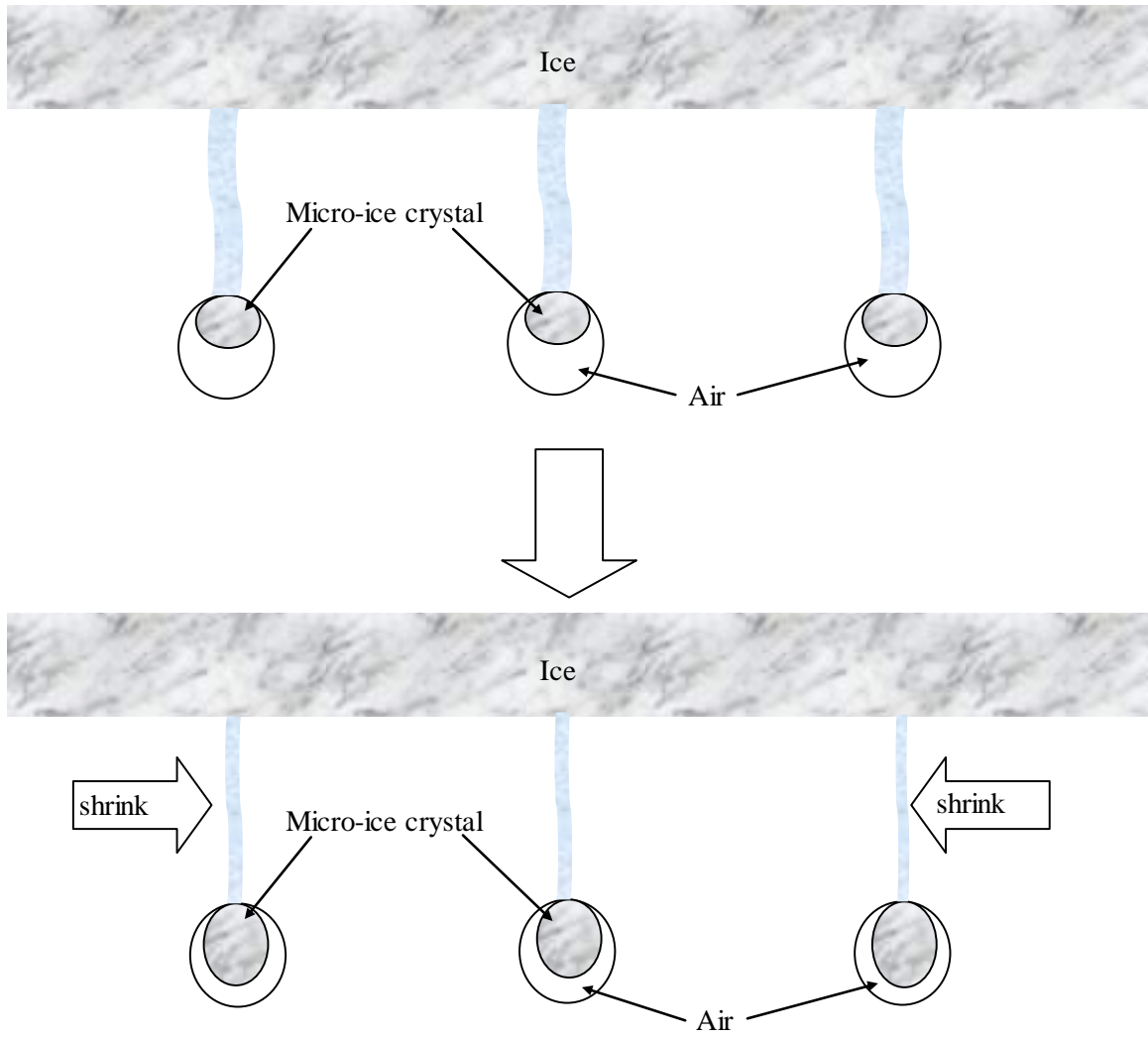


**Figure 7- 13 Schematic explanation of expelling air burbles in salt solution during freezing**

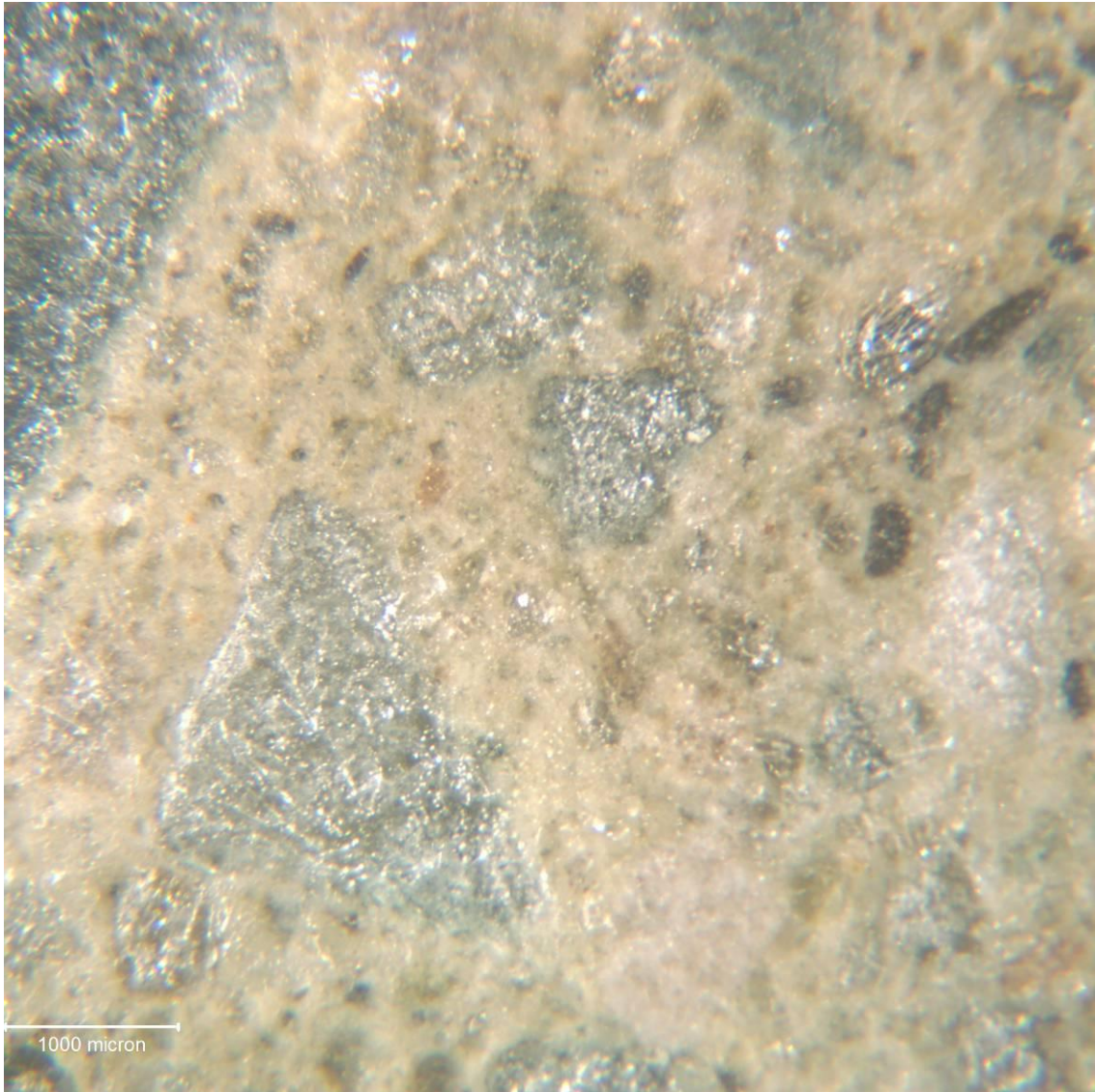


**Figure 7- 14 Microscopic photo of the ice layer on concrete surface at -20C (3%NaCl Solution, 2F-T cycles)**

When surface liquid, however, is pure water, surface liquid is totally frozen and micro-ice crystal may not filled the voids so that air may not be expelled. Not many air burbles have been found in ice of water.



**Figure 7- 15 Schematic explanation when surface liquid is water**



**Figure 7- 16 Microscopic photo of the ice layer on concrete surface at -20C (water, 2F-T cycles)**



### **7.4.3 Air voids clustering and ITZ**

As a result, not only is air content essential factor but spacing factor is also key factor. However, air voids system with sufficient numbers of air content and spacing factor can work properly when the voids are spread out through whole paste. In fact, air-void clustering and agglomerates were reported in [47]. According to the report, the air-void clustering can cause low compressive but the cause of the clustering has not been established. The air void-clustering also has been observed in this study. It is noticeable that the clustering seems to coincide with ITZ around aggregates. In the early stages of hydration there is much solution-filled space. The mass content of this water-rich zone is very low (i.e. very porous zone) even after long duration of hydration [48]. See Figure 7.17. Thus, high local water-cement ratios seem to create very porous zone called ITZ around aggregates [48, 49, 50]. In case of air entrained concrete, Air-Entrain-Agent (AEA) can flow along with water. Then, water-rich zone can contain a higher portion of AEA. As a very porous zone, the ITZ can be easily damaged by frost attack due to high local degree of saturation as well as low strength. In fact, the ITZ was damaged in early freeze-thaw cycles in this study.

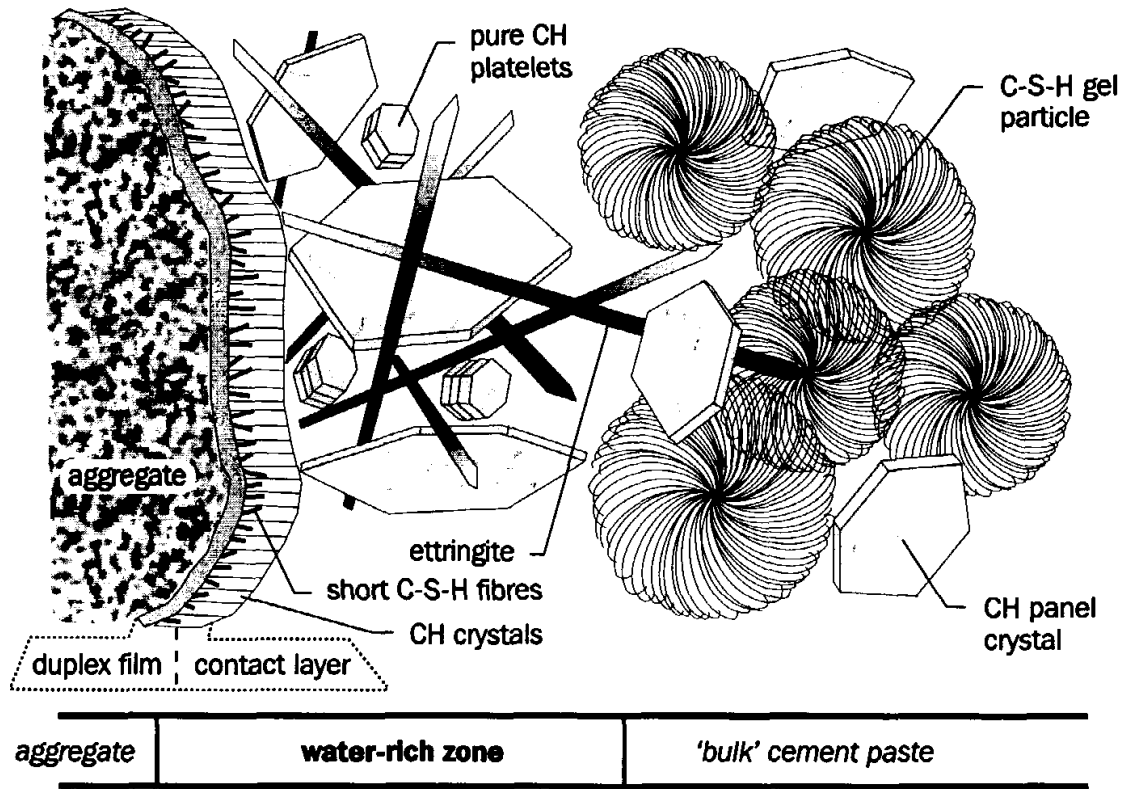
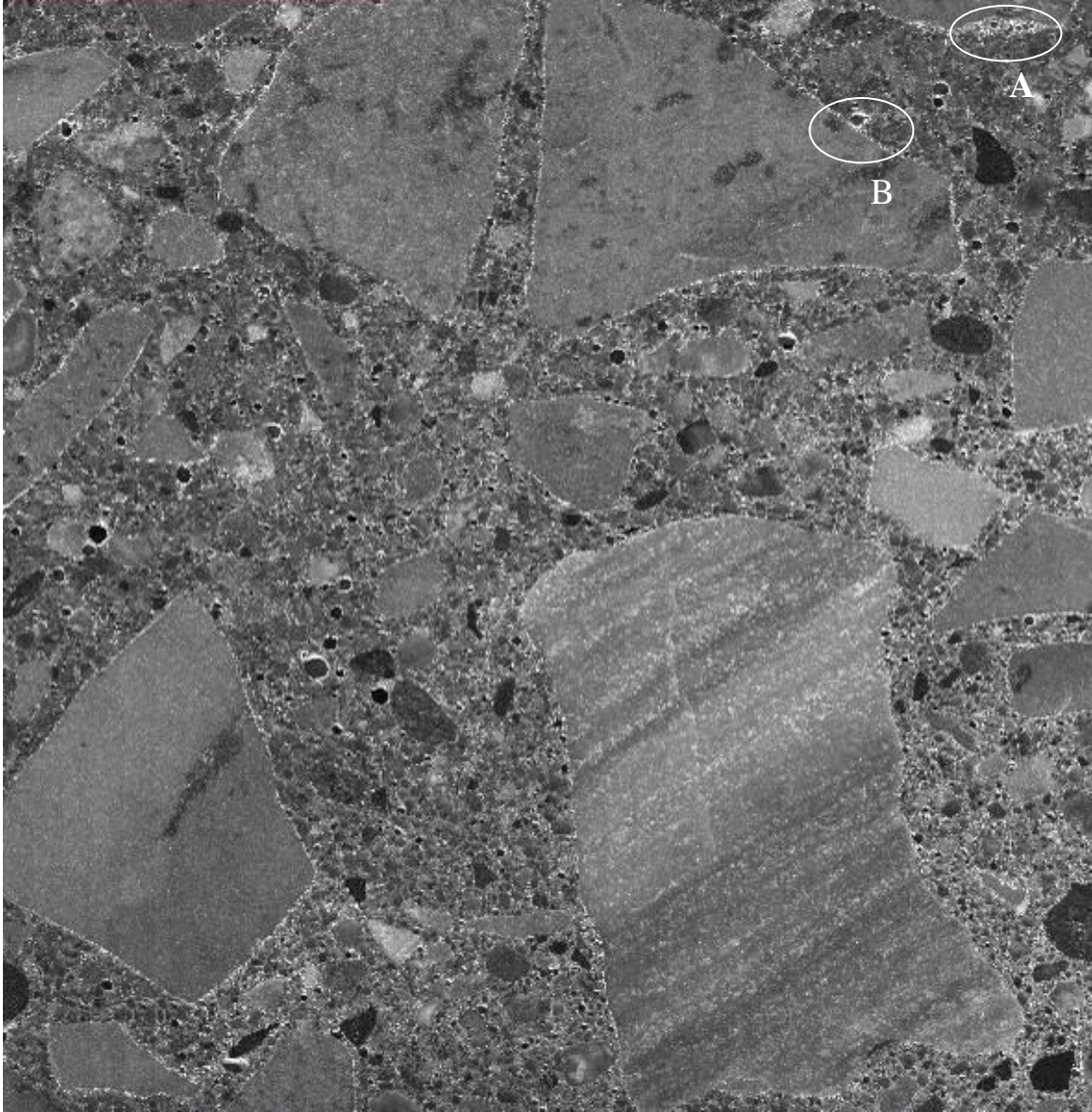


Figure 7- 17 Schematic impression of the interfacial transition zone [48]

#### 7.4.3.1 Microscopic examination air voids clustering on OPC specimens

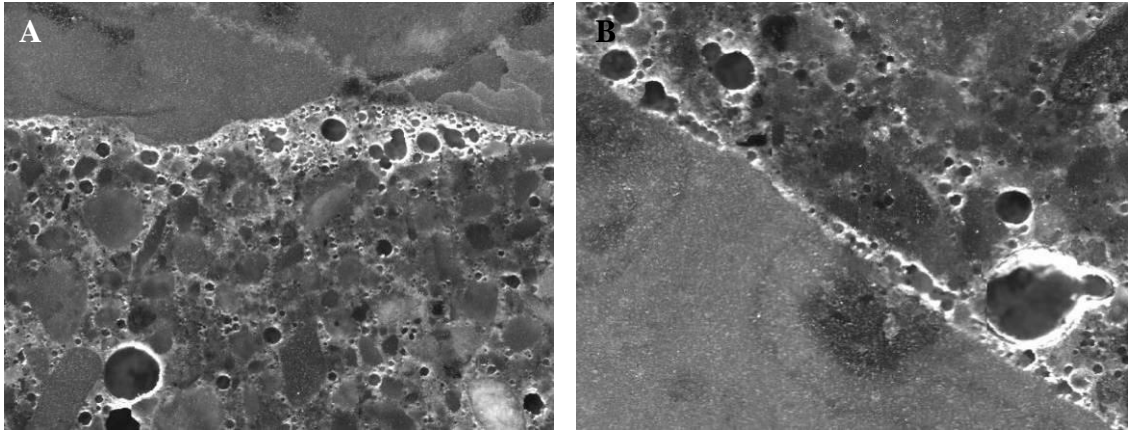
To find out how serious the ITZ and air-void clustering are, the surfaces of OPC 1 and OPC 2 concrete have been observed at microscopic level.



**Figure 7- 18 Polished surface of OPC-I specimen**

In the Figure 7.18, it is seen that air voids tend to congregate around aggregates. For a close look, spot A and B are magnified.





**Figure 7- 19 Spot A and B of OPC-I specimen in Figure 7.18**

Fine voids gathered around aggregates and some voids were united. This phenomenon reduced the efficiency of air voids system. Besides, the gathering voids prevent paste from bonding to aggregates. As the air contents increase, the phenomenon became more significant. See Figure 7.20 and 7.21.

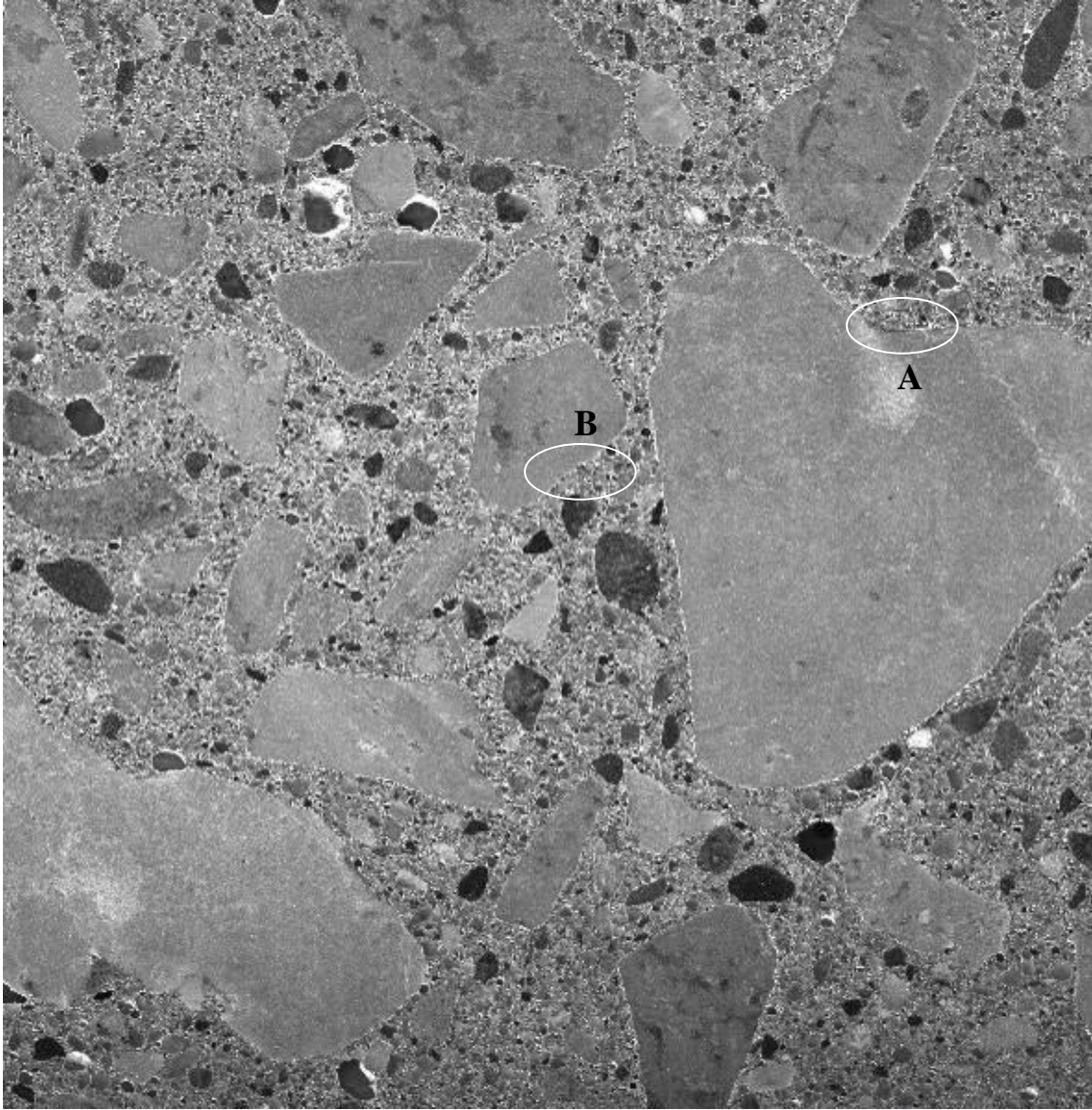


Figure 7- 20 Polished surface of OPC-II specimen

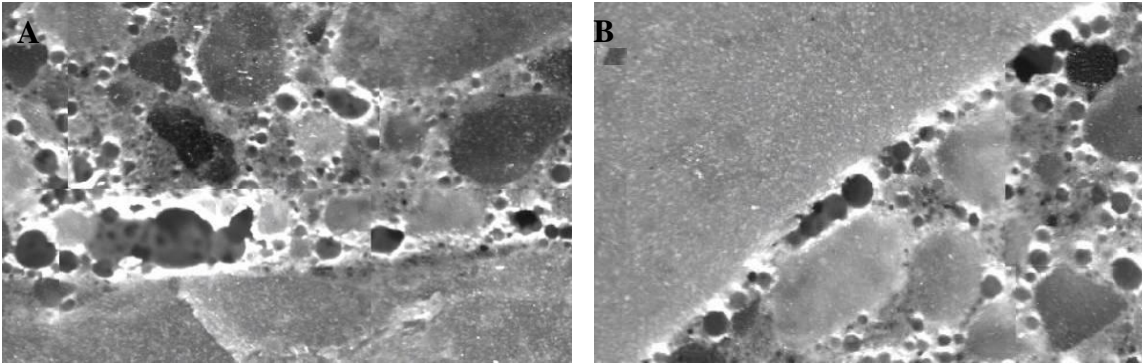
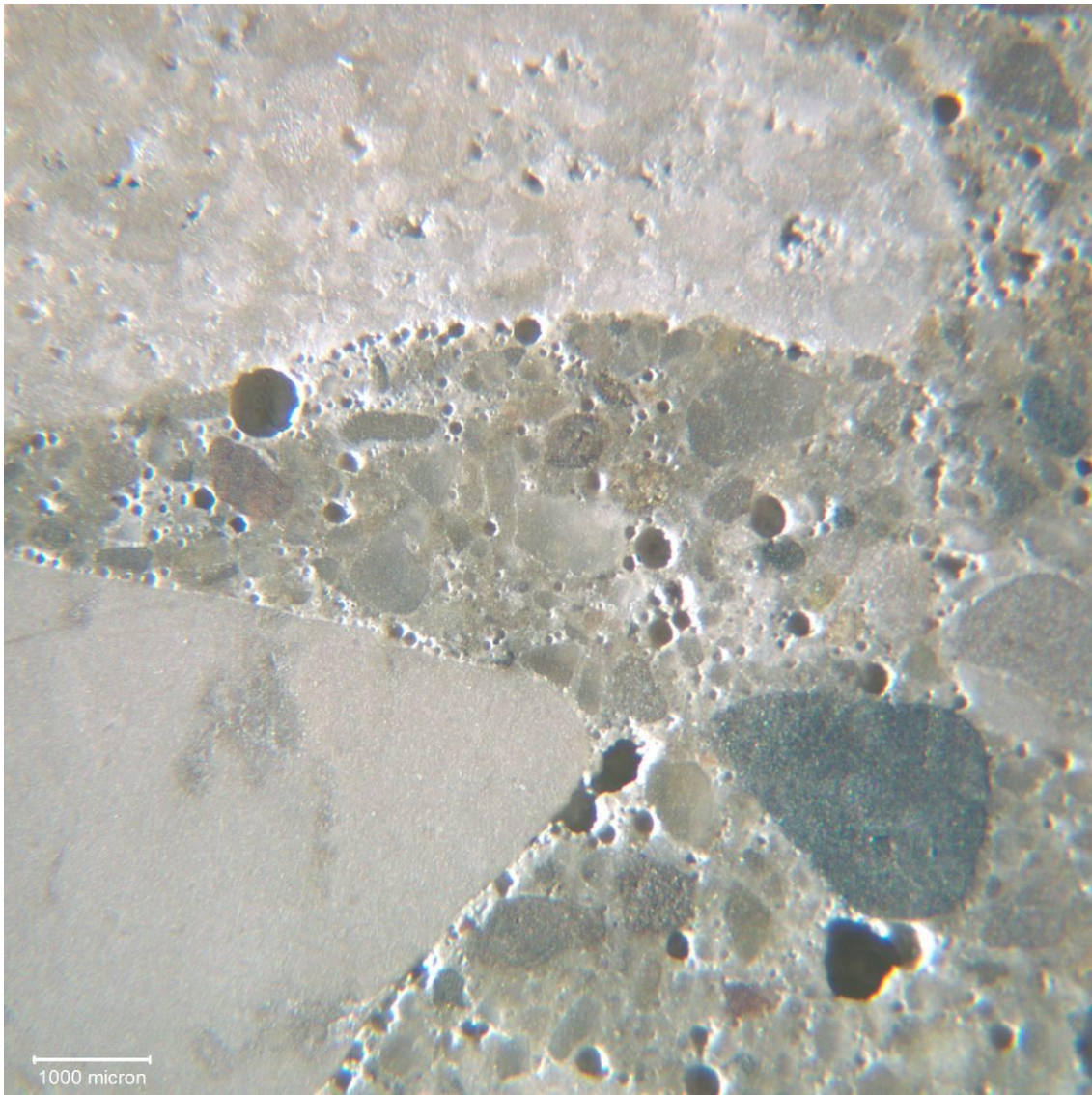


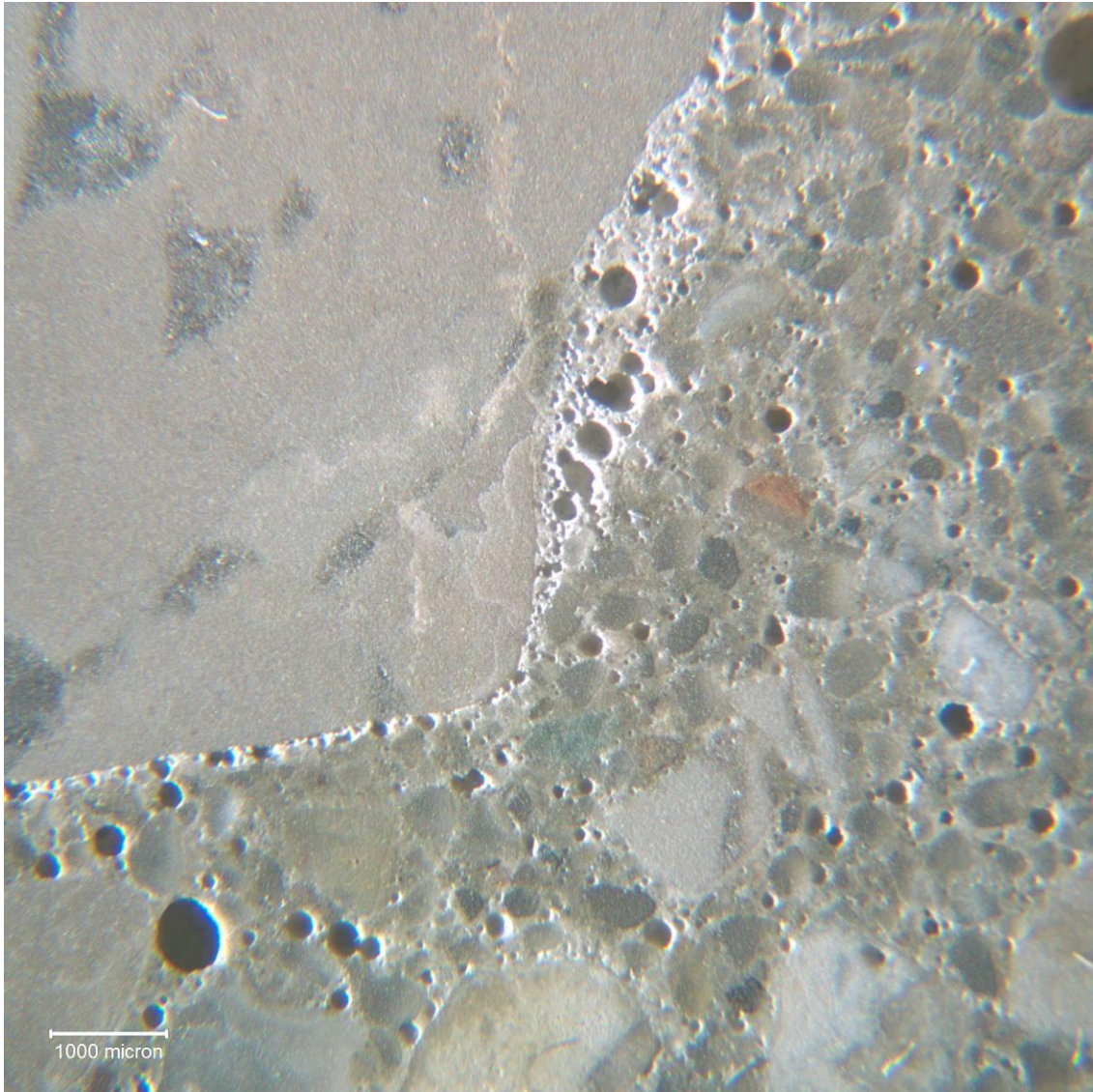
Figure 7- 21 Spot A and B of OPC-II specimen in Figure 7.20



The congregated air voids may not protect paste from hydraulic pressure but weaken bond strength between paste and aggregates. The drawbacks have been observed almost every interface between paste and aggregates on OPC concrete. See Figure 7.22 and Figure 7.23.



**Figure 7- 22 Interface between aggregates and paste (OPC-I)**

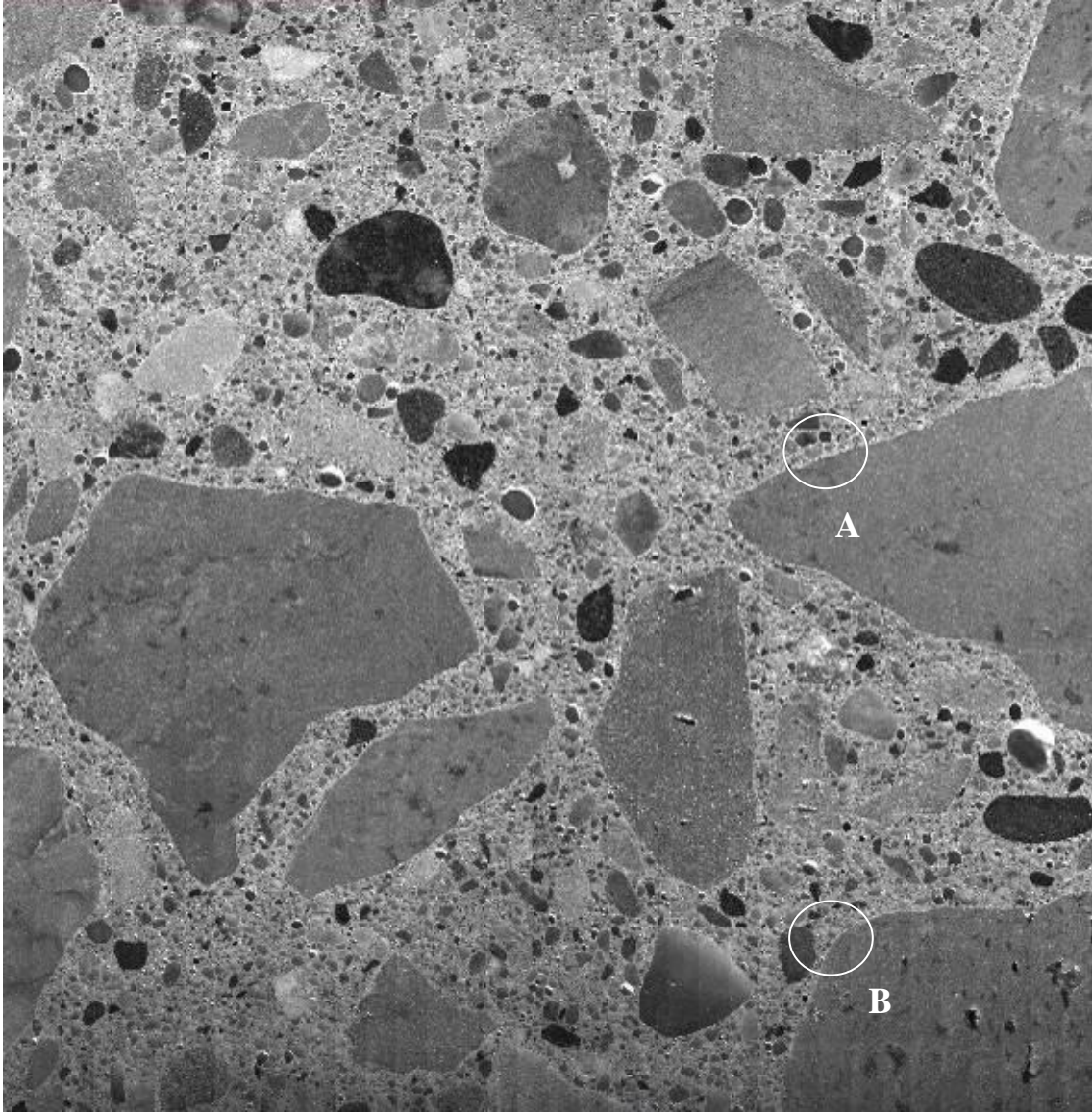


**Figure 7- 23 Interface between aggregates and paste (OPC-II)**

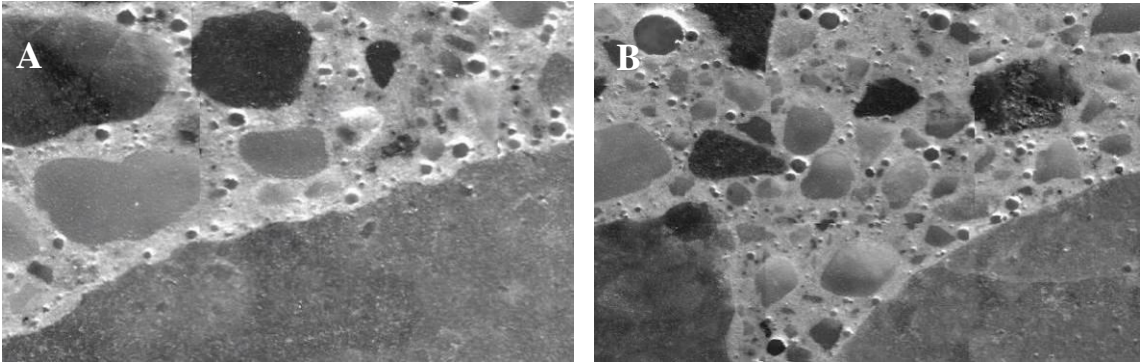
#### **7.4.3.2 Microscopic examination air voids on HPC specimens**

Among many structural advantages, the use of GGBFS can improve the fluidity of fresh concrete. This benefit seems to reduce water-rich zone and therefore air-void clustering. See Figure 7.24 and 7.25.



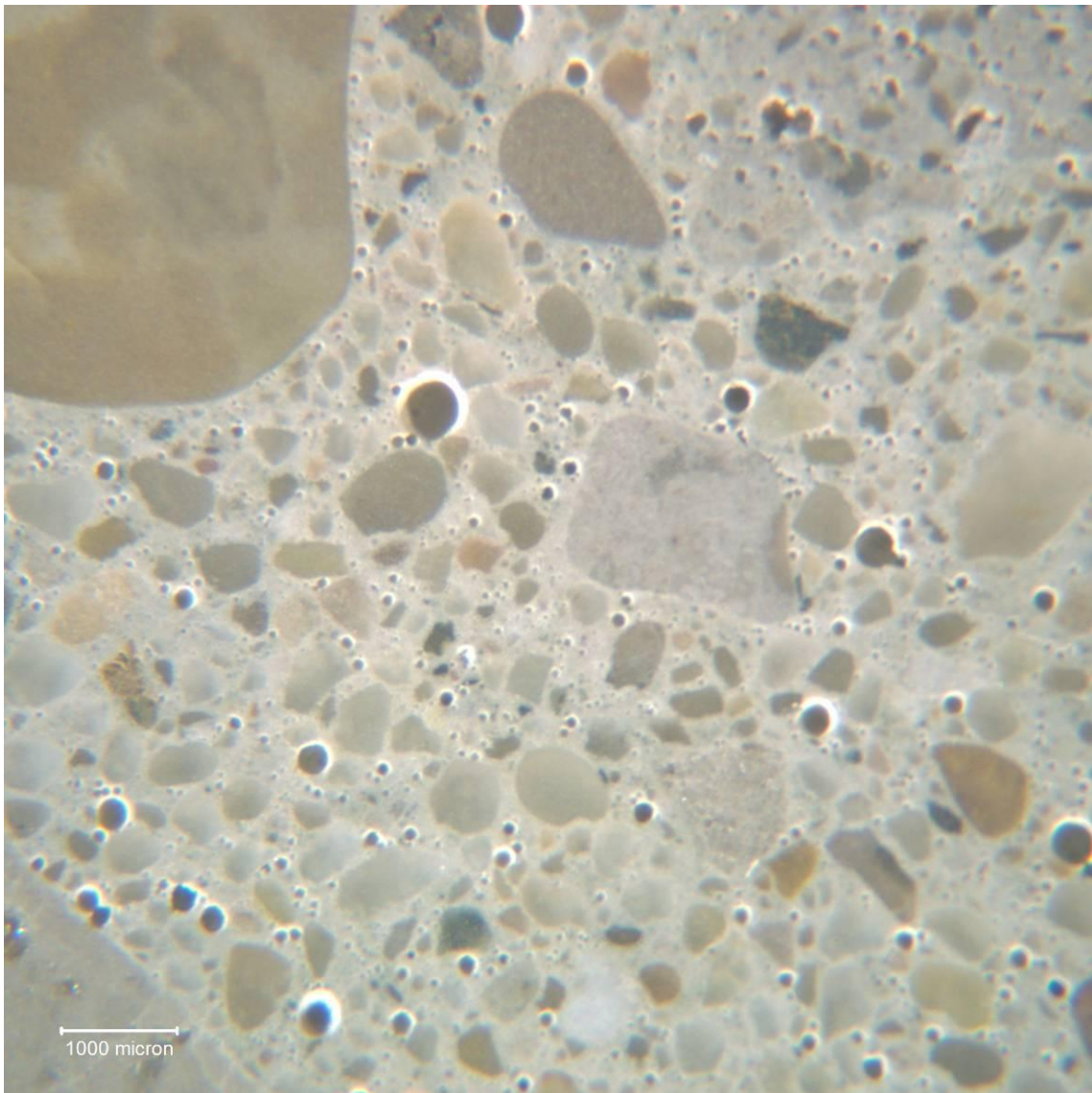


**Figure 7- 24 Polished surface of HPC-II specimen**



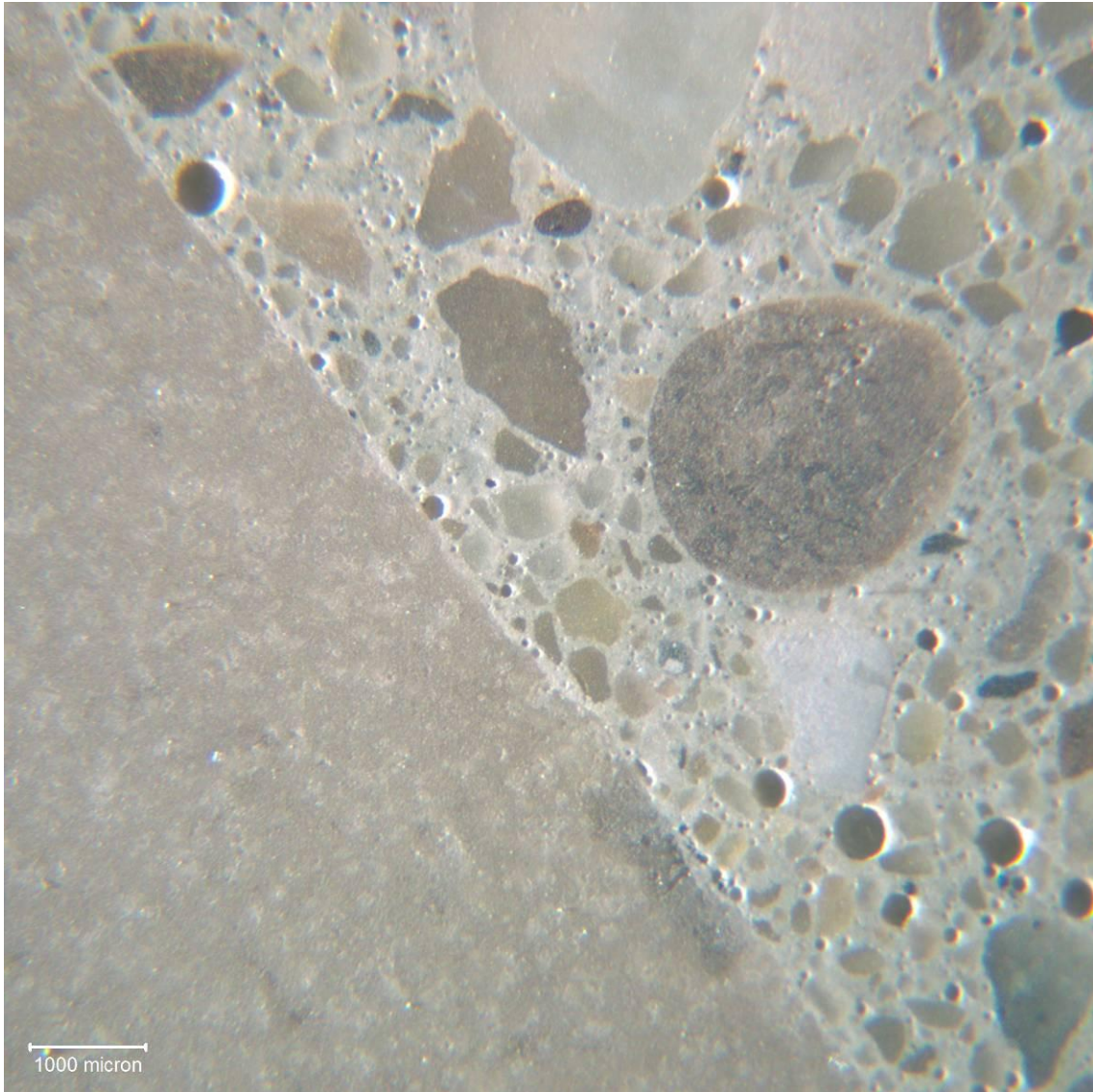
**Figure 7- 25 Spot A and B of HPC-II specimen in Figure 7.24**

The air-void clustering has not been observed almost every interface between paste and aggregates on HPC concrete. See Figure 7.26 and Figure 7.27.



**Figure 7- 26 Interface between aggregates and paste (HPC-II)**





**Figure 7- 27 Interface between aggregates and paste (HPC-III)**

#### **7.4.3.3 ITZ and air voids with in the ITZ of OPC concrete**

As concrete is a composite material the cement paste cannot be considered as a homogeneous phase. In fact, hydrated cement paste surround sand and coarse aggregate called Interfacial Transition Zone (ITZ). The ITZ has very high porosity so it has higher degree of saturation than bulk past. The diffusivity is rely on porosity. The effective

diffusion coefficient for transport through the pores,  $D_e$ , is estimated as follows:

$$D_e = \frac{D\varepsilon_t\delta}{\tau} \quad (7.4)$$

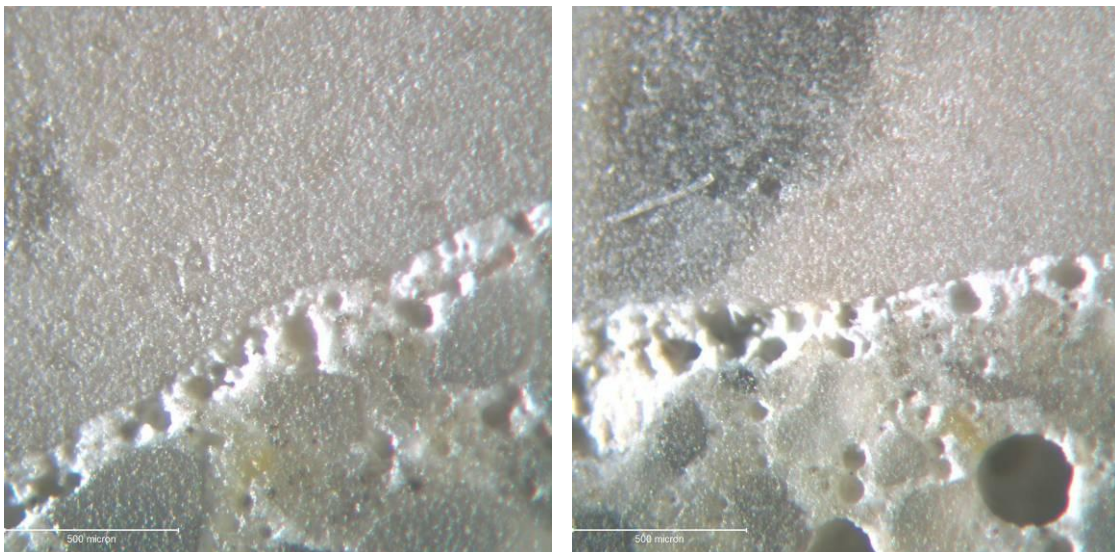
Where:

$D$ : diffusion coefficient in gas or liquid filling the pores ( $m^2s^{-1}$ )

$\varepsilon_t$ : porosity available for the transport (dimensionless)

$\tau$ : tortuosity (dimensionless)

Porosity is linearly related with diffusivity and pore pressure. As results, ITZ may have higher water contents and consequently higher pore pressure during freezing.



**Figure 7- 28 ITZ and air voids in the zone (OPC-I)**

In addition to high porosity, ITZ tends to draw fine air voids rather than coarse voids. It has been observed that many fine air voids have been entrapped in ITZ reducing the efficiency of air void system of bulk paste. See Figure 7.29 and 7.30.

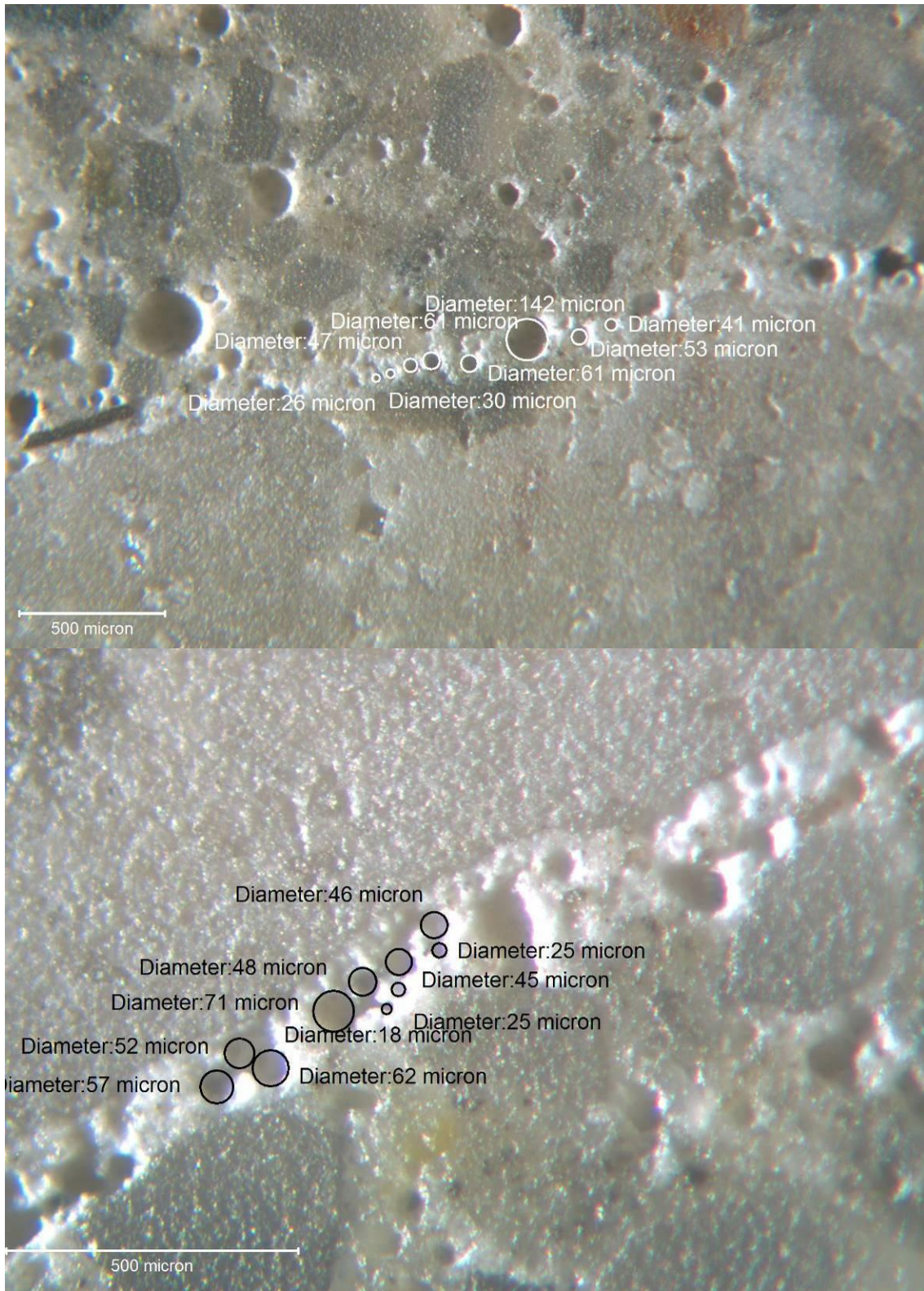
A lot of fine air voids in ranges from 10microns to 100microns are entrapped and place very closely. The air voids are surrounded by very porous paste thus they can be easily



filled with liquid. Once the voids are filled they cannot be considered as protection method but as resources creating cryogenic pump.

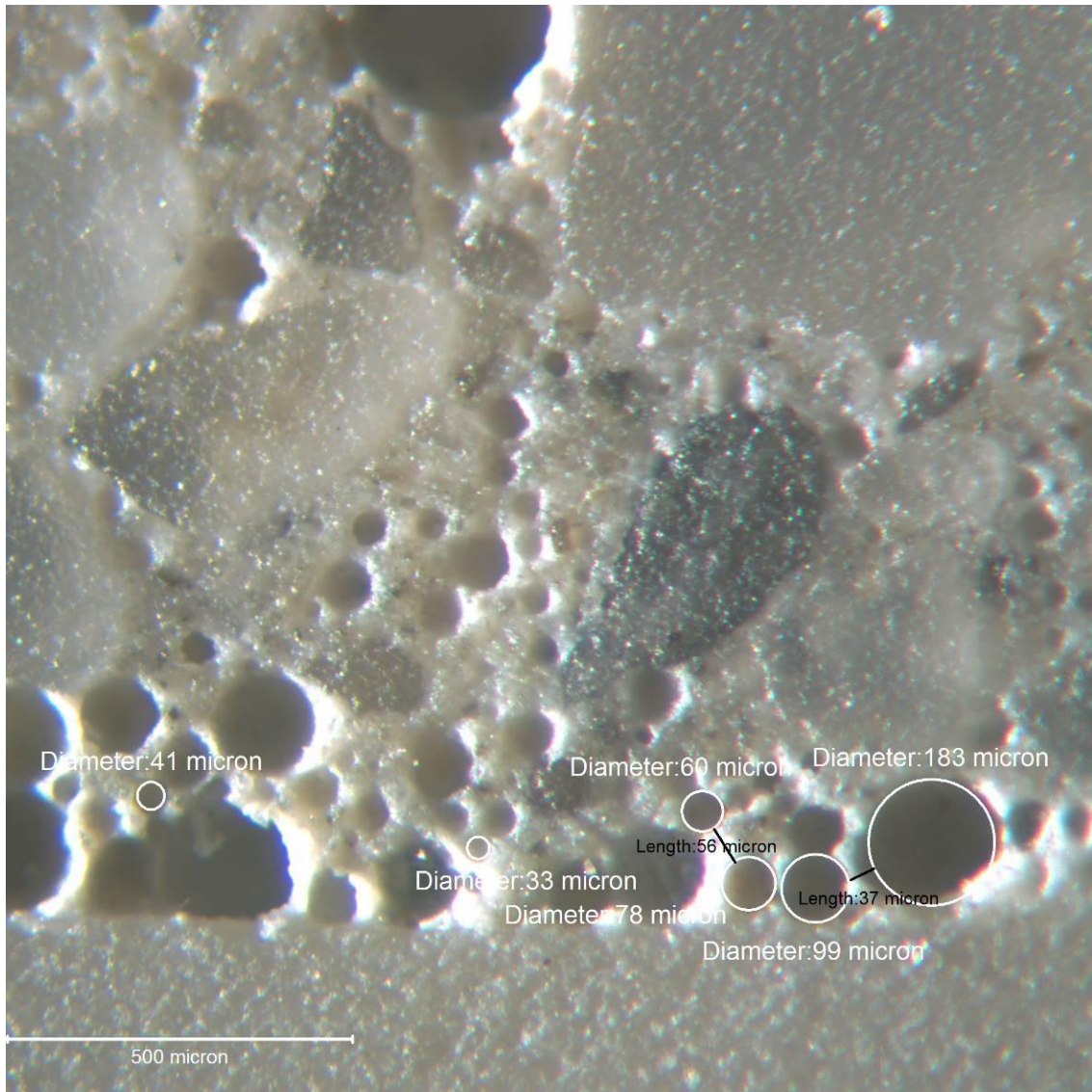
As fine air voids are entrapped in ITZ, there are relatively coarse air voids in bulk paste causing longer flow distances. The drawbacks are getting worse with higher air content.

See Figure 7.31 to 7.33.

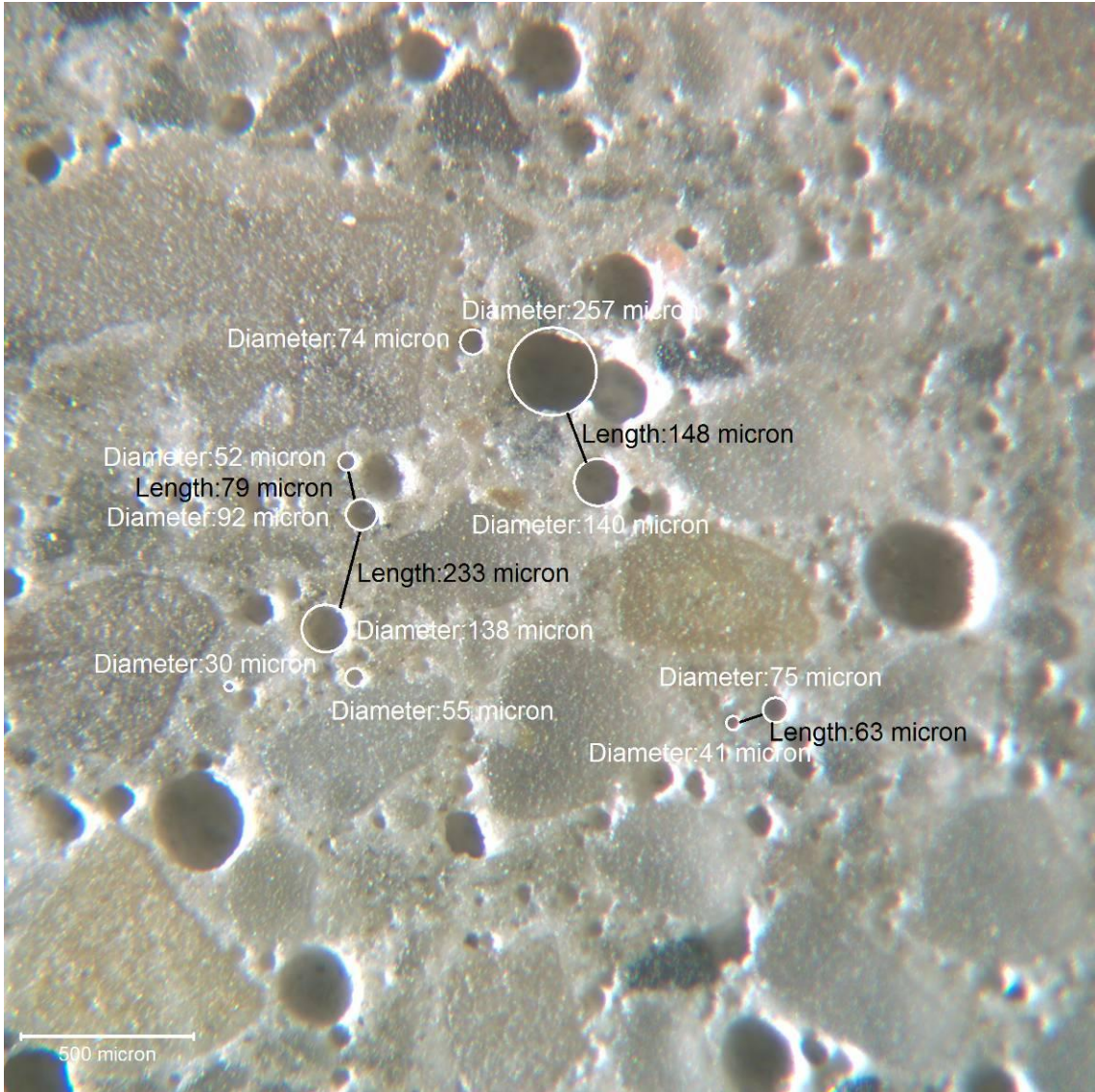


**Figure 7- 29 Air voids in ITZ of OPC-I**



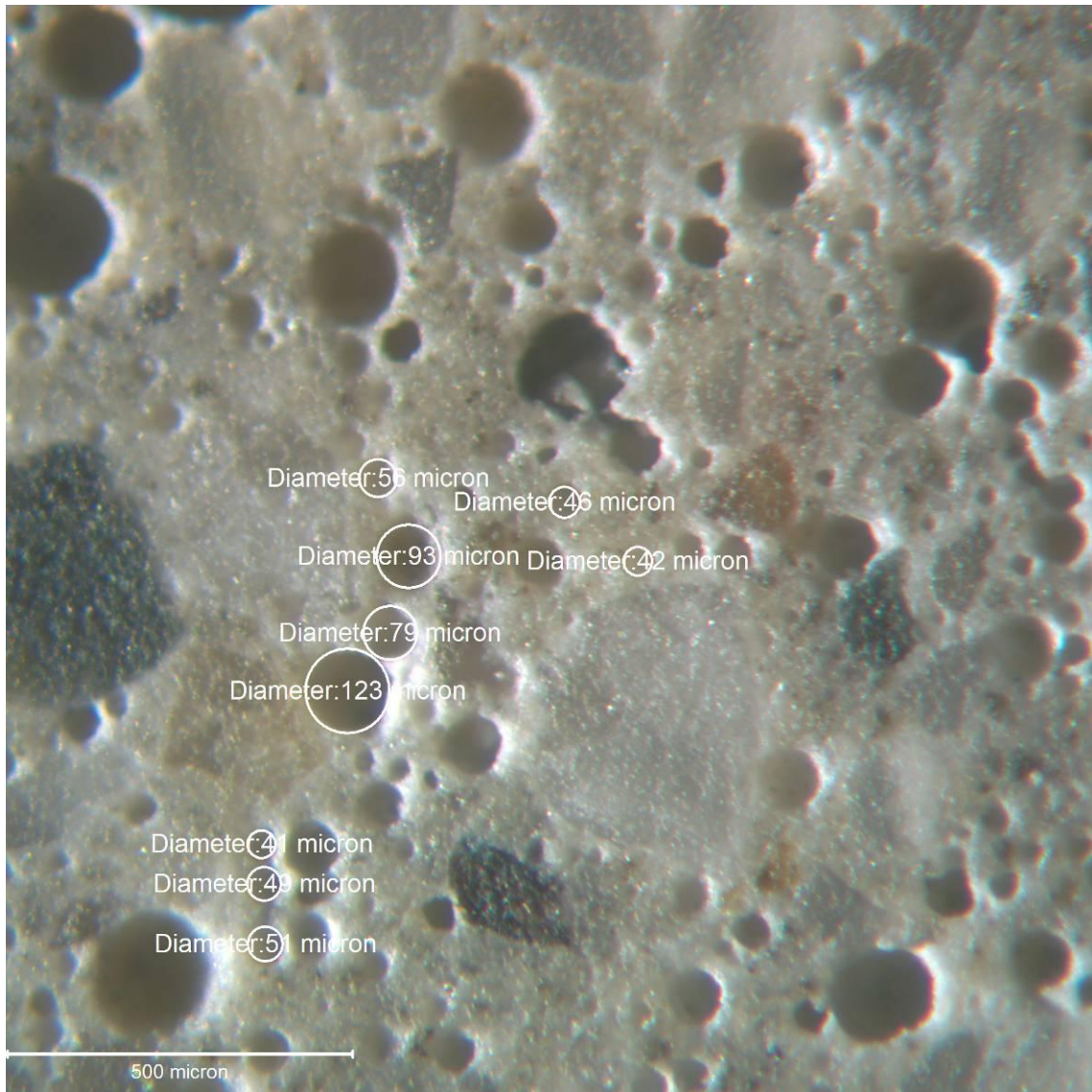


**Figure 7- 30 Air voids in ITZ of OPC-II**

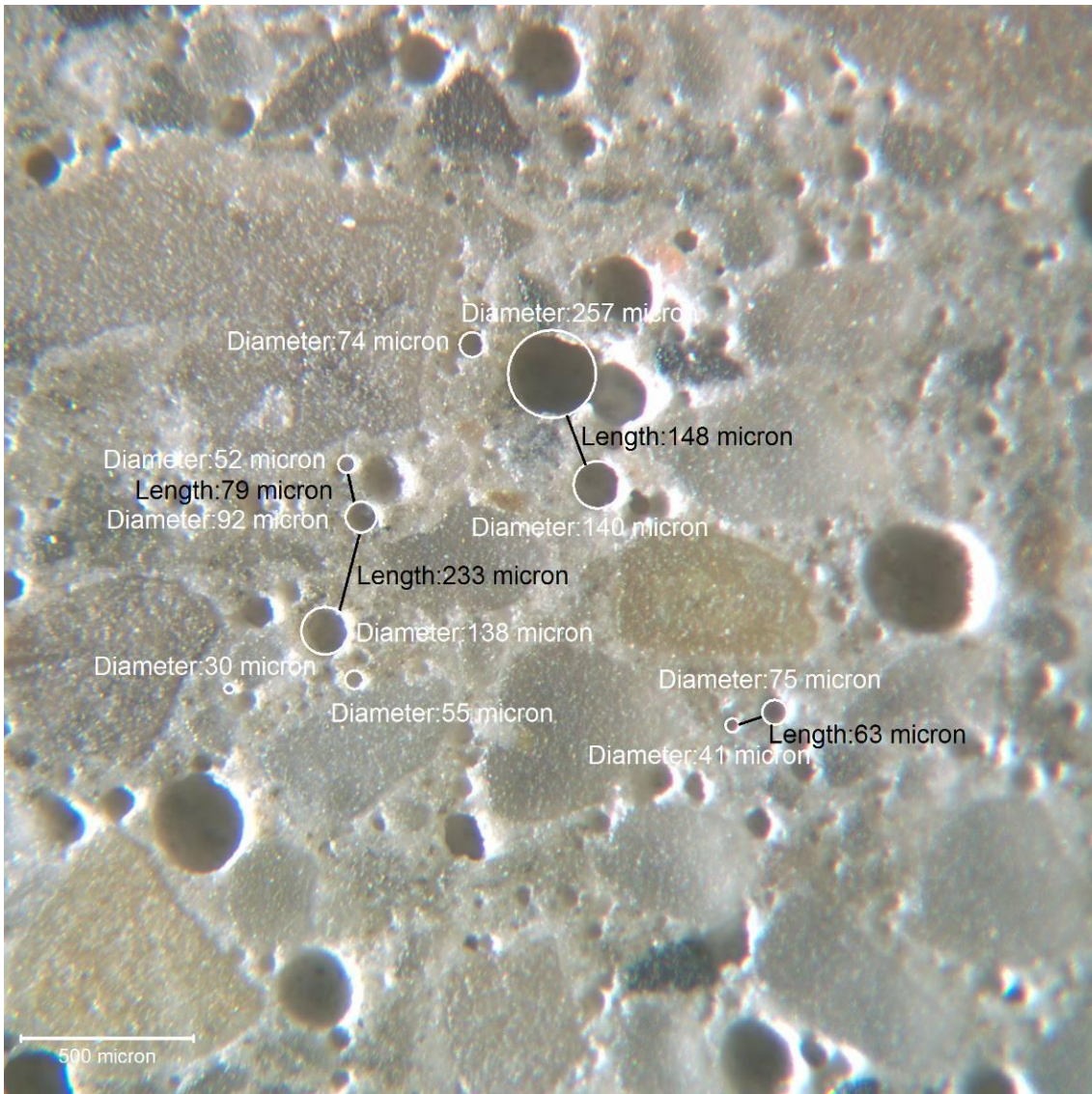


**Figure 7- 31 Air voids in bulk paste of OPC-I**





**Figure 7- 32 Air voids in bulk paste of OPC-II**

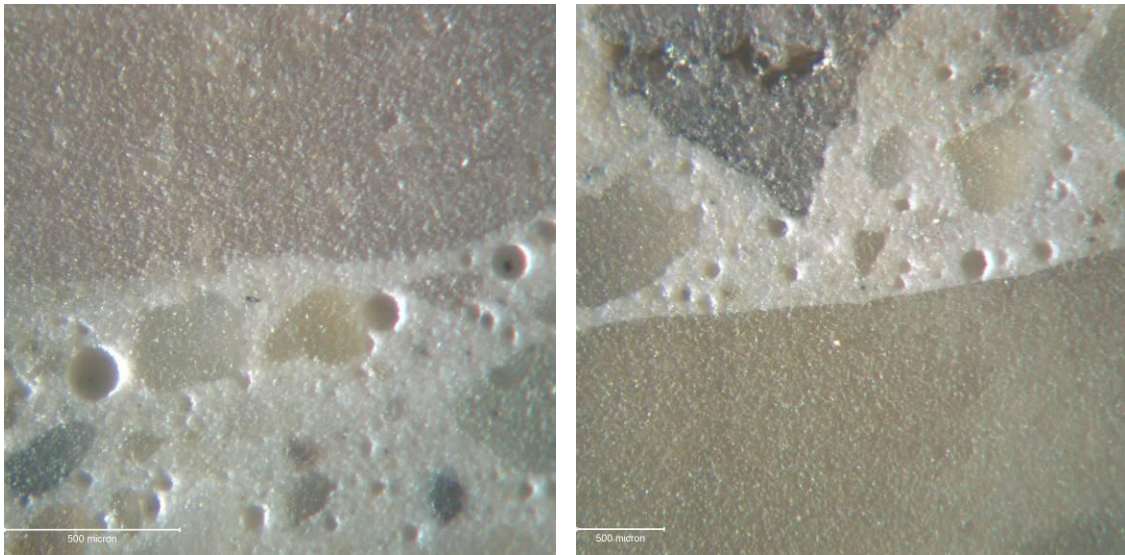


**Figure 7- 33 Another examination of air voids in bulk paste of OPC-II**



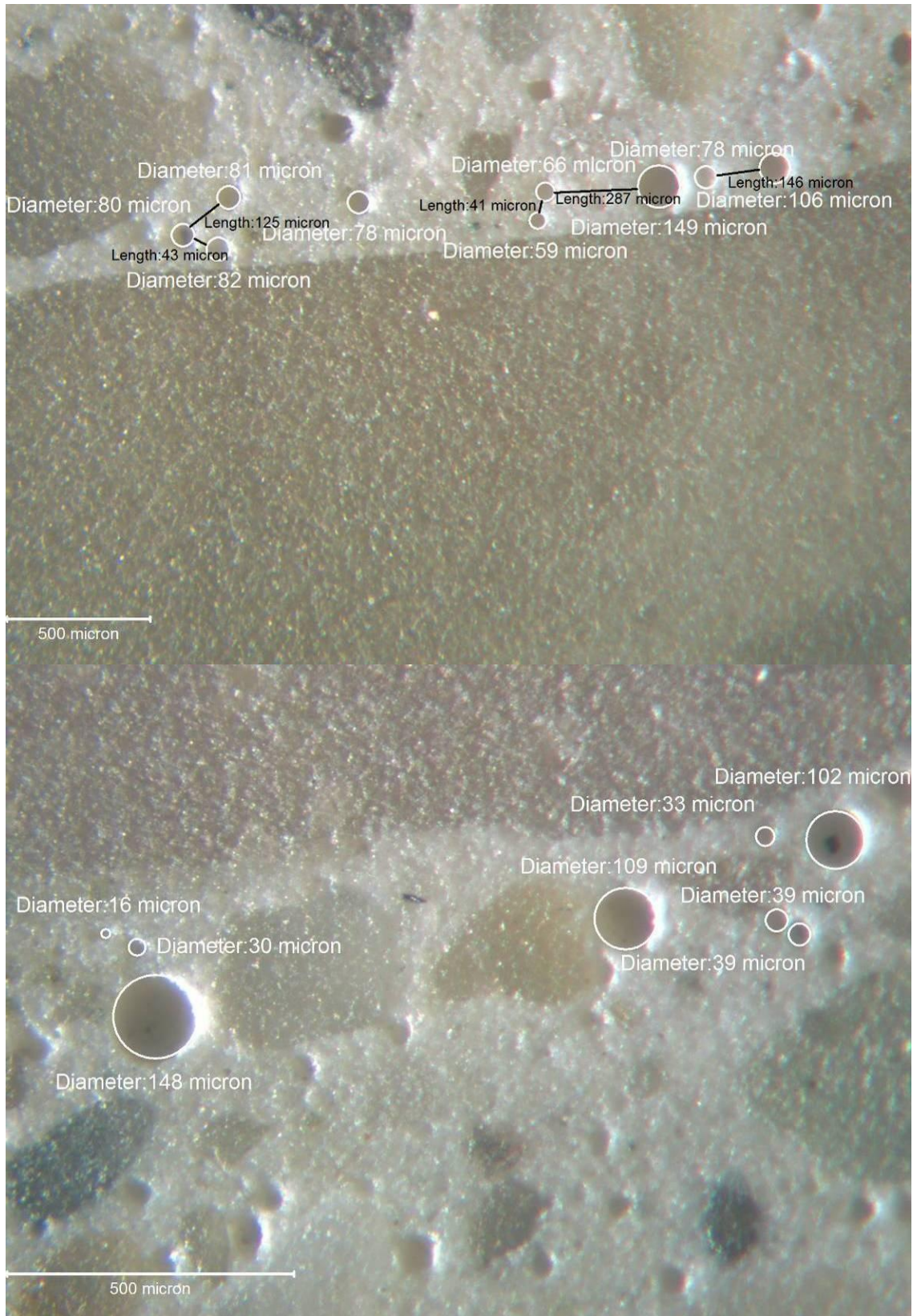
#### 7.4.3.4 ITZ and air voids with in the ITZ of concrete containing GGBFS

ITZ has not been observed significantly in HPC concrete. Air voids are well distributed. Congregations of air voids do not occur as well. The properties of air voids are consistent between interfaces and bulk concrete. See Figures 7-34.



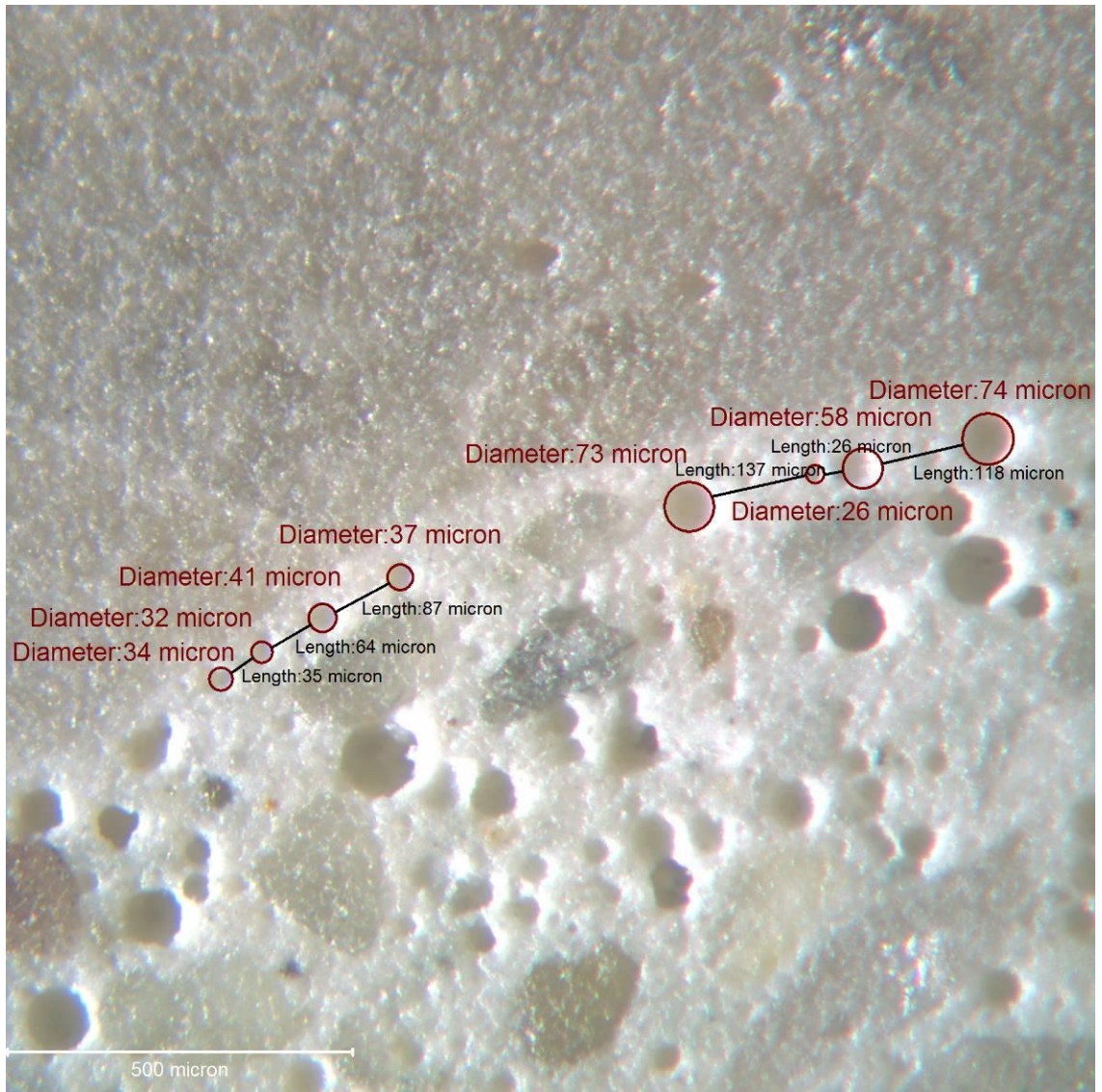
**Figure 7- 34 Interface of HPC-II**

Air voids at interface of HPC concrete seems to distribute well in terms of radius as well as distance between voids. It seems not to be different both in HPC-2 (Figure 7.35) and HPC-3 (Figure 7.36). As a result, bulk paste also has well distributed air voids system. See Figure 7.37 through 7.39.

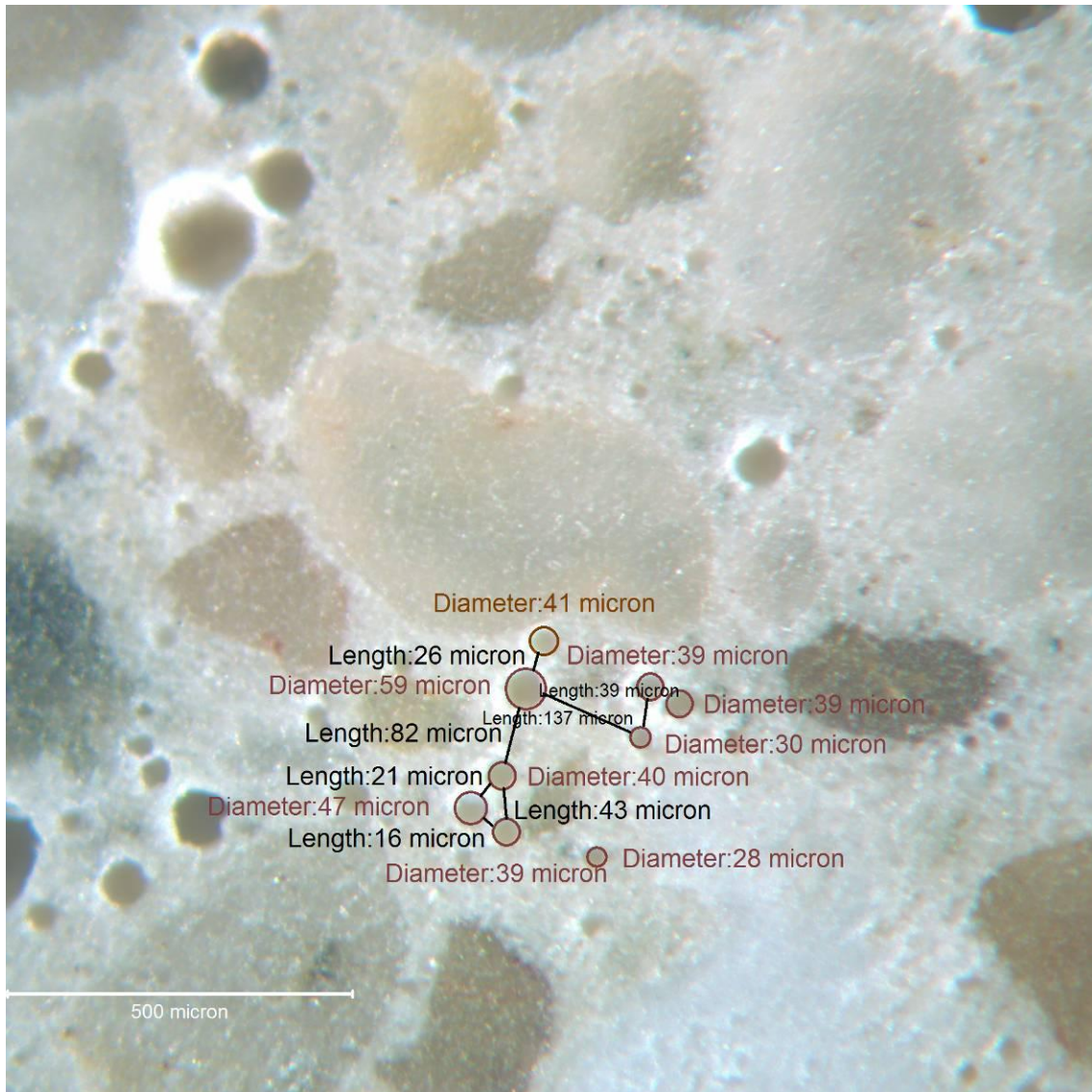


**Figure 7- 35 Air voids in interface of HPC-II**



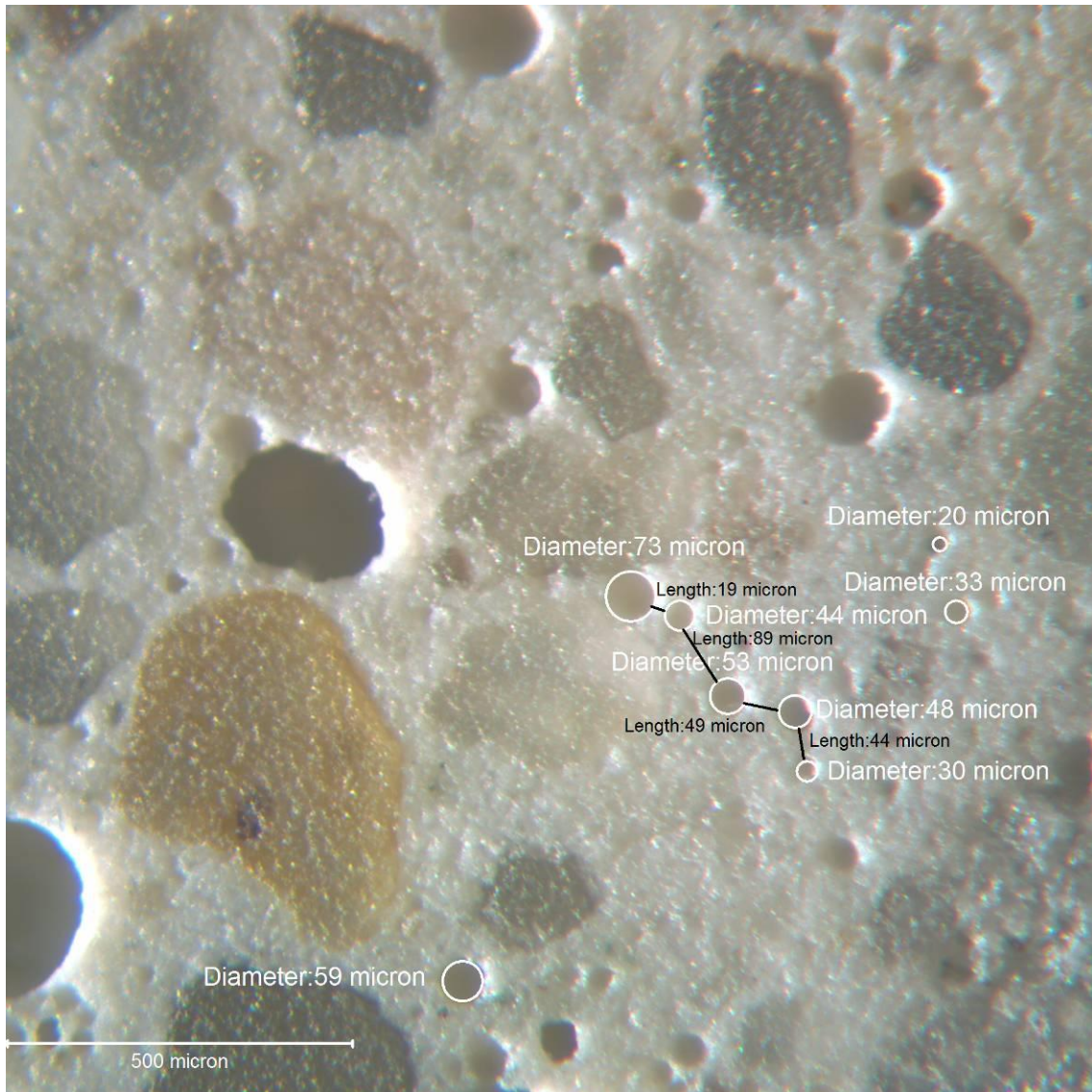


**Figure 7- 36 Air voids in interface of HPC-III**

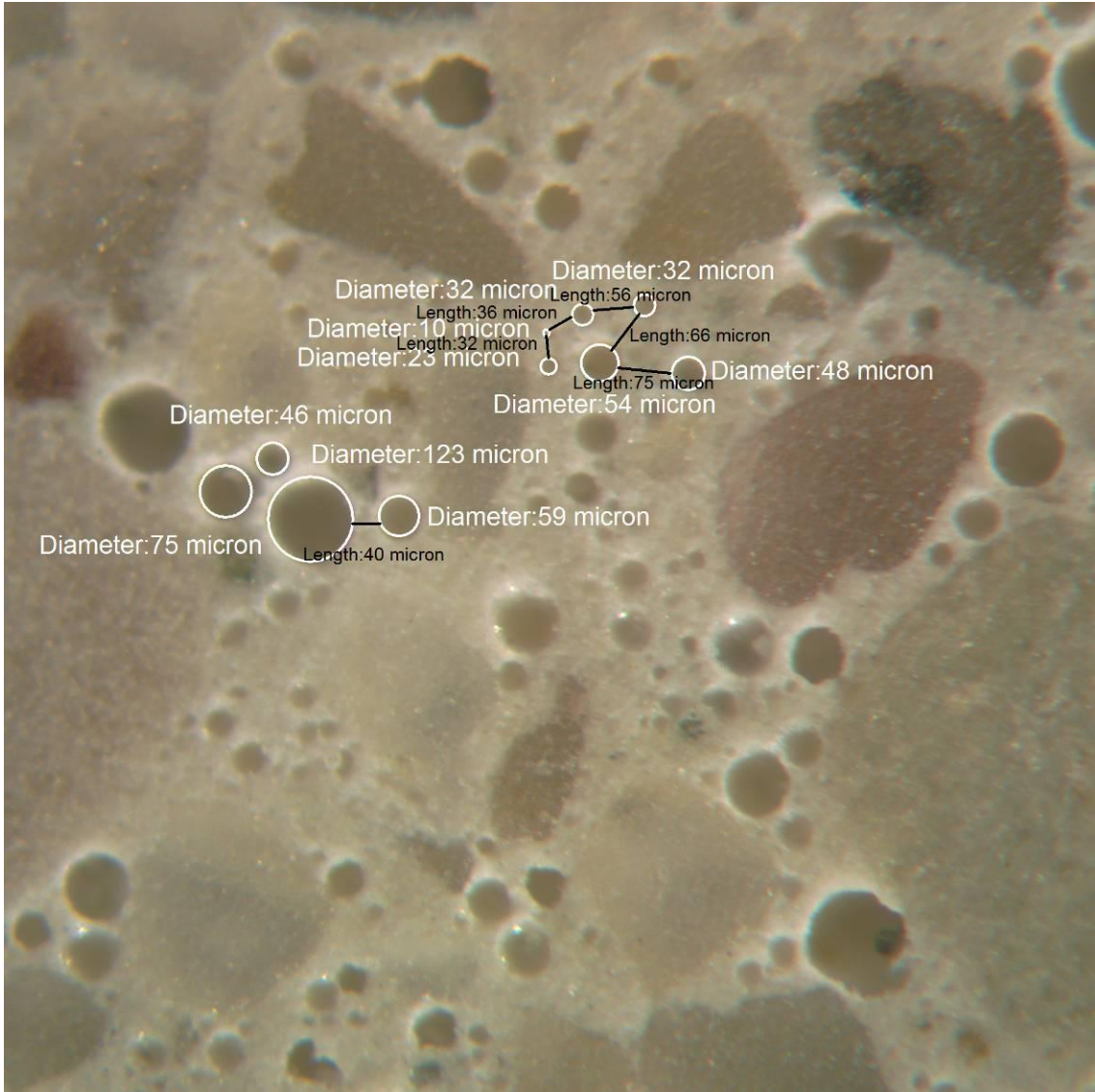


**Figure 7- 37 Air voids in bulk paste of HPC-III**





**Figure 7- 38 Another air voids in bulk paste of HPC-III**



**Figure 7- 39 Air voids in bulk paste of HPC-III**

### 7.4.3.5 Damage of ITZ by expansion during F-T cycles

Concrete paste can be protected by air voids from destructive hydraulic pressure until degree of saturation reach to the critical point. The porosity of ITZ may be extremely high up to 40% which is 10times of bulk paste. Thus, the degree of saturation of ITZ can be easily reached to critical point while that of bulk paste sill remain under critical point. Once temperature drop under freezing point, the water content of ITZ increases by cryogenic pump. As a results, expansion can be concentrated within ITZ. The strain of paste can be divided as strain of ITZ and strain of bulk paste.

$$\varepsilon_{total} = \varepsilon_{ITZ} + \varepsilon_{paste} \quad (7.5)$$

$$\varepsilon_{ITZ} = \frac{\Delta l_{ITZ}}{l_{ITZ}} \approx \frac{\overline{l_{agg}} \cdot \Delta l_{ITZ}}{2 \cdot P_{agg} \cdot l \cdot \overline{l_{ITZ}}} \quad (7.6)$$

$$\varepsilon_{paste} = \frac{\Delta l_{paste}}{l_{paste}} \approx \frac{\Delta l_{paste}}{P_{paste} \cdot l} \quad (7.7)$$

$$\Delta l = \Delta l_{ITZ} + \Delta l_{paste} \quad (7.8)$$

Where,

$l$  is total length of concrete

$\Delta l_{ITZ}$  is the length change of ITZ

$l_{ITZ}$  is the length of ITZ

$\overline{l_{agg}}$  is the mean value of aggregate diameter

$P_{agg}$  is aggregate content

$\Delta l_{paste}$  is the length change of paste

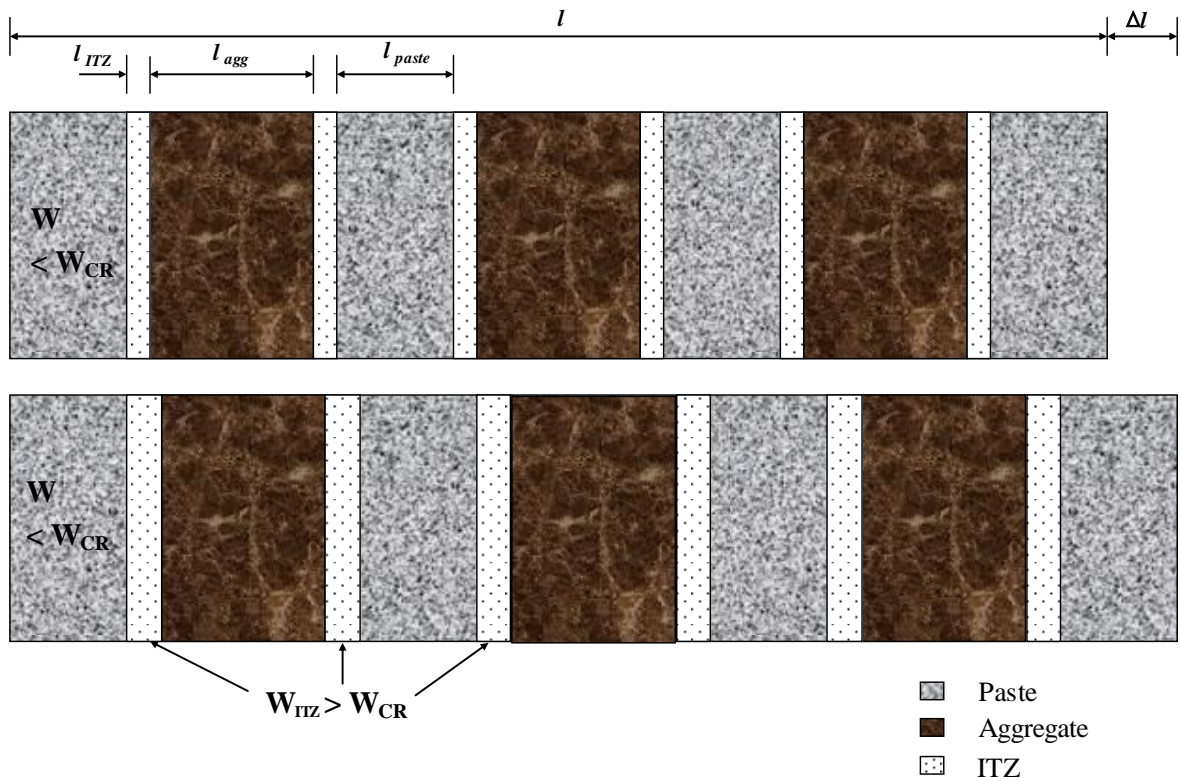
$l_{paste}$  is the length of paste

Assuming that paste is protected perfectly from expansion by air voids, and then the equations can be;

$$\varepsilon_{total} = \varepsilon_{ITZ} \approx \frac{\overline{l_{agg}} \cdot \Delta l_{ITZ}}{2 \cdot P_{agg} \cdot l \cdot \overline{l_{ITZ}}} \quad (7.9)$$

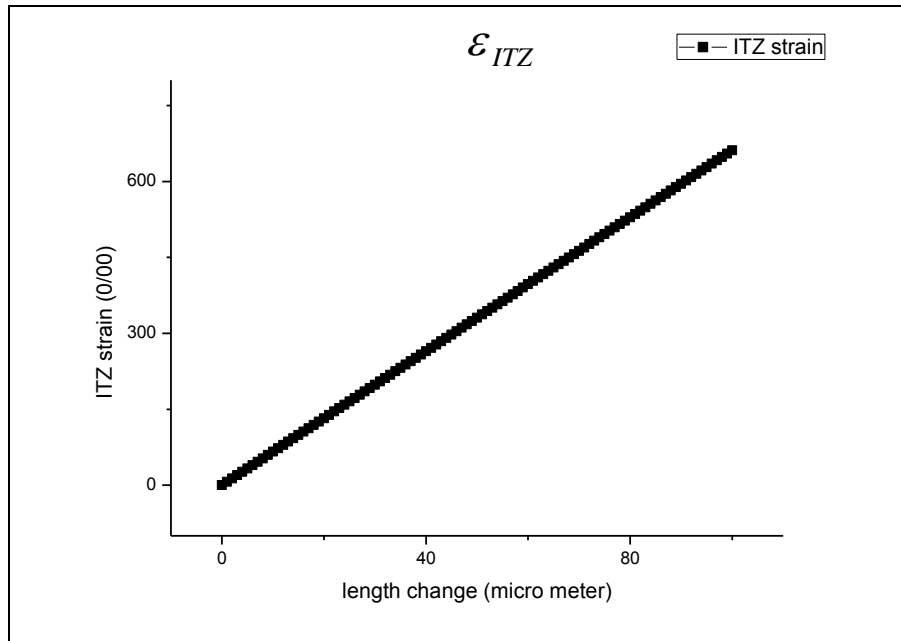
$$\Delta l = \Delta l_{ITZ} \quad (7.10)$$

It is simulated in Figure 7.40.



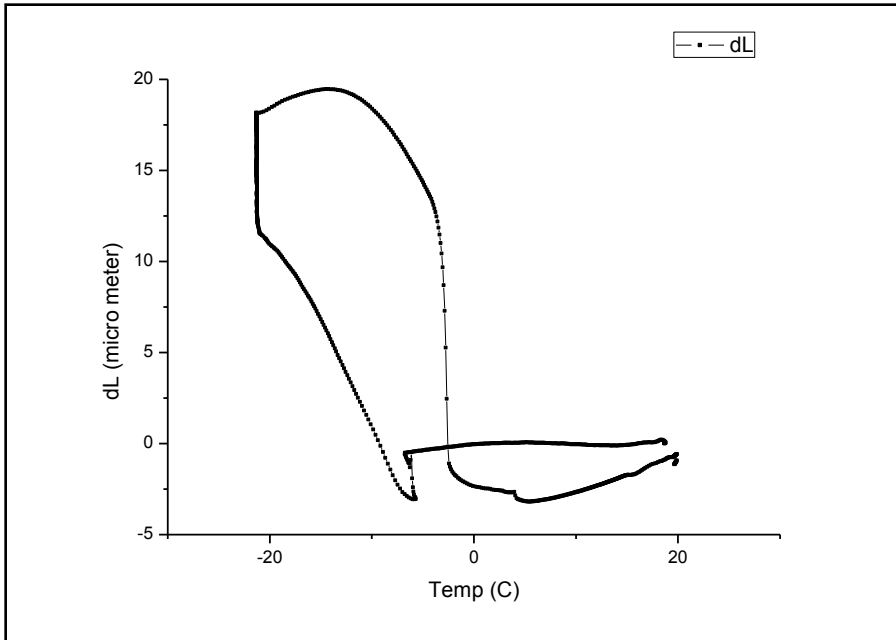
**Figure 7- 40 Schematic explanation of expansion in ITZ during F-T cycles**

In fact, the average width of ITZ may be 30 to 40 micro-meters[49][50][51]. The ITZ strain of LTD test prism is shown in Figure 7.41.



**Figure 7- 41 ITZ strain (ITZ width =30micron, aggregate content = 70% and average diameter of coarse aggregates = 25mm) for LTD test prism (Length=90mm)**

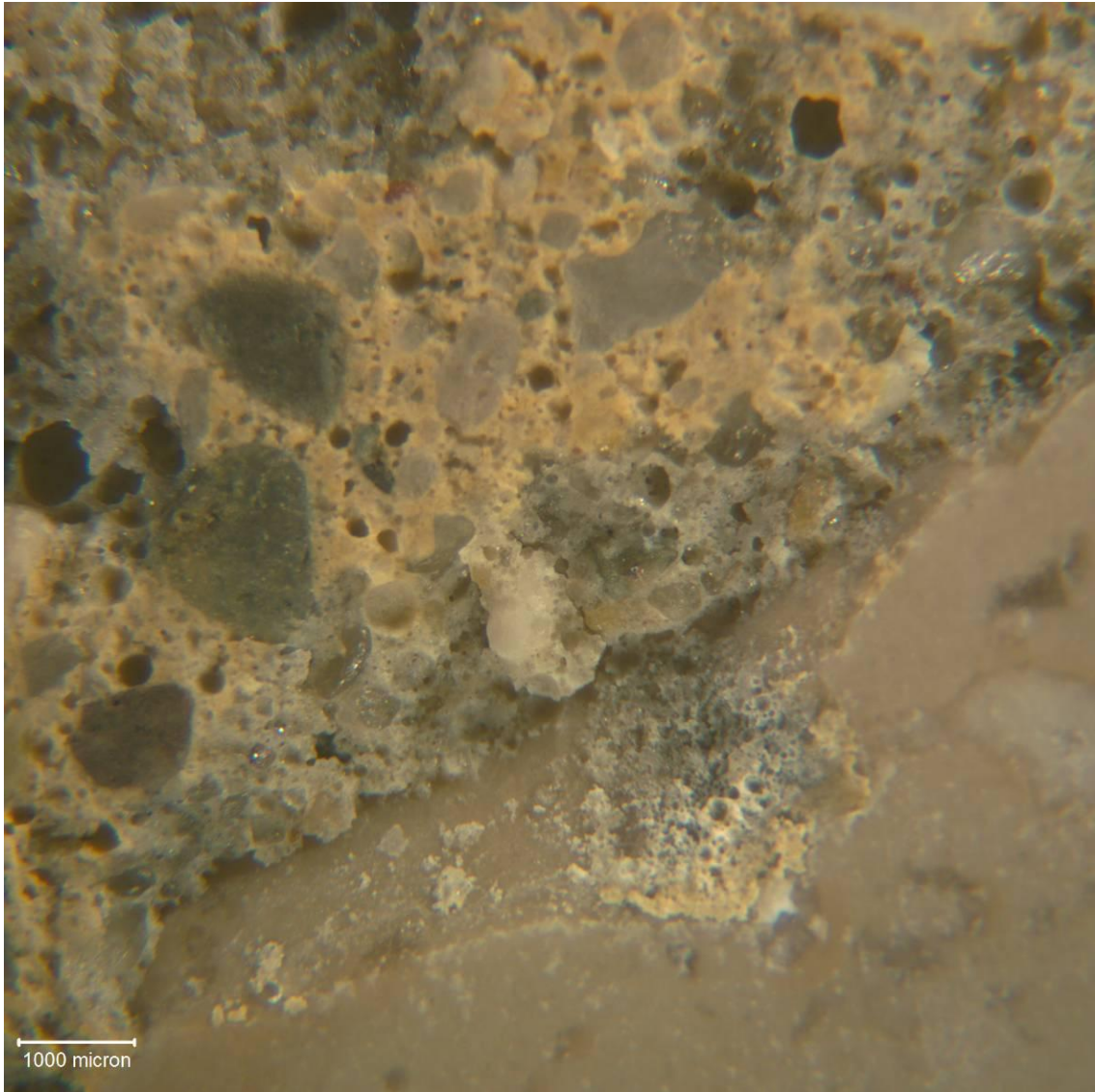
OPC-2 concrete has very high air content and short flow distance. Although the bulk paste reaches seldom to critical water content, the concrete has experienced cryogenic expansion during freezing thawing cycle.



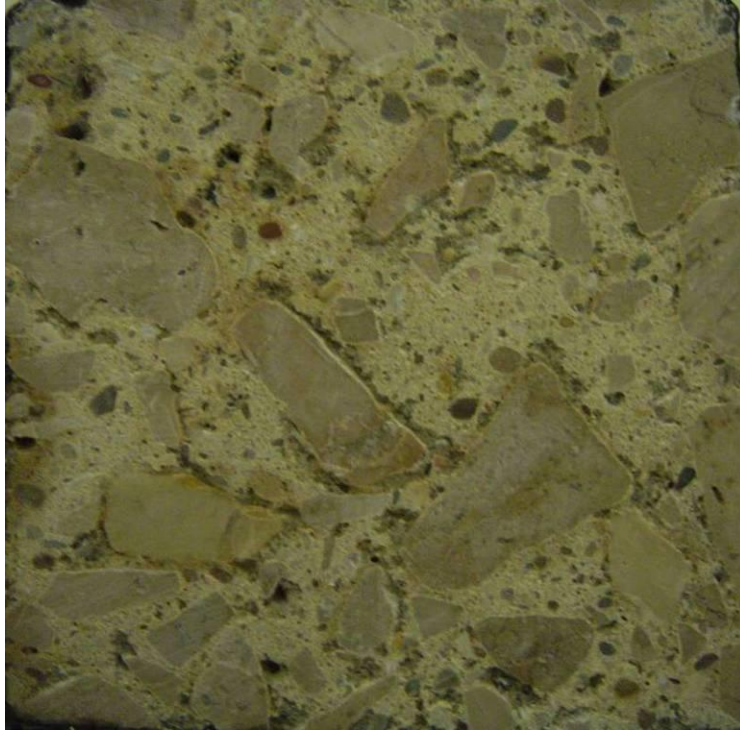
**Figure 7- 42 Dilatation of OPC-2 during a F-T cycle**

Even though OPC concrete has excellent air voids system, ITZ of the concrete can be easily damaged by cryogenic pump. The damages of ITZ have been observed on OPC concrete surface from early freezing thawing cycles. See Figure 7.43 to Figure 7.45.





**Figure 7- 43 OPC-II Specimen after 4 F-T cycles in 3% NaCl solution**



**Figure 7- 44 OPC-II (after 4 F-T cycles in 3% NaCl solution)**

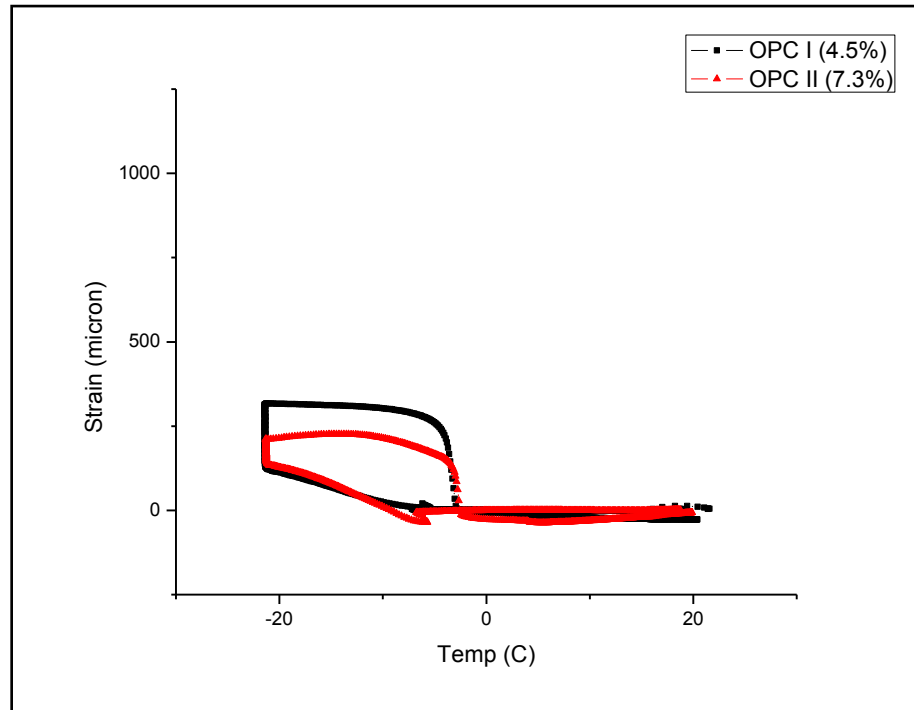


**Figure 7- 45 OPC-II (after 10 F-T cycles in 3% NaCl solution)**

## 7.5 TEST RESULTS WITH LABORATORY CONCRETE SPECIMENS

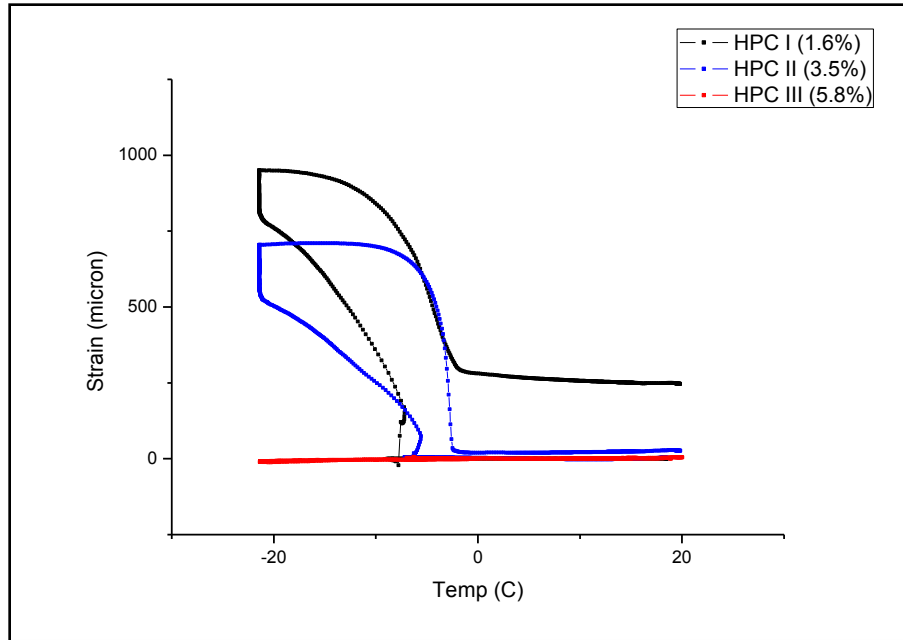
### 7.5.1 LTD test

LTD tests were performed with laboratory mix concrete specimens. As found out in previous studies, cryogenic pump effect seems to be related with the air voids system. However, the expansion of OPC specimen may not be fully removed by increasing air content. Expansion within ITZ seems to be independent of air voids system. See Figure 7.46.



**Figure 7- 46 Expansion of OPC concrete specimens due to cryogenic pump effect ( $\Delta\varepsilon$ )**

The use of GGBFS seems to be beneficial to reduce ITZ. Thus, the expansion of concrete can be successfully removed by sufficient air voids. See Figure 7.47.

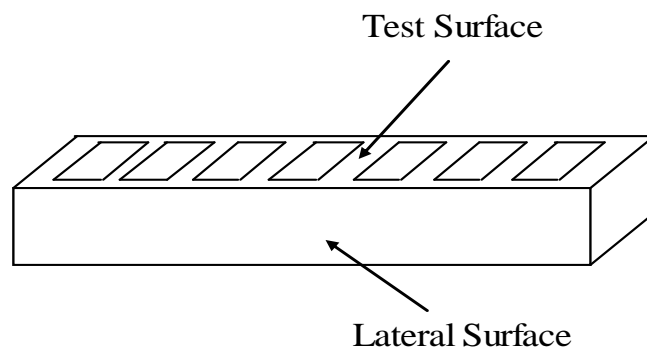


**Figure 7- 47 Expansion of HPC concrete specimens due to cryogenic pump effect ( $\Delta\varepsilon$ )**

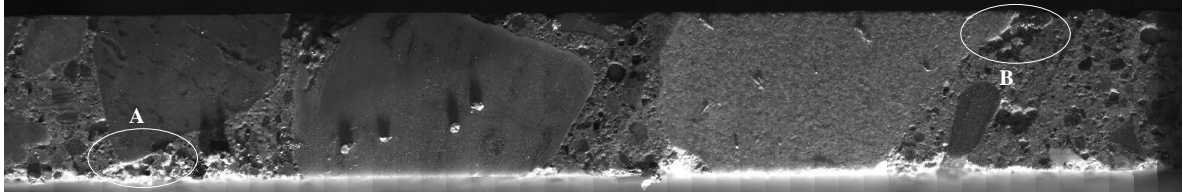
### 7.5.2 Microscopic examination into damage of LTD specimens of OPC concrete

After 5 F-T cycles of LTD test, the surfaces of OPC I LTD prism were examined.

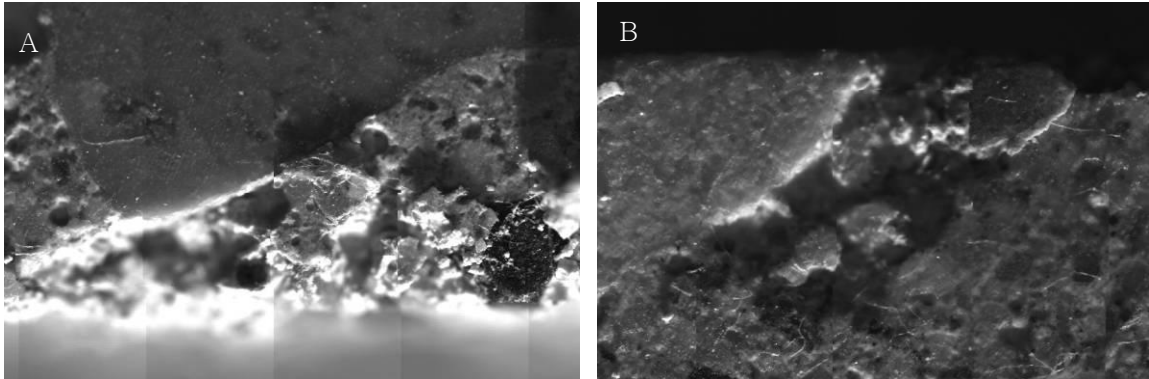
Figure 7. 48 shows the locations of surface of LTD prism.



**Figure 7- 48 The locations of surfaces of LTD prism**

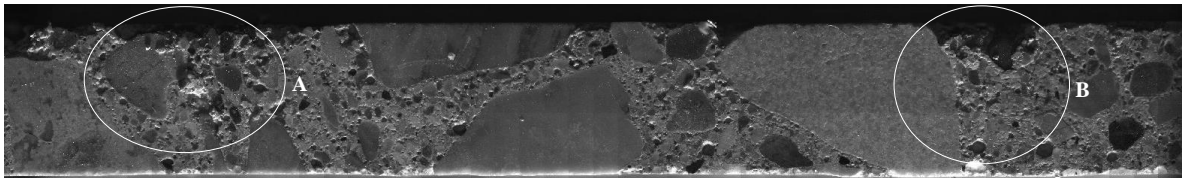


**Figure 7- 49 The test surface of OPC I LTD prism after 5 Freeze-Thaw cycles**



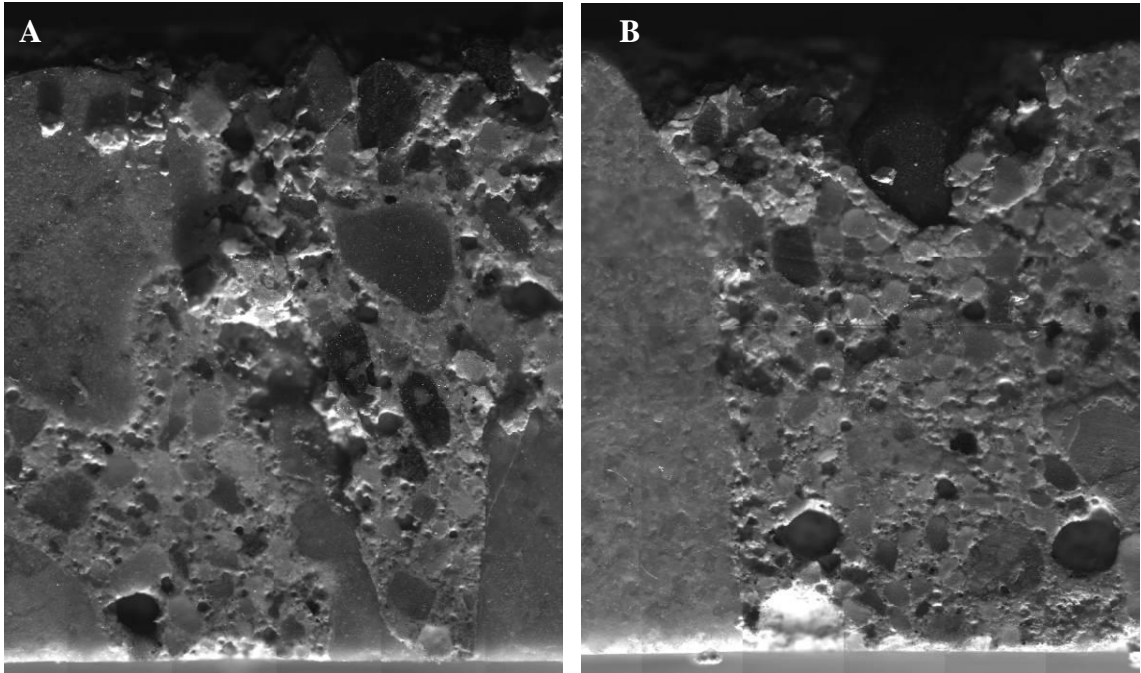
**Figure 7- 50 Spot A and B of OPC-I LTD prism in Figure 7.49**

Scaling centralized to edge and interfaces between aggregates and paste on the test surface of OPC-II specimen.



**Figure 7- 51 The lateral surface of OPC I LTD prism after 5 Freeze-Thaw cycles**



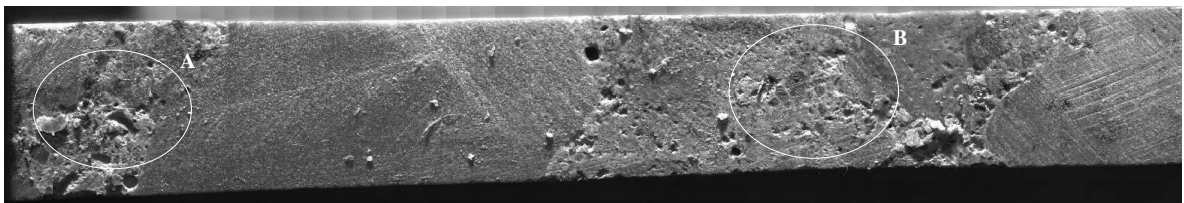


**Figure 7- 52 Spot A and B of OPC-I LTD prism in Figure 7.51**

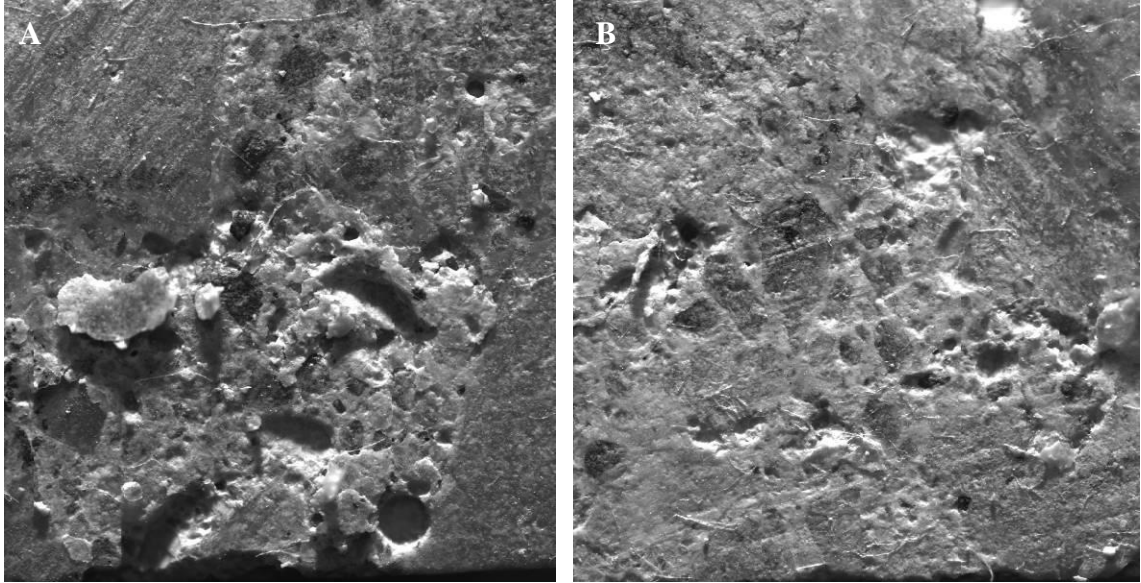
The cracks on lateral surface prolonged from the top to the middle of lateral surface along the interface. In addition, most paste close to test surface was removed so that aggregates were uncovered. The scaling and cracks seem to be concentrated to ITZ.

### **7.5.2 Microscopic examination into damage of LTD specimens of HPC concrete**

After 5 F-T cycles and 10 F-T cycles of LTD test, the surfaces of HPC II LTD prism were examined.

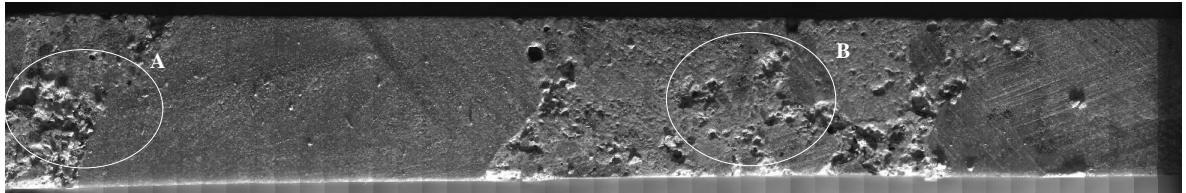


**Figure 7- 53 The test surface of HPC-II LTD prism after 5 F-T cycles**

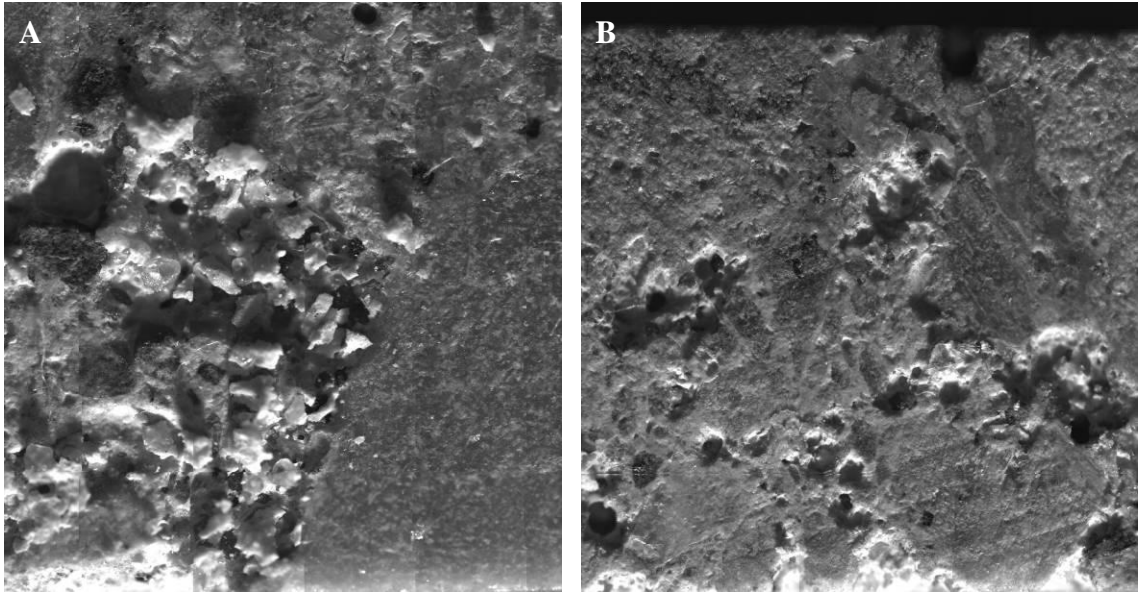


**Figure 7- 54 Spot A and B of HPC-II LTD prism in Figure 7.53**

Only few scaled particles were observed on the test surface of HPC-II LTD prism after 5 freeze-thaw cycles.

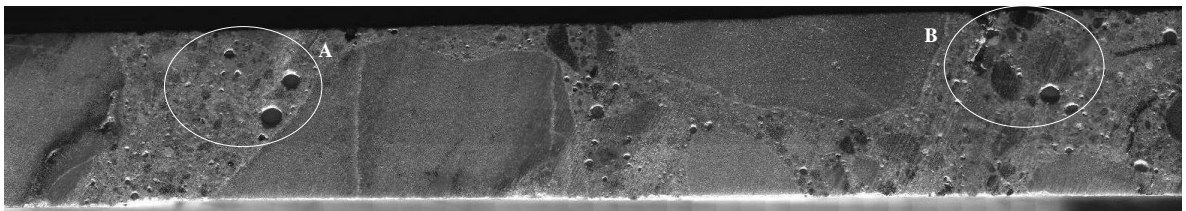


**Figure 7- 55 The test surface of HPC-II LTD prism after 10 F-T cycles**



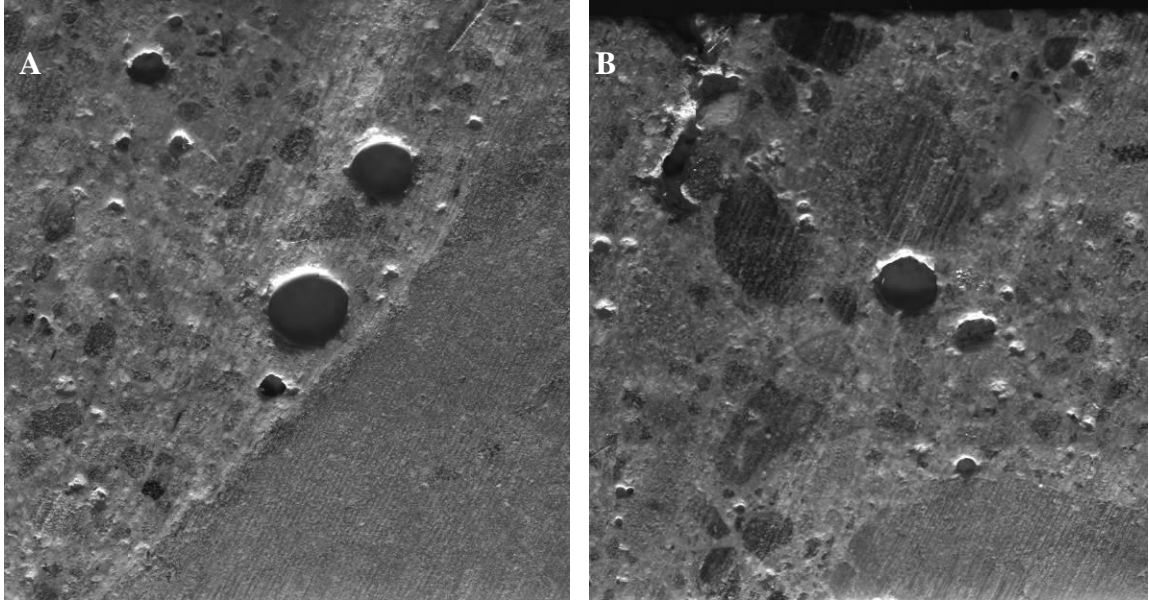
**Figure 7- 56 Spot A and B of HPC-II LTD prism in Figure 7.55**

The scaling was observed occasionally through entire paste after 10 freeze-thaw cycles. Interfaces between paste and aggregates do not seem to be damaged severely.



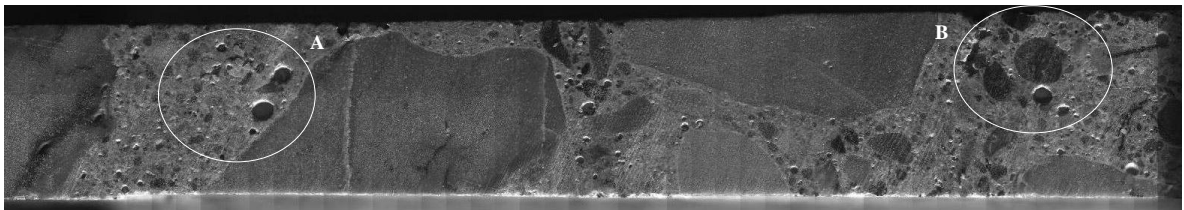
**Figure 7- 57 The lateral surface of HPC-II LTD prism after 5 F-T cycles**



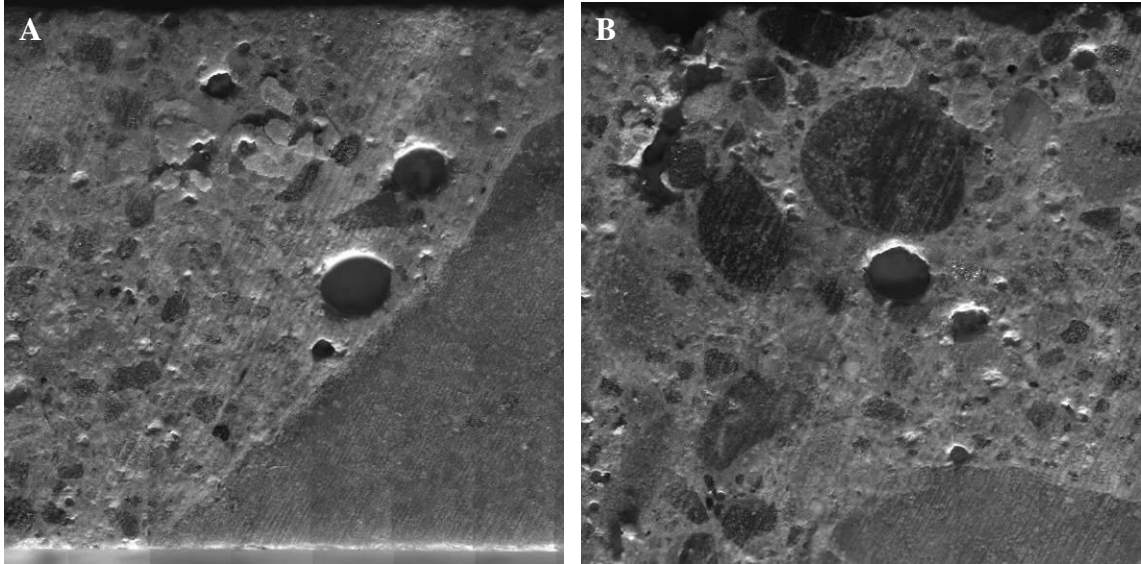


**Figure 7- 58 Spot A and B of HPC-II LTD prism in Figure 7.57**

Almost no scaled particles were observed on the lateral surface of HPC-II LTD prism after 5 freeze-thaw cycles.

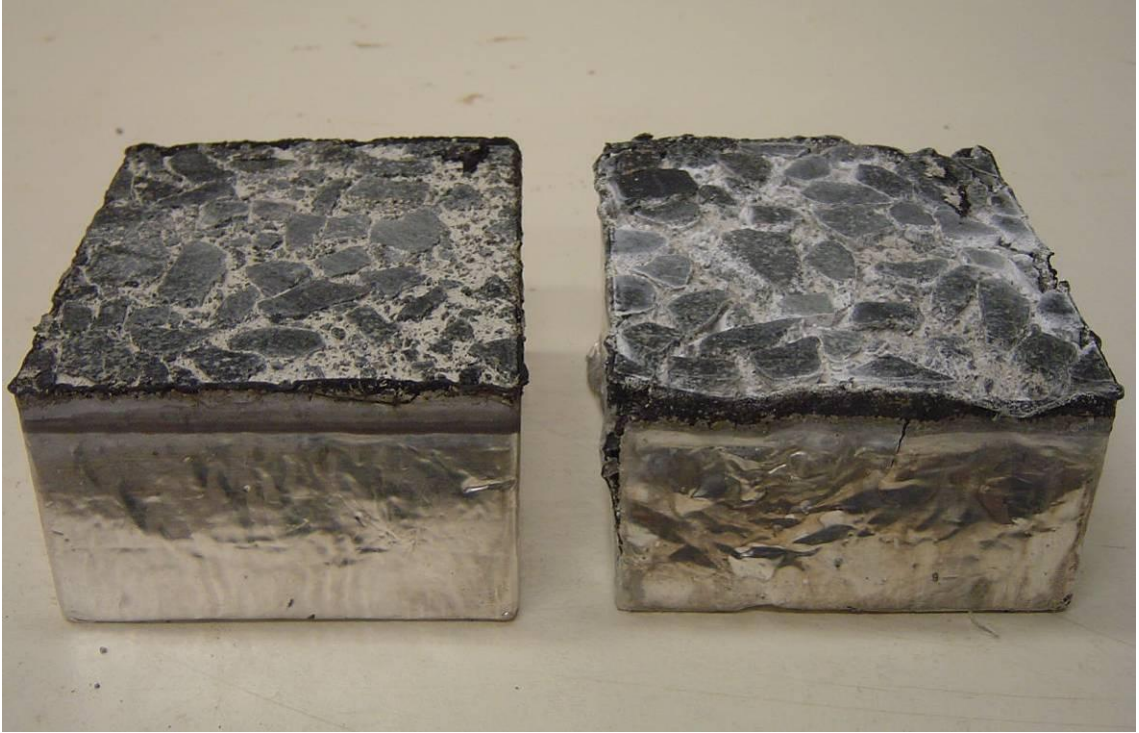


**Figure 7- 59 The lateral surface of HPC-II LTD prism after 10 F-T cycles**



**Figure 7- 60 Spot A and B of HPC-II LTD prism in Figure 7.59**

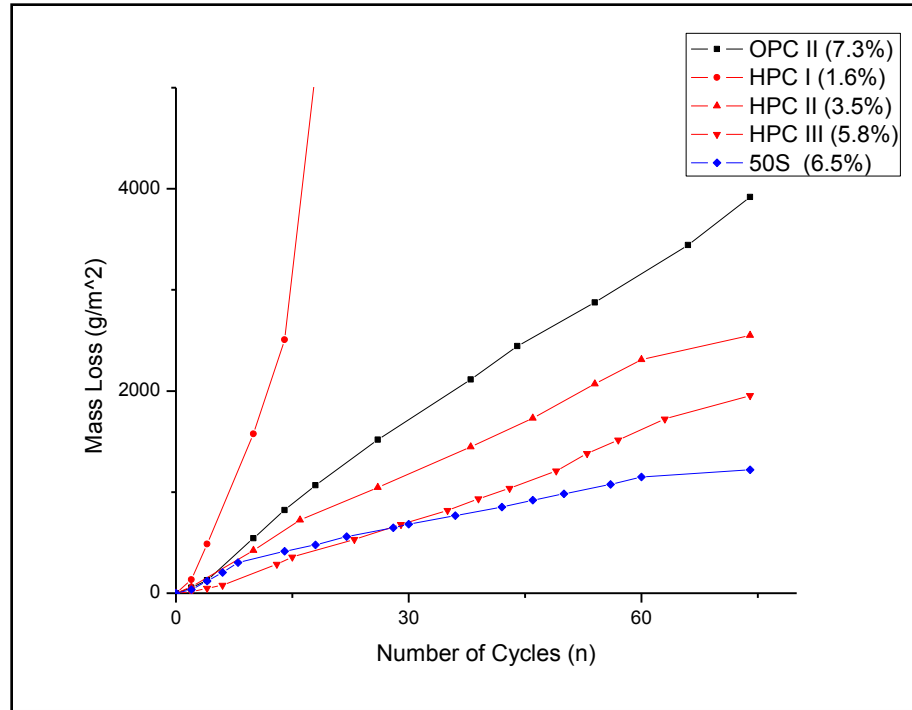
Only few scaled particles were observed on top parts of the lateral surface of HPC-II LTD prism after 10 freeze-thaw cycles. Due to improved ITZ, scaling, damage and cracks of concrete containing GGBFS seem to be shallow. Long-term durability can be improved by the improved interfaces. See Figure 7.61.



**Figure 7- 61 After 130 F-T cycles in 3%NaCl solution (concrete containing GGBFS (left) and Ordinary Portland Cement Concrete (right))**

### **7.5.3 Surface scaling test**

RILEM CDF tests were carried out with laboratory concrete specimens. The results of surface scaling are plotted in Figure 7.62.



**Figure 7- 62 The evaluation of surface scaling of laboratory specimens**

The mass loss results of HPC specimens are proportionally related with the air contents. However, OPC concrete specimen with high air content had more mass loss compared with any other HPC and 50S specimens except HPC concrete with no entrained air. 50S specimen had more scaling than HPC III specimen in early freeze-thaw cycles but the scaling rate of 50S specimen decreased after 6 to 8 freeze-thaw cycles.

## 7.6 SUMMARY OF FINDINGS

Adequate air content seems to improve surface scaling resistance. On the other hand, too much air can reduce strength of concrete. Therefore, it is needed to minimize air content of concrete as much as it has scaling resistance. In order to optimize the air content, well distributed air voids are required. Thus, microscopic observations were performed on polished surfaces of laboratory mix concretes as well as image analysis of RapidAir C 457.

In addition to air voids, properties of paste such as sorptivity and homogeneity are important factor for surface resistance. Absorption tests were performed and paste damage by surface scaling was examined.

LTD tests were conducted with OPC concrete and concrete containing 35%GGBFS of various air contents. The effects of improved properties of air void system and paste on cryogenic pump expansion were studied. Furthermore, cracks of LTD prisms were monitored after LTD tests.

### Air-Void system

- HPC concrete specimen seems to have more fine air voids compared to OPC concrete specimen. This was observed in both moderated air content and high air content.
- Air voids clustering were observed in OPC concrete specimens. The clustering occurred around aggregates so that the aggregates were separated from paste. The concentrated air voids can create a localized zone of weakness. Furthermore, fine air voids were united so that the clustered air voids do not seem to work effectively as a frost protection method.
- Air voids clustering around aggregates seem to reduce effectivity of air voids of bulk paste.
- The use of GGBFS successfully minimized the air void clustering.

### Paste properties

- Absorption rates reduced with increasing portion of GGBFS replacement up to 35%. Concrete containing GGBFS seems to have less sorptivity.
- Highly porous zones, ITZ, were observed interfaces between aggregates and paste of OPC concrete. ITZ seems to occur with air voids clustering. The coincidence seems to worsen the resistance of scaling as well as the strength of interface.
- Due to the defects of interface between aggregates and paste, ITZ of OPC concrete were easily damaged by frost attack and the depth of damage became deeper with more F-T cycles.
- The defects of interface were significantly reduced by the use of GGBFS

#### Expansion by cryogenic pump

- Due to ITZ, highly porous zone, OPC concrete does not seem to protect from cryogenic pump expansion just by increasing air void. In fact, OPC I (4.5% air) and OPC II (7.3% air) expanded similarly during the LTD test.
- With improved air voids distribution and paste properties, the cryogenic pump expansion of HPC-II specimen, 35% of replacement by GGBFS with 5.8% air, was successfully removed.

#### Microscopic observation after LTD test

- Damage of OPC concrete was concentrated to ITZ on the test surface of LTD specimen. In addition, the cracks on lateral surface were prolonged through ITZ and reached the

middle of height of specimen

- Damage of concrete containing GGBFS was observed only on the test surface and top of lateral surface which is close to top surface. The damage seemed to spread evenly through entire test surface.

#### Surface scaling resistance

- Surface scaling resistance seems to be obviously improved by the use of GGBFS. HPC II specimen (3.5% air) had less mass loss up to 70 F-T cycles than OPC II specimen (7.3% air).
- As a result, the use of GGBFS can replace some of air content.
- HPC I (no entrained air) concrete specimens were severely scaled off by frost attack. The use of GGBFS may not be able to replace entire air voids.

## **CHAPTER 8**

### **MAJOR FINDINGS AND RECOMMENDATIONS FOR FUTURE WORK**

The major focus of this work was to investigate the surface scaling property from a comprehensive laboratory testing program of a variety of highway field concretes of different air-contents and field performance. Additionally, laboratory concretes of different air-content and GGBFS content were investigated. Another major focus was to study the mechanism of surface scaling. This part was investigated from unrestrained specimen dilation versus temperature relation from freeze-thaw tests between 20 C and – 20 C on small specimens. Scaling tests were conducted based on the German CDF (Capillary Suction, De-icing agent and Freeze-thaw Test) and CIF tests (Capillary Suction, Internal damage and Freeze-thaw Test). Specimen sizes used for these tests were 70 mm thick and 80 mm by 80 mm is width and length???. Air void analysis was based on ASTM C 457 Linear Traverse method. Capillary sorptivity was determined from specimen sorption tests on 37 mm thick discs of 100 mm diameter size. Microscopic observations were based on digital stereomicroscope measurements using high resolution CCD camera.



## **8.1 Major Findings**

In this study the driving force responsible for developing surface scaling can be explained by means of an exiting theory known as the Cryogenic Suction Pump. This mechanism is thermodynamic-based. As ice starts forming inside a large pore, capillary transport will form within triple-phases zone. If the surface liquid is unfrozen, then a cryogenic pump keeps activating within a surface region. Surface liquid consisting of Salt-water is an example, because salt-water does not freeze instantly as opposed pure water because the solutes lowers the freezing point while increasing the solute concentration in remaining solution, which keeps a 3% salt solution unfrozen above the eutectic point (-21.2 C).

Surface scaling can develop as a result of excessive internal pore pressure from either critically saturated pores within the paste without air-entrainment as pressure relief, or when surface liquid is present, then the cryogenic pump exacerbates the problem as this creates an additional sink for ice formation.

This study is a first to identify a link between surface scaling due to pure water and salt-water (i.e. 3 % sodium chloride concentration). For pure water the cryogenic pump is limited to capillary pore-suction, and is less severe than if additional liquid is available in the case of deicer salt.

Also, another first to identify is the connection between surface scaling and Interfacial Transit Zone (ITZ) which is a localized zone around the aggregate consisting of higher porosity. Due to the larger pore-size and high porosity damage from cryogenic pump initiates in this region. Scaling is localized and propagates with depth and width. This

type of scaling is more severe than regular surface scaling which is spread out over more surface area, but less deep. Substantial improvement in surface scaling resistance was achieved by eliminating the weak-ITZ by means of pozzolanic reactions between the Portland cement paste and GGBFS. The pozzolanic reactions further reduced capillary sorptivity (i.e. rate of capillary suction versus  $\sqrt{time}$ ) as seen from water sorption results and thus reduced the rate of transport by cryogenic pump.

Entrained air was found to be the major factor in mitigating the cryogenic suction pump. The cryogenic suction pump starts as soon as freezing inside the larger pores is initiated. Specimen expansion as determined by the LTD test does not develop until ice expansion has filled part of the large pores. Initial freezing in these pores is due to pure water from the fully saturated capillary pores. This freezing initiates the cryogenic suction pump. Cryogenic pump expansion is reduced with increasing entrained air content as air decreases pore-filling and creates capillary discontinuity, which inhibits suction.

However, increased entrained air alone cannot stop the cryogenic suction pump as long as surface liquid is available during freezing (i.e. temperatures down to -20 C). Freezing exposure to pure surface water is much less severe as liquid transport is only possible within the pore system. Increasing entrained air content in a fully saturated pore-system can prevent internal frost damage, but cannot prevent salt-scaling surface damage.

Paste sorptivity was found to be a measure of the liquid transport property as affected by entrained air content, and pozzolanic reactions. Once the expansion was initiated, a gradient of expansion was related with a cryogenic pump flow rate which was controlled by paste sorptivity. The cryogenic suction pump accelerates critical saturation levels in the

paste.

The cryogenic pump mechanism was found to be essential to understanding frost actions, especially surface-scaling, which is a surface phenomenon of the porous paste. Surface scaling occurs regardless of whether the surface liquid is pure water or contains salt-solution. However, surface scaling in terms of rate of mass-loss is about an order of magnitude greater when the surface liquid contains about 3% salt-solution.

The cryogenic pump was studied using LTD method, which measures continuously the specimen free deformation versus temperature on smaller specimens where temperature gradients are small. The results seem to agree with predictions based on the cryogenic pump mechanisms.

## **8.2 RECOMMENDATIONS FOR FUTURE RESEARCH**

In the course of this research, major variables affecting surface scaling resistance, frost actions during repeated freeze-thaw cycles, laboratory tests with field specimens and lab specimens, and microscopic and macroscopic examinations on damaged surface by frost actions were studied. The results of these examinations raise several questions that merit further investigation. Recommendations regarding the questions are categorized as follows:

### Cryogenic pump mechanisms of surface scaling

Based on cryogenic pump mechanisms, the effects of air voids and use of GGBFS during frost actions can be explained. However, it is still very complicated to quantify the deteriorations due to lack of information of microstructure of concrete. Furthermore, flow rates toward ice crystals in concrete are varied along temperature and freezing gradients

as well as liquid characteristics. Therefore, there seems to be no quantification of the flow rate during freeze-thaw cycles. It should be valuable to quantify frost actions and flow rates during free-thaw cycles.

#### Laboratory versus field

There does not seem to be a criterion of laboratory tests for durable concrete in the field. It is thus important to pay attention to laboratory versus field performance. As studied in this research, frost deterioration seems to be proportionally related with air contents as frost protection method and paste qualities such as sorptivity and ITZ. However, side effects of overuse should be counted. For instance, too much entrained air can reduce the strength of concrete. Furthermore, RILEM CIF-CDF tests seem to represent very harsh weather conditions. Every specimen in the range of this study eventually failed in terms of surface scaling. However, many road pavements do not seem to be deteriorated severely by surface scaling during their service lives. It is highly recommended that it should be decided how many CIF-CDF cycles represent the real service life of pavement concrete under a certain conditions. Once this is identified, concrete mix properties can be optimized under real weather conditions.

#### Air voids system as frost protection method

Entrained air is one of most important properties for frost durability. On the other hand, the entrained air seems to be very difficult to control in the field. In fact, the efficiency of air voids seems to decrease by size of air burbles and unexpected phenomena such as clustering around aggregates and infillings of air voids. Thus, the air void contents should

be optimized by improving distributions of air voids and removing defects such as clustering.

#### Supplementary Cementitious Material, GGBFS

ITZ and sorptivity of concrete paste seem to be correlated with surface scaling resistance. The use of GGBFS successfully recued the ITZ and decreased sorptivity in the range of this study. The portion of replacing cement by GGBFS was limited up to 50%. In fact, the portion of GGBFS has been limited due to scaling resistance. However, any defects of GGBFS have not been found during this research except weak skins. As a result, it is suggested that the content of GGBFS needs to be increased followed by monitoring of how surface scaling resistance is affected as well as weak skins.

#### Other variables

It has been reported that there are many variables affecting surface scaling such as water to cement ratio, curing method and duration, and high concentrations of deicer solution. In this study, water to cement ration was fixed at 0.45, curing duration was fixed to 28 days, and the concentration of solution was kept at 3%. It may be valuable to perfume test with high concentrations of deicer solutions for a better understating of the mechanisms. In addition, if there is a request to increase frost durability of concrete after air voids contents and GGBFS replacement are optimized, w/c ratio and curing process may be considered.

## References

1. Max J. Setzer, *Modeling and Testing the Freeze-Thaw Attack by Micro-Ice-Lens Model and CDF/CIF-Test*, University Duisburg-Essen, IBPM-Institute of Building Physics and Materials Science, Essen, Germany (2004)
2. M. Pigeon, C. Talbot, J. Marchand and H. Hornain, *Surface Microstructure and Scaling Resistance of Concrete*, Cement and Concrete Research, Vol. 26, No. 10 : 1555-1566 (1996)
3. Andrzej Cwirzen, Vesa Penttala, *Aggregate-Cement paste transition zone properties affecting the salt-frost damage of high-performance concretes*, Cement and Concrete Research 35 : 671-679 (2004)
4. L. Basheer, P.A.M. Basheer and A.E. Long, *Influence of coarse aggregate on the permeation, durability and the microstructure characteristics of ordinary Portland cement concrete*, Construction and Building Materials 19 : 682-690 (2005)
5. Daria Jozwiak-Niedzwiedzka, *Scaling resistance of high performance concretes containing a small portion of pre-wetted lightweight fine aggregate*, Cement & Concrete Composites, 27 : 709-715 (2005)
6. An Cheng, Ran Huang, Jiann-Kuo Wu and Cheng-Hsin Chen, *Influence of GGBS on durability and corrosion behavior of reinforced concrete*, Materials Chemistry and Physics 93 : 404-411
7. Powers, T.C, Brownyard , T.L, *Studies of the Physical Properties of Hardened Portland Cement Paste*, Research Laboratories of the Portland Cement Association, Bull. 22 (1948)
8. M.J. Setzer, *Basis of testing the freeze-thaw resistance: surface and internal deterioration*, RILEM Proceedings 34 : 158-173
9. Hallet, B, Walder, J.S, Stubbs, C.W, *Weathering by Segregation Ice Growth in Microcracks at Sustained Subzero Temperatures: Verification from an Experimental Study Using Acoustic Emissions*, Permafrost and Periglacial Processes, Vol 2: 283-3000 (1991)
10. F. Belaid, G. Arliguie, R. Francois, *Porous Structure of the ITZ around galvanized and ordinary steel reinforcements*, Cement and Concrete Research 31 (2001) 1561-1566.
11. Fletcher, N.H., *The Chemical Physics of Ice*, Cambridge University Press (1970)
12. G. Fagerlund, *A service life model for internal frost damage in concrete*, Div. Building Materials, Lund Institute of Technology, Report TVBM-3119 (2004)
13. G. Hadenblad, *Moisture permeability of mature concrete, cement mortar and paste*, Div. Building Materials, Lund Institute of Technology, Report TVBM1014 (1993)
14. *Handbook of Chemistry and Physics*, 70<sup>th</sup> Ed. CRC Press, Florida, 1989-1990.
15. Fletcher, N.H., *The Chemical Physics of Ice*, Cambridge University Press (1970)

16. Nyame, B.K., and Illston, J.M., *Relationships Between Permeability and Pore Structure of Hardened Cement Paste*, Magazine of Concrete Research 33 : 139-146 (1981)
17. Powers, T.C, *The Air Requirement of Frost-Resistant Concrete*, Proceedings, Highway Research Board 29, PCA Bull. 33 (1949)
18. Pigeon, M. and Lachance. M., *Critical Air Void Spacing Factors for Concrete Submitted to Slow Freeze Thaw Cycles*, Proc. ACI, 78 : 282 (1981)
19. Pigeon, M., Perranton, D., and Pleau, R., *Scaling Tests of Silica Fume Concrete and the Critical Spacing Factor Concept*, ACI Spec. Pub., 100: 1155 (1987)
20. DeFontenay, C. and Sellevold, E.J., *Ice Formation in Hardened Cement Paste, I: Mature Water Saturated Pastes*, ASTM Spec. Tech. Pub., 691:425 (1980)
21. Vesa Penttala and Fahim Al-Neshawy, *Stress and strain of concrete during freezing and thawing cycles*, Cement and Concrete Research 32:1407-1420 (2002)
22. M. Burn, A. Lallemand, J.F. Quinson and C. Eyraud, *A new method for the simultaneous determination of the size and shape of pores: The thermoporometry*, Thermochim. Acta 21 : 59-88 (1977)
23. V. Penttala, *Freezing-induced strains and pressures in wet porous materials and especially in concrete mortar*, Adv. Cem. Based Mater. 7: 8-19 (1998)
24. V. Penttala, *Strains and pressures induced by freezing mortars exposed in sodium chloride solution*, Concr. Sci. Eng. 1 (1) : 2-14 (1999)
25. Stefan Jacobson, Frank Melandso and Hung Thanh Nguyen, *Flow calculation and thermodynamics in wet frost exposure of cement based materials*, Narvik University College, University of Tromso, Norway.
26. George W. Scherer, *Stress from crystallization of salt*, Cement and Concrete Research 34: 1613-1624 (2004)
27. Niels Thaulow and Sadananda Sahu, *Mechanism of concrete deterioration due to salt crystallization*, Materials Characterization 53: 123-127 (2004)
28. O. Wowra, *Effects of carbonation to microstructure and pore solution*, RILEM Proceedings 27:61-67
29. J. Stark, *Frost resistance with and without deicing salt – a purely physical problem?*, RILEM Proceeding 34:83-99
30. John J. Valenza ng 34:83-99e W. Scherer, *Mechanism for Salt Scaling of a Cementitious Surface*, Princeton University, Civil & Env. Eng. / PRISM, Eng. Quad. E-319, Priceton, NJ
31. Zdenek P. Bazant, Jenn-Chuan Chern, Arnold M. Rosenberg and James M. Gaidis, *Mathematical Model for Freeze-Thaw Durability of Concrete*, J. Am. Ceram. Soc. 71 [9] 776-83 (1988)
32. Hesstvedt, E., *The interfacial Energy Ice/Water*, Norwegian Geotech. Inst., Pub. No. 56 (1964)
33. NRMCA, *CIP2-Scaling Concrete Surfaces*, 2pp., 1998.
34. John J. Valenza II and George W. Scherer, *Mechanism for Salt Scaling*, The American Ceramic Society 89 [4] 1161-1179 (2006)
35. J. Marchand. M. Pigeon, D. Bager, and C. Talbot, *Influence of Chloride Solution Concentration on Deicer Salt Scaling Deterioration of Concrete*, ACI Material Journal Title no, 96-M53
36. Correns CW, *Growth and dissolution of crystals under linear pressure*, Discuss

Faraday Soc 1949;5:267-71

37. Chatterji S, Thaulow N. *Unambiguous demonstration of destructive crustal growth pressure*. Cem Concr Res 1997;27:811-6
38. G. Fagerlund, *The international cooperative test of the critical degree of saturation method of assessing the freeze/thaw resistance of concrete*, VOL. 10, No. 58 – MATERIAUX ET CONSTRUCTIONS
39. P. Grathwohl, *Diffusion in natural porous media: Contaminant transport, sorption / desorption and dissolution kinetics*. Kluwer Academic Publishers, 1998, [ISBN 0-7923-8102-5](#)
40. J.D. Shane, T.O. Mason and H.M. Jennings, *Conductivity and microstructure of the interfacial transition zone measured by impedance spectroscopy*. In: M.G. Alexander, G. Arliguie, G. Ballivy, A. Bentur and J. Marchand, Editors, *Engineering and Transport Properties of the Interfacial Transition Zone in Cementitious Composites*, E & FN Spon, London (1999), pp. 173 of th
41. S. Jacobsen, *Liquid uptake mechanisms in wet freeze/thaw: Review and modeling*, in: D.J. Janssen, M.J. Setzer, M.B. Snyder (Eds.), RILEM Proceeding PRO 25, Cachan, France, 2002, pp. 41-51
42. S. Jacobsen, *Calculating liquid transport into high-performance concrete during wet freeze/thaw*, Cement and Concrete Research 35 (2005) 213-219
43. J. Crank, *The Mathematics of Diffusion*, end ed., University Press, Oxford, 1975, 414 pp.
44. D.K. Panesar, S.E. Chidiac, *Multi-variable statistical analysis for scaling resistance of concrete containing GGBFS*, Cement & Concrete Composites 29 (2007) 38-48
45. J.M. Gao, C.X. Qian, H.F. Liu, B. Wang, L. Li, *ITZ microstructure of concrete containing GGBS*, Cement and Concrete Research 35 (2005) 1299-1304
46. Tan Ke-Feng, Xin-Cheng Pu, *Strengthening effects of FGFA, GGBS and their combination*, Cem. Concr. Res. 28(12)(1998) 1819-1825
47. Ronald L. Kozikowski Jr., David B. Vollmer, Peter C. Taylor, and Steven H. Gebler, *Factors Affecting the Origin of Air-Void Clustering*, PCA R&D Serial No. 2789 (2005)
48. Mario Robert DE ROOIJ, *Syneresis in cement paster systems*, Doctoral Thesis, Delft University (2000)
49. Sidney Diamond, *Considerations in image analysis as applied to investigations of the ITZ in concrete*, Cement & Concrete Composites 23 (2001) 171-178
50. J.C. Nadeau, *A multi-scale model for effective moduli of concrete incorporating ITZ water-cement ratio gradients, aggregate size distributions, and entrapped voids*, Cement and Concrete Research 33 (2003) 103-113
51. Sidney Diamond, Jingdong Huang, *The ITZ in concrete-a different view based on image analysis and SEM observations*, Cement & Concrete Composites 23 (2001) 179-188
52. Olivier Coussy, Paulo J.M. Monteiro, *Poreelastic model for concrete exposed to freezing temperatures*, Cement and Concrete Research 38 (2008) 40-48